Title

Modulation of P-glycoprotein (P-gp/MDR1) expression and function by sex-steroid hormones and its effect on HIV protease inhibitor pharmacokinetics

Author

Kim, Winnie Young

Publication Date

2004

Peer reviewed|Thesis/dissertation

MODULATION OF P-GLYCOPROTEIN (P-gp/*MDR1*) EXPRESSION AND FUNCTION BY SEX-STEROID HORMONES AND ITS EFFECT ON HIV PROTEASE INHIBITOR PHARMACOKINETICS

by

WINNIE YOUNG KIM

DISSERTATION

Submitted in partial satisfaction of the requirements for the degree of

DOCTOR OF PHILOSOPHY

in

PHARMACEUTICAL CHEMISTRY

in the

GRADUATE DIVISION

of the

UNIVERSITY OF CALIFORNIA, SAN FRANCISCO

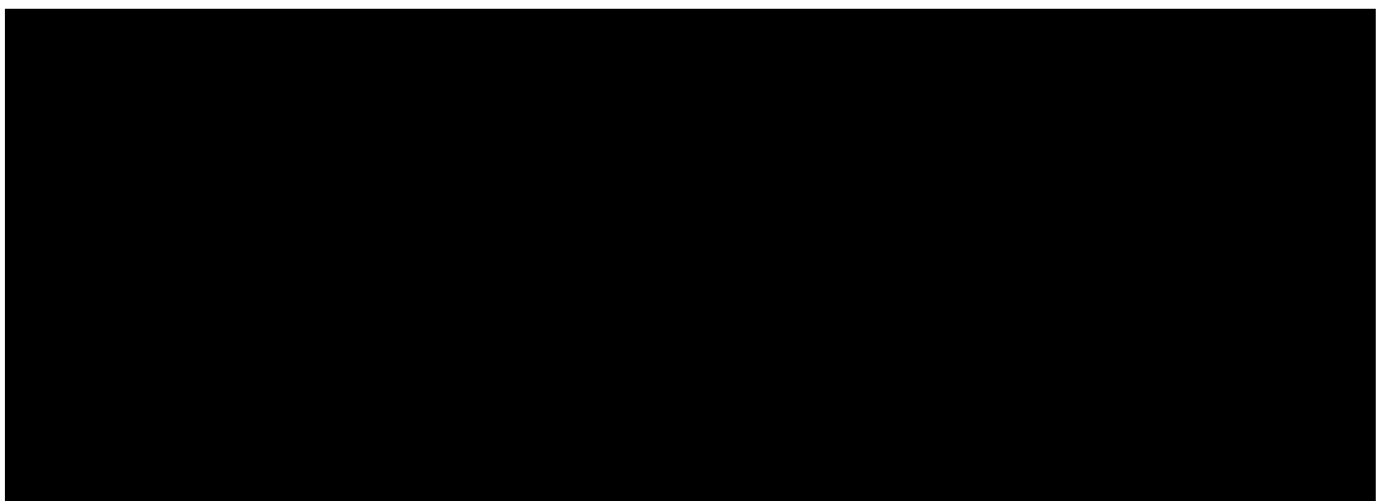

Date University Librarian

Degree Conferred:.....

This dissertation is dedicated to:

My parents, Jung Eun and Young Sil Kim,
for their selfless love and encouragement throughout my life.

ACKNOWLEDGEMENTS

First and foremost, I give thanks and all glory to God, who has blessed me in more ways than I could fathom. I am extremely grateful that I have had the privilege of being mentored by my advisor, Dr. Leslie Z. Benet, who has been a truly outstanding example of an ingenious and superb scientist with no limits to creative discovery. When I first entered graduate school, I prayed that God would provide me with a kind and understanding advisor. As always, the answer to my prayers exceeded my expectations. My deepest thanks to Les for his encouragement and patience during preparations for my oral qualifying exam, the arduously intricate clinical study, the completion of this dissertation and all the support in between. I have been inspired tremendously to pursue discovery in the scientific interactions between body and drug, ultimately helping to relieve suffering in mankind for this generation and those to come.

I would like to thank the members of my thesis committee, Dr. Rob Taylor for all his help and patience with the clinical study and Dr. Synthia Mellon for all her enthusiastic and helpful ideas as both my thesis and orals committee member, and both for taking time out of their busy schedules to review this thesis and share advice from their individual wealth of expert knowledge. I also thank the rest of my orals committee, Dr. Kathleen Giacomini, Dr. Deanna Kroetz and Dr. Nancy Sambol, for providing further insight into my project.

I thank Dr. Carolyn Cummins for helping me get started in the lab, being a patient and thorough instructor in many techniques, including the quintessential transport studies

and LC/MS methodology. Drs. Jae Chang, Wendy Putnam and Miki Susanto were and continue to be wonderful friends and colleagues, providing both emotional and scientific support through sound advice and long talks. I am also very grateful to both current and former lab group members, Dr. Uwe Christians, Dr. Wolfgang Jacobsen, Dr. Noboru Okamura, Dr. Nobuyuki Murayama, Dr. Hideaki Okochi, Dr. Nobuaki Watanabe, Dr. Muhammed Baluom, Dr. Chi-Yuan Wu, Dr. William Chen, Dr. Chunze Li, Dr. Hong Sun, Sumiko Hirai, Mike Goldenberg, Frances Peterson and fellow graduate students Justine Lu and Yvonne Lau for being a wonderfully warm and enthusiastic group of friends, creating a scientifically invigorating environment in which to work.

My sincere thanks to Dr. Dhaval Desai who was instrumentally key in jumpstarting the clinical study, coordinating the entire first half of the study and Dr. Lynda Frassetto for all her expert support and skills during the second half of the rigorous yet exciting study. Dr Muhammed Baluom, Dr. William Chen and Dr. Emil Lin were very generous in their help, also responsible for the nelfinavir sample LC/MS analyses. I owe special thanks to Dr. Uri Ladabaum and Dr. Richard Weisiger for their kind willingness to help via 50+ endoscopies that were carried out to complete this study. My deepest gratitude is due to Dr. Rob Taylor, Dr. Danielle Lane and Dr. Karen Purcell for their perpetual help in executing the seemingly endless number of endometrial scans and biopsies. I thank Hank Matallana at the UCSF DNA Bank, Jon Woo at the Genotyping Core Facility, Dr. Peter Bacchetti for statistical support, the LCA core lab, Dr. Jay Levy's lab and Dr. Deanna Kroetz's lab for their generous help and use of their instrumentation and facilities.

I would like to thank my father, Jung Eun Kim, and mother, Young Sil Kim, for their unconditional love, consistently being there to support me emotionally, spiritually and intellectually in all my endeavors. I could not have asked for better role models of what hard work, discipline and perserverance can accomplish, all the while being loving and dedicated parents. My younger sisters, Anna and Susan, have been my best sidekick buddies, also always encouraging me to no end. I look forward to the many things they will teach me as they mature into lovely, sensible women. Thanks to my friends at Eastbay Baptist Church who were vital in helping to preserve my sanity and for giving me many happy years of fellowship and friendship. Finally, my love and most heartfelt thanks go to my best friend, Dr. Eugene Sohn, who despite his own hectic life as an intern, has been my biggest fan and bestest friend, encouraging me to grow into a more confident, loving and patient woman and now, scientist.

ABSTRACT

Ovulatory Cycle Effects on P-glycoprotein (P-gp/*MDR1*) Modulating HIV Protease Inhibitor Pharmacokinetics

Winnie Young Kim

This dissertation shows that hormonal fluctuations during the menstrual cycle can modulate P-glycoprotein (P-gp/*MDR1*) expression and function, thereby controlling substrate drug bioavailability and disposition. The mechanisms by which ovarian steroid hormones can regulate P-gp, and the extent to which this translates into clinical significance in women's health are still unknown. We hypothesize that estrogens and progestins, synthetic and endogenous, can upregulate the multidrug resistance transporter, P-gp/*MDR1*, thereby interacting synergistically with metabolizing enzymes to influence P-gp substrate drug levels in women. In our *in vitro* studies, induction of P-gp by various synthetic and natural sex-steroid hormones was observed in a human colon carcinoma cell line, LS180. Bidirectional transport and inhibition studies revealed that various estrogens were transported by P-gp. To investigate our thesis *in vivo*, we conducted an extensive clinical study in 21 premenopausal HIV+/- African-American and Caucasian women, using the anti-retroviral HIV drug, nelfinavir, a known P-gp and CYP2C19 substrate, as a probe drug. The goal of this study was to determine whether changes in estrogen and progestin levels during the menstrual cycle could affect P-gp expression in the intestine and endometrium, and P-gp function in lymphocytes. Results from our study showed that endometrial *MDR1* mRNA expression was upregulated during the midluteal phase of the menstrual cycle, when estradiol and progesterone levels peak, while

intestinal expression levels remained relatively unchanged. P-gp function examined in calcein-AM efflux assays in isolated lymphocytes demonstrated increased P-gp activity during the midluteal phase. A comparative pharmacokinetic analysis of nelfinavir between follicular and luteal phases showed a large overall increase in AUC and Cmax during the luteal phase, suggesting a hepatic P-gp effect. The significance of the results from these studies point to the role of the ovulatory cycle and its hormonal effects on the use of P-gp substrate drugs. Since one known factor in the development of HIV viral resistance to antiretroviral PIs is inadequate drug therapy, it is possible that many female subjects are being inadequately treated during the follicular phase of the menstrual cycle. Hence, the interactions between transporters and hormones require further investigation with significant implications for future drug therapy in women.

TABLE OF CONTENTS

CHAPTER III

Bi-directional Transport of Sex-Steroid Hormones

CHAPTER IV

Ovulatory Cycle Effects on P-gp Expression and Function in HIV+/- Women

CHAPTER V

In Vivo Pharmacokinetics of Nelfinavir, Effects of HIV Status and MDR1 Polymorphisms in African-American and Caucasian Females

LIST OF TABLES

LIST OF FIGURES

CHAPTER 1

Introduction

1.1 Overview

Ovarian steroid hormones can modulate P-glycoprotein expression and function that may in turn alter the pharmacokinetics of drugs that are transported by P-gp in women. It had been previously demonstrated that the combination of estradiol and progesterone was able to upregulate *mdr*1a expression in the murine uterus. To further investigate the relationship between transporter and sex-steroid hormones, a series of *in vitro* experiments were carried out. Our objective was to demonstrate that in a female human cell line, ovarian steroid hormones could induce and regulate P-gp expression and ATPase catalytic activity. Another important goal was to determine whether any of these steroid hormones were P-gp substrates. These studies shed light on potential drug-drug interactions in women, in whom multiple hormone-drug therapy regimens are the norm. Since the effects of the menstrual cycle on P-gp expression and function are yet unknown, our clinical research study disclosing significant changes in P-gp substrate drug pharmacokinetics could have a profound impact on the treatment of women in many therapeutic areas including anti-HIV and cancer chemotherapy. Moreover, additional areas of critical research have been exposed regarding the role of P-gp in HIV infectivity and the development of resistance to protease inhibitors (PIs).

1.2 P-glycoprotein

1.2.1 Structure

Encoded by the human *ABCB1* gene (subfamily B), also known as the multidrug resistance gene, *MDR1,* P-glycoprotein (P-gp) is a 170 kDa transmembrane efflux pump for a plethora of structurally unrelated cytotoxic compounds (1, 2). P-gp is a member of the ATP-binding cassette transporter family (ABC). Overexpression of P-gp is one of the major mechanisms by which cells develop multidrug resistance during cancer and AIDS chemotherapy (3). Consequences of increased P-gp activity include limited oral bioavailability and accumulation of drug in P-gp expressing cells, as well as reduced access to blood-tissue barriers, such as the blood-brain barrier (BBB) and the materno-fetal barrier (MFB) (4, 5). There are two known forms of the *MDR* gene in humans, *MDR1* and *MDR3*. In rodents, three genes are expressed- *mdr1a, mdr1b* and *mdr*2 (6). Of these genes, only *MDR1* in humans, and *mdr1a/b* in rodents, encode P-gp proteins with drug transporting capabilities (7). The human *MDR3* and murine *mdr*2 encode a P-glycoprotein responsible for the secretion of phosphatidylcholine into bile, which is most likely a phospholipid transport protein or flippase (8-11).

Comprised of 1280 amino acids, P-gp is a transmembrane protein (Figure 1.1) with two symmetric, homologous halves, each comprised of 610 amino acids joined by a flexible linker region of 60 amino acid. Each half encompasses a short hydrophilic N-terminal segment, six putative transmembrane domains (TMD) identified by hydropathy plots, and a hydrophilic C-terminal region (12). Surrounding the linker region are the Walker A, B

and C sequence motifs followed by a nucleotide binding site, which can bind ATP, triggering ATP hydrolysis. P-gp ATPase catalytic activity requires that both nucleotide binding sites be coordinately stimulated (13). An extracellular region susceptible to considerable posttranslational modification located between TMD 1 and 2 is glycosylated in amino acid positions g1, g4 and g9 (14). Point mutational analyses and photoaffinity labeling studies investigating substrate specificity show that transmembrane domains (TMD) 5, 6, 11, 12 and the extracellular loops linking each pair are important for drug-binding. Transmembrane domains 3 and 10 contribute to drug translocation activities, while domains 6 and 11or 12 are predicted to modulate P-gp activity and substrate specificity (15-17).

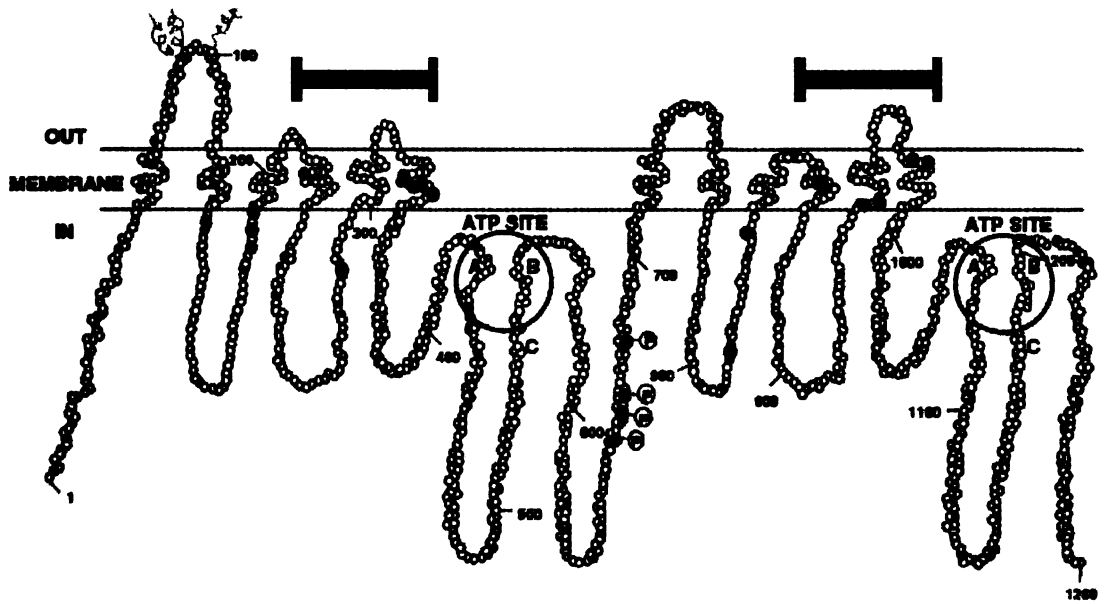

Figure 1.1 A proposed schematic model of the secondary structure of P-glycoprotein. This representation after Ambudkar *et al.* (18) illustrates the amino acids responsible for substrate specificity (blue circles) including glycosylation sites (yellow curls), ATP-binding sites, the Walker A, B and C motifs and phosphorylation sites.

Although stable expression of each individual half has been observed, studies suggest that both halves are required to be linked and interact in a synchronized manner for the molecule to be fully functional (19, 20). It has also been established that interaction between the ATP sites and the drug binding domain sites is critical for drug transport.

Despite numerous attempts, the 3-dimensional structure had not been fully determined. Electron microscopy and image analyses by Rosenberg *et al.* (21) suggest that P-gp is shaped similar to a donut with 6-fold symmetry. When viewed looking down through the pore into the cell, a diameter of 10 nm and a pore diameter of ~5nm has been observed. Half of the entire molecule reputedly lies within the plasma membrane. Furthermore, the central pore is closed off at the intracellular cytoplasmic side, modeling a cup-like chamber that is open to the extracellular medium.

1.2.2 Expression

Multidrug resistance was first observed when cancers treated with multiple chemotherapeutic drugs showed resistance to previously unexposed cytotoxic agents. P-glycoprotein was first identified by Juliano and Ling (3) in Chinese hamster ovary (CHO) cells selected for colchicine resistance and was shown to be responsible for cross-resistance to a wide spectrum of amphilic compounds. Expressed on the apical surface of normal epithelial cells located in major drug eliminating organs in the body, P-gp serves important detoxification functions (Table 1.1). High levels of P-gp have been observed in columnar epithelial cells of the jejunum and colon, adrenal gland, the luminal surface of

biliary hepatocytes and on the intraluminal surface of capillary endothelial cells in both the brain and the testes.

Table 1.1 Tissue localization of P-glycoprotein. Adapted and expanded from Thiebaut *et al.* (22), Young *et al.* (23), Rao *et al.* (24), van der Valk *et al.* (25) and Chaudhary *et al.* (26).

Tissue	**Localization**
Liver	Biliary canalicular front and apical (luminal or central canal) surface of epithelial cells in small biliary ductules
Pancreas	Apical surface of small ductile epithelial cells; not larger in larger pancreatic ducts
Kidney	Brush border of proximal tubule epithelial cells
Colon & Jejunum	High concentrations on apical surfaces of superficial columnar epithelial cells
Adrenal gland	Apical surface of cells in both medulla and cortex
Brain	Sub-apical epithelial surface of choroid plexus of brain (cerebral spinal fluid) as well as luminal surface of endothelium of brain capillaries of the blood brain barrier (BBB)
Placenta	Maternal surface of trophoblasts
Female genital tract and ovary	Endocervical glandular epithelium, ovarian surface epithelium, ectocervical squamous epithelium, endothelial cells in the cortex of the ovary and in the stromal tissue of the myometrium, endometrium and endocervix
Lymphocytes	Peripheral blood mononuclear cells – CD56+ > CD8+ > CD20+ > CD4+
Murine intestine	Regional variation- moderate expression in duodenum and jejunum and maximal expression in ileum

Through immunohistochemical staining using monoclonal antibody MRK16, Thiebaut *et al.* (22) showed high expression levels of P-gp on the apical surfaces of cells facing the excretory compartment in most tissues. Results from this localization study suggested that P-gp served an important role as a detoxification pump to protect the body at the cellular level from toxins. In the adrenal gland, P-gp is believed to be responsible for secretion of steroids, thereby regulating intracellular steroid concentrations to prevent high toxic accumulation (27). P-gp expressed on the biliary canilicular surface of hepatocytes is known to excrete toxic xenobiotics into the bile, causing increased clearance and decreased drug plasma levels. In the gut lumen, P-gp functions to efflux drugs that passively diffuse into the mucosal epithelial cells back out into the lumen so as to prevent drug absorption and decrease bioavailability. Protective mechanisms by P-gp at blood-tissue barriers (i.e. BBB) are well illustrated by numerous knockout mice studies in which penetration is enhanced in mice deficient for mdr1a/b. This is found to be true not only for administered toxic compounds, but also for several endogenous steroid hormones such as cortisol, progesterone, corticosterone and aldosterone (28). Additional studies by van der Valk *et al.* (25) discovered P-gp also to be expressed in the epithelia of bronchi, mammary gland, prostate gland, salivary gland and sweat glands of the skin. However, P-gp expression was not detected in the stomach, lung, spleen and skin.

Multidrug resistance associated DNA sequences (mdr1 and mdr2) from various cancer cell lines were identified, amplified and localized to chromosome 7 (7q21.1) (29-31). The gene encompasses 28 exons spanning >100 kb of DNA (32) that transcribed into an mRNA of 4.5 kb, which encodes a 1280 amino acid glycoprotein.

1.2.3 Mechanism

Traditionally, intestinal and hepatic drug metabolism have been considered to be the primary determinants of drug disposition. However, the discovery of drug transporters has opened different doors in our current understanding of the mechanisms of drug absorption, distribution and disposition. Recent research regarding ABC transporters and drug metabolizing enzymes has evolved to recognize an interaction and synergy between the two, in which the efflux and/or uptake transporters function to regulate the intracellular drug concentration and exposure to metabolizing enzymes (33, 34). For example, intestinal P-gp activity may increase the efflux/passive absorption cycling on the apical cell membrane/lumen periphery for drugs that are substrates for both P-gp and CYP3A. This cycling would increase the exposure and opportunity for a drug to be metabolized by intracellular CYP enzymes, thereby working coordinately to control drug absorption and oral bioavailability.

At the physiologic level, it is still not clear exactly how P-gp functions. Like most conventional ABC transporters, P-gp undergoes a conformational change in response to ATP binding and hydrolysis. This change alters both the affinity and orientation of substrate binding sites. Crystal structures of intact P-gp from Salmonella typhimurium (35) and Escherichia coli (MsbA lipid transporter) (36) have provided significant insights as models for *MDR1* P-gp. However, the relevance of these modeled conformations to actual P-gp function is still questionable. Currently, there are several proposed models of how P-gp translocates its unusually broad range of substrates across cellular membranes.

It was initially thought that P-gp acted as a hydrophilic passageway, allowing drugs to be transported from the cytoplasm to extracellular medium so as to protect drugs from the hydrophobic lipid membrane. However, subsequent evidence implied otherwise (37, 38). Roepe *et al.* (39) hypothesized that transported drugs do not physically bind to P-gp, but rather indirectly stimulate the efflux of cationic compounds and decrease intracellular retention of drug by altering the plasma membrane potential. Other suggested permutations of transport mechanisms include the pump, flippase and vacuum cleaner models. The "pump" hypothesis suggests that energy derived from ATP hydrolysis is used for drug removal from the membrane or cytoplasm. There is also evidence that substrates of the MDR protein are expelled from the inner leaflet of the cytoplasmic membrane rather than from the cytoplasm (40, 41). This led to the "flippase" model where P-gp is predicted to "flip" the drug from the inner cytoplasmic membrane leaflet to the outer leaflet of the bilayer. Eventual transfer of drug to the extracellular medium prevents intracellular drug accumulation. The third model hypothesis proposes P-gp to be a "hydrophobic vacuum cleaner," describing P-gp to be perpetually "vacuuming" the membrane of all toxic chemicals and indiscriminately expelling most hydrophobic substrates (12).

In comparison to these proposed models that require more detailed clarification, abundant evidence points to a direct interaction between transporter and substrate. This direct interaction is confirmed by studies that show that structurally altered substrates can change transport affinity (42). P-gp mutational studies show shifts in transport properties and affinities for specific compounds (43). It can be stated conclusively that the

multidrug transporters, including P-gp, are substrate-specific with multiple sites of interaction/binding for different substrates and inhibitors (1, 44-55).

As previously mentioned, compounds transported by P-gp are diverse in chemical structure, properties and size (Table 1.2). Most seem to share the properties of being hydrophobic and cationic with a molecular mass between 300-2000 Da. The hydrophobic properties allow for passive diffusion. It has been suggested that based on biophysical characteristics, P-gp substrates are linked by the spatial separation of electron donor groups (56, 57). Other groups have demonstrated that substrate specificity is dependant upon the number and strength of hydrogen bonds (58). A diverse array of studies have been implemented in the past decade to identify regions of P-gp that interact with substrate drugs and inhibitors (Table 1.3) (51-53, 59-64).

At the molecular level, the various puzzle pieces of *MDR1* transcriptional regulation are slowly being pieced together. It is has been established that the multidrug resistance phenotype can result from stabilization of the *MDR1* mRNA, regulation at the translational level and alterations in protein processing (65). The *MDR1* gene has both a proximal and distal promoter region. The distal promoter is more commonly expressed in tissues and cultured cells. Thus, this region is considered a critical element in the regulation and expression of the gene (66, 67). Within this region, *MDR1* lacks a consensus TATA box, but does contain an inverted CCAAT element [-82 to –73] and a

Table 1.2 Selected P-gp substrates. Adapted and expanded from Ambudkar *et al.*(1), Seelig *et al.* (56, 57), Silverman *et al.* (68), Wacher *et al.* (69) and Marzolini *et al.* (70).

SUBSTRATES	
Actinomycin D	Dexniguldipine
Aldosterone	Dibucaine
Amitriptyline	Digitoxin
Amprenavir	Digoxin
Atorvastatin	Diltiazem
Bepredil	Dipyridamole
BIBW22 BS	Docetaxel
Bisantrene	Domperidone
Calcein	Doxorubicin
Cefazolin	Emitine
Cefoperazone	Epirubicin
Cefotetan	Erythromycin
Celiprolol	Estradiol
Cepharanthine	Estrogen-glucuronide
Cerivastatin	Ethidium bromide
Cevuronium	Etoposide
Cimetidine	Fexofenadine
Cinchonidine	Fluphenazine
Cis-flupenthixol	Fluvastatin
Colchicine	Gallopamil
Corticosterone	Gramicidin D
Cortisol	Hoechst 33342
CP100356	Hydrocortisone
Cyclosporine	Indinavir
Daunorubicin	Itraconazole
Dexamethasone	Ivermectin

Loperamide	S9788
Losartin	Saquinavir
Lovastatin	SDB-ethylenediamine
Mefloquine	Simvastatin
Methadone HCl	Sparfloxacin
Methylbenzoylreserpate	Spiperone
Methylreserpate	Tacrolimus
Mithramycin	Talinolol
Mitomycin C	Teniposide
Mitoxantrone	Terfenadine
Monensin	Tetracycline
Morphine	Tetraphenylphosphonium bromide
Morphine-6-glucuronide	Thioridazine
N-Acetyl-leucyl-leucyl-norleucine	Topotecan
Nelfinavir	Trifluoroperazine
Nicardipine	Triflupromazine
Nifedipine	Triton X-100
Ondansentron	Valinomycin
Paclitaxel	Valspodar
Perphenazine	Verapamil
Phenoxazine	Vinblastine
Phenytoin	Vincristine
Puromycin	Vindolin
Quinidine	Yeast factor pheremone
Rhodamine 123	Yohimbine
Ritonavir	

Table 1.3 Selected P-gp inhibitors. Adapted and expanded from Wacher *et al.* (69) and Marzolini *et al.* (70).

INHIBITORS	
Amiodarone**	Methadone*
Atorvastatin*	Mifopristone (RU486)
Azithromycin	Nelfinavir***
BIBW22	Nevirapine
Bromocriptine	Nicardipine*
Carvedilol	Nitrendipine
Chlorpromazine	Orange juice
Clarithromycin	Paroxetine
Cyclosporine***	Pentazocine
Delavirdine	Prednisone
Diltiazem*	Progesterone
Dipyridamole*	Quercetin
Efavirenz	Quinidine*
Erythromycin**	Reserpine**
Felodipine	Ritonavir***
Fluconazole	Saquinavir***
Flupenthixol	Sertraline
Fluoxetine	Simvastatin*
GG918 (GF120918)	Sirolimus*
Hydrocortisone*	Spironolactone
Indinavir***	Staurosporine
Itraconazole*	Tacrolimus***
Ketoconazole	Tamoxifen**
Lidocaine	Terfenadine*
Lovastatin*	Testosterone
LY335979	Trifluoroperizine*
Mefloquine*	Troleandomycin**

Valspodar*	VX-710
Verapamil**	

* Also P-gp substrate
** Also P-gp inducer
*** Also P-gp substrate and inducer

Table 1.4 Selected inducers of P-gp. Adapted from Marzolini *et al.* (70).

INDUCERS	
Actinomycin D*	Phenobarbital
Amiodarone**	Phenothiazine
Amprenavir*	Reserpine**
Clotrimazole	Retinoic acid
Colchicine*	Rifabutin
Cyclosporine***	Rifampin*
Daunorubicin*	Ritonavir***
Dexamethasone*	Saquinavir***
Doxorubicin*	Sirolimus***
Erythromycin*	St. John's Wort
Etoposide*	Tacrolimus***
Indinavir***	Tamoxifen**
Mitoxantrone*	Trazodone
Nefazodone	Troleandomycin**
Nelfinavir***	Vinblastine*
Nifedipine*	Vincristine*

* Also P-gp substrate
** Also P-gp inhibitor
*** Also P-gp substrate and inhibitor

GC-rich element [-56 to -43], which interact with Sp transcription factors (71-75). Basal transcription is controlled by a Y-box, to which transcription factor NF-Y binds, and an initiator (Inr) sequence that is believed to be the site of a RNA Pol II pre-initiation complex (76, 77). Downstream overlapping a second GC-rich region, an inverted MED-1 (Multiple start site Element Downstream 1) was found to be a critical element in maintaining constitutive *MDR1* transcription in human cell lines (78). In normal tissue, the *MDR1* gene is differentially expressed, inducible by a versatile assortment of environmental triggers including chemical carcinogens, cytokines, heat shock, UV and x-ray irradiation, hormones and antibiotics (Table 1.4). This inducible regulation is not only species, but tissue and cell dependent.

1.3 Ovarian Hormones

1.3.1 Classes

Steroid hormones are a group of biologically active compounds that are derived from cholesterol and all have in common a cyclopentanoperhydrophenanthrene ring. The cholesterol precursor (Figure 1.2) comes from 2 major sources: (1) it is synthesized directly from acetate, or (2) LDL cholesterol is taken up by cells via cholesterol ester stores in intracellular lipid droplets or from uptake of low-density lipoproteins (LDL). Free cholesterol moves from the cytoplasm to the outer mitochondrial membrane. Within the mitochondria, C_{27} cholesterol is converted to its respective 18-, 19-, 21-carbon steroid hormones. This involves a rate-limiting and irreversible cleavage of a 6-carbon residue by enzyme P450scc (CYP11A1; cholesteraol side-chain cleavage; desmolase), resulting in pregnenolone (C_{21}), a precursor for the synthesis of all steroid hormones (Figure 1.2).

Steroids with 21-carbon structures are labeled pregnanes, 19-carbon compounds are known as androstanes and 18-carbon compounds, estranes. The main sites of steroid hormone production are the adrenal cortex, testis, ovary and the placenta (79).

Figure 1.2 Chemical structure of cholesterol and metabolite pregnenolone.

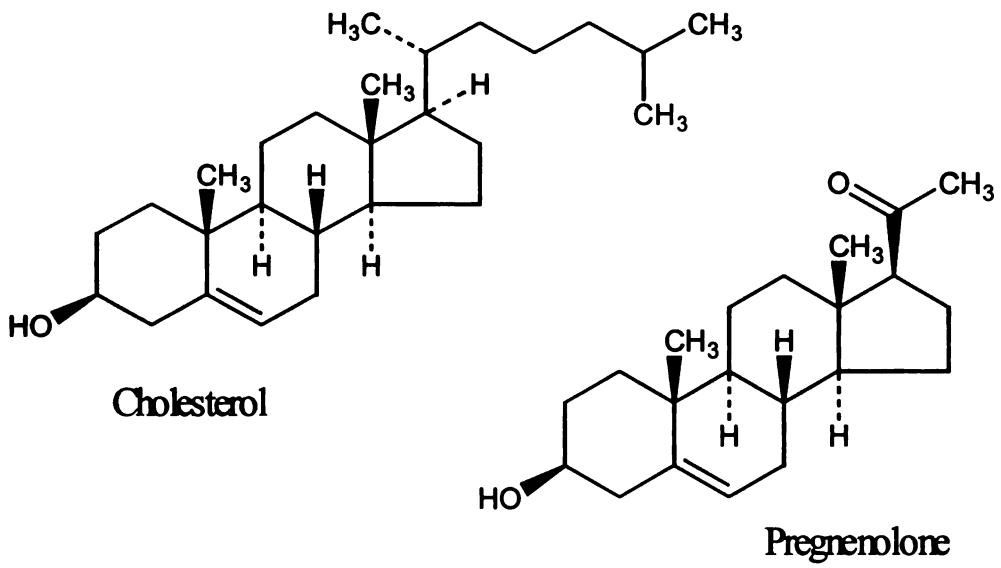

Secreted steroid hormones are classified into five groups of molecules, based primarily on receptor binding specificity. The adrenal cortex produces 3 major classes of these steroid hormones: glucocorticoids (carbohydrate metabolism regulation), mineralocorticoids (Na^+/K^+ level regulation) and androgens. The adrenal cortex consists of a cortex and a medulla. The cortex is the site for steroid production and consists of 3 major tissue regions known as the zona glomerulosa, zona fasciculata and zona reticularis. The medulla is a neuroectoderm-denied tissue and produces catecholamines. The remaining 2 classes of steroid hormones are the ovarian steroid hormones, estrogens

and progestogens (also known as progestins). In women, these endogenous hormones have significant developmental effects, neuroendocrine actions for ovulatory control, and major actions on mineral, carbohydrate, protein and lipid metabolism. They are produced primarily in the ovaries and the placenta (80).

It has long been known that the ovaries produce steroid hormones that control and regulate the female reproductive system. Under tight biosynthetic control, secretion of estrogens and progestins are regulated by the anterior pituitary gonadotropins (Figure 1.3). This is executed via negative and a unique positive feedback loop, which directs hypothalamic secretion of gonadotropin releasing hormone (GnRH). The GnRH then triggers pituitary secretion of follicule stimulating hormone (FSH) and luteinizing hormone (LH) and. In turn, the gonadotropins (LH and FSH) play a critical role in the maturation of the follicle by stimulating production of estrogen and progesterone by the ovary. The ovarian follicle that matures into a corpus luteum during the course of the ovulatory cycle contains granulosa, theca interna and luteal cells, which are the predominant hormone-secreting cells. The ovaries release progesterone in large amounts during the luteal phase, which exerts feedback regulation on the pituitary and hypothalamus. Estrogen exerts feedback regulation primarily on the pituitary (81).

Figure 1.3 Neuroendocrine control of steroid hormone secretion.

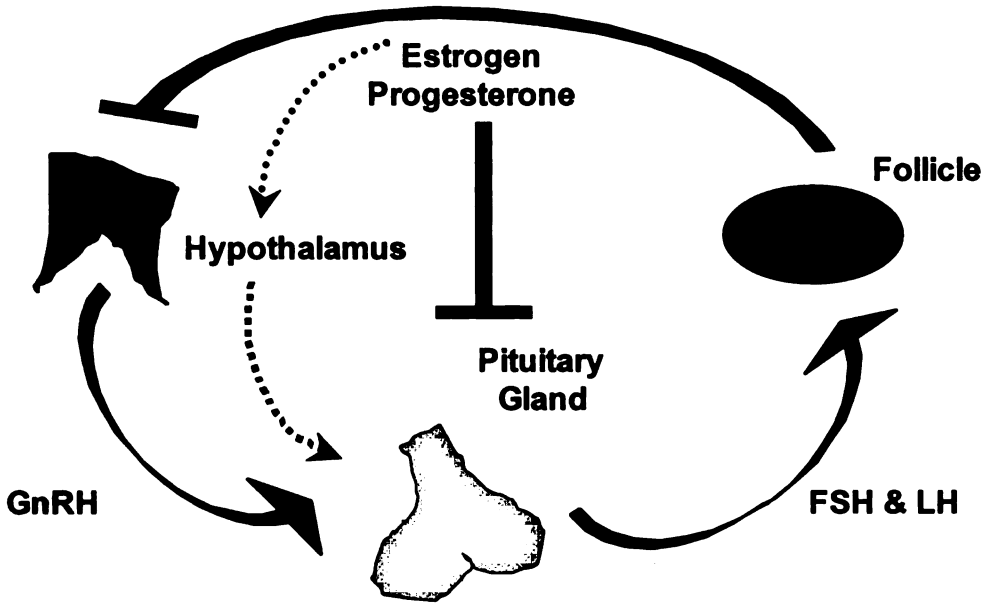

1.3.2 Metabolism

The biosynthesis and metabolism of steroid hormones as depicted in Figure 1.4 begins with the cleavage of cholesterol to form pregnenolone, the common precursor to all steroids, and a six-carbon fragment, isocaproic acid (not shown). This rate-limiting step is controlled by the gonadotropins, FSH and LH from the anterior pituitary. Gonadotropins bind to gonadal tissue and stimulate P450scc activity, stimulating cAMP and PKA mediated pathways that activate overall production of sex hormones. The biochemical pathways are similar in the ovaries, testis and adrenal glands.

Figure 1.4 Major pathways in steroid biosynthesis and metabolism.

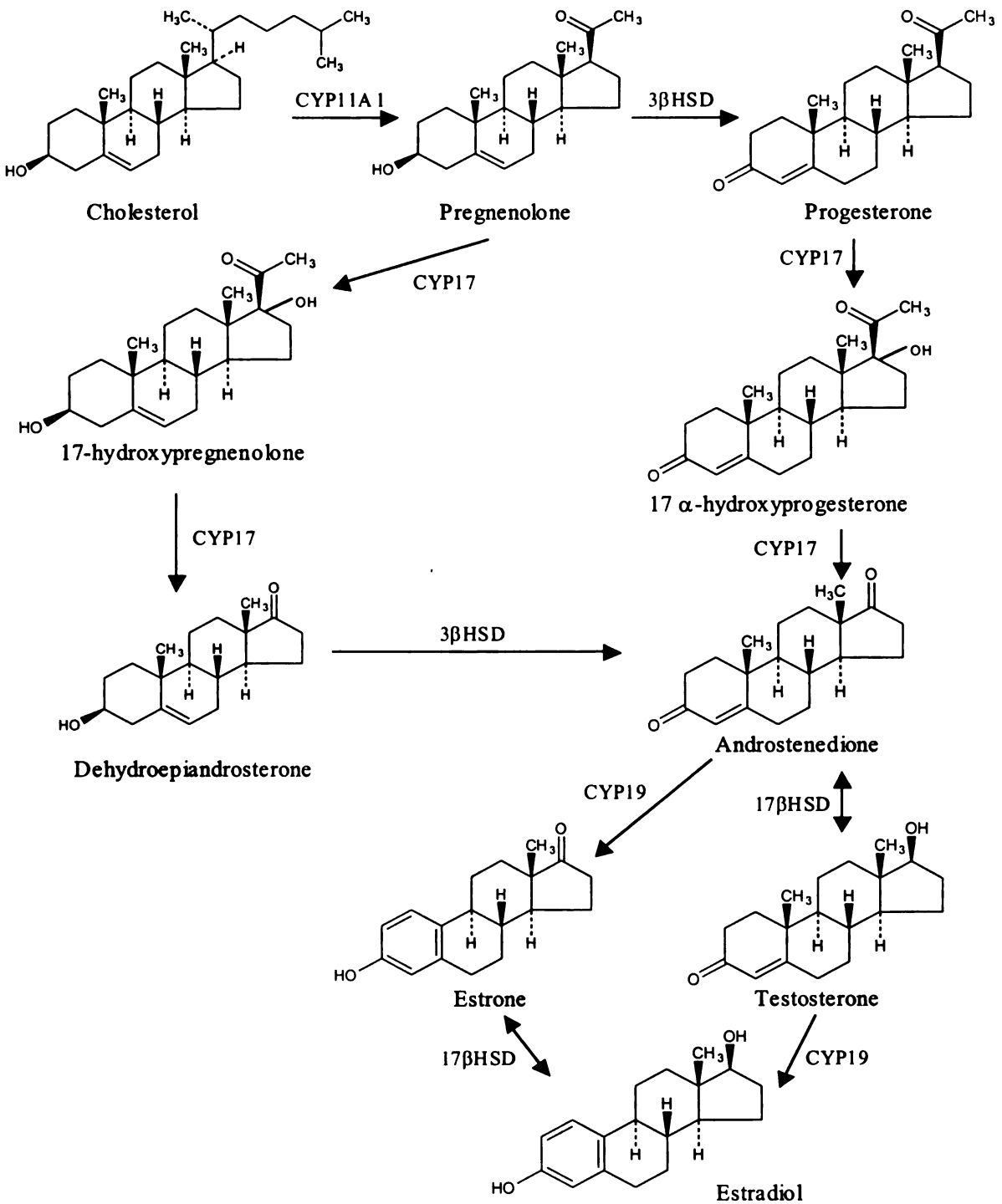

In the ovaries, pregnenolone is converted either to 17-hydroxy pregnenolone by CYP17 (17 α-hydroxylase) or progesterone by 3 β–hydroxy steroid dehydrogenase (3 β–HSD) (Figure 1.4). Alternatively, pregnenolone can be metabolized to 11-deoxycorticosterone, which is then converted to the mineralocorticoid, aldosterone (not shown). Progesterone is secreted in large amounts during the luteal phase of the menstrual cycle, following ovulation. It is a substrate for the enzyme 17 α-hydroxylase, which converts it to 17-hydroxy progesterone (Figure 1.4). Testes and ovaries both contain an additional enzyme, a 17 β-hydroxysteroid dehydrogenase that enables androgens to ultimately be converted into testosterone. Androstenedione is further metabolized by an aromatase enzyme (CYP19) into estrone and by 17 β -hydroxy steroid dehydrogenase into testosterone. Estradiol, the most active and abundant estrogen is synthesized from the androgen, testosterone through the aromatase enzyme (CYP19). Estrone is synthesized in a similar mechanism by the same enzyme from androstenedione (82) (Figure 1.4).

1.3.3 Estrogens

The predominant ovarian steroids in women are estrogens and progestins. The major and most potent estrogen produced by women is estradiol (estradiol-17 β) (Figure 1.5). It is produced by the ovary from granulosa cells, synthesized from androgens by P450 aromatase. Estradiol is converted to estrone in the ovaries by 17 β-hydroxysteroid dehydrogenase, which is then further metabolized in the liver to its 16 α-hydroxyestrone conjugated derivative and subsequently excreted in the bile (Figure 1.5). Another route is for estrone to be converted to 2- or 4-hydroxyestrone. The metabolite of estrone, 16 α-

hydroxyestrone, is the precursor for estriol, a less potent estrogen that is also known as the "pregnancy hormone" and is produced in the liver. Of the three main estrogens, estrone is the least potent and is found to be the most prevalent estrogen found in postmenopausal women. It is a produced primarily from peripheral and adipose tissue.

Figure 1.5 Metabolic pathway of estrogens.

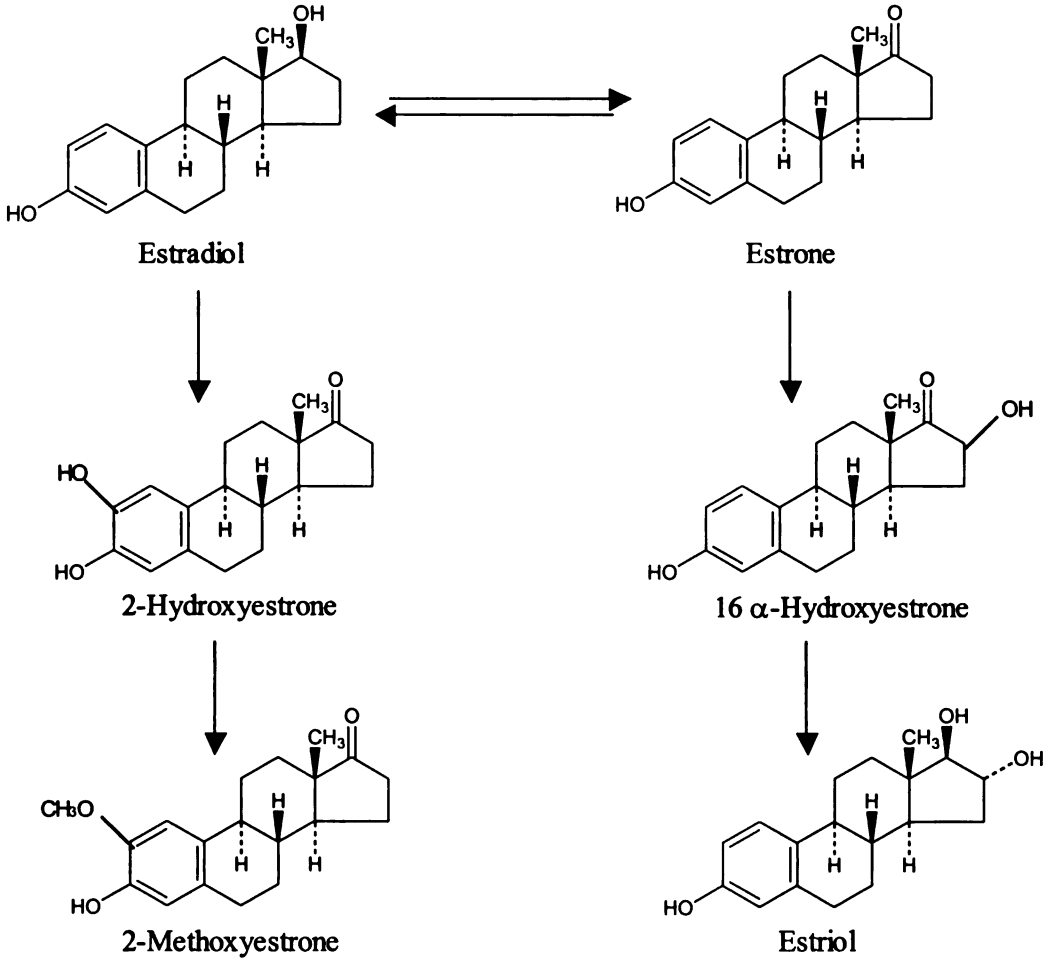

Because significant amounts of estrogens and their active metabolites are excreted in the bile, they can be reabsorbed from the intestine and the resulting enterohepatic circulation ensures that orally administered estrogens will have a high ratio of hepatic to peripheral effect (82).

All steroid hormones exert their action by passing through the plasma membrane and binding to intracellular receptors. The actual biologic effects of the steroids are mediated by their specific hormone receptors (Figure 1.6). Plasma estradiol also acts in the same way, entering the cell by diffusion where it is then transported to the nucleus to be bound to its appropriate receptors. Estrogen receptors found as two isoforms, α or β, are bound to several different heat shock (hsp 90, hsp 70, hsp 56) or chaperone proteins in a multimeric complex. It is thought that this binding stabilizes the estrogen receptor's basal conformation. When estrogens bind to their receptor, there is a conformational change that causes dissociation of the receptor from its heat shock proteins, and exposure of a nuclear translocation signal previously "hidden" within the receptor structure (Figure 1.6). This signal initiates transport of the receptor-hormone ligand complex to the nucleus, where it binds as a homodimer (αα or ββ) or heterodimer (αβ) to its respective hormone response element (HRE). The HRE consists of a consensus recognition sequence in the nuclear DNA, which is bound by a specific DNA-binding region on the receptor. The canonical recognition sequence for estrogen (ERE) is as follows: (5')AGGTCA-NNN-TGACCT(3').

Figure 1.6 Structural schematic representation of steroid receptors. Adapted from Gardner et al. (82).

- ***NH_2-terminal:*** designated as ligand-independent transactivation (AF-1).
- ***DBD (DNA-binding domain):*** responsible for receptor dimerization.
- ***LBD (Ligand-binding domain):*** responsible for hetero- and homo-dimerization, steroid-ligand binding, nuclear translocation and association with heat shock proteins (AF-2).

The "N" denotes an A, G, C or T nucleotide. For the other major classes of nuclear hormone receptors, which include glucocorticoid, mineralocorticoid, progesterone and androgen, the response element (HRE) sequence is (5')AGAACA-NNN-TGTTCT(3'). Subsequent binding attracts core transcription factors and co-activators or co-repressors that function to drive or inhibit transcriptional activity (82).

Developmentally, estrogens are key factors in the maturation of female-specific organs such as the uterine muscle, endometrial lining, vagina and breast ductules. This occurs by stimulating synthesis of enzymes responsible for cellular propagation and growth. Estrogens are also thought to play an important role in intestinal absorption by reducing the motility of the bowel. In the liver, estrogens can increase synthesis of binding or hormone-transport proteins (82).

1.3.4 Progestins

Progesterone is the major physiologic progestin in humans, as it serves as the precursor to estrogens, androgens and adrenocortical steroids. A known P-gp inhibitor, progesterone has been shown to inhibit the efflux transport of P-gp substrates such as cyclosporine across intestinal cells (83). Known to have a short half-life of five minutes, progesterone is rapidly converted into 20 α-hydroxyprogesterone and then to pregnanediol (Figure 1.7). Pregnanediol is then conjugated with glucuronide in the liver, which is ultimately

Figure 1.7 Metabolic pathway for progesterone.

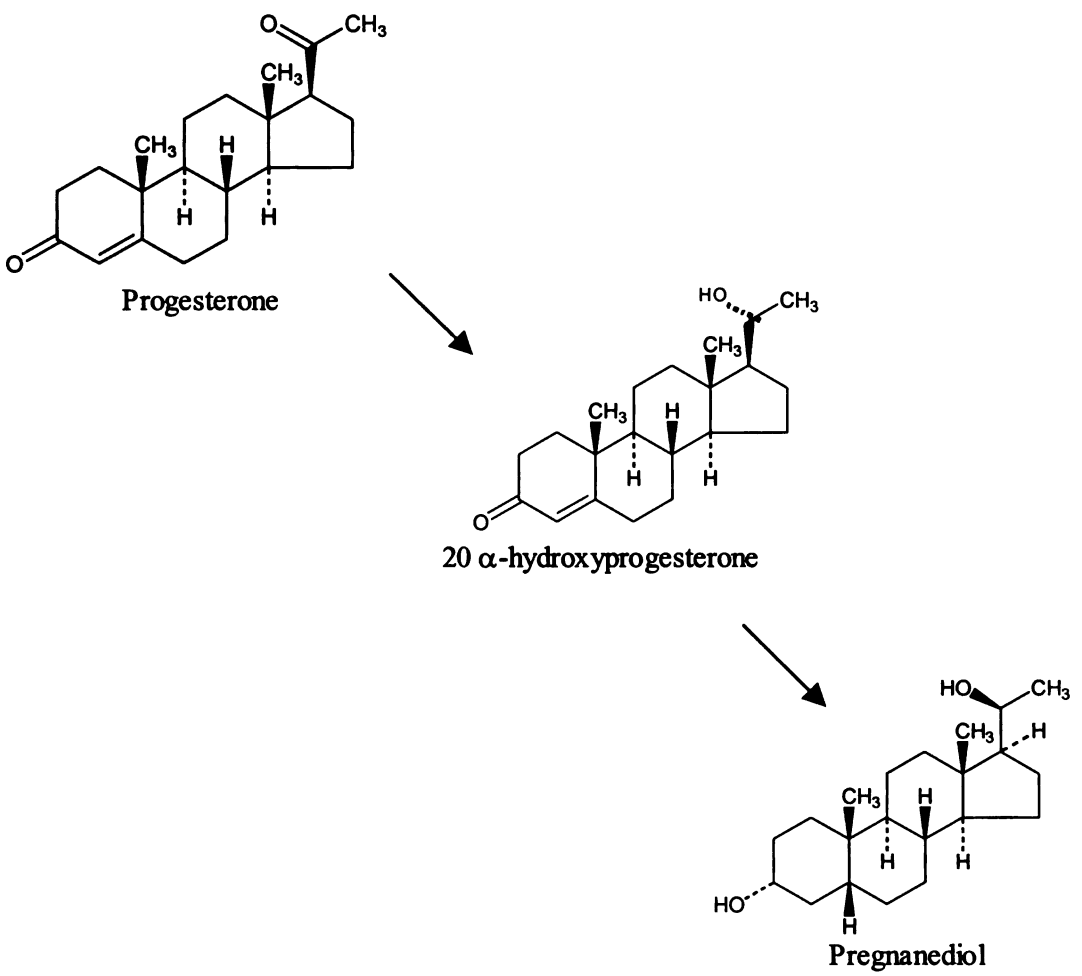

excreted in the urine. Similar to estrogens, progesterone also enters the cell and binds to its progesterone receptors (PR-A and PR-B), that are found in both cytoplasm and nucleus. These receptors form homo- and heterodimers, before binding as a ligand-receptor complex to a DNA response element in target genes, thereby regulating target gene expression (84). The expression of the two forms of the same progesterone receptor gene is cell-type specific. Furthermore, the A receptor is a truncated version of the B receptor. The specificity of a response following transcriptional activation is dependent upon several factors: the volume of a specific type of receptor population within a particular cell type and cell-specific transcription factors (82). Progesterone is secreted mainly from the corpus luteum during the second half of the menstrual cycle, the luteal phase. Synthesis and secretion is stimulated by LH, which is mediated by a membrane-bound receptor linked to a G-protein coupled signal transduction pathway that stimulates adenylyl cyclase and increases the synthesis of cyclic AMP (85). In plasma, progesterone is primarily bound to albumin and corticosteroid binding globulin (CBG).

Progestins have physiologic developmental effects on the breasts and endometrium. It is also a critical hormone in maintaining pregnancy following implantation by sustaining endometrial differentiation. In mammalian systems, progestins enhance differentiation and oppose estrogenic actions of cellular proliferation. The antagonizing characteristic may be mediated by causing a decrease in estrogen receptor synthesis and increases in estrogen metabolism. However, there are many instances in which progestins and estrogens work synergistically to bring about proliferative effects such as in the acini of the mammary gland (80). Furthermore, estradiol stimulates expression of the

progesterone receptor, which is then stimulated by progesterone. Interestingly, it was demonstrated *in vivo* that the combination of 17β-estradiol and progesterone was necessary in order to induce *mdr1* expression in the secretory epithelium of murine uterus (86).

1.3.5 Synthetic steroids

There are a significant number of synthetic estrogens and progestins that have been developed for oral, parenteral, transdermal or topical administration due to extensive first-pass hepatic metabolism of endogenous β-estradiol and progesterone. These high-dose oral micronized preparations of synthetic estrogens and progestins are one of the most commonly prescribed class of drugs in the U.S. They are prescribed for oral contraceptive action and to a lesser extent, hormone replacement therapy. After becoming globally available for use in the mid-twentieth century, hormone contraceptives have transformed lifestyles for billions and radically reformed and improved planned parenthood. Furthermore, it was realized that there were substantial health benefits, aside from the dose-dependent side effects, which were quickly adjusted to prevent unnecessary overdosing. More recent studies have investigated the health benefit to risk ratio, particularly for estrogens and progestins used in hormone replacement therapy for postmenopausal women. Conclusive results are still yet to be determined.

The chemical alterations on the natural steroid hormones play a significant role in increasing the oral efficacy by decreasing the rate of metabolism and clearance,

prolonging half-life and increasing overall blood concentrations. Some synthetic estrogens (see Figure 1.8) that are commonly used include ethynyl estradiol, mestranol and quinestrol. The ethynyl substitution in the C17 position of ethynyl estradiol serves to inhibit first-pass hepatic metabolism. Quinestrol is a long-acting oral preparation that is stored in body fat and released slowly over a period of several days, eventually converted into ethynyl estradiol. A variety of nonsteroidal synthetic estrogens have also been developed for clinical use and include diethylstilbestrol, hexestrol, chlorotrianisene and methallenestril. Estradiol and its naturally occurring metabolites are highly bound to sex-hormone binding globulin (SHBG) and to a lesser extent to albumin, whereas a synthetic estrogen such as ethynyl estradiol is more highly bound to serum albumin.

Progestins are used in combination with various estrogens for contraception, hormone replacement therapy, ovarian suppression, dysmenorrhea, hirsutism and uterine bleeding, to name a few indications. Synthetic progestins (see Figure 1.8) include medroxyprogesterone acetate (MPA), norethindrone, noregestrel and norgestimate. The last three of these progestin analogs belong to a class of compounds known as 19-nor compounds, possessing an ethynyl substitution at the C17 position. These progestin derivatives have significantly longer half-lives and reduced hepatic first-pass metabolism. The mechanism of action for the combinations of estrogens and progestins used for contraception is mainly through inhibition of pituitary function, which in turn inhibits ovulation (82).

Figure 1.8 Structures for various synthetic estrogen and progestin derivatives.

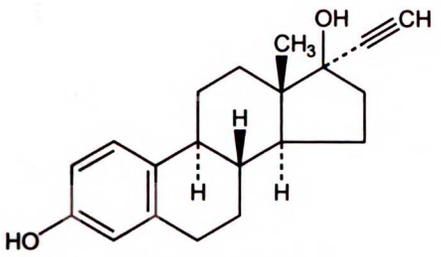

Ethynyl Estradiol

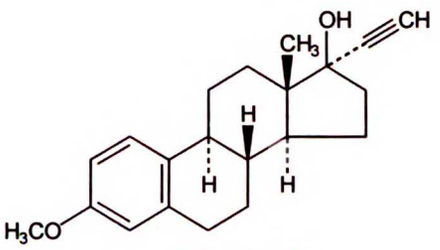

Mestranol

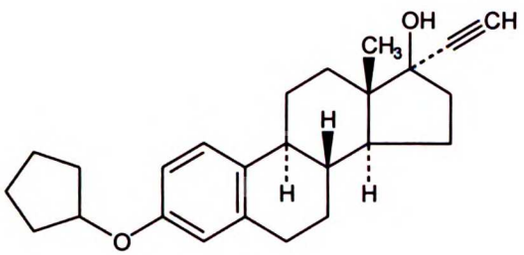

Quinestrol

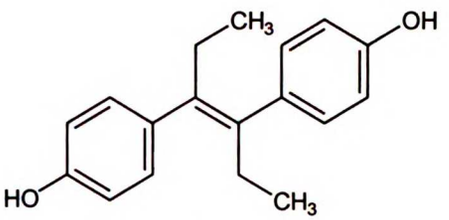

Diethylstilbestrol

Synthetic Estrogens

Synthetic Progestins

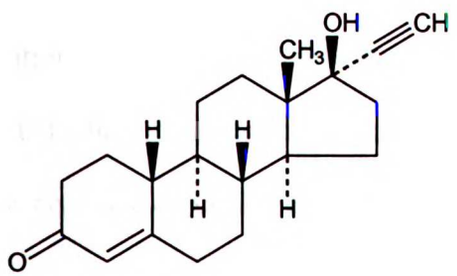

Norethindrone

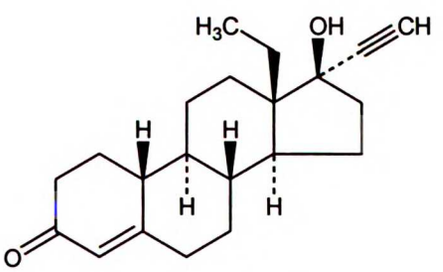

Norgestrel

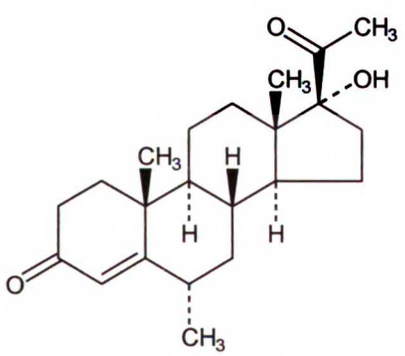

Medroxyprogesterone

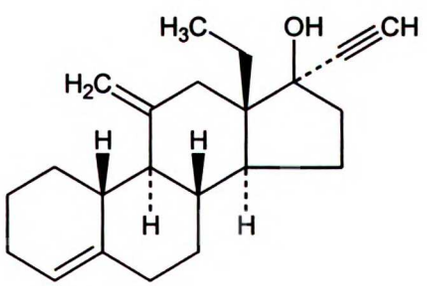

Desogestrel

1.4 Women's Health

1.4.1 Ovulatory cycle

Also known as the menstrual cycle, the ovulatory cycle is an intricate cycling of changes in the female reproductive system. The hypothalamus, anterior pituitary and ovaries interact with each other via inhibition, release and stimulation of sex-steroid hormones for the end goal of ovulation. This cycling occurs in three different phases over a period of, in general, 28-30 days (Figure 1.9). During this time, the ovary regulates the synthesis and secretion of sex-steroids as well as the eventual release of the ovum. For most women, the beginning of menstruation (or menarche) occurs soon after a pubertal and the adrenarche stages between ages 10-16, in which adrenal androgen synthesis commences. During the time of puberty, FSH and LH levels rise. However, FSH levels exceed LH levels due to the immature development of gonadotropin negative and inhibin feedback regulation. Consequently, unregulated gonadotropin serum levels reach those similar to a castrated adult, resulting in well-known pubertal qualities. The reproductive years that follow continue on until menopause is reached at an average age of 50.

The menstrual cycle is tightly controlled by a neuroendocrine cascade involving the hypothalamus, pituitary and ovaries. Gonadotropin-releasing hormone (GnRH) is released like clockwork at hourly intervals, regulated by an inherent pulsatility of the GnRH neuron. GnRH then stimulates intermittent release of LH and FSH from the anterior pituitary, completely dependent upon the frequency and amplitude of the pulsatile release of GnRH by the hypothalamic neuronal "clock." The GnRH pulse frequency is greatest during the follicular phase compared to the second-half of the cycle,

reflective of the inhibitory effects of progesterone on the pulse generator. The by-product is a "pulse"-like plasma profile of LH and FSH. These gonadotropins exert their action by stimulating estrogen and progestin secretion in the ovaries, which in turn exert feedback controls in order to maintain obligatory concentrations during the course of the cycle (80).

The first phase of the cycle starts at day one (see Figure 1.9), which consists of a three to seven-day period of menstruation. This first phase continues on to be characterized by the

Figure 1.9 Menstrual cycle phase and ovarian steroid hormone levels.

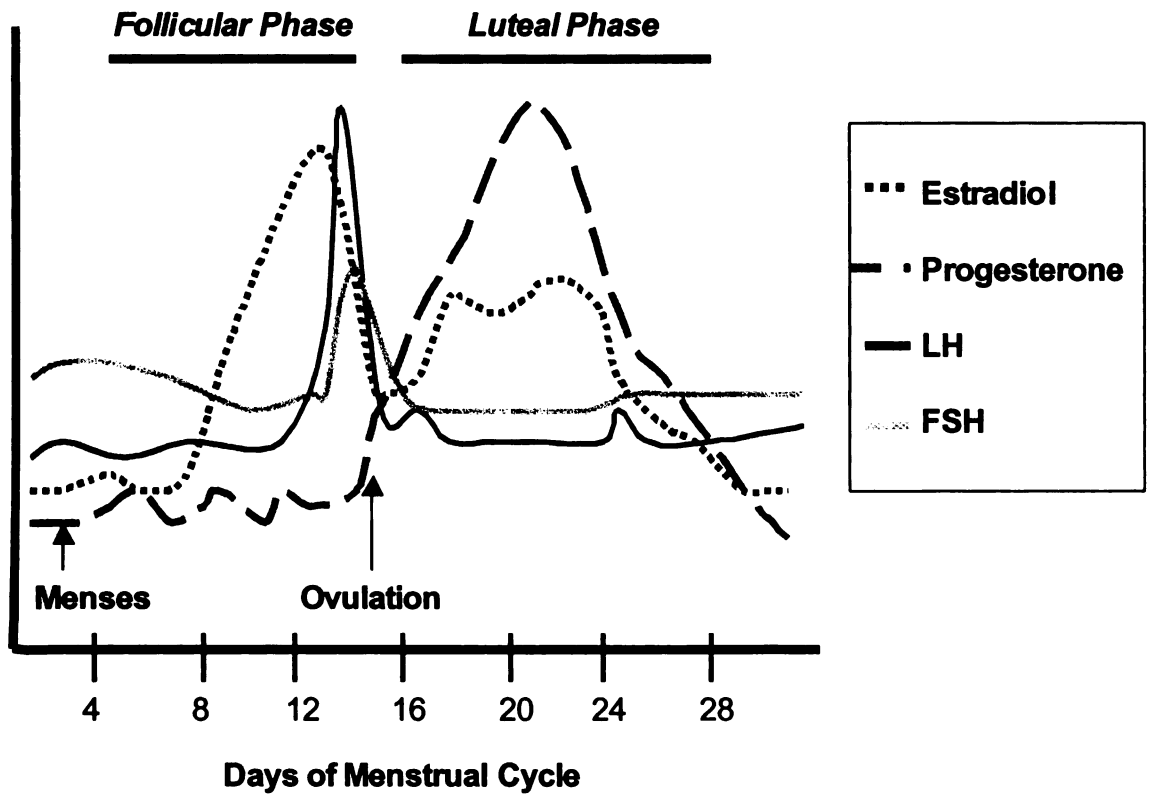

growth and development of 6-12 primary follicles, hence known as the follicular or proliferative phase. Prior to onset of menses, FSH and LH levels begin to rise. Follicular development is dependent upon the continuous rise in FSH levels and the estrogen produced, stimulated by FSH early during the cycle. Simultaneously, increasing luteinizing hormone (LH) levels are also responsible for androgen synthesis, which is converted to estrogen. Soon after reaching peak levels during the midcycle surge, FSH gradually declines until reaching its lowest levels during the second half of the first cycle. This is an effect of rising estrogen levels, which act to suppress FSH. However, as estrogen levels peak pre-ovulation, it exerts positive feedback to the hypothalamus and pituitary, stimulating GnRH release and a surge in both LH and FSH levels during ovulation (approximately mid-cycle; day14), the second phase (81, 82).

During the follicular phase, the primordial follicles are found to grow near the outer cortex of the ovary, along the germinal epithelium. Of these, only one will continue growing to be transformed into a dominant follicle in the developing oocyte. At the time of ovulation, the surge in gonadotropin release causes the dominant, antral follicle to rupture and release the ovum, or egg, into one of the fallopian tubes. This ruptured follicle becomes the corpus luteum, marking the beginning of the third phase- the luteal or secretory phase (81).

During the luteal phase, the lining of the uterus, the endometrium, continues to thicken from the follicular phase in preparation for implantation of a fertilized egg. The corpus luteum, composed of granulosa and theca cells that develop into luteal cells, releases

large amounts of progesterone. For this reason, progesterone levels rise and peak mid-cycle, while estrogen serum levels also rise, but reach a plateau. Progesterone acts to suppress the proliferative effects of estrogens on the endometrium and instead, stimulates differentiation. Progesterone is the principal steroid hormone necessary to prepare the endometrium for implantation and maintain pregnancy. Progesterone is also known to have inhibitory effects on the pulsatile release of LH. Because of this, during the luteal phase, the hypothalamic GnRH pulse generator produces relatively less frequent pulses of larger amplitude as compared to the follicular phase. If the egg is not fertilized by a sperm, the corpus luteum degenerates (luteolysis), steroid synthesis declines and the endometrium disintegrates and sheds via menstruation. However, if conception occurs, the fertilized egg enters the uterus, latches onto the lining, and commences growth (80, 81).

1.4.2 Menopause

Menopause was originally thought to be caused by primary ovarian deficiency due to a depletion of functional primordial follicles. This is still the most accepted theory. However, the observation of some normal oocytes present in postmenopausal ovaries suggested otherwise. Presently, it is generally believed that menopause is brought about by neuroendocrine changes such as in the critical pulsatile release of GnRH due to increasing age. The lack of follicular growth in response to LH and FSH secretion causes estrogen and progesterone levels to drop. During this phase in life, women are no longer able to produce offspring, characterized by the end of menstrual bleeding.

Production of estrogens and progestins begin to decline possibly even more than two years before menopause and continue to decline for several years afterward. Serum estrogen levels in menopausal women constitute approximately one-sixth the mean levels of premenopausal women and progesterone levels drop to about one-third of that found in younger, cycling women (81). The primary source of steroid hormones reverts from the ovary to androgens derived from the adrenal gland and peripheral tissues. Estrone is the predominant circulating estrogen in menopausal women, synthesized in adipose tissue. Physiological changes associated with menopause include vaginal dryness and thinning of the epithelium, osteoporosis, hot flashes from periodic increases in core temperature and a higher incidence and risk for cardiovascular disease. Emotional changes may be manifest as anxiety, depression and irritability, particularly around the onset of menopause. Management for such symptoms requires careful assessment of the individual patient's symptoms, risks and genetic predispositions for disease, particularly cardiac and breast cancer. Hormone therapy is commonly used for the treatment of menopausal symptoms. Treatment may include estrogen and progestins, individually or combined, depending on the therapeutic target and patient needs.

1.5 HIV

1.5.1 Molecular aspects of HIV

Human immunodeficiency virus (HIV) was first identified in 1983 to be the cause of AIDS. It was discovered to be a retrovirus, a member of the lentivirus genus. The clinical manifestations that are characterized by HIV infection are a marked reduction in CD4+ cell counts and the vulnerability to and development of a plethora of infections and

cancers (87). Subsequent work and progress in the research of HIV pathogenesis, replication and interaction with its cellular host in the past three decades have produced several promising points of attack via a myriad of anti-HIV drug therapies.

HIV was originally isolated from the lymph node of a man with persistent lymphadenopathy syndrome (LAS). Following several years of investigation and the discovery of HIV-1, a separate subtype HIV-2 was identified in West Africa (88). Both viruses when viewed by electron microscopy have characteristics similar to lentivirus, with the capsid of the virus containing two identical strands of RNA, a viral RNA-dependent DNA polymerase Pol (RT) and the nucleocapsid proteins, p9 and p6.

1.5.2 Structure, expression and mechanism

The genomic size of HIV (Figure 1.10) is approximately 9.8 kb in length, containing nine different genes encoding 15 proteins. The full length mRNA transcript is translated into Gag, Pol and Env proteins. The Gag precursor p55, cleaves into 4 smaller proteins: p24, p17, p9 and p6. The Pol precursor protein is also proteolytically separated into the RT, protease and integrase viral enzymes. The envelope (Env) protein is processed into the proteins p120 (surface protein) and p41, the envelope transmembrane protein. In order for HIV to effectively infect a target cell, it first enters the cell by fusing its viral envelope with host cell membrane via interaction of specific cell surface receptors.

Figure 1.10 HIV virion structure. Adapted from Levy *et al.* (89) and Leis *et al.* (90).

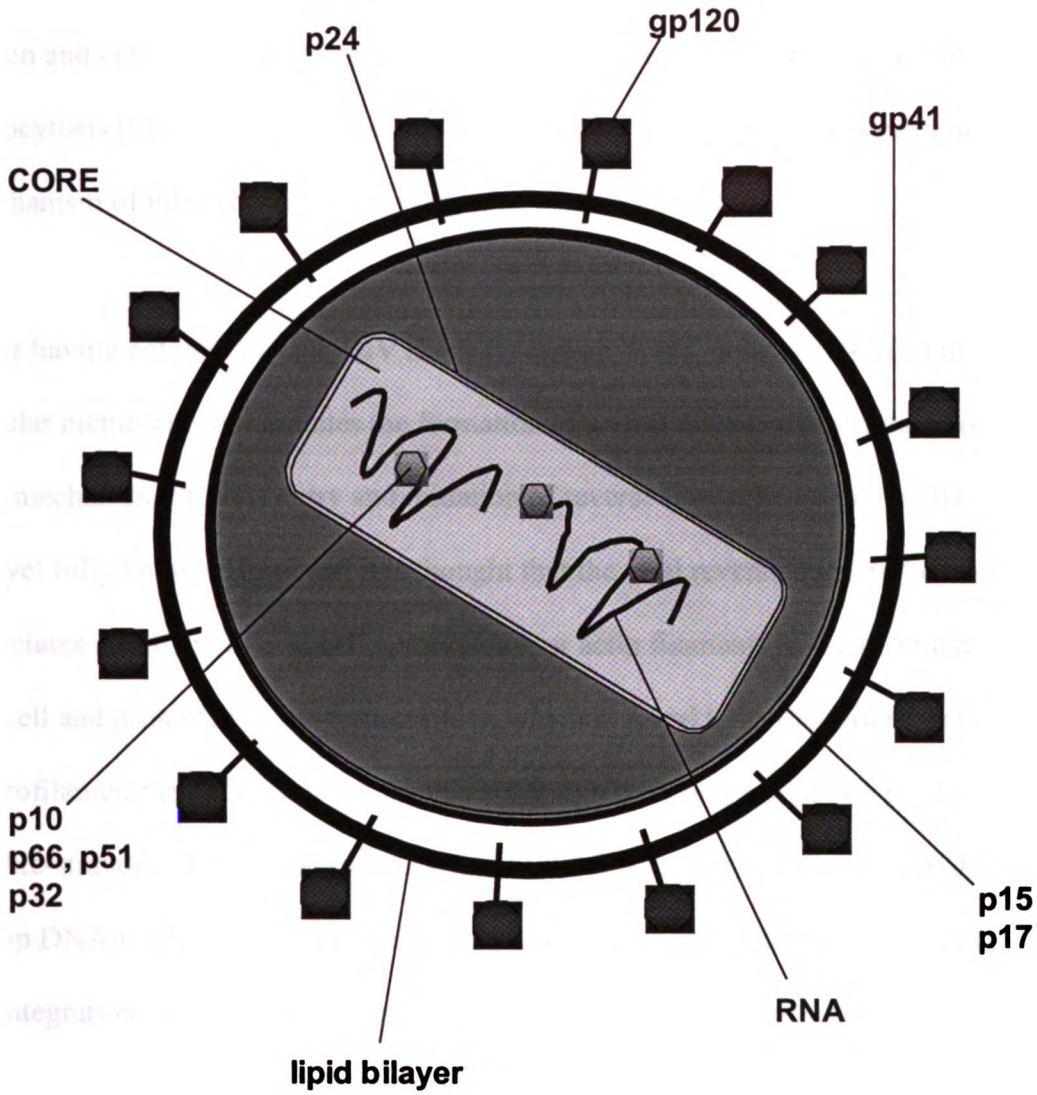

The two primary viral envelope proteins as mentioned earlier are gp120 and gp41, in which gp120 is exposed on the surface and is associated with gp41, imbedded within the viral lipid membrane. The inevitable interaction between the viral surface protein, gp120

and the CD4 receptor on the surface of target cells causes a conformational change to facilitate binding of the virion to nearby chemokine receptors on the target cell. The cascade of conformational changes and binding to various factors allow for optimal fusion and entry of virus. It has also been shown that HIV virions can also enter a cell by endocytosis (91). Furthermore, cell-to-cell transfer of HIV may be a more rapid mechanism of infection than direct infection by free virus (89).

After having entered the cell, HIV sheds its capsid "coat," detaches itself from the cellular membrane and initiates the formation of a viral reverse transcriptase complex. The mechanism of virus entry and initiation of reverse transcription in the infected cell is not yet fully known. However, it is thought that the viral reverse transcriptase complex associates rapidly with host cell cytoskeleton or actin filaments to establish itself within the cell and promote reverse transcriptase, which is found to be dependent on intact actin microfilaments (92). Viral DNA synthesis through reverse transcription produces a double-stranded cDNA, reverse transcriptase, integrase, Vpr, matrix and a high mobility group DNA-binding cellular protein HMGI. All of these components make up the HIV preintegration complex (PIC) (93). The PIC utilizes microtubular structures to direct itself toward the nucleus (94). The precise mechanism of viral entry into the nucleus is still being investigated. Once inside the nucleus, PIC initiates integration of its viral genome, double-stranded DNA, into the host chromosome, mediated by viral protein integrase. Studies show that viral integration can lead to either latent or active replication of HIV and is controlled at the level of transcriptional elongation (95).

The details of viral transcriptional regulation once integrated into host genome, are still under investigation. Viral transcription requires expression of a combination of both host cellular and viral genes. For HIV, there are two classes of genes: the early viral genes *tat, rev* and *nef*, which regulate expression and the late genes: *gag, pol, env, vpr, vpu* and *vif*. Each of these polypeptide proteins have important structural, replicative and regulatory roles (96, 97). Initial activation of the LTR by transcription factors leads to the production of the above-mentioned short and some complete transcripts (98). The complete transcripts allow the Tat protein to be produced, which causes the level of viral RNA transcription to be enhanced. The Tat protein is key for not only activating, but also maintaining a high level of viral transcription.

HIV is a polytropic virus that can infect many cell types. CD4+ lymphocytes are known to carry and produce the highest levels of the virus. Infected macrophages act as reservoirs of HIV, while more highly differentiated macrophages in lymphoid tissues are thought to be the first site of viral replication. In the brain, HIV infects macrophages and microglia with the highest frequency, but is also known to infect astrocytes, oligodendrocytes and capillary endothelial cells to varying degrees (89). In peripheral blood, most lymphocytes that are infected by HIV remain in the latent state, which at some unknown point can be activated to release active virus.

1.5.3 Mechanisms of antiretroviral drug activity

Although much progress has been made in understanding the pathogenesis of HIV infection, there are still many questions that remain unanswered with regard to HIV

interactions within the host. Better understanding of the mechanisms of HIV infection and how our body's defense system reacts to HIV, will be most useful in the advancement of detecting and effectively treating HIV in individuals.

Currently, there are many therapeutic approaches to control HIV infection. There are three distinct classes of drugs: nucleoside reverse transcriptase inhibitors (NRTIs), non-nucleoside reverse transcriptase inhibitors (NNRTIs) and protease inhibitors (PIs). Other classes of anti-HIV drugs are in development, but not yet available. Effective drug therapy "cocktails" include a combination of one or more drugs from all three classes. The NRTIs work by mimicking nucleosides that assist in the replication of viral DNA in the host cell. Once they are taken up in the cell by reverse transcriptase, they impair the function of replication. There are six nucleoside RT inhibitors presently available- AZT, ddI, ddC, d4T, 3TC and ABC. NNRTIs include nevirapine, delavirdine and efavirenz, which are given usually in combination with other agents as they are not as effective given alone.

There are currently six commonly used protease inhibitors, which include nelfinavir, saquinavir, ritonavir, indinavir, amprenavir and a combination of lopinavir and ritonavir (LPV; Kaletra®). HIV protease inhibitors are reversible competitive inhibitors of HIV protease, enzymes responsible for cleaving the polyprotein Gag-Pol into proteins that form the capsid (p19), nucleocapsid (p24) for immature virions, reverse transcriptase, proteases and integrase, which facilitates viral genome integration into host DNA. Their mechanism of action is to bind HIV proteases and inhibit proteolytic cleavage of viral

DNA and RNA into the functional proteins that are used to produce new virion particles. PIs are a crucial element to almost all anti-HIV drug regimens.

Nelfinavir mesylate is a nonpeptidic HIV protease inhibitor used in conjunction with other anti-retroviral agents. It is well-absorbed following oral administration, with a peak plasma concentration attained withing 2 to 4 hours at a dose of 500-800 mg. Animal studies show extensive tissue distribution after oral administration and it is ~98% plasma protein bound. Plasma elimination half-life is 3.5 to 5 hours and nelfinavir is excreted primarily in the feces, both as parent drug and metabolites. The chief site of nelfinavir metabolism occurs in the liver. Although its metabolism is mediated by several CYP450 isoenzymes, including CYP3A4, nelfinavir is metabolized principally by CYP2C19, which is predominantly expressed in the liver compared to the gastrointestinal tract. As depicted in Figure 1.11, the bulk of nelfinavir is metabolized into its active hydroxy-*t*-butylamide metabolite also known as M8 (99, 100), and a smaller portion to its inactive 3'-methoxy-4'-hydroxynelfinavir, M1 metabolite. The M8 metabolite, like nelfinavir, is largely bound to plasma proteins and also demonstrates similar *in vitro* anti-viral activities (100).

Figure 1.11 Chemical structure of HIV protease inhibitor, nelfinavir, and metabolites. The bold arrow indicates the major pathway to active metabolite, M8.

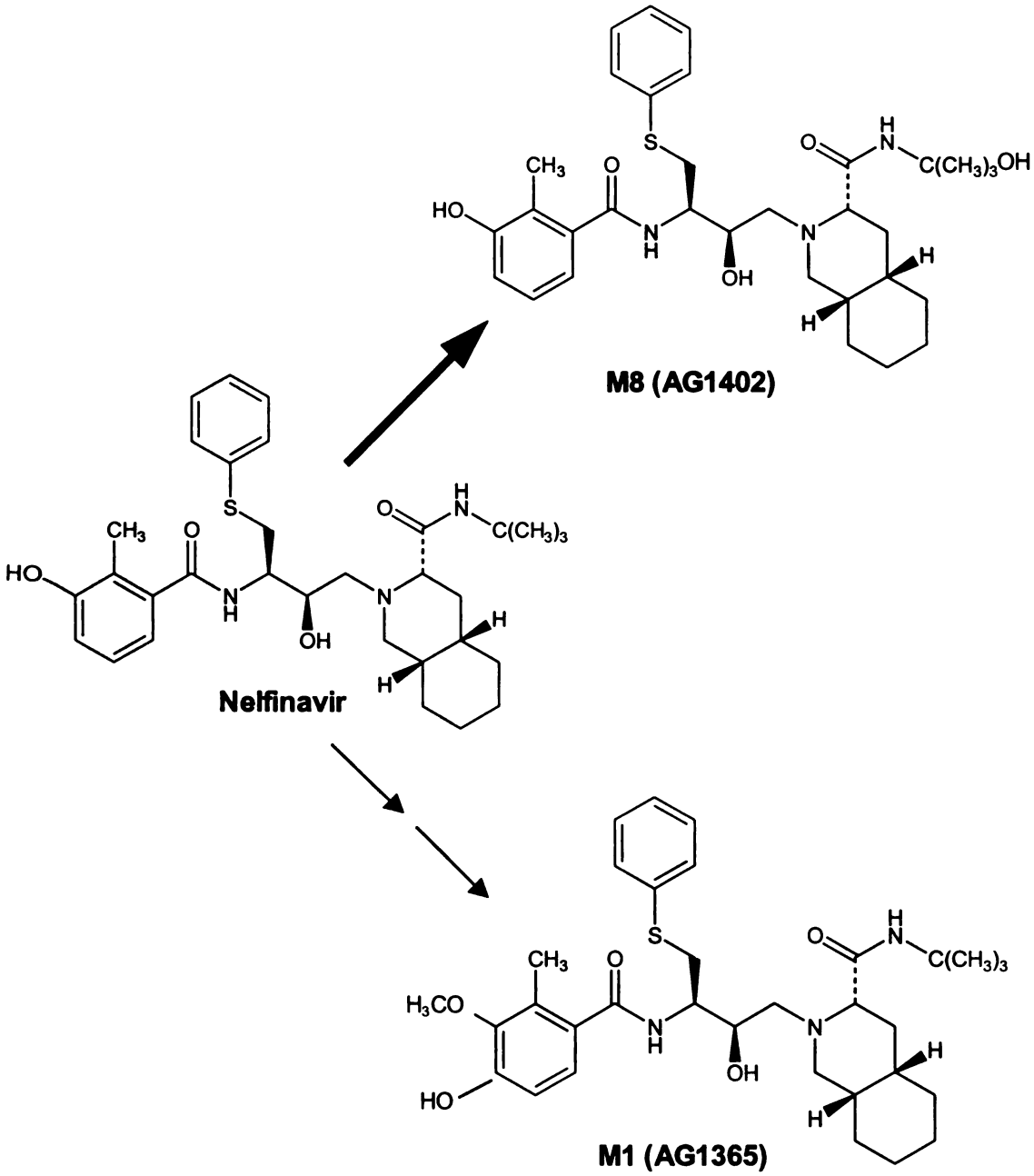

1.5.4 HIV in women

In the last quarter of the 20th century, a breakthrough occurred in women's health. Following several milestones, it was ensured that the subpopulations of women and members of minorities would no longer be excluded from human clinical research. However, even in 2001, it was concluded that there was still a dearth of research investigating the effect of sex differences on drug safety and efficacy. Throughout the rest of the world, there continue to exist gender inequalities in social, economic and power status. Because of this, women are given dosages of drugs that were originally tested predominantly in males without any adjustments based on their obvious physiological differences.

Sexually-transmitted diseases such as HIV are widespread and rapidly rising throughout countries in Africa and South East Asia. Gender and social inequalities contribute to the HIV epidemic where prostitution runs rampant and women are particularly susceptible and vulnerable to infection. One reason for higher risk of infection in women may be due to substantially higher mucosal exposure to seminal fluids. Obvious sex differences in pathology calls out for clinical management tailored to women's particular symptomatology, disease progression and other related illnesses based on issues such as hormonal changes during the menstrual cycle, pregnancy and menopause among others. Currently, there are 12-13 African women infected for every 10 African men. Additionally, half-a-million infections in children were passed on to them from their mothers. In the U.S., HIV was the 5th leading cause of death for U.S. women (ages 25-44) and among black women aged 25-44, HIV infection was the third leading cause of death

(101, 102). The epidemic has increased most dramatically among women of color. African-American and Hispanic women together represent less than one-fourth the population of U.S. women, yet they account for almost 80% of U.S. AIDS cases reported among women in 2000 (103). Further research into the relationship between HIV infectivity and P-gp based on ethnically-related SNP genotype may prove to be extremely insightful as it is known that African-Americans, compared to Caucasians are predominantly homozygous wildtype for the *MDR1* C3435T polymorphism.

1.5.5 The P-glycoprotein, HIV and sex-steroid triangle

Many studies have shown that all HIV protease inhibitors currently in use (indinavir, saquinavir, nelfinavir, ritonavir, aprenavir) are transported by P-gp (104-106). P-gp functions to pump these drugs out of cells, decreasing the intracellular therapeutic efficacy. However it has been demonstrated *in vivo* that in *mdr1a* (-/-) knockout mice, plasma concentrations of HIV PIs, such as indinavir, nelfinavir and saquinavir, were elevated 2 to 5-fold after oral administration and brain concentrations were increased 7 to 36-fold after an intravenous administration compared to control mice (107). It was also noted that IV administration of the P-gp inhibitor LY335979 in mice caused a 4-fold, dose-dependent increase of nelfinavir concentration in testes (104). These data demonstrate that P-gp can limit systemic oral bioavailability of these agents as well as penetration into the brain and testis.

P-gp may also largely affect the penetration of protease inhibitors into tissue compartments such as the vagina/endometrium and the central nervous system that could

serve as sanctuary sites for HIV. This raises the possibility that increased P-gp activity due to high sex-steroid hormone circulating levels during the luteal phase may affect the efficacy of HIV-drug therapy. The effect of P-gp on limiting oral bioavailability and tissue distribution of PIs has significant implications for the effectiveness of anti-HIV therapy today. Insufficient therapeutic drug levels resulting in poor penetration into sanctuary sites such as the brain, testis and very possibly the vagina/endometrium, may result in ineffective treatment, continued HIV replication and development of resistance.

Another area of ongoing research involves the dynamic relationship between P-gp and HIV-1 expression and infectivity. It has been suggested that P-gp expression may affect HIV-infectivity. A study reported by Lee *et al.* (108) demonstrated that virus production and infectivity was significantly attenuated when P-gp was overexpressed at the surface of CD4+ cells infected with HIV-1. The overexpression of P-gp did not alter membrane expression or distribution of either the HIV-1 receptor CD4 or the coreceptor CXCR4. Reichelderfer *et al.* (109) investigated the effect of menstrual cycle phase on HIV-1 levels in PBMCs and the genital tract in women. Their studies demonstrated that HIV-1 RNA expression levels in the genital tract were highest during the luteal phase, when estrogen/progestin levels peak. Retrospective studies by the Axiotis *et al.* (110, 111) demonstrated that P-gp was expressed in human secretory and gestational endometrium. A further examination of endometrial P-gp expression via immunohistochemical staining in pre- and postmenopausal women during the menstrual cycle, showed increased P-gp expression during the luteal phase, compared to the follicular phase. These studies led us to hypothesize that increased P-gp expression and function may be regulated by ovarian

hormones, which during the luteal phase may act to limit effective intracellular concentrations of PIs within the vaginal/endometrial tract, a potential sanctuary site for HIV, thereby allowing viral replication and infectivity.

Hence, the relevance of exploring hormonal effects during the menstrual cycle on the pharmacokinetics of P-gp substrate drugs becomes more significant. The involvement of steroid hormones as P-gp substrates as shown in our *in vitro* data, and in the steroidal modulation of P-gp expression, points to a much needed investigation between reproductive hormones and P-gp in order to identify areas of compromised drug efficacy during the menstrual cycle for the optimal health and safety of women.

1.6 Specific Aims

The goal of this research is to determine if female sex-steroid hormones and both their natural and synthetic metabolites can enhance P-gp expression and function. This in turn would lead to alterations in the pharmacokinetic profile of P-gp substrate drugs during hormone fluctuations of the ovulatory cycle in women, based on *MDR1* genotype, ethnicity and HIV status. The specific aims are as follows:

1. Characterize the human LS180 colon cell line that endogenously express P-gp, and determine whether progestins and estrogens modulate P-glycoprotein expression and activity in this cell line.

2. Using MDCK cells, test whether sex-steroid hormones and their metabolites are substrates of P-gp and examine the effects and interaction of sex-steroids on P-gp mediated transport of HIV protease inhibitor, nelfinavir.

3. Conduct a clinical study in Caucasian and African-American pre-menopausal HIV-positive and negative women to determine the effects of sex-steroid hormone changes during the ovulatory cycle on the pharmacokinetics of protease inhibitor and expression and function of P-gp.

CHAPTER II

Hormonal Modulation of P-glycoprotein/MDR1 in vitro [1]

2.1 Objectives

The purpose of the following *in vitro* studies is to determine whether female sex-steroid hormones and their metabolites can modulate P-gp expression and ATPase catalytic activity and to investigate whether steroid hormones can induce *MDR1* transcription at the transcriptional level. We sought to characterize the expression and inducibility of *MDR1* in a female human intestinal cell line that endogenously expresses P-gp to examine the effects of various estrogens and progestins crucial in women's health, serving as a model for absorption of drugs. To do this, we employed the LS180 colorectal (colon) adenocarcinoma cell line, which was originally derived from a Caucasian female. Most recently, Pfrunder *et al.* (112) showed that *MDR1* and CYP3A4 were inducible in LS180 cells by rifampin, a known P-gp inducer, and the levels of hPXR mRNA detected in LS180 were significantly higher than in Caco-2 or TC-7 cells, thus making it a suitable model for *MDR1* induction. We also investigated whether various steroid hormones could transcriptionally activate *MDR1* in LS180 cells transfected with a plasmid reporter vector

[1] This chapter was published in part within a manuscript entitled, "P-glycoprotein (P-gp/*MDR2*) Mediated Efflux of Sex-Steroid Hormones and Modulation of P-gp Expression *In Vitro*." by W.Y. Kim and L.Z. Benet, *Pharm Res* 21:1284-1293 (2004).

containing a 4 kb region of the *MDR1* promoter. Knowing that P-gp ultilizes energy gained from ATP hydrolysis to transport an assortment of structurally unrelated compounds out of cells, we further investigated how steroids affect transporter function by conducting a series of ATPase assays. These studies revealed that hormones could interact with the ATP-binding site, stimulating catalytic ATPase activity, a function critical for transport.

2.2 Introduction

2.2.1 Molecular insights: *MDR1* regulation by steroids

Several key studies have increased our understanding of the influence of hormones on multidrug resistance. Atuvia *et al.* (113) evaluated the regulation of P-gp expression and function in rodent adrenal cells, where mdr1b expression was enhanced by steroid hormones and inhibition of steroid biosynthesis markedly decreased mdr1b mRNA levels. Furthermore, disruption of the mdr1b allele resulted in greater intracellular accumulation of vinblastine and daunomycin. In another study investigating the absorption of steroid hormones in rat intestine, progesterone was found to decrease intestinal absorption of vinblastine, a P-gp substrate (114). We postulate that progesterone may be inducing P-gp activity in the rat intestine and changes in hormone levels may affect the pharmacokinetics of other P-gp substrate drugs.

Of importance to our hypothesis, P-gp expression and function have been found to vary with ovulatory function and phase in women. The highest levels were found during the midluteal phase of the menstrual cycle, when estrogen and progestin levels

peak (111). Studies in rats demonstrate highly increased levels of mdr1-type P-gp RNA in the luminal and glandular epithelia of uterus and placenta during pregnancy (115). In mice, the levels of P-gp expression parallel that of progesterone in the serum, peaking during days 15-17 of gestation, then declining (116). Furthermore, the combination of β-estradiol and progesterone induce *mdr1* in the secretory epithelium of the uterus (86). As P-gp is also found in human placental trophoblasts and in human secretory and gestational endometria (111), these observations suggest possible interactions between P-gp and steroids in humans. Therefore, an *in vitro* investigation of the physiological interaction between the ingested hormone-drug and an *in vitro* cell system was carried out.

In women, the predominant circulating sex-steroids are estrogen and progesterone, produced primarily in the ovaries and placenta. The major estrogens produced by women are estradiol (17 β-estradiol, E_2), estrone (E_1) and estriol (E_3). 17 β-Estradiol is converted to estrone, estriol, their 2-hydroxylated derivatives and conjugated metabolites by the liver and subsequently excreted in the bile. These compounds control a myriad of biochemical reactions, acting as chemical messengers to induce or repress enzyme regulation and protein synthesis. Their mechanism of action is defined by passive intracellular diffusion, binding to intracellular receptors and as dimer complexes, initiating or repressing transcription via interaction with specific nucleotide sequences called hormone response elements (HRE) present in target genes (117).

Hormonal effects on the pharmacokinetics of drugs that are substrates for P-gp have never been evaluated. However Axiotis *et al.* (111) demonstrated, in a retrospective study, that expression, distribution and intracellular localization of P-gp in human endometrium is dependent on the menstrual cycle. In a more recent study, estradiol increased cytoplasmic concentrations of P-gp in ERα-positive MCF7 breast cancer carcinoma cells, which were resistant to doxorubicin cytotoxicity, while ERα-negative, ERβ-positive T47D breast cancer cells were sensitive to doxorubicin cytotoxicity (118). Both ERα and ERβ bind estradiol and initiate transcriptional activation, mediated by the estrogen-response element (ERE) (119, 120). Estrogen receptors are also capable of modulating transcription by binding to AP1 and Sp1 responsive DNA sequences(121, 122). Both AP1 and Sp1 *cis*-elements are located in the *MDR1* promoter region (123). Paech *et al.* (121) showed that ERα usually activates transcription at AP1 sites, while ERβ inhibits transcription at these sites. This suggests that in ERα-positive MCF-7 cells, estradiol stimulates P-gp expression. This increased P-gp expression may thus explain the observation of increased multidrug resistance in ERα-positive MCF7 cells.

As orally administered synthetic derivatives of estrogens and progestins are among the most widely prescribed drugs for women, the studies here aim to investigate the effects of both natural and synthetic derivatives of estradiol and progesterone on P-gp expression *in vitro*.

2.2.2 P-gp catalytic ATPase activity

P-gp transport activity utilizes the energy derived from ATP hydrolysis to drive the transport of cytotoxic compounds against a concentration gradient. It also appears that in

order for transport to occur, drug must somehow physically bind to the protein to elicit an effect on the ATP catalytic pathway. It is known that there are specific drug binding sites on transmembrane domains 5, 6 and 11, 12 and that some binding sites interact with transport substrates as well as non-transported modulators (124-126). There is also direct evidence of communication between the drug-binding sites and the ATP catalytic domains, shown by allosteric alterations in the fluorescence of a cysteine residue probe within the Walker A motif of the nucleotide-binding domain (127-129).

Compounds including verapamil, vinblastine and rhodamine 123 are known to bind to P-gp and a few are also known to be substrates (130, 131). This suggests that compounds that can bind to P-gp and stimulate P-gp ATPase catalytic activity are not necessarily transported by P-gp. Another prime example is progesterone, which is not a P-gp substrate, but is instead a potent inhibitor (27, 47, 132-134). Our studies show that it can stimulate P-gp ATPase activity in a concentration-dependent manner. This potent inhibition strongly suggests a direct physical interaction between P-gp and drug via a mechanism that is yet to be determined.

2.3 Materials and Methods

2.3.1 Hormones and materials

17 β-Estradiol, ethynyl estradiol (EE), estrone, estriol, progesterone, norethindrone, norgestrel, and 6-α methyl-hydroxy progesterone acetate (6α-MPA) were all purchased from Sigma Chemical Company (St. Louis, MO). The cell lines used for induction studies were all purchased from ATCC and kept frozen in liquid nitrogen at the UCSF

cell culture facility (UCSF-CCF; San Francisco, CA). The following cell lines were used: LS180, HepG2, RL95-2, HCC1500 and TM3. Growth and maintenance of these cells utilized the following materials, which were all purchased from the UCSF-CCF: PBS Ca^{2+}/Mg^{2+} free, PBS with Ca^{2+}/Mg^{2+}, DME-H21 (Dulbecco's Modified Eagle's Medium containing 8.5 g/L glucose, 25 mM Hepes, 2.2 g/L $NaHCO_3$ and non-essential amino acids), RPMI 1640, DMEM EBSS, HAM-F12(K), trypsin (0.25, 0.5%) Hepes, fetal bovine serum (FBS, Hyclone), horse serum, insulin, penicillin, streptomycin, Na-pyruvate, non-essential amino acids (NEAA) and glutamine. The following materials were purchased separately for cell culture predominantly from Fisher Scientific (Santa Clara, CA): Falcon polyethylene six-well plates, Falcon high-density (3 μm pore-size) cell culture inserts, T75 culture flasks, disposable aspirating and serological polypropylene pipettes, Nalgene CN filtration units (50, 100, 250, 500 and 1000 mL), disposable polypropylene conical vials (15 and 50mL), pipet tips, pipets, pipet-aid, disposable cell scrapers, TRIZOL, inverted microscope TMS (Nikon Corp.), CO_2 incubator (Revco Scientific) and a Millicell-ERS transepithelial resistance (TEER) measurement system (Millipore).

2.3.2 Cell culture growth conditions

The LS180 cells were grown in RPMI 1640 phenol-red free media, 10% FBS, 1% penicillin/streptomycin (Pen/Strep at 100x) and 1% glutamine. HepG2 cells were grown in DMEM EBSS, 10% FBS, 1% pen/strep, 1% Na-pyruvate and 1% non-essential amino acids (NEAA). RL95-2 endometrial cells were grown in a 1:1 ratio of DME-H21 and HAM-F12K along with 10% FBS, 1% Hepes (1 M), 0.5% insulin and 1% Pen/Strep. The

TM2 cell line was grown in a 1:1 ratio of DME-H21 and Ham's-F12K, 5% horse serum, 2.5% FBS, 1% glutamine and 1% Na-pyruvate. All cell lines were grown in phenol-red free media to eschew any potential estrogenic effects caused by the red dye. Consequently, most phenol-red free media are light sensitive. All feeding, induction and experimental conditions were performed with minimal light exposure. Cells were grown on either 6-well plates at a density of ~300,000 cells/insert or 75-cm^2 flasks at a density of 1E6. Cells were grown to confluence for 4-7 days at 37°C in 5% CO_2.

2.3.3 Characterization of various cell lines

The following cell lines were screened and tested for *MDR1* inducibility: LS180 (human colon), HepG2 (human liver), RL95-2 (human endometrium), HCC-1500 (human breast) and TM3 (mouse testis). LS180 colon adenocarcinoma cells originate from a female Caucasian, blood type O and express HLA A2, B13 and B50 antigens. They were deposited in the ATCC by Northwestern University at passage #34. They have an epithelial morphology, adherent growth properties, are positive for Colon Antigen 3, negative for p53 antigen expression and express interleukin-10 (IL-10) and IL-6. The HCC-1500 cells are primary ductal carcinoma cells, obtained from an African-American female with a breast tumor classified as TNM stage IIB, grade 2. Cells have an epithelial morphology, adherent growth properties, are positive for expression of both estrogen and progesterone receptors, and positive for p53 expression. RL95-2 are endometrial carcinoma cells obtained from a Caucasian female with an epithelial morphology and adherent growth properties. They express both α and β estrogen receptors, possess α-keratin, well-defined junctions, tonofilaments and surface microvilli. HepG2 liver cells

are derived from hepatocellular carcinoma tissue from an adolescent Caucasian male. Also adherent and epithelial, these cells are known to express many proteins including albumin, plasminogen, α-fetoprotein and retinal binding protein. The TM3 cell line originates from normal male mouse testis tissue, expressing LH, epidermal growth factor (EGF), androgen, estrogen and progesterone receptors. It responds to LH with an increase in cAMP production, and capabilities to metabolize cholesterol, but does not respond to FSH. Monolayer confluence was tested by measuring the transepithelial electrical resistance (TEER) values using the Millicell-ERS transepithelial resistance measurement system. Measurements were made prior to cell collection for each individual well in growth medium.

2.3.4 Induction

2.3.4.1 Materials

The human colon carcinoma cell line, LS180, was purchased through the UCSF Cell Culture Facility (CCF; San Francisco, CA) from American Type Culture Collection (ATCC; Rockville, MD). Dulbecco's modified Eagle's medium (DME-H21) was obtained from UCSF CCF. RPMI 1640 (without phenol red) was custom-ordered through CCF and supplemented with the following: 10% fetal bovine serum (HyClone Laboratories), 100 U/mL penicillin, 100 μg/mL streptomycin and 1% glutamine. Falcon polyethlylene terephthalate (PET) cell culture inserts (Becton Dickinson) and their companion Costar 6-well plates (Costar Corp.) were purchased from Fisher Scientific (Santa Clara, CA). Acetonitrile (ACN) was obtained from Fisher Scientific.

2.3.4.2 Cell splitting, induction and lysis

For all induction experiments, hormones were first dissolved in ethanol, DMSO, acetonitrile (ACN) or water and appropriate concentrations were added to media before filtration. LS180 colon cells were cultured on six-well inserts or 75-cm^2 flasks, prior to seeding into six-well plates and rinsed twice with PBS (Ca^{2+}/Mg^{2+} free) and allowed to incubate in PBS during the second rinse for 15 minutes at 37°C, 5% CO_2. When cellular tight junctions were slightly loosened, viewed under microscope, PBS was aspirated and 0.25-0.5% trypsin was added and swirled to coat adherent cells. Cells were returned to the CO_2 incubator at 37°C for ~5 minutes. When cells had separated, forming white circular globes, flasks were tapped to gently loosen off the surface and gently resuspended in media for allocation into six-well plates for induction. Cells were seeded at a density of ~300,000 cells/insert in a 1.5 mL aliquot on the apical side. The basolateral side, cradling the insert, contained a 2.5 mL aliquot of cell-free media. Cells were grown in the CO_2 incubator at 37°C and allowed to adhere overnight. They were then fed 24 h post-seeding and then induced with hormone-containing media replacement (both apical and basolateral sides of the insert) every 24 hours, 3 days (72 h) before confluence. Before harvesting, TEER values were measured.

For mRNA analysis, cells were harvested when confluent (~ 4 to 7 days) by washing twice in ice-cold PBS without Ca^{2+}/Mg^{2+}, with gentle rocking and careful aspiration of PBS. Cells were lysed by the addition of TRIZOL (1mL/insert) into each well and allowed to sit for approximately 30 sec. They were then homogenized by passing cell lysate several times through the pipette. Lysates were then transferred to 1.5 mL

DNase/RNase-free microcentrifuge tubes for total RNA isolation. For Western blot protein analysis, cells were rinsed twice in PBS (Ca^{2+}/Mg^{2+} free) and immediately scraped off in PBS using different cell scrapers for different hormone samples into 15mL polypropylene conical tubes when confluent.

2.3.5 Semi-quantitative RT-PCR

2.3.5.1 Materials

The 18s Classic I internal standard with competimer technology was purchased from Ambion, Inc. (Austin, TX) and *MDR1* primers were ordered from BD Gentest (Woburn, MA). SuperScript OneStep RT-PCR with Platinum TAQ, 25x Reaction Mix and DEPC-treated H_20 were purchased from UCSF CCF. PCR RNase/DNase free tubes were obtained from Ambion, Inc. PCR reactions were done using PCR Express Thermal Hybaid Cycler. 2% agarose e-gels and apparatus were purchased from Invitrogen, and pictures were taken using Polaroid film.

2.3.5.2 Total RNA isolation

After cell lysates were collected and transferred into 1.5 mL microcentrifuge tubes in TRIZOL (Gibco-BRL), a monophasic solution of phenol and guanidine isothiocyanate, they were incubated for 5 minutes in a 20-30°C water bath to permit complete dissociation of nucleoprotein complexes. To each tube, 0.2mL chloroform was added, shaken vigorously by hand for 15 sec and incubated in the 20-30°C water bath for 3 minutes. Samples were then centrifuged at 12,000xg for 15 minutes at 4°C, which

allowed the mixture to separate into a lower red, phenol-chloroform phase, a middle interphase, and a colorless aqueous phase (RNA remains exclusively in the aqueous phase). Following phase separation, the aqueous phase was transferred to a fresh 1.5 mL microcentrifuge tube and RNA precipitated by the addition of 0.5 mL isopropyl alcohol/tube. After incubation at 20-30°C for 10 minutes, samples were again centrifuged for 10 minutes at 12,000xg in 4°C. The RNA precipitate formed a white, opaque gelatin-like pellet on the bottom of the tube. To wash RNA, supernatant was carefully removed with a pipet and 75% ethanol was added (1mL/tube), vortexed and centrifuged at <7500xg for 5 minutes at 4°C. Each sample was drained free of ethanol and air-dried for 20-30 minutes until the pellet became transparent with no residual ethanol. The RNA pellet was dissolved in ~40-60 µL of RNase-free water by passing the solution several times through the pipette tip and incubated for 10 minutes at 55°C. The concentration and purity of isolated RNA samples were measured using an ultraviolet spectrophotometer, confirming $A_{260/280}$ ratio values between 1.6-1.8. Samples were diluted into 0.5 µg/µL aliquots and frozen at -80°C until RT-PCR.

2.3.5.3 *MDR1* primer design

The following gene specific, intron-spanning primer sequence was used for h*MDR1*:

Primer	Sequence	Base Location
Sense	5'- GCCTGGCAGCTGGAAGACAAATACACAAAAT -3'	834-864
Anti-Sense	5'- AGACAGCAGCTGACAGTCCAAGAACAGGACT -3'	1088-1118

The expected amplified product length was 284 bp.

2.3.5.4 RT linearity range test

For optimal semi-quantitative analysis, the linear range of PCR and optimal 18S Primer:Competimer ratio (3:7) was determined based on cycle number and pixel band density (Figure 2.1). Competimer technology involves modification of 18s competimers at their 3' ends to block extension by DNA polymerase. By mixing 18s primers with increasing amounts of 18s competimers, the overall PCR amplification efficiency of 18s cDNA can be reduced without the primers becoming limiting and maintaining quantitative abilities. PCR reactions were conducted with a cycle number between 30-33, within the acceptable linear range to eliminate mRNA band saturation and allow optimal range for band density variability.

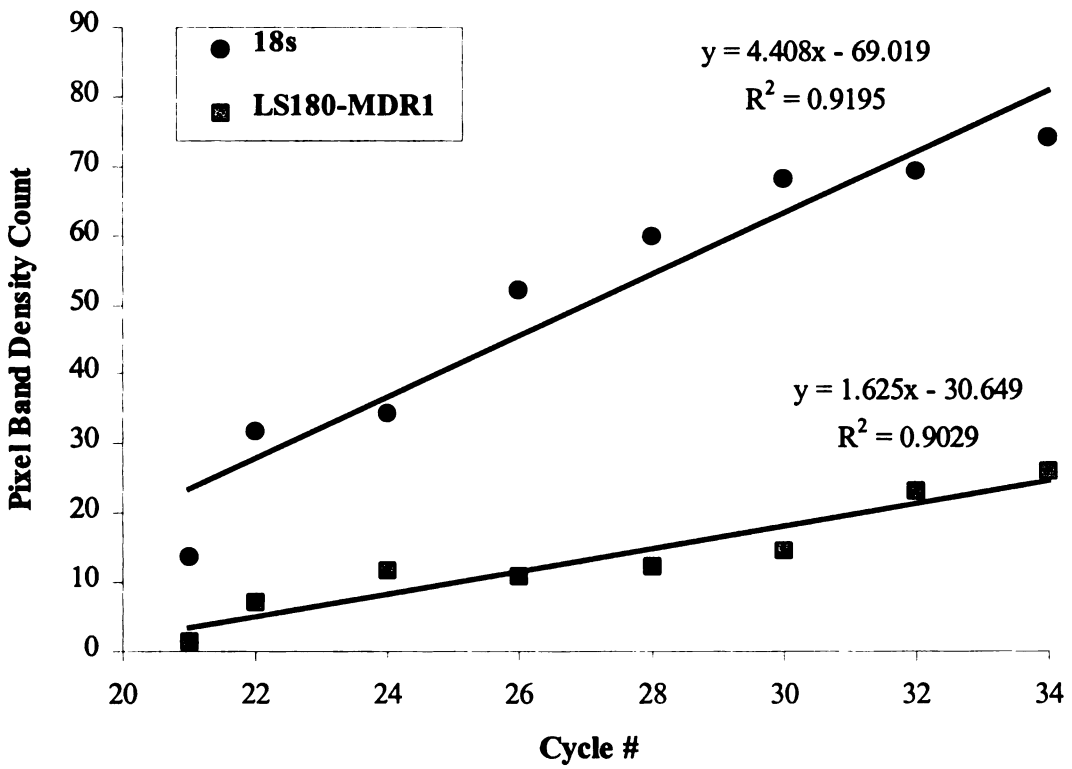

Figure 2.1 Plot of pixel band density *vs.* PCR cycle # to determine linear range for RT-PCR reactions for both 18s internal standard and *MDR1* mRNAexpression in the LS180 cell line.

2.3.5.5 One-step RT-PCR

Superscript™ One-Step with Platinum® *Taq* (Gibco-BRL) was used to detect RNA by RT-PCR, in which both cDNA synthesis and PCR was performed in a single tube. The PCR reaction was performed by thawing of all components including 2x Reaction Mix (Gibco-BRL), Template RNA, *MDR1* (Sense/Anti-Sense) primers, Ambion 18s Primer:Competimer mix, and DEPC-H_20. Individual PCR reaction tubes were prepared on ice, each containing the following in the listed order:

a. 2x Reaction Mix (final concentration: 1x; 25 µL/tube)
b. DEPC-H_20 (50% v/v; 14 µL/tube)
c. 10 µM Sense and Anti-sense *MDR1* primer (0.2 µM each; 1 µL/tube)
d. 0.5 µg/µL Template RNA (2µg; 4 µL/tube)
e. 18s (3:7) 0.5 µg/µL Primer:Competimer (2 µg; 4µL/tube)
g. RT/Platinum *Taq* Mix (1µL/tube)

The final volume was attained with water up to 50 µL. Samples were briefly centrifuged to make sure all components settled at bottom of the amplification tube and analyzed in the PCR Express Thermal Hybaid as depicted in Figure 2.2:

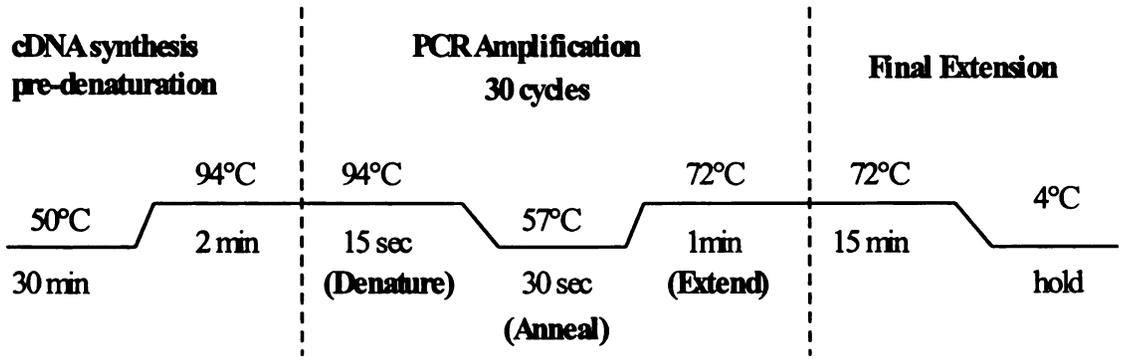

Figure 2.2 RT-PCR cycling conditions for *MDR1* cDNA amplification.

RT-PCR products were separated on 2% agarose e-gels. Before loading, samples were kept on ice while e-gels were pre-run at 62 V for 2 minutes. Samples were then diluted (5 μL sample + 15 μL DEPC-H_20) and loaded onto lanes. A 100 bp DNA ladder (7 μL ladder + 13 μL DEPC-H_20) was also loaded in the first lane. Gel was run for 30 minutes at 60 V, immediately viewed under a UV transilluminator and photographed using a UV Polaroid camera.

Human liver total RNA obtained from Ambion, Inc. was used as a positive control. Integrity of RNA was confirmed by use of the18S ribosomal RNA internal standard (Ambion), which yielded an expected amplified product of 489 bp.

2.3.5.6 Semi-quantitative analysis

Polaroid pictures of gels were scanned and captured electronically. Images were imported into the NIH Scion image analysis software and the image inverted for optimal quantification of band density. Pixel band density values measured were subtracted from background values and ratio values were calculated for *MDR1*/18s to normalize for inter-individual lane and loading variability.

2.3.6 Western blot

2.3.6.1 Materials

The P-gp antibody, C219, was obtained from Signet (Dedham, MA). For the Western blotting procedure, the following materials were utilized: QiaShredder (Qiagen), BioRad

gradient Tris-HCl polyacrylamide gels (4-20%), PAGE electrophoresis apparatus, PVDF membrane, nitrocellulose membrane, pre-stained broad range protein standard (BioRad), 10x Tris/Glycine/SDS running buffer (BioRad), Laemmli sample buffer, β-mercaptoethanol, microcentrifuge tubes, non-fat dry milk, Tris-HCl, Tris, glycine, NaCl, deionized H_20, Tween-20, transfer cassettes, sponges, filter paper, Saran wrap, timer, 15 mL Falcon disposable polypropylene conical tubes, ECL reagents (Amersham), Hyperfilm (Kodak) and film developer.

2.3.6.2 Cell lysis

LS180 colon cells were cultured on six-well inserts or 75-cm^2 flasks and harvested when confluent (~4 to 5 days). Cells were washed in ice-cold PBS without Ca^{2+}/Mg^{2+}, scraped and centrifuged at 4000xg for 10 minutes (4°C). The pellet was washed again with PBS and resuspended in lysis buffer containing 1μg/ml pepstatin, 20 μg/ml leupeptin, 20 μg/ml aprotinin, 1 mM PMSF and a supplemental protease inhibitor cocktail in hypotonic buffer (Tris-HCl, KCl, $MgCl_2$). Samples were sonicated on ice (15 sec x2) and stored at -80°C.

2.3.6.3 Western blot protocol

The presence and expression level of P-gp was detected using Western blot analysis. The protein concentration of LS180 cell lysate samples were quantified using a BioRad assay kit utilizing bovine serum albumin (BSA) as the protein standard. All samples were diluted 1:1 with Laemmli buffer (containing 5% β-mercaptoethanol) and adjusted to

obtain a final loading concentration of 100 μg protein. Samples were then immediately transferred to a QiaShredder and spun for 20 sec at 13,000 x g in 4°C. This step ensured more accurate loading by precluding the sample from becoming overly viscous. Samples were then loaded unboiled onto a BioRad gradient Tris-HCl polyacrylamide gel (4-20%) electrophoresis (PAGE) in running buffer (recipe as shown in Table 2.1) at a constant 100V for 90 minutes. The pre-stained SDS broad range marker was also loaded (7μL) in the first lane.

During transfer, nitrocellulose membrane was soaked briefly in methanol, then in transfer buffer (Table 2.1) for at least 15 minutes in 4°C. Sponges and filter paper were also kept soaking in transfer buffer. Gels were then blotted in transfer buffer along with nitrocellulose, sponges and filter paper overnight at 26V in 4°C. The nitrocellulose membrane was then blocked in 5% non-fat milk at room temperature for 1 hour and then washed twice for 10 minutes in TTBS (Table 2.1) before probing with the primary P-gp antibody (C219; 1:100 in 1% non-fat milk) for another hour at room temperature. The membrane was again washed with TTBS once for 15 minutes, twice for 10 minutes and then probed with secondary goat anti-mouse horseradish peroxidase (HRP)-conjugated antibody (diluted 1:15,000 in 1% non-fat milk) for 50 minutes at room temperature. Membrane was then washed with TTBS once for 15 minutes and twice for 10 minutes, then the same set of washes repeated with TBS (Table 2.1). Membranes were then taken to the darkroom with a film developer and washed in a mixture of ECL reagents for 1 minute, blotted with Kimwipes, wrapped in plastic and exposed to film that was subsequently developed. P-gp protein was detected with the enhanced

chemiluminescence system (ECL- Amersham). The resulting P-gp protein bands ran at an apparent molecular weight of ~170 kDa. Band density was scanned and quantified using the same method described above for RT-PCR.

Table 2.1 Western blot solution recipes.

Solution	Ingredient	Amount Added	Final Concentration
Running buffer	10x Tris/Gly/SDS	100mL	10%
	DDI H_20	to 1L	90%
Transfer buffer	Tris	3.03 g	25 mM
	Glycine	14.4 g	190 mM
	Methanol	200 mL	20% (v/v)
	DDI H_20	to 1L	
TBS	Tris-HCl	4.87 g	20 mM
(Tris-buffered saline)	NaCl	58.44 g	0.5 M
	DDI H_20	to 2L	
	*Adjust to pH 7.5 with concentrated HCl.		
TTBS	Tween-20	500 µL	0.05% (v/v)
	TBS	to 1L	

2.3.7 Transfection

2.3.7.1 Materials

The *MDR1*-pGL3 vector containing a 4-kb upstream *MDR1* promoter region that was used for these experiments was graciously provided by Yan Shu from Dr. Kathleen

Giacomini's lab. Materials used for calcium phosphate transfection of LS180 cells include: 6-well plates, ProFection® Mammalian Transfection System- Calcium Phosphate (Promega; Madison, WI), Hepes-buffered saline (HBS), nuclease-free H_20, plasmid DNA, control plasmid DNA, empty vector plasmid DNA, and inducing hormones, Promega Luciferase Assay System (luciferase assay substrate, luciferase assay buffer, luciferase cell culture lysis reagent 5x), spectrophotometer, Falcon disposable cell scraper, microcentrifuge tubes, 96-well plates, sodium carbonate, multi-channel pipettor, Fisher vortex mixer, Sarstedt 5mL polystyrene round-bottom tubes and luminometer.

2.3.7.2 Transfection of *MDR1* plasmid vector into LS180 cell line

Calcium phosphate-mediated transfection was used for transient expression of the MDR1 promoter via plasmid into the LS180 cell line. This particular procedure involves mixing the plasmid DNA with $CaCl_2$ and a phosphate buffer to form a fine precipitate, which is dispersed over the cultured cells. Coprecipitation of the DNA with calcium phosphate enhances transfection efficiency. This method was first established by Graham *et al.* (135).

LS180 cells were grown to 30-50% confluence on 6-well plates with 2-3 mL media. Three hours prior to experimentation, cells were fed with fresh media. DNA was quantified at 260/280 nm. To each well, the following DNA mixtures were added in duplicate for LS180 cell transfection and incubated at RT for 30 minutes:

1. (+) Positive control: 2 μg control pGL3 plasmid (w/ endogenous promoter, no luciferase gene), 1.5 μg pSV (internal control for β-gal to confirm positive transfection and functional promoter), 0.25 M $CaCl_2$ and DDI H_20.
2. (-) Negative control: 2μg pGL3 Basic empty vector, 1.5 μg pSV internal control, 0.25 M $CaCl_2$ and DDI H_20.
3. *MDR1*-promoter vector: 2 μg *MDR1*-pGL3 plasmid vector, 1.5 μg pSV internal control, 0.25 M $CaCl_2$ and DDI H_20.

The next day, cells were induced by replacing media with fresh media containing hormones. Cells were continuously induced with replacement media every 24 hours for 3 days (72 hours total), then harvested when confluent.

The β-galactosidase enzyme assay was utilized to obtain a β-gal standard curve. The pSV-β-galactosidase control vector is a positive control vector, co-transfected with the *MDR1*-pGL3 plasmid vector, and used for monitoring transfection efficiencies of mammalian cells. The SV40 early promoter and enhancer drive transcription of the *lacZ* gene embedded within the vector, which encodes the β-galactosidase enzyme. The β-gal enzyme is used as a reporter enzyme that is assayed directly from cell lysates and can be measured spectrophotometrically. A negative control, pGL3 basic empty vector, prepared from transfected cells is also assayed for the presence of endogenous β-gal activity.

The β-gal enzyme assay was performed by washing cells in a duplicate 6-well plate with PBS Ca^{2+}/Mg^{2+} free buffer twice. Diluted reporter lysis buffer 1x (RLB) was added to coat cells (300 μL/35 mm well) and incubated for 15 minutes at RT. Cells were then scraped off, transferred to a microcentrifuge tube, briefly vortex mixed and centrifuged at

13,000xg for 2 minutes at 4°C. Supernatant was transferred to fresh tubes, diluted 2:1 in 1x RLB, and a portion was then diluted again 1:1 in assay 2x buffer. The assay 2x buffer contains the yellow substrate ONPG (*o*-nitrophenyl-β-D-galactopyranoside), which is hydrolyzed by β-gal to the colorless substrate *o*-nitrophenyl. The samples were vortex mixed and incubated at 37°C for 30 minutes until a faint yellow color appeared, indicating β-gal enzyme activity. Reactions were stopped with 1M sodium carbonate and absorbance read at 420 nm.

The luciferase assay is known to be very sensitive with immediate results as the luciferase protein does not require any post-translational processing. In this assay, the luciferase enzyme transcribed from the pGL3 plasmid vector catalyzes the conversion of the added substrate, luciferin, to produce oxyluciferin and light. This is done by the conversion of chemical energy derived of luciferin oxidation by luciferase, using ATP-Mg^{2+} as a co-substrate. Sample preparations for the luciferase assay were the same as for the β-gal assay. A 100μL aliquot of luciferase assay reagent was added to each Sarstedt tube. The luminometer was programmed to perform a 2-second measurement delay followed by a 10-second measurement reading for luciferase activity. A 20 μL aliquot of cell lysate sample was added to tube containing the luciferase assay reagent prior to placing each tube in the luminometer for reading.

For data analysis, duplicate absorbances were measured spectrophotometrically for each sample using the β-galactosidase enzyme assay to construct a standard curve, acquiring specific β-gal milliunit measurements (β-gal). Emission of luciferin luminescence was

measured in a separate, duplicate set of samples. Total luciferase activity (RLU) measurements were calculated using the ratio: RLU/β-gal, so as to normalize RLU values.

2.3.8 P-gp ATPase activity assays

2.3.8.1 Materials

Human P-gp and control membranes for the ATPase activity assay were obtained from Gentest (Woburn, MA). The following materials were also used to measure P-gp ATPase activity: a microplate spectrophotometer (OD 630-850 nm), 96-well microtiter plates, multichannel pipettor, 0.5 M KPO_4 (monobasic and dibasic), deionized H_20, 0.1 M KPO_4, verapamil, MgATP, Tris-MES buffer, EGTA, KCl, dithiothreitol (DTT), sodium azide, Tris-base, Nalgene filter unit, zinc acetate, ammonium molybdate, ascorbic acid, NaOH, SDS, anti-foam A, sodium orthovanadate, 17β-estradiol, progesterone, estriol, estrone and ethynyl estradiol.

2.3.8.2 P-gp ATPase assay

Stimulation of P-gp ATPase catalytic activity was measured in membranes of Sf9 insect cells transfected with a recombinant baculovirus containing *MDR1* cDNA (Gentest©). The P-gp ATPase assay method used was a modification of the original assay described by Sarkadi *et al.* (136) and as per manufacturer's procedures. Control and P-gp membranes were separately incubated at 37 °C for 20 minutes with positive control (20 μM verapamil) or varying concentrations of test hormone-drug, 3 mM MgATP and

buffer solution (50 mM Tris-Mes, 2mM EGTA, 50 mM KCl, 2 mM dithiothreitol, and 5 mM sodium azide). A duplicate reaction mixture also containing a P-gp ATPase inhibitor, sodium orthovanadate (100 μM), was assayed in parallel as a negative control.

ATPase activity measured in the presence of sodium orthovanadate (non P-gp ATPase activity) was subtracted from the activity produced without vanadate to determine vanadate-sensitive ATPase activity. Addition of 10% SDS was used to terminate the reaction. Reaction mixtures were then incubated for 20 minutes in a zinc acetate (15 mM) solution containing ammonium molybdate (35 mM) to measure levels of inorganic phosphates released by its absorbance at 800 nm. A phosphate standard curve was used to compare and quantify absorbance measurements.

2.4 Results

2.4.1 Expression and Inducibility of P-gp in various female cell lines

Several cell lines were screened and tested for the presence and inducibility of P-gp expression by steroid hormones, specifically 17β-estradiol and progesterone, to obtain a diagnostic tool with which to investigate the mechanisms of P-gp induction. The cell lines that were screened for P-gp expression included HepG2 (hepatic), RL95-2 (endometrial), HCC1500 (breast), TM3 (murine testis) and LS180 (colon). Of these cell lines, those that exhibited endogenous P-gp expression via Western blotting were induced by the predominant female steroids, 17β-estradiol and/or progesterone as well other related regulatory hormones such as the somatotropin, hGH (anterior pituitary growth hormone), dexamethasone, luteinizing and follicle-stimulating hormone. Induction was

conducted by growing the individual cell lines in their respective media and growth supplements until attaining 30-50% confluence with feeding on an as-needed basis. Three days before 90-100% confluence and harvesting, cell lines were fed with replacement media containing hormone(s) and replaced with fresh hormone-containing media every 24 hours for 72 hours total. Continuous visual inspections of cell lines for cellular integrity, health and confluence were performed on a daily basis.

In a series of studies, the endocrine regulation of the estrogen receptor (ER) concentration in primary cultures of rat hepatocytes was studied. The combination of the human somatotropic anterior pituitary growth hormone, hGH, and dexamethasone was utilized to upregulate estrogen receptor (ER) levels as was shown by Stavreus-Evers *et al.* (137-139) in which the combination increased ER protein levels 6-fold and ER mRNA levels 2.5-fold. These effects were not significantly different from those hepatocytes that were treated with only hGH. The aim of our studies was to upregulate ER in a human liver cell line, HepG2, in order to maximize steroid hormone induction of P-gp at the regulatory level, as some of our previous studies showed that estradiol and progesterone alone did not have a significant effect (individually or in combination) on P-gp expression in HepG2 cells.

In Figure 2.3, HepG2 liver cells were induced for 72 hours with various hormones, harvested, and probed for P-gp protein expression using the P-gp specific monoclonal antibody, C219, in Western blotting. The molecular weight for P-gp is approximately 170 kDa, running between the molecular weight markers, 207 and 118 kDa, as shown at the

top of Figure 2.3. Band images were electronically analyzed using NIH Scion Imaging software and results show an approximate 40% and 50% increase in P-gp expression in the presence of both 10 μM β-estradiol (E_2) and 10 μM progesterone (P) with either 0.005 pM hGH + 10 nM dexamethasone (open bars) or 0.005 pM hGH alone (closed bars). There was no significant increase in P-gp expression in the presence of E_2 alone in either condition, but a slight increase of 20% was observed in the presence of progesterone and hGH + dexamethasone.

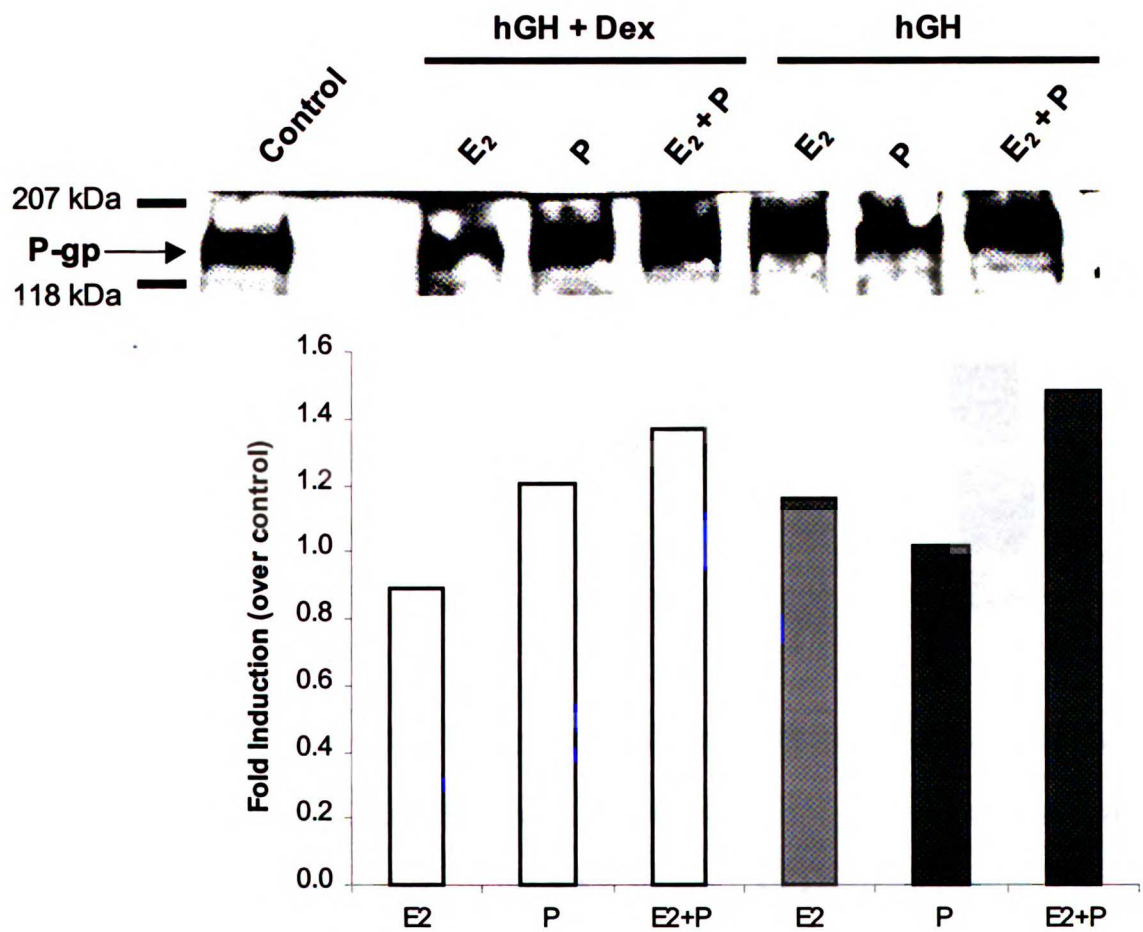

Figure 2.3 Western blot of P-gp expression and induction by 17β-estradiol (E_2) or progesterone (P), pituitary growth hormone alone (hGH; closed, gray bars) or with dexamethasone (hGH + Dex; open bars) in HepG2 cell line.

To determine whether steroid hormones induce P-gp, we examined the effect of various steroid hormones on P-gp expression in HepG2 liver, RL95-2 endometrial and TM3 mouse testis cells. Figure 2.4 shows Western blotting for P-gp in these various cell lines. Induction occurred over a period of 72 hours and nitrocellulose membrane was probed for P-gp using the C219 antibody.

Figure 2.4 Western blotting of P-gp expression in *MDR1*-MDCK, HepG2, RL95-2 and TM3 cell lines.

MDR1-transfected MDCK (Madine-Darby Canine Kidney) cells were used as a positive control. In HepG2 liver cells, 10 μM rifampin, a known inducer of P-gp was also used to determine whether P-gp expression was inducible compared to control (lane 5). In HepG2 cells, P-gp expression levels were only slightly increased in the presence of rifampin, compared to control. Testosterone (1 μM) was used to determine if any male steroid hormones would have a regulatory impact on P-gp expression as this particular

cell line is derived from a Caucasian male. However, no obvious changes in expression were observed. The combination of 1μM estradiol and progesterone (E_2 + P) seemed to show a slight, but insignificant decrease in P-gp expression compared to control, whereas the combination of the gonadotropins, LH and FSH (lane 6) showed no change in expression. 17β-Estradiol (500 nM) seemed to slightly decrease P-gp expression compared to control. In the endometrial RL95-2 and murine testis TM3 cell lines, expression of P-gp was undetectable, indicating low or no endogenous levels of P-gp. Western blotting of the breast cancer cell line, HCC1500 also showed no detectable levels of endogenous P-gp. RT-PCR experiments were conducted to examine the effect of these same hormones on *MDR1* mRNA expression. The results also showed no significant changes of *MDR1* at the transcriptional level, using 18s as an internal standard.

Figure 2.5 RT-PCR of *MDR1* mRNA expression in the HepG2 cell line. Lanes 1-2 are control HepG2 cells with no hormone induction. Lanes 3-4 were HepG2 cells induced with 0.1 I.U./mL hCG, lanes 5-6 with 0.1 I.U./mL hG, lane 7 with 0.1 I.U./mL LH, lane 8 with 0.1 I.U./mL FSH and lanes 9-10 with the combination of LH + FSH. The cDNA samples were run on a 2% agarose e-gel.

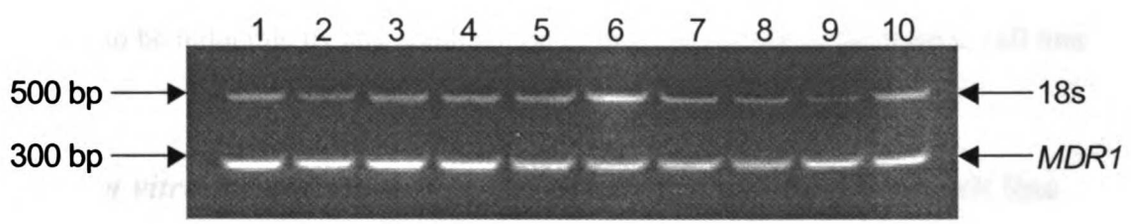

We tested HepG2 cells for inducibility of *MDR1*-mRNA at the transcriptional level by other various gonadotropins including human chorionic gonadotropin (hCG), gonadotropin (hG), LH and FSH. Figure 2.5 illustrates the reverse transcription of total RNA isolated from HepG2 cells, synthesis and amplification of human *MDR1* primer-specific cDNA via a polymerase chain reaction (PCR). The classic 18s primer-competimer (3:7) set was used as an internal standard, which amplifies a sequence of approximately 488 bp in length. The *MDR1* primers amplify a product sequence that has a length of 284 bp. A control mouse liver was used as a negative control (not shown, but in lane 0). *MDR1* mRNA expression was not significantly induced by any of the gonadotropins, confirming results observed at the protein level.

Extended and brief induction times were also investigated and it was concluded that maximal expression of P-gp was attained after 72 hours of exposure. Additional experiments were performed inducing HepG2 cells for 72 hours with the combination of 17β-estradiol or progesterone with the various gonadotropins utilized in Figure 2.5. This included a dose-dependent increase from 50 nM to 50 μM of either 17β-estradiol or progesterone combined with hCG or human gonadotropin (hG), showing no visible effect on P-gp expression at the protein level. At the mRNA level, *MDR1* expression was also not seen to be inducible by any combination of these hormones in the HepG2 cell line.

2.4.2 *In vitro* induction of P-gp/*MDR1* by steroids in LS180 cell line

Expression and induction of P-gp expression by hormones was investigated in the LS180 human colon carcinoma cell line. The LS180 cell line is purported to express the

pregnane X receptor, hPXR (112), a key regulator of xenobiotic metabolism, which several studies have shown may be important for *MDR1* induction (140-142). Several PXR response elements forming a complex regulatory cluster (including a DR4-motif) were identified in the 5'-upstream promoter region of human *MDR1* that may serve as binding sites for PXR ligands such as rifampin, phenobarbital, statins and St. John's wort. Recent studies demonstrate that the compounds that induce *MDR1* do so by activating the nuclear receptor PXR as well as the constitutive androstane receptor, CAR.

Figure 2.6 Induction of *MDR1* mRNA in LS180 cell line.

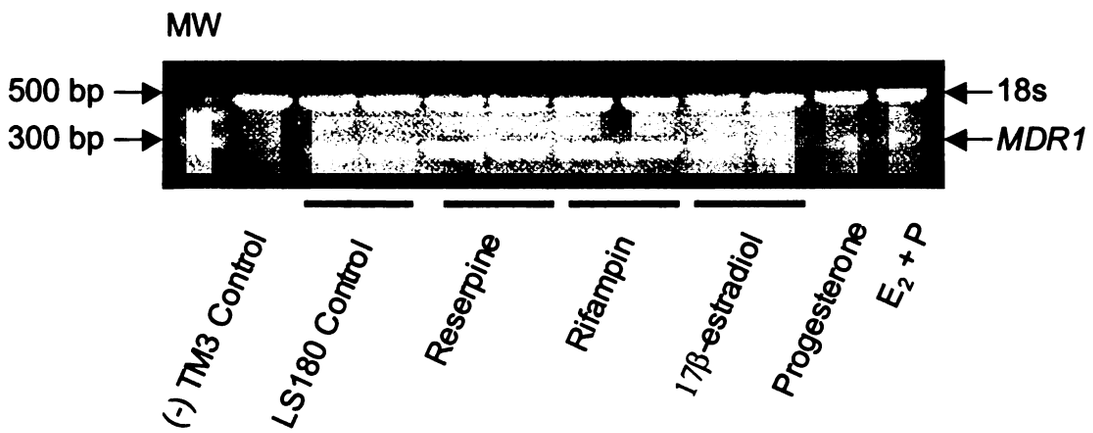

Figure 2.6 illustrates induction of LS180 colon cells by known P-gp inducers, reserpine and rifampin. The TM3 mouse cell line was used as a negative control as no endogenous human *MDR1* is present. Reserpine (10μM) induced *MDR1* mRNA 2.4-fold while 10 μM rifampin caused a 2.6-fold induction in *MDR1* mRNA compared to the LS180 control cells expressing basal endogenous levels of *MDR1*. 17β-estradiol (500 nM) showed a slight 29% decrease in *MDR1* mRNA expression. The combination of β-estradiol and

progesterone significantly decreased *MDR1* mRNA expression approximately 87% compared to control.

In Figure 2.7, the Western blot exhibits induced P-gp expression levels that are similar to that observed at the mRNA level. Reserpine (10 μM) and 10 μM rifampin were found to significantly induce *MDR1* expression approximately 7.3 and 6.4-fold, respectively, over control (LS180). In the presence of 500 nM 17β-estradiol, *MDR1* mRNA was slightly

Figure 2.7 Western blotting of P-gp induction in LS180 cell line.

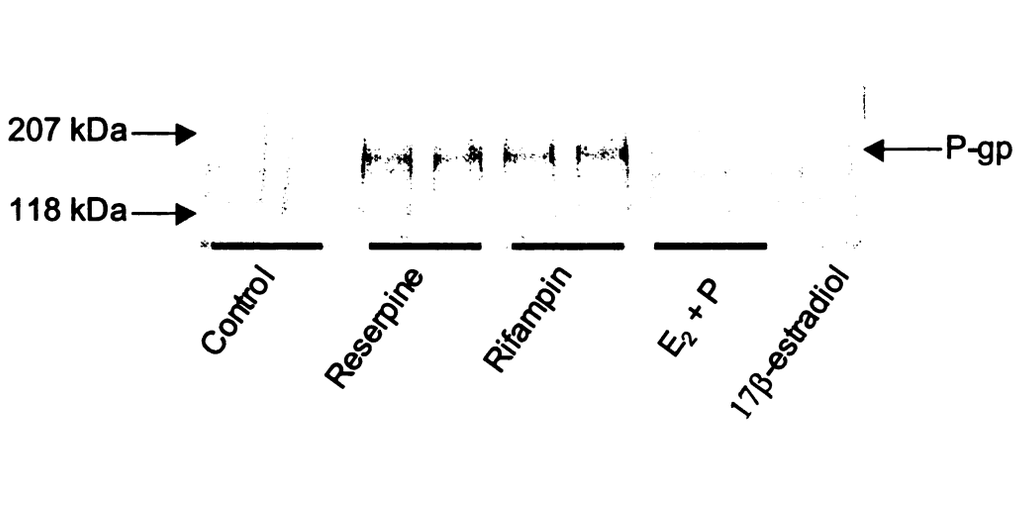

induced 1.4-fold over control, while the combination of 500 nM 17β-estradiol and 500 nM progesterone decreased P-gp expression ~20% compared to control LS180 cells. The consistent level of expression observed at the mRNA level was also observed at the protein level, suggesting that induction or repression via transcriptional regulation of *MDR1* is translated into increased or decreased P-gp protein expression.

In Figure 2.8, first-strand cDNA was synthesized from total RNA isolated from LS180 cells treated with either 5 μM of selected hormones (top panels) or 50 μM (bottom panels) as indicated- *lanes 1*: positive control (10 μM rifampin), *lanes 2*: negative control (media only), *lanes 3*: negative control (with 50 μM DMSO), *lanes 4*: β-estradiol, *lanes 5*: progesterone, *lanes 6*: estrone, *lanes 7*: estriol, *lanes 8*: ethynyl estradiol. The amplification products were resolved on 2% agarose gels stained with EtBr.

Figure 2.8 Amplification of *MDR1* from untreated control or hormone-treated LS180 cells using RT-PCR.

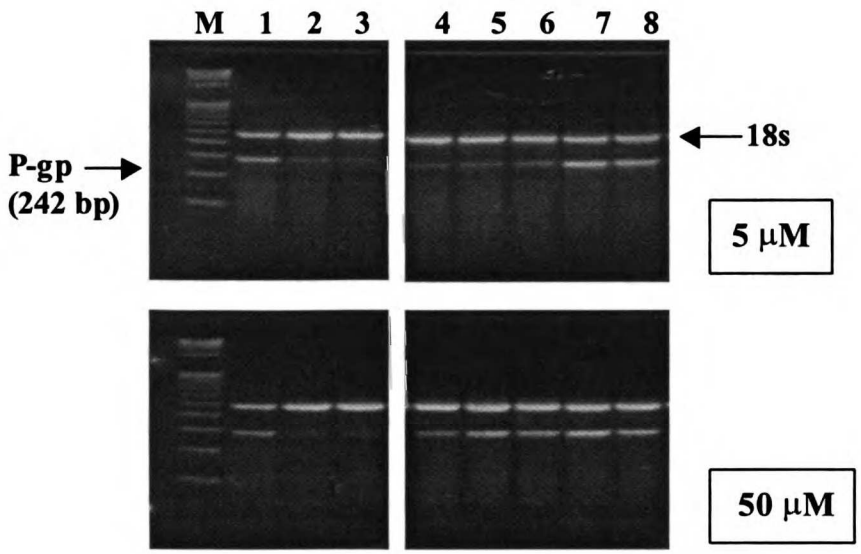

To investigate the effect of steroid hormones on *MDR1* expression, LS180 cells were used as an *in vitro* model. Rifampin, confirmed to be a known inducer of intestinal P-glycoprotein *in vivo* (143) and *in vitro* (142) via the PXR response element, was used as a positive control. LS180 cells were incubated with various estrogens and progestins for 48

or 72 hours prior to harvesting and isolation of total RNA. Maximal induction was observed at 72 hours indicating time-dependent induction. Using RT-PCR, endogenous *MDR1* mRNA expression levels as shown in Figure 2.8 were inducible 10.7-fold (over control) by 5 μM ethynyl estradiol and 11.0-fold by 5 μM estriol. Both estrone and progesterone, at 5 μM, similarly induced *MDR1* approximately 2-fold, while 17 β-estradiol showed no significant induction over 18s control. However, at 50 μM, estrone and estriol demonstrated significant *MDR1* induction (7.2 and 6.3-fold, respectively) on *par* with ethynyl estradiol (9-fold). Progesterone also showed a smaller, but significant increase in *MDR1* induction at the 50 μM level (3.2-fold), while only a slight induction was observed with 17 β-estradiol (Figure 2.8).

In Figure 2.9, *MDR1* mRNA induction was within the physiologic linear range from 25 nM to 10 μM for ethynyl estradiol and estrone (top panel) as indicated- *lane 1*: negative control LS180 cells, *lanes 2-6*: respectively 10 μM, 1 μM, 500 nM, 50 nM, 25 nM ethynyl estradiol and *lanes 7-11*: same sequence of concentrations for estrone. Cells were also induced with norethindrone and D-norgestrel (bottom panel) as indicated- *lane 1*: negative control, *lane 2*- positive control (10μM rifampin), *lanes 3-7*: respectively 10 μM, 1 μM, 500 nM, 50 nM, 25 nM norethindrone, *lanes 8-12*: same sequence for D-norgestrel. *M*: Marker 100 bp DNA ladder.

Figure 2.9 Concentration-dependent induction of *MDR1* mRNA using RT-PCR

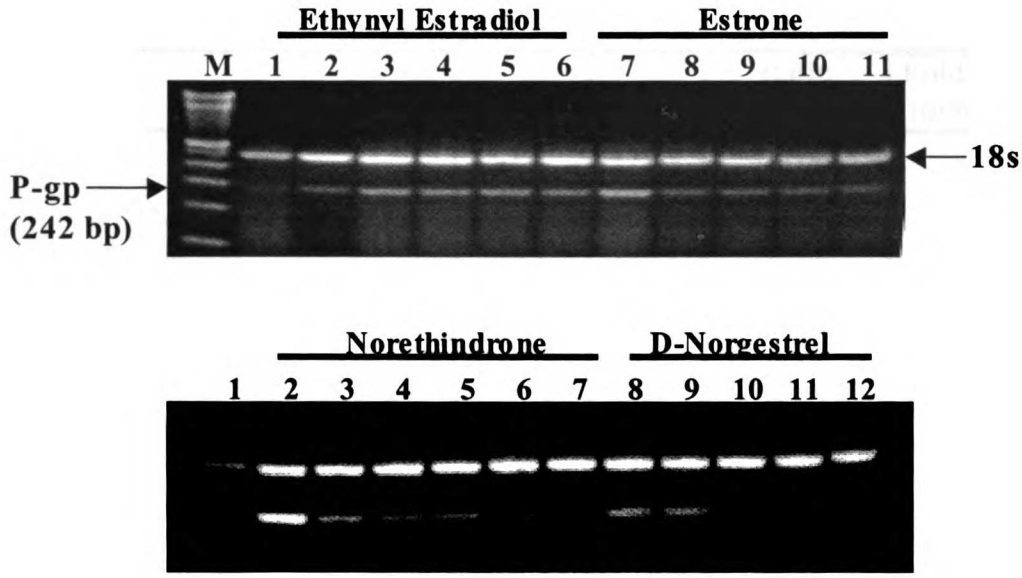

LS180 cells were treated with increasing concentrations of four steroid hormones ranging from 25 nM to 10 μM. A concentration-dependent induction of *MDR1* mRNA was observed with D-norgestrel (Figure 2.9, bottom panel, lanes 8-12) and estrone (Figure 2.9, upper panel, lanes 7-11). For norethindrone and ethynyl estradiol, a more constant level of induction was observed over the concentration range tested. Induction in some lanes seemed to look weaker at higher concentrations. However, calculated *MDR1*/18s ratio values using NIH imaging software suggest otherwise, indicating that the amount of cDNA loaded per lane may fluctuate slightly due to inherent variability in technique from lane to lane. These results indicate that *MDR1* mRNA is inducible by both natural and synthetic sex-steroid hormones suggesting regulation of the multi-drug resistance gene at the transcriptional level. The levels of these transcripts were quantitatively measured using NIH Scion imaging software and normalized to uninduced control cells. The results of the quantification are given in Table 2.2.

Table 2.2 Semi-quantitative measurements of P-gp and *MDR1* induction by various steroid hormones.

Figure 2.8		*MDR1**	18s*	Ratio (MDR1/18s)	Fold Induction (over control)
10 μM Rifampin		17.7	113.3	0.16	1.9
Control		10.0	119.0	0.08	-
Control (+50μM DMSO)		13.7	120.7	0.11	1.3
5 μM	β-Estradiol	10.4	114.2	0.09	1.1
	Progesterone	22.5	114.9	0.20	2.3
	Estrone	19.9	108.1	0.18	2.2
	Estriol	86.5	96.3	0.90	11.0
	Ethynyl Estradiol	70.8	90.1	0.79	10.7
Control		10.9	119.9	0.09	-
50 μM	β-Estradiol	14.5	115.1	0.13	1.4
	Progesterone	35.0	121.7	0.29	3.2
	Estrone	79.4	121.9	0.65	7.2
	Estriol	68.9	121.0	0.57	6.3
	Ethynyl Estradiol	99.2	121.7	0.82	9.0
Figure 2.9					
Control		50.9	79.6	0.08	-
10 μM	Ethynyl Estradiol	61.0	94.6	0.27	3.4
1 μM		22.8	62.3	0.37	4.6
500 nM		23.4	64.3	0.36	4.5
50 nM		25.1	62.0	0.39	4.9
25 nM		19.8	62.3	0.31	3.9
10 μM	Estrone	29.2	60.5	0.48	6.0
1 μM		12.3	52.7	0.23	2.9
500 nM		10.8	49.3	0.22	2.8
50 nM		7.8	43.6	0.18	2.3
25 nM		5.0	34.4	0.14	1.8
Control		13.8	68.4	0.20	-
10 μM	Norethindrone	57.9	92.3	0.63	3.1
1 μM		47.4	91.0	0.52	2.6
500 nM		48.5	87.7	0.55	2.7
50 nM		44.5	87.5	0.51	2.5
25 nM		32.9	86.4	0.38	1.9
10 μM	Norgestrel	42.4	80.4	0.53	2.6
1 μM		38.2	72.7	0.53	2.6
500 nM		18.8	72.0	0.26	1.3
50 nM		13.4	65.4	0.21	1.0
25 nM		0.4	40.3	0.01	0.0

Figure 3	MDR1**	SD	Fold Induction
10 μM Tamoxifen	95.8	-	3.9
50 μM Estrone	71.1	2.12	2.9
50 μM Estriol	54.7	0.04	2.2
50 μM Ethynyl Estradiol	84.1	1.06	3.4
50 μM MPA	26.7	-	1.1

* Values for MDR1 and 18s were subtracted from background pixel count.
** Values reflect average of duplicates when applicable.

Figure 2.10 Western blot of P-gp in the LS180 colon cell line.

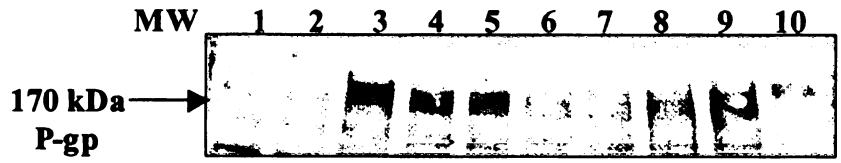

In Figure 2.10, LS180 cells were incubated in media containing various steroid hormones 72 hours prior to harvesting. Samples are shown as indicated- *lanes 1,2*: negative control (cells grown in media only), *lane 3*: positive control (10 μM tamoxifen), *lanes 4,5*: 50 μM estrone, *lanes 6,7*: 50 μM estriol, *lanes 8,9*: 50 μM ethynyl estradiol, *lane 10*: 50 μM 6α-methyl hydroxy progesterone acetate (MPA). Fifty μg samples were run on a 4-20% gradient gel, transferred to nitrocellulose and hybridized with C219 monoclonal Ab.

The presence and expression level of P-gp was detected using Western blot analysis. LS180 cell lysate samples were run unboiled on a gradient Tris-HCl polyacrylamide gel electrophoresis (PAGE), transferred to nitrocellulose and cross-reacted with the P-gp antibody, C219. The resulting P-gp protein bands ran at an apparent molecular weight of ~170 kDa. P-gp protein levels were significantly induced over control cells by 50 μM estrone (3-fold), estriol (2.2-fold) and ethynyl estradiol (3.4-fold) in LS180 cells (Fig. 2.10). Tamoxifen (10 μM), an estrogen receptor agonist, was used as a positive control of P-gp induction with a 4-fold increase over control. The synthetic progestin derivative, 6α-methyl progesterone acetate (6α-MPA) was also investigated for P-gp inducibility. Interestingly, there was only a 0.1-fold induction of P-gp at the protein level, but at the same concentration (50μM), 6α-MPA induced *MDR1* mRNA 3.7-fold over control, normalized to the 18s internal standard. Protein band intensities were scanned and pixel counts measured against control cells using the same method as described above for RT-PCR.

2.4.3 Transcriptional regulation of *MDR1*

To determine whether *MDR1* induction caused by steroid hormones was directly related to transactivation of the *MDR1* promoter, we utilized a pGL3 reporter gene plasmid containing a 4-kb upstream promoter region spanning exons 1 and 2 of the *MDR1* gene and a downstream luciferase gene. This plasmid DNA vector was transiently transfected into LS180 cells by co-precipitation with $CaCl_2$-phophate for 5 hours to enhance transfection efficiency. The LS180 cells were induced with various steroid hormones for 72 hours to determine whether hormones could bind and activate transcription of the

MDR1 promoter. This would be confirmed by continued transcription of the downstream luciferase reporter gene. The β-galactosidase containing plasmid vector, pSV, was also included in every well to serve as an internal standard and to verify occurrence of successful transfection and promoter function. After induction, cells were subjected to β-galactosidase and luciferase reporter gene assays.

Figure 2.11 Transcriptional activation of *MDR1* promoter by 10 μM steroid hormones in LS180 cell line.

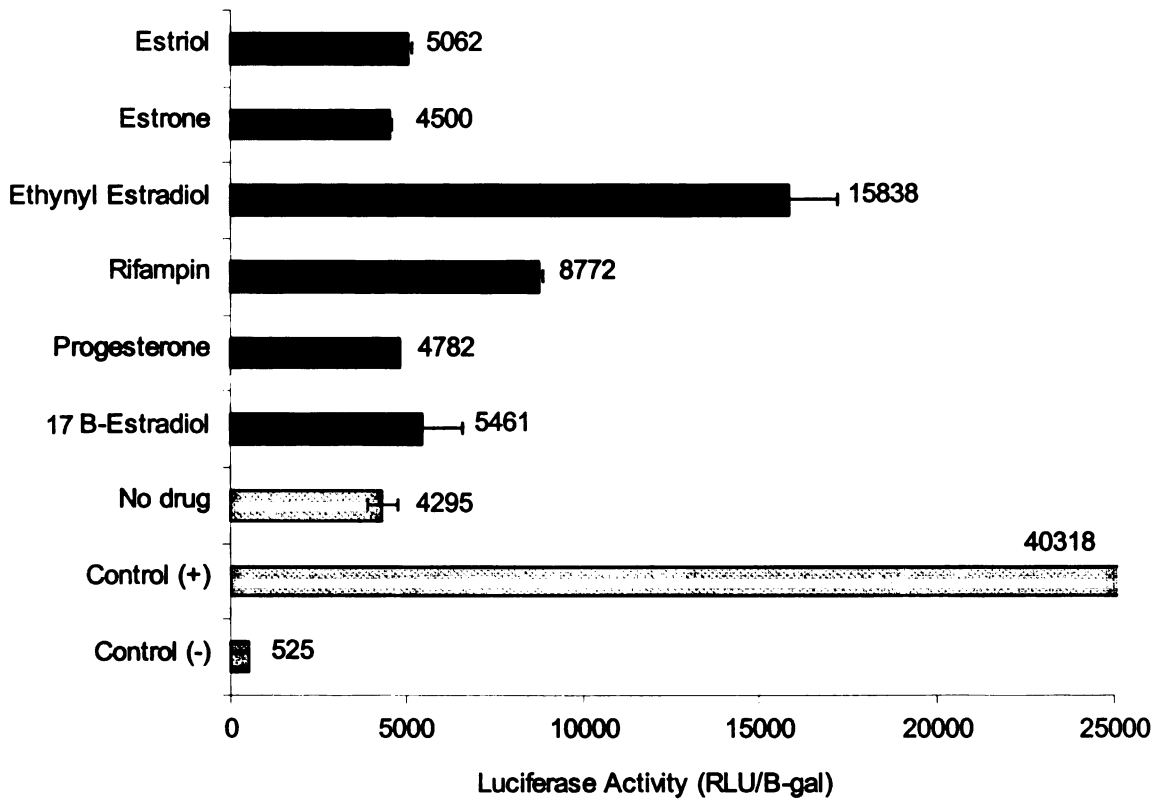

In Figure 2.11, investigation of P-gp regulation was done by examining the potential for transcriptional activation of the *MDR1* promoter by various sex-steroid hormones at 10

μM in LS180 cells. A 4-kb section of the *MDR1* promoter region was inserted into the pGL3 reporter gene plasmid and transfected into cells that were induced with hormones. After 72 hours, cells were harvested and analyzed for luciferase and β-galactosidase activity. We observed that rifampin, a known inducer of P-gp expression transcriptionally activated *MDR1* approximately 2.0-fold compared to control, while ethynyl estradiol also significantly stimulated *MDR1* transcription 3.7-fold. β-Estradiol, estrone, estriol and progesterone (all 10μM) did not seem to significantly activate *MDR1* transcription at 1.3, 1.0, 1.2 and 1.1-fold increases compared to control, respectively.

Figure 2.12 Fold Activation of luciferase activity by 10 μM steroid hormones.

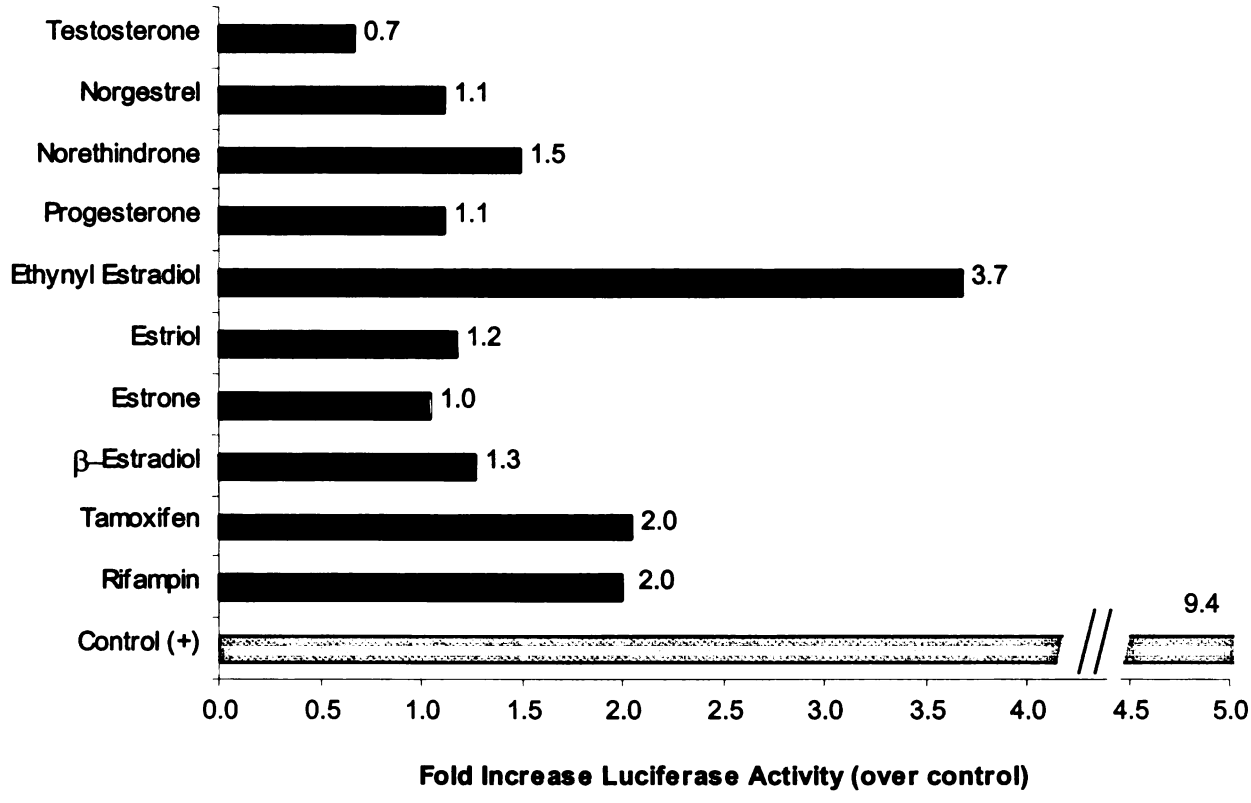

In Figure 2.12, several more steroid hormones were tested for the ability to transactivate the *MDR1* promoter. The synthetic progestin derivative, norethindrone, commonly used in oral contraception was able to transcriptionally activate *MDR1* at a 1.5-fold increase compared to no drug control. Tamoxifen, an anti-estrogen, also transactivated *MDR1* to a similar extent as observed with rifampin. However, testosterone and norgestrel, another synthetic progestin derivative, showed no significant transactivation at the 4-kb upstream promoter region of the *MDR1* promoter compared to no drug control. This suggests that the induction observed at both the protein and mRNA level by these hormones may be caused instead by an alternate binding site, or hormone response element further downstream than the 4-kb section we analyzed. These studies also suggest that the mechanism by which ethynyl estradiol, tamoxifen and possibly norethindrone mediate activation of the *MDR1* promoter may be similar to that of rifampin via the PXR/RXR activation complex. However, the mechanisms of *MDR1* transactivation and induction still remain largely unknown.

2.4.4 Stimulation of P-gp ATPase activity

Active transport of compounds by P-gp is mediated by energy derived from the ATP hydrolysis to ADP and inorganic phosphates (P_i). In order to measure P-gp specific ATPase activity, a baculovirus expression system transfected with human P-gp cDNA was used (Gentest). The *MDR1*-expressing recombinant baculovirus was constructed by co-transfection of Sf9 cells with Bsu36I digested AcMNPV genomic DNA and the pBacPAK9 transfer vector with the human *MDR1* cDNA inserted in a BamHI site. The cDNA encodes six histidine residues at the N-terminus.

It is unknown whether sex-steroid hormones can stimulate vanadate-sensitive P-gp ATPase activity. Therefore, the following steroid hormones were tested: 17β-estradiol, progesterone, testosterone, estrone, estriol, ethynyl estradiol, norgestrel and norethindrone. Several anti-estrogens including tamoxifen, metabolites of tamoxifen, droloxifen and toremifine were found to stimulate P-gp ATPase activity, in certain cases with potencies near that of verapamil (144). Clomifene, nafoxidene, diethylstilbestrol and progesterone were also found to act as P-gp ATPase stimulators, suggesting direct interaction with P-gp, thereby interfering with its cytotoxic extrusion activity.

Figure 2.13 Stimulation of P-gp ATPase activity by progesterone (—▲—) and ethynyl estradiol (--- ● ---).

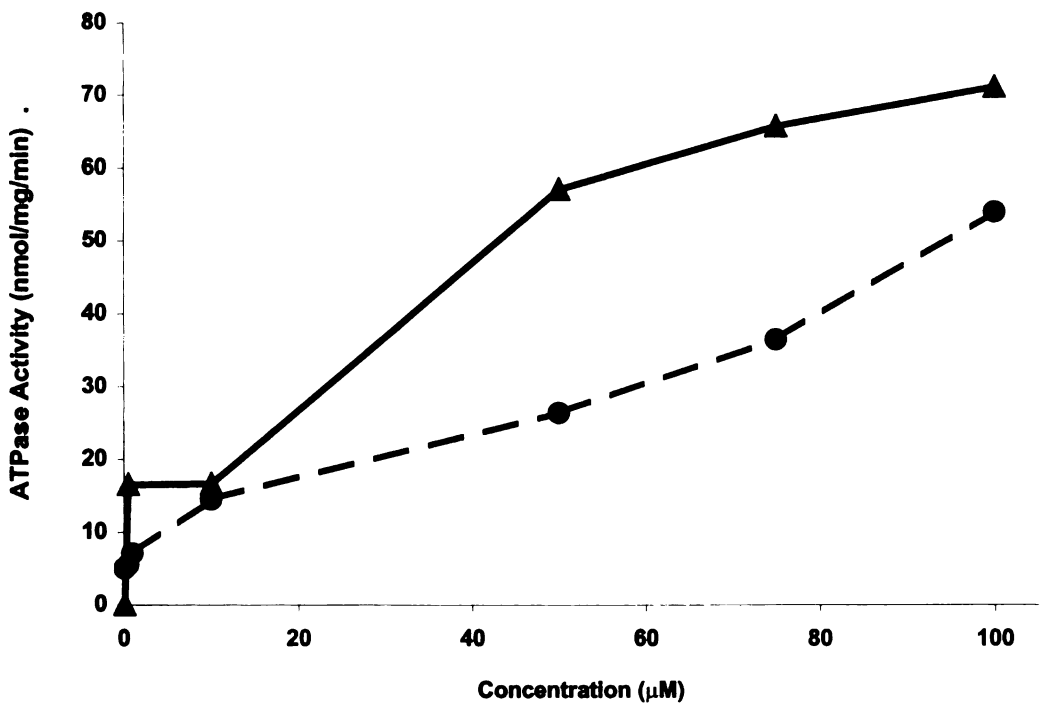

Figure 2.13 demonstrates the concentration-dependent stimulation of vanadate-sensitive ATPase activity of P-gp by progesterone and ethynyl estradiol over a range of 0.1 μM to100 μM. The P-gp ATPase activity was measured in membranes of Sf9 insect cells transfected with a recombinant baculovirus containing *MDR1* cDNA used with appropriate control membranes. Verapamil was used as a positive control as it is a known substrate of P-gp as well as a potent stimulator of P-gp ATPase activity. Each data point is the average of duplicate determinations.

Other steroid hormones that were also tested include 17β-estradiol, estrone, estriol, norethindrone, norgestrel, 6α-methyl hydroxy progesterone (MPA) and testosterone. Of these, norethindrone, testosterone and 6α-MPA exhibited potent stimulation of P-gp ATPase activity in a concentration-dependent manner, similar to that for progesterone and ethynyl estradiol. Estrone, estriol and norgestrel also stimulated P-gp ATPase activity, but to a lesser extent, demonstrating activity at an average of ~10 nmol/mg/min.

2.5 Discussion and Conclusions

Studying the integral elements that dictate the role of P-gp in major drug-eliminating organs (i.e. intestine, liver) is essential for better understanding the absorption and elimination of many administered drugs and hormones prevalent in women's health. We hypothesize that steroid hormones and both their natural and synthetic metabolites can modulate the expression and function of P-gp. This in turn can affect the pharmacokinetics and bioavailability of drugs that are substrates for P-gp in women.

Of importance to our hypothesis, P-gp expression and function has been found to vary with ovulatory function and phase. The highest levels were found during the midluteal phase of the menstrual cycle, when estrogen and progestin levels peak (111). Studies in rats demonstrate highly increased levels of mdr1-type P-gp RNA in the luminal and glandular epithelium of uterus and placenta during pregnancy (115). In mice, the levels of P-gp expression parallel that of progesterone in the serum, peaking during days 15-17 of gestation, then declining (116). Furthermore, *mdr1* expression was induced by the combination of β-estradiol and progesterone in the secretory epithelium of the uterus (86). Piekarz *et al.* (145) demonstrated that a progesterone agonist, acting through the A form of the progesterone receptor (PR_A) was able to increase expression of the *mdr1b* gene approximately 3-fold in T47D cells that were co-transfected with an expression vector for the A form of the progesterone receptor, but not the B form. As P-gp is also found in human placental trophoblasts and in human secretory and gestational endometrium (111), these observations suggest possible interactions between P-gp and steroids in humans. Therefore, an *in vitro* investigation of the physiological interaction between the ingested hormone-drug and simulated model cell system was carried out.

Our studies have shown that various sex-steroid hormones can induce *MDR1* mRNA expression in a time and concentration-dependent manner in the LS180 colon carcinoma cell line, establishing it to be a suitable model for intestinal *MDR1* induction. These hormones include both endogenous (17β-estradiol, estrone, estriol, progesterone) and synthetic hormone derivatives (ethynyl estradiol, norethindrone, norgestrel, 6α-MPA) commonly used in oral contraception and hormone replacement therapies. Induction at

the mRNA level was also observed at the protein level for nearly all of the steroid hormones, except for the synthetic progestin, 6α-HPA, albeit at higher concentrations than observed *in vivo*. The slight decrease in P-gp expression observed in HepG2 cells in the presence of only 17β-estradiol and progesterone, compared to the increase in P-gp expression observed in HepG2 (compared to control) when also induced in the presence of hGH alone or with dexamethasone, suggests that the presence of estrogen receptors as well as the combination of both β-estradiol and progesterone may be necessary for inducing P-gp.

Endogenous peak serum estrogen and progestin concentrations in normal, premenopausal women have been observed for estradiol at 1.5 nM, estriol at 10 nM, estrone at 1 nM and progesterone at 40 nM. Since these estrogens are highly bound to plasma proteins such as albumin and SHBG (sex-hormone binding globulin) at a range from 50-99%, serum concentrations of unbound or free estrogens can be determined from serum hormone and plasma protein concentrations. Estradiol is protein bound to SHBG at 37% and albumin at 61% for a total bound fraction of ~98%. Hence, the unbound fraction for circulating estradiol is determined to be approximately 30 pM. Unbound concentrations of estriol range from 1.3-2 nM, while estrone is ~ 20 pM. Maximum serum concentrations of synthetic steroids from low-dose oral hormone therapies were measured at 15 nM for norgestrel (100 μg dose), 47 nM for norethindrone (1 mg) and 0.3 nM for ethynyl estradiol (10 μg) (146-148). Unbound plasma concentrations of these various synthetic steroids typically range from 0.01-20 nM. Despite low unbound circulating concentrations, these hormones are significantly potent. Our studies show *in vitro*

induction of *MDR1* mRNA by various steroids at concentration ranges that are albeit higher, but significantly low enough to suggest *MDR1* mRNA induction may very well be observed *in vivo*.

Rifampin, used as a positive control, has been shown to transcriptionally induce *MDR1* by binding a PXR response element (DR4 motif) in the upstream enhancer region of the *MDR1* gene (142). Our data in hormone-induced LS180 cells transfected with a pGL3 plasmid vector containing a 4-kb section of the upstream promoter region of *MDR1*, demonstrated 2-fold (over no drug control) transcriptional activation of the *MDR1* promoter by both 10 μM rifampin and tamoxifen, a 1.5-fold activation by 10 μM norethindrone and a 4-fold activation by 10 μM ethynyl estradiol. One can speculate that the mechanism of *MDR1* induction by these steroid hormones may be similar to that of rifampin (via PXR) or possibly by other hormone response elements (e.g. ERE) present in the upstream promoter region of the *MDR1* gene.

It was originally believed that stimulation of P-gp ATPase activity was a direct reflection of its drug transport capabilities. However, although many drugs have been shown to stimulate the P-gp ATPase activity, certain drugs have been shown to bind tightly to the drug-binding sites of P-gp without eliciting ATP hydrolysis. Using ATPase activity assays, ethynyl estradiol, progesterone, testosterone, norethindrone and 6α-MPA were all found to significantly stimulate P-gp ATPase activity in a concentration-dependent manner. These results suggest direct interactions of steroid hormones with P-gp and perhaps functional regulation to some degree. Progesterone is known not to be a substrate

of P-gp, but our studies show that it can stimulate P-gp ATPase activity, suggesting it to be a potent competitive inhibitor. It is yet to be determined whether ethynyl estradiol is also transported by P-gp. However, estrone, estriol, norgestrel and β-estradiol did not have the potent capability to significantly stimulate P-gp ATPase activity, suggesting weaker interactions, but not negating the capacity for transport.

While the physiological interaction between steroids and P-gp is poorly understood, efforts have been made to probe this relationship. Our studies show that various female steroid hormones, both natural and synthetic, can induce P-gp and *MDR1* mRNA expression in the LS180 intestinal cell line, indicating significant potential for altering absorption of P-gp substrate drugs in women, perhaps during the ovulatory cycle or concomitant hormone therapy. Furthermore, several of these hormones were also able to activate transcription at the *MDR1* promoter with implications that those that did not may require a more downstream promoter site that was not included in our plasmid vector. Insight into the physical interaction between P-gp and steroid hormones was revealed with the discovery that many steroid hormones were able to significantly stimulate P-gp ATPase activity. These experiments give further evidence that steroid hormones can modulate P-gp expression and activity, giving clues to comprehend the mysterious and intricate relationship between steroids and multidrug resistance.

CHAPTER III

Bi-directional Transport of Sex-Steroid Hormones[2]

3.1 Objective

To understand the intricate relationship between steroid hormones and P-gp better, the following *in vitro* studies were carried out to determine whether sex-steroid hormones are substrates of P-gp. In examining the potential for hormones to be subject to P-gp mediated transport, evidence gained from our studies will help to identify potential drug-drug interactions, especially for synthetic steroids used for oral contraception and hormone replacement therapy. This will contribute to current knowledge on the effect of fluctuating endogenous steroids during the ovulatory cycle on P-gp activity. These studies were carried out in an established bi-directional transport system involving *MDR1*-transfected MDCK (Madine-Darby Canine Kidney) cells that over-express human P-gp/*MDR1*, and also in control MDCK cells. The potent and specific P-gp inhibitor, GG918 was experimentally utilized to examine and confirm substrate selectivity of P-gp for hormones. Intracellular concentrations were also measured for hormones that exhibited active efflux to confirm P-gp function and transport.

[2] This chapter was published in part within a manuscript entitled, "P-glycoprotein (P-gp/*MDR2*) Mediated Efflux of Sex-Steroid Hormones and Modulation of P-gp Expression *In Vitro*." by W.Y. Kim and L.Z. Benet, *Pharm Res* 21:1284-1293 (2004).

3.2 Introduction

It has been postulated that P-gp, which is highly expressed in the adrenal gland (149-151), may play an important physiologic role in regulating intracellular steroid concentrations. Earlier studies have suggested that P-gp may function to actively secrete steroid hormones, precluding toxic accumulation of intracellular steroid levels (134). It should be noted that several adrenal steroids such as cortisol, aldosterone and dexamethasone were found to be actively transported by P-gp (27, 28, 133), while progesterone and several of its natural metabolites (132), although not P-gp substrates, were discovered to be potent P-gp inhibitors. In fact, numerous studies have shown that progesterone blocks P-gp mediated efflux of other steroids and P-gp substrate drugs and is capable of reversing drug resistance in P-gp expressing cells (152, 153). Although estradiol (E_2) is not transported by P-gp (154), estradiol and diethylstilbestrol (DES) induced P-gp and decreased accumulation of intracellular adriamycin, causing drug resistance (155). It is likely that steroid transport by P-gp is linked to the hydrophobic nature of steroids. It has also been suggested by Barnes *et al.* (152) that the phosphorylation of P-gp modulates P-gp-steroid interactions and may also be responsible for the steroid-induced antagonism of P-gp mediated transport observed for some steroids such as progesterone and its derivatives (e.g. methylhydroxyprogesterone acetate, 16 α-methyl progesterone). Hence, both transport and antagonism may be dependent upon steroid hydrophobicity.

We sought to determine whether female sex-steroid hormones, their natural metabolites and synthetic derivatives were substrates of P-gp so as to identify potential interactions between hormones and P-gp substrate drugs. In order to do this, Madine Darby Kidney (MDCK) cells, a dog renal epithelia cell line, were transfected with an *MDR1* cDNA to overexpress human *MDR1*, and grown as monolayers on cell culture Transwell inserts (156). For directional transport to occur, these cells form tight junctions and grow in a polarized fashion so that the basolateral membrane faces and attaches to a supporting surface such as a petri dish or a polycarbonate filter membrane (used in our studies) on which they are grown, and the P-gp expressing apical side of the cell faces the growth medium. This mimics the gut lumen where epithelial cells grow in a polarized fashion with the brush-border membrane of intestinal mucosa apical side facing the lumen and the basolateral side exposed to capillaries in the gut interstitium. When grown to confluency, a monolayer of epithelial cells, with differentiated tight junctions, form a selective permeability barrier through which only water and selected solutes and compounds can cross by transcellular passive diffusion. Compounds can also pass through cells via two types of membrane transport proteins, carrier and channel proteins present within the cellular membrane (157). Tight junctions mitigate the opportunity for compounds to pass between cells through the paracellular route.

Different cell lines regulate the P-gp transporter based on culture conditions including, growth factors in the medium, the surface structure to which cells attach, and intracellular transcription factors (158). Although many transport studies have been conducted in the Caco-2 human intestinal cell line, the time required to reach confluency (21-28 days) and

for P-gp to become fully functional (17-27 days) places it at a disadvantage for high through-put screening of drug permeability transport characteristics (158, 159). Furthermore, variability in phenotype and transporter expression has been noted depending on cell culturing conditions, so that data generated from these cells can be misleading (160). MDCK cells, however, are among the most well-defined epithelial cell lines with respect to lipid composition and protein expression (161). They are characterized by more stable transporter expression and the classical two-chamber transport assay developed with these cells has proven to be a better model with which to study P-gp mediated drug efflux. In this cell transport system, compounds that are substrates for P-gp can bind to P-gp and be actively transported in the basolateral to apical (B→A) direction. Therefore, we investigated the polarized efflux of various steroid hormones in *MDR1*-MDCK cells compared to control MDCK cells.

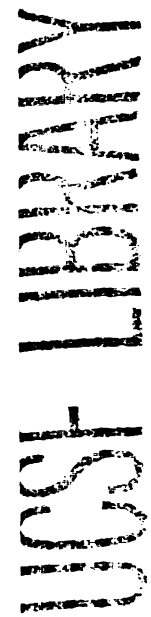

3.2.1 Characterization of MDCK and *MDR1*-MDCK cell lines

Few selected cell culture models have been used in the past for studying transport and are being used today in industry as tools for predicting *in vivo* barrier-passage of compounds. The MDCK cell line was first established in the 1950's, at a time when cryopreservation was not yet available, hence the high passage number (~200) currently used in many studies today. Typical TEER (transepithelial electrical resistance) values that have been recorded are ~200-400 Ω cm^2 for MDCK cells and ~1000-5000 Ω cm^2 for *MDR1*-MDCK cells (162). If seeded at an approximate density of $5x10^4$ cells/cm^2 on polycarbonate membranes, 80% confluence is reached in 2-3 days, plateauing to a stationary growth phase after 6-7 days with a cell density of $5x10^5$ cells/cm^2. When the tight junction

network is established (days 3-4), mannitol permeation tests during the stationary phase have been conducted to determine tightness of cell-cell contact. P_{app} values for mannitol were recorded to be ~$3x10^{-6}$ cm/s for *MDR1*-MDCK cells and ~$4x10^{-7}$ cm/s for MDCK cells (163). Mannitol P_{app} values were ten times higher for MDCK cells, which corresponds with data generated from our studies in which *MDR1*-MDCK cells grow at a faster rate and to a higher density than MDCK cells for unknown reasons, characterized by TEER values ~8-10 times higher in *MDR1*-MDCK cells.

The MDCK cells differentiate into columnar epithelia and form tight junctions within a period of 3-5 days. The *MDR1*-MDCK cell line has been shown to exhibit polarized efflux of P-gp substrates (164-169) with P-gp localization on the apical surface of cells (170). As estimated by Western blotting, P-gp is found to be expressed in two isoforms, migrating at molecular weights of 150 and 170 kDa, with the 150 kDa isoform being the predominant isoform expressed in *MDR1*-MDCK cells (171). MDCK cells are reported to share many common epithelial cell characteristics observed in situ and have been used as a model for intestinal mucosa (163).

3.2.2 Transport experiment set-up

The goal of these studies is to determine whether steroid hormones are actively transported by P-gp. An established experimental set-up that is used in our laboratory consists of the Falcon® horizontal insert system in 6-well plates in which the cell membrane inserts supporting the cell monolayer is placed horizontal between apical (medium within the insert) and basolateral (medium in wells, cradling the insert)

chambers (Figure 3.1). High pore density (HD) translucent polyethylene terephthalate (PET) track-etched membranes are used with a specific 0.4 μM pore density ($1x10^8$ pores/cm^2). They allow for high rates of basolateral diffusion of nutrients and compounds for optimal transport, secretion and binding studies. Prior to experimentation, drug-hormones were solubilized in DMSO (final concentrations are less than 0.05%) and added to cell culture medium to use for "donor" solutions alongside no-drug transport buffer "receiver" controls. Hormones were then added to the donor compartment (either apical or basolateral side) and control transport buffer to the receiver compartment. The final volume for each compartment was 1.5 mL for the apical side and 2.5 mL for the basolateral side.

Figure 3.1 Falcon cell culture horizontal transport system. Inserts used with a companion 6-well tissue culture plate. Adapted from Becton Dickinson technical bulletin for Falcon cell culture inserts.

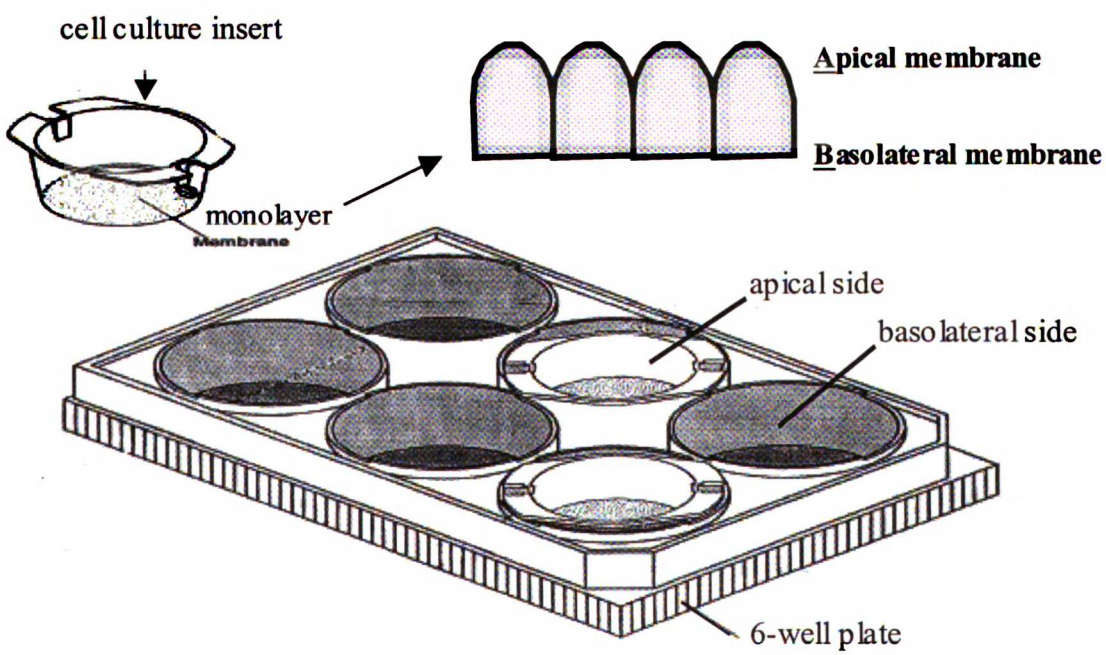

3.3 Materials and Methods

3.3.1 Materials

17 β-Estradiol, ethynyl estradiol (EE), estrone, estriol, progesterone, norethindrone, norgestrel and colchicine were purchased from Sigma Chemical Company (St. Louis, MO). GG918 (GF120918) was a kind donation from Glaxo-Wellcome. The *MDR1*-MDCK and MDCK cell lines were kindly provided by Dr. Ira Pastan (National Cancer Institute, Bethesda, MD). Dulbecco's modified Eagle's medium (DME-H21) was obtained from the UCSF cell culture facility (CCF; San Francisco). Fetal bovine serum, penicillin and streptomycin were purchased directly from UCSF CCF. Trypsin/EDTA solution (0.25% and 0.5%), Dulbecco's phosphate-buffered saline (PBS) and Hanks' balanced salts (HBSS) modified were also purchased from UCSF CCF. Falcon polyethylene terephthalate (PET) cell culture inserts (Becton Dickinson) and their companion Costar six-well plates (Costar Corp.) were purchased from Fisher Scientific (Santa Clara, CA). Acetonitrile (ACN), methanol and ammonium acetate (NH_2-Ac) were obtained from Fisher Scientific.

3.3.2 Cell culture conditions

MDR1-MDCK and MDCK cells were grown in DME-H21 on Falcon cell culture inserts placed into 6-well plates at a seeding density of ~300,000 cells/insert. Colchicine (80 ng/mL) was added to *MDR1*-MDCK cells to select for P-gp expressing cells. Both cell lines were grown to confluence for 3-6 days at 37°C in 5% CO_2 humidity. Prior to a transport experiment, transepithelial electrical resistance (TEER) was measured in each

well to ensure cellular integrity and confluence. Approximate MDCK TEER values measured were 150-300 Ω cm^2, while *MDR1*-MDCK values ranged from 900-1900 Ω cm^2.

3.3.3 Transport experiment protocol

Bidirectional transport across *MDR1*-MDCK and MDCK cell monolayer experiments were conducted as originally described (172) with minor adjustments. After TEER measurements, cells on inserts were pre-washed with Hank's Balanced Salt Solution (HBSS-FH) containing 1% FBS and 22.5 mM HEPES (pH 7.4) and then incubated in a 37°C rocking shaker for 30 min. To measure P-gp mediated transport of selected sex-steroid hormones (B→A), hormone-containing HBSS-FH was added to the basolateral (B) chamber, while HBSS-FH alone was added to the apical (A) chamber of the Transwell insert-plate unit. At the same time, (A→B) was measured via hormone dosing on the (A) side and time point sampling on the (B) side. Each measurement was evaluated in triplicate on up to 3 separate occasions. Cells were incubated in a 37°C shaker and 150 µL aliquots were taken from the receiver side at 0.5, 1 and 2 hour timepoints.

Throughout the experiment, the final volume was maintained at 1.5 mL on the (A) side and 2.5 mL on the (B) side via addition of 150 µL replacement fresh media after aliquot samples were taken. Inhibition of P-gp transport activity was obtained by addition of 1 µM GG918 in the HBSS-FH media (+/- hormone) to both chambers. To measure

intracellular concentrations, cell inserts were immediately removed and washed quickly by dipping twice into 3 separate solutions of ice-cold PBS. Membrane inserts were then air-dried, cut out with a needle and placed into scintillation vials containing 1 mL of ACN:H_20 (70:30, v/v) using tweezers. Vials were sonicated in a water bath for 10 minutes and centrifuged for 10 minutes at 12,000 g. The supernatant was extracted by pipet and analyzed via LC/MS.

3.3.4 Transport calculations

Apparent permeability coefficient values (P_{app}) were determined as follows:

$$P_{app} = (\Delta Q/\Delta t) \div (C_0 \bullet A)$$

where ΔQ is the linear accumulation of drug concentration in the receiver (basolateral) chamber over a time interval (Δt) , C_0 is the initial concentration of the test compounds and A is the surface area of the filter (4.2 cm^2). This coefficient was used to quantify transport of drug molecules from the donor to the receiver side for both apical and basolateral chambers. The transfer of drug was measured as an increase in drug concentration over time. Experiments were performed under "sink" conditions in which drug concentrations in the receiver compartment remained less than 10% of donor compartment drug concentrations. The net efflux of the compound was calculated by taking the ratio of the P_{app} (B→A) over the P_{app} (A→B) values. A minimum net efflux ratio of 2.0 was used as the threshold value to identify P-gp mediated transport.

3.3.5 Analytical methods

All test and hormone compounds were detected and quantified via electrospray ionization interface (ESI) using a Hewlett Packard Series 1100 LC/LC-MSD equipped with an on-line six-port column switching extraction step. The first HPLC system comprises an autosampler with a quarternary pump (G1311A), while the second consists of a selective mass detector (G1946A) and binary pump (G1312). In brief, 50 μL of sample was injected into a MOS Hypersil extraction precolumn (Hewlett Packard). After 2 minutes, samples were backflushed and separation was achieved using a Prodigy 5μ ODS column [50 x 2 mm] via activation of the switching valve. The mobile phase consisted of 2 mM ammonium acetate and 9:1 acetonitrile:H_20. A flow rate of 2 mL/min was used. Using selected ion monitoring (SIM), steroid estrogen ions $(M-H)^-$ were detected in negative ion polarity (NI) while progestins were measured in positive ion mode (PI).

3.4 Results

3.4.1 β-Estradiol

Transport of β-estradiol mediated by P-gp is controversial. Barnes *et al.* (152), examined the effect of P-gp on the accumulation of various [^{3}H] labeled steroids in the multidrug-resistant human colon cell line, SW620 Ad300 subline (P-gp expressing cells induced by Adriamycin) expressed as a percent decrease in accumulation relative to that in the parental SW620 cell line. It was confirmed that progesterone, methylhydroxy-progesterone acetate and androstenedione were not transported by P-gp with no significant decrease in accumulation. However, β-estradiol, and its precursors

dehydroepiandrosterone, testosterone and pregnenolone all exhibited significantly (p <0.01) decreased intracellular SW620 Ad300 accumulation by 28%, 18%, 12% and 14%, respectively. In contrast, Fujise *et al.* (154) showed in LLC-PK cells (porcine kidney cells) transfected with P-gp, that the net transport of β-estradiol was not detectable. Although these results suggest that P-gp can reduce the accumulation of a wide range of steroids, we determined whether β-estradiol was truly a P-gp substrate or not.

17 β-Estradiol was tested for substrate selective transport mediated by P-gp in *MDR1*-overexpressing MDCK cells and control MDCK cells at the following concentrations: 500 nM, 5 μM and 20 μM. We did not observe any significant transport at 500 nM and 5 μM due to quantification detection limits, as characterized by a significantly higher P_{app} B→A value over P_{app} A→B, resulting in a net efflux ratio value greater than 2.0 in *MDR1*-MDCK cells and a net efflux ratio of approximately 1.0 in MDCK cells. However, at 20 μM, we detected active transport of β-estradiol with a significantly higher B→A efflux transport in *MDR1*-MDCK cells than that observed in the A→B absorptive direction (Figure 3.2). Table 3.1 summarizes the apparent permeability values for efflux and absorptive transport directions (B→A and A→ B) as well as the net efflux ratios of 20 μM β-estradiol across *MDR1*-MDCK and MDCK cells, which were 3.5 and 1.0, respectively. Intracellular concentrations were measured as depicted in Figure 3.3, illustrating a significant decrease in intracellular concentrations from both an apical and basolateral dose (35.8% and 68%, respectively) in *MDR1*-MDCK cells compared to control MDCK cells. These studies suggest that β-estradiol is involved in carrier-mediated transport by P-gp.

Figure 3.2 Bi-directional transport of 20 μM β-estradiol across *MDR1*-MDCK and MDCK cell lines.

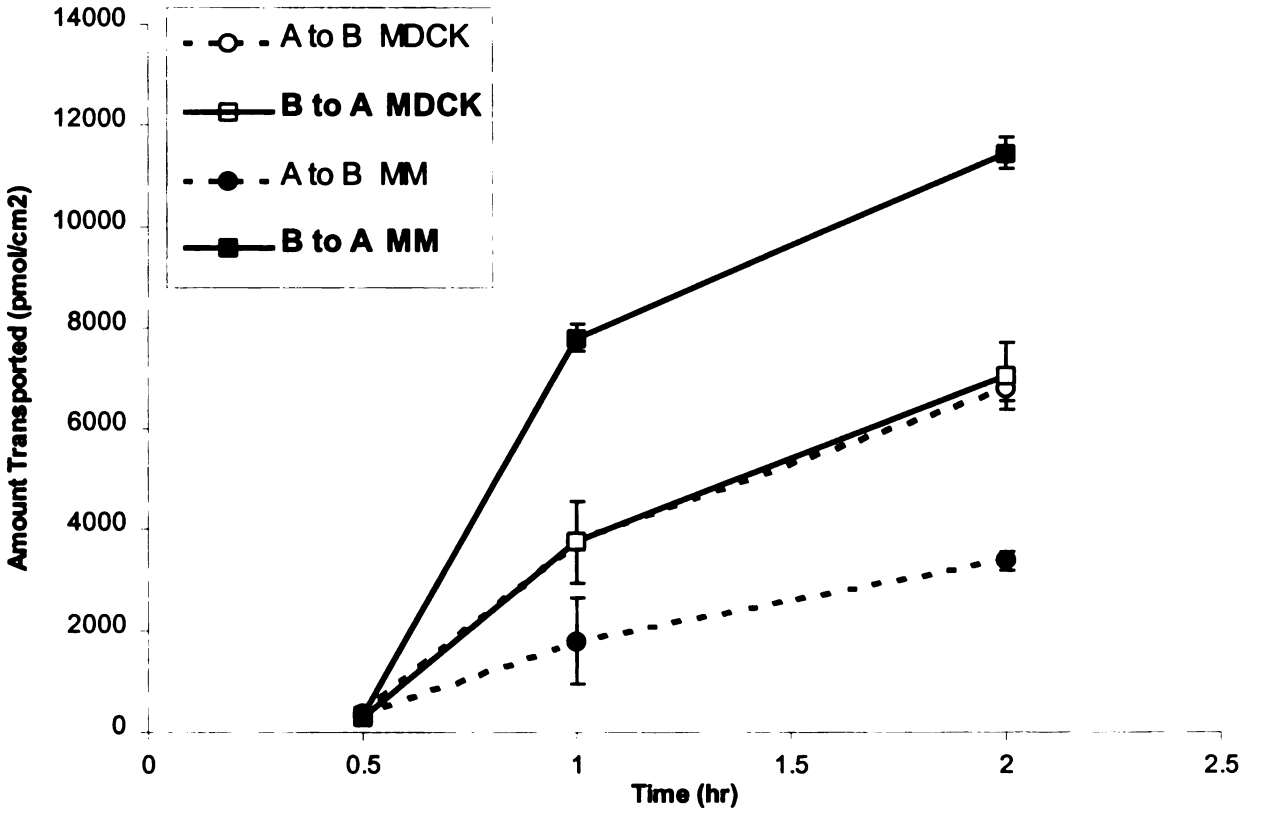

Table 3.1 Bi-directional transport of 20 μM β-estradiol across *MDR1*-MDCK and MDCK cell lines.

	P_{app} x 10^{-7} cm/s (avg ± SE, n=3)		Net Efflux Ratio:
Cell Line	**B→A**	**A→B**	**(B→A/A→B)**
***MDR1*-MDCK**	955 ± 778	273 ± 123	3.5
MDCK	601 ± 133	589 ± 123	1.0

Figure 3.3 Intracellular levels for β-estradiol (20 μM donor side concentration) in *MDR1*-MDCK and MDCK cell lines. Apical to Cell (A to C) measures intracellular levels after an apical dose and Basolateral to Cell (B to C) measures intracellular levels after a basolateral dose. Data are represented as mean ± SD (n=3).

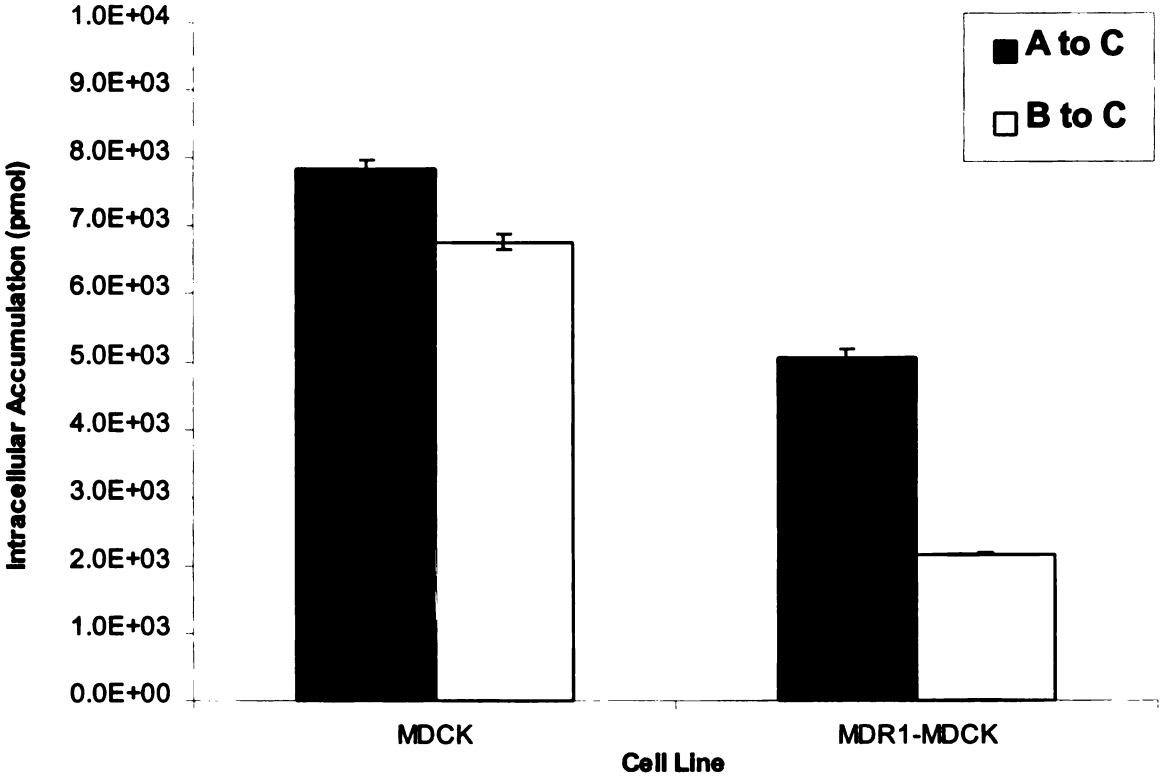

3.4.2 Estrone

Estrone, a naturally occurring metabolite of β-estradiol, was tested to determine whether it is actively transported by P-gp. No prior studies exist in literature showing that estrone is a substrate of P-gp. Hence, bi-directional transport studies were conducted in *MDR1*-MDCK and MDCK cell lines and assessed to determine whether there is active efflux in the B→A direction. Figure 3.4 illustrates the transport of 1 μM estrone across both cell lines, revealing a higher net flux in the B→A direction in P-gp expressing MDCK cells

compared to absorptive flux in the A→B direction. MDCK cells exhibited no obvious changes in either direction. This suggests P-gp carrier-mediated efflux transport into the apical compartment in *MDR1*-MDCK cells. The apparent permeabilities were determined (Table 3.2) with an observed net efflux ratio of 6.6 in *MDR1*-MDCK cells and 0.97 in MDCK cells. The ratio of net efflux values for *MDR1*-MDCK/MDCK is calculated to be 6.8, suggesting that estrone is a good substrate for P-gp.

Figure 3.4 Bi-directional transport of 1 μM estrone across *MDR1*-MDCK and MDCK cell lines.

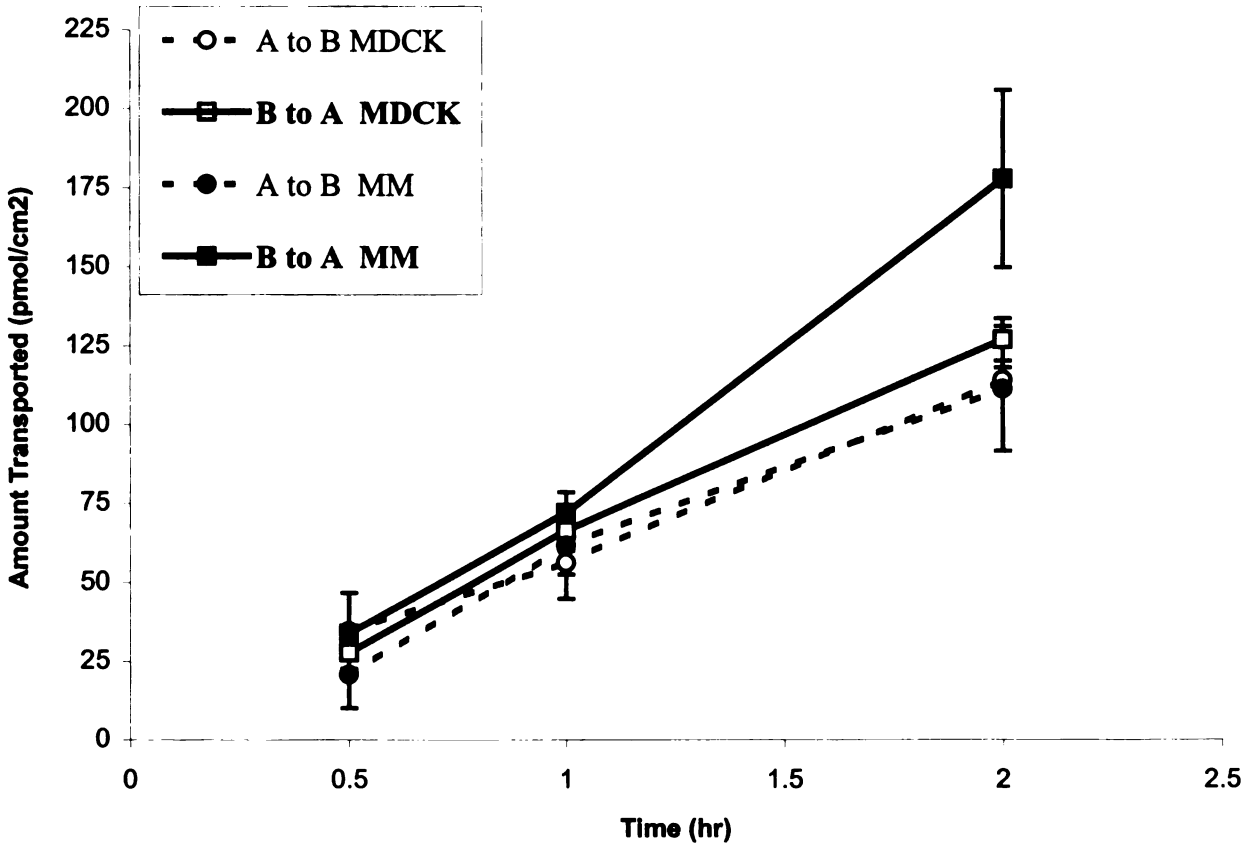

Table 3.2 Bi-directional transport of 1 μM estrone in the presence and absence of 1μM P-gp inhibitor, GG918, across *MDR1*-MDCK and MDCK cell lines.

	P_{app} x 10^{-7} cm/s (avg ± SE, n=3)		Net Efflux Ratio:
Cell Line	**B→A**	**A→B**	**(B→A/A→B)**
***MDR1*-MDCK**	38.7 ± 6.4	5.90 ± 1.39	6.6
+ GG918	7.54 ± 3.34	6.28 ± 3.61	1.2
MDCK	5.90 ± 0.24	6.10 ± 0.38	0.97
+ GG918	6.23 ± 1.65	6.86 ± 1.29	0.91

To confirm that estrone is a substrate for P-gp, the effect of a P-gp inhibitor, GG918 at 1μM, was also tested on transport of estrone across both cell lines (Table 3.2). Results show that in the presence of the P-gp inhibitor, GG918, efflux in the B→ A direction is significantly diminished in the *MDR1*-MDCK cell line. The net efflux ratio (B→A/A→B) was decreased almost 6-fold in the presence of GG918. As expected with a compound that is actively transported by P-gp, there were no apparent effects in the MDCK cell line for either direction and no change in net flux.

Intracellular levels of estrone were measured in both MDCK and *MDR1*-MDCK cell lines (Figure 3.5). Intracellular estrone levels when applied on the apical and basolateral side were significantly decreased in *MDR1*-MDCK cells, suggesting efflux transport. There was a 23.1% and 69% decrease in intracellular estrone concentration from an

apical and basolateral dose, respectively, in *MDR1*-MDCK cells compared to MDCK cells. Higher intracellular uptake was observed to be higher from an apical dose most likely due to easier access to cells (no membrane filter barrier as seen with the basolateral side) allowing for more passive diffusion. This illustrates and confirms the polarized efflux of estrone mediated by P-gp.

Figure 3.5 Intracellular levels for 1 μM estrone in *MDR1*-MDCK and MDCK cell lines. Apical to Cell (A to C) measures intracellular levels after an apical dose and Basolateral to Cell (B to C) measures intracellular levels after a basolateral dose. Data are means ± SD (n=3).

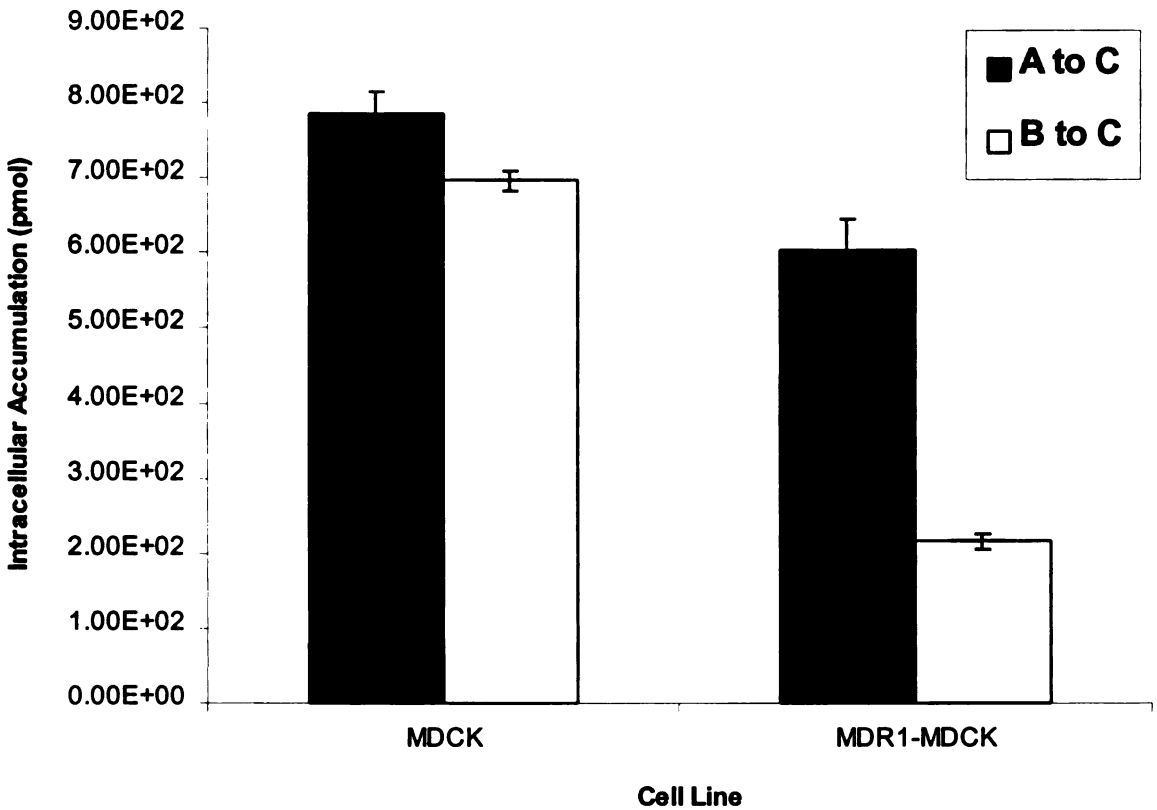

3.4.3 Estriol

To test the selectivity of P-gp transport for estriol, we examined the bi-directional transport of 20 μM estriol across both MDCK control and *MDR1*-MDCK monolayers in our established transport model system. The net transport of estriol across *MDR1*-overexpressing MDCK cells was found to be significantly greater in the Basolateral to Apical (B→A) direction compared to that in the Apical to Basolateral (A→B) direction (Figure 3.6). The overall transport of estriol over time was over 3-fold higher in the efflux direction than in the absorptive direction in the *MDR1*-MDCK cell line. However, no relevant differences in net transport were observed across MDCK cells.

Figure 3.6 Transport of 20 μM estriol across MDCK and *MDR1*-MDCK cell lines.

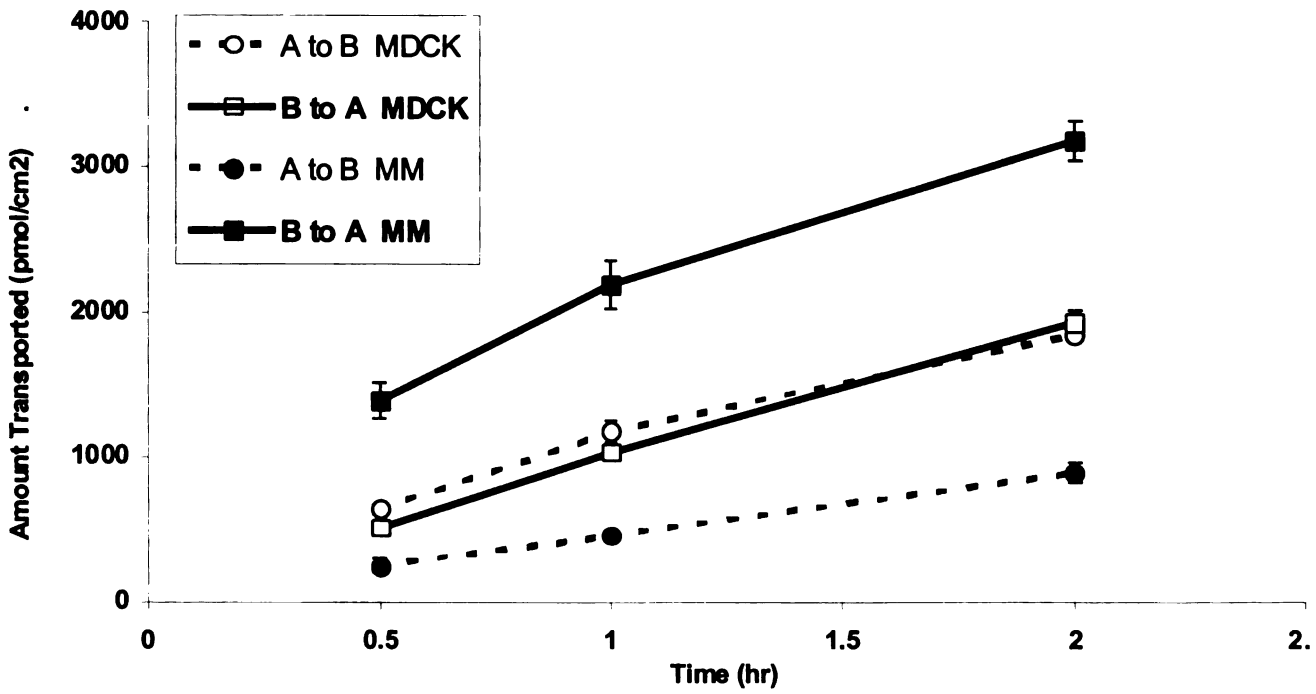

The apparent permeability efflux ratio as calculated (B→A/A→B) was 3.2 in *MDR1*-MDCK, while in MDCK the value was 1.1 (Table 3.3). The higher net efflux ratio observed in *MDR1*-MDCK cells suggests estriol to be a good substrate for P-gp. Figure 3.6 is a representative depiction of the results presented in Table 3.3 for the transepithelial transport of 20 μM estriol across MDCK and *MDR1*-MDCK cell monolayers. Drug was added to apical (A→B) or basolateral (B→A) compartments and sampled on the opposite side at 0.5, 1, 2 h timepoints in 37°C. Each point represents the mean of ~3 monolayers from a typical experiment.

Table 3.3 Bi-directional transport of 20 μM estriol in the presence and absence of 1μM P-gp inhibitor, GG918, across *MDR1*-MDCK and MDCK cell lines.

	P_{app} x 10^{-7} cm/s (avg ± SE, n=3)		Net Efflux Ratio:
Cell Line	**B→A**	**A→B**	**(B→A/A→B)**
***MDR1*-MDCK**	147 ± 10	46.5 ± 19.4	3.2
+ GG918	16.3 ± 7.2	12.3 ± 9.0	1.3
MDCK	112 ± 3	97.5 ± 3.9	1.1
+ GG918	20.0 ± 4.4	13.2 ± 2.1	1.5

Transport of estriol was also tested in the presence of 1 μM GG918 to confirm P-gp-mediated transport. The overall net efflux ratio of the permeability values for *MDR1*-

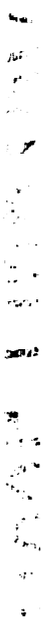

MDCK in the presence of the P-gp inhibitor was decreased 2.5-fold. The flux values in MDCK cells were decreased 6 to 7-fold in the B→A and A→B directions, respectively, but decreased proportionately. Hence, the net efflux ratio in the presence of GG918 demonstrated no significant change. This provides further evidence that estriol is also a substrate for P-gp. Figure 3.7 depicts intracellular levels of estriol that were extracted and measured following the last timepoint (2 hour). The marked decrease in intracellular

Figure 3.7 Intracellular concentrations of 20 μM estriol in MDCK versus *MDR1*-MDCK cells after bi-directional transport indicates active efflux. Apical to Cell describes amount of intracellular estriol after an apical dose of estriol, while Basolateral to Cell indicates the same after a basolateral dose. Solid bars (■) and open bars (□) reflect intracellular measurements in absence and presence of the P-gp inhibitor, GG918, respectively.

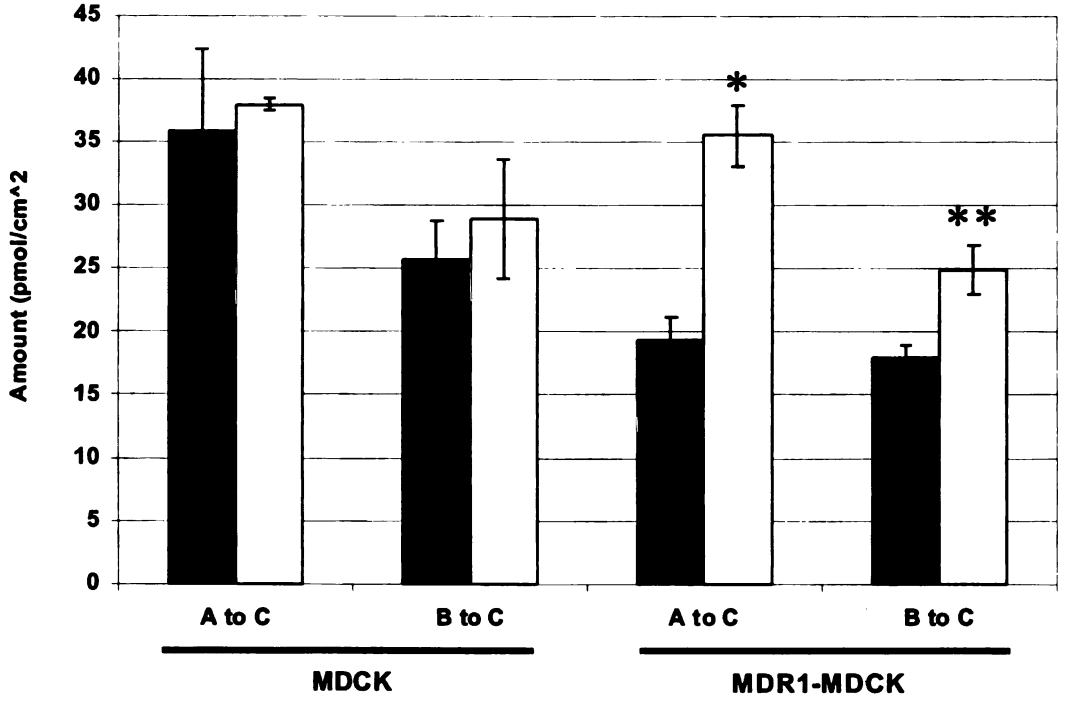

* p<0.001, Statistical difference observed in *MDR1*-MDCK cells (A to C) between cells treated with and those without GG918, using paired, two-tailed t-test.
** p<0.01, Statistical difference observed in *MDR1*-MDCK cells (B to C), as defined above.

estriol levels for *MDR1*-MDCK cells suggest active efflux transport mediated by P-gp. We observed a 46% and 30% decrease from an apical and basolaterally administered dose, respectively. For intracellular concentrations measured in the presence of the P-gp inhibitor, GG918, there was an 81% and 40% increase in intracellular estriol accumulation from an apical and basolateral dose, respectively, in P-gp expressing cells. P-gp inhibition restored intracellular levels close to those observed in control MDCK cells. These studies confirm that estriol is a substrate for P-gp.

3.4.4 Ethynyl Estradiol

Ethynyl estradiol, a synthetic derivative of β-estradiol, was tested for transport by P-gp in the same model transport system as used for the previous compounds. The bi-directional transport (Figure 3.8) that was measured in both *MDR1*-MDCK and MDCK cells showed a significantly higher flux in the basolateral-to-apical (B→A) direction in *MDR1*-MDCK cells. The B→A flux in MDCK cells was significantly lower and non-distinguishablefrom the A→B flux values. The net efflux ratio values as detailed in Table 3.4 show a 13.8-fold increase for ethynyl estradiol transport in *MDR1*-MDCK cells over MDCK cells. In the presence of the P-gp inhibitor, GG18, net efflux ratios were decreased 9.2-fold in *MDR1*-MDCK cells. No change was observed in net flux across MDCK cells in the presence of GG918, further corroborating that ethynyl estradiol is indeed transported by P-gp. Intracellular concentrations of ethynyl estradiol were measured following transport. There were significant decreases of ethynyl estradiol

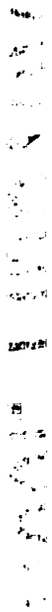

Figure 3.8 Transport of 5 μM ethynyl estradiol.

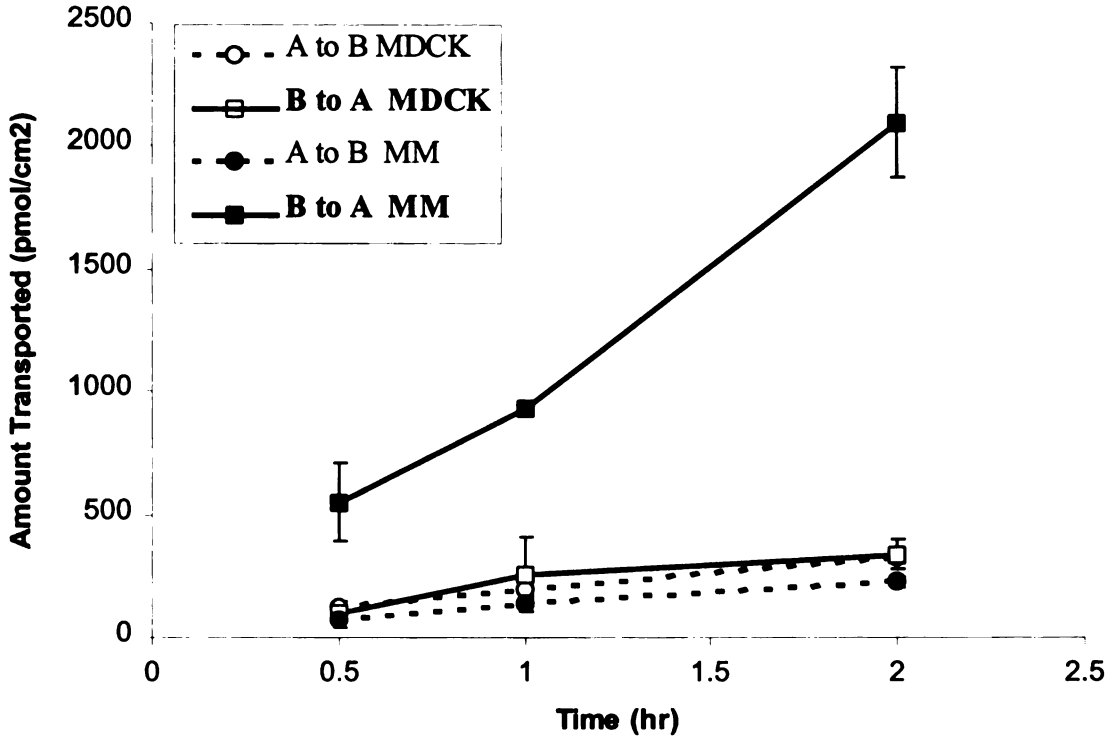

Table 3.4 Bi-directional transport of 5 μM ethynyl estradiol in the presence and absence of 1 μM P-gp inhibitor, GG918, across *MDR1*-MDCK and MDCK cell lines.

	P_{app} x 10^{-7} cm/s (avg ± SE, n=3)		Net Efflux Ratio:
Cell Line	**B→A**	**A→B**	**(B→A/A→B)**
***MDR1*-MDCK**	467 ± 9	41.6 ± 2.2	11
+ GG918	27.6 ± 1.4	22.6 ± 2.5	1.2
MDCK	50.1 ± 0.9	63.3 ± 1.3	0.8
+ GG918	28.5 ± 6.7	27.7 ± 8.9	1.0

Figure 3.9 Intracellular levels of 5 μM ethynyl estradiol in *MDR1*-MDCK and MDCK cell lines.

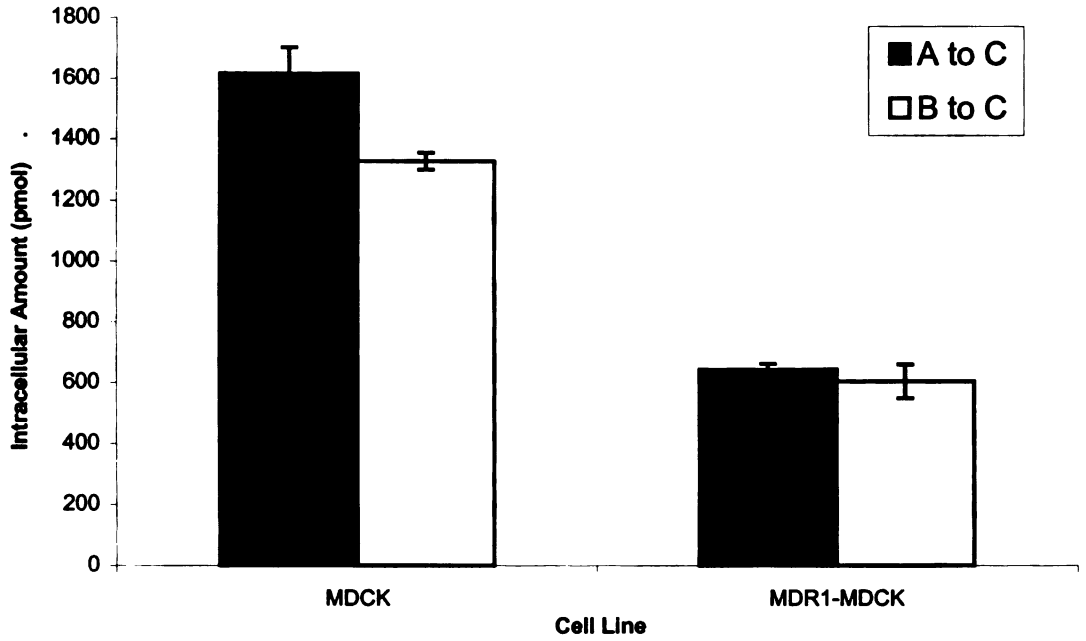

following an apical or basolateral dose in the *MDR1*-MDCK cell line compared to MDCK. We observed a 62% intracellular decrease after an apical dose and a 54.6% decrease following a basolateral dose (Figure 3.9). These experiments provide supporting evidence that P-gp acts to efflux ethynyl estradiol out of cells and that ethynyl estradiol is a substrate of P-gp. The studies are the first to demonstrate that ethynyl estradiol, a commonly prescribed oral contraceptive, is not only metabolized by CYP3A4, but is also a very good substrate for P-gp transport. There are many potential drug-drug interactions that may arise from concomitant administration of other P-gp substrate drugs due to the transporter-enzyme interplay that has proven to have profound impacts on drug absorption.

3.4.5 Norethindrone

Norethindrone, a synthetic progestin derivative used primarily for oral contraception, was tested to examine whether it is a substrate for P-gp. Since norethindrone was able to induce *MDR1* mRNA in a concentration dependent manner, we were curious as to whether there may be a physical interactive relationship as well. Transport of 10 μM norethindrone was examined across both *MDR1*-MDCK and MDCK cell lines in the same manner as for previous compounds (Figure 3.10).

We discovered that norethindrone was not actively effluxed by P-gp as we did not observe any difference in the B→A flux between *MDR1*-MDCK and MDCK cell lines. There was no difference between the B→A flux and A→B flux in the *MDR1*-MDCK cells. However, MDCK cells exhibited higher permeability in the A→B direction, hinting perhaps that norethindrone may be a substrate for an unidentified transporter in MDCK cells since the net efflux ratio is less than 1.0 (Table 3.5). The efflux ratios of the permeabilities for both directions as displayed in Table 3.5, shows the lack of increase in efflux in the B→A direction as is observed for better P-gp substrates. Furthermore, intracellular concentrations of norethindrone after transport were not found to differ between cell lines (Figure 3.11). In fact, there was a slight increase in norethindrone intracellular concentrations following a basolateral dose in *MDR1*-MDCK cell lines. This demonstrates that norethindrone is not a likely substrate for P-gp.

Figure 3.10 Bi-directional transport of 10 μM norethindrone across *MDR1*-MDCK and MDCK cell lines.

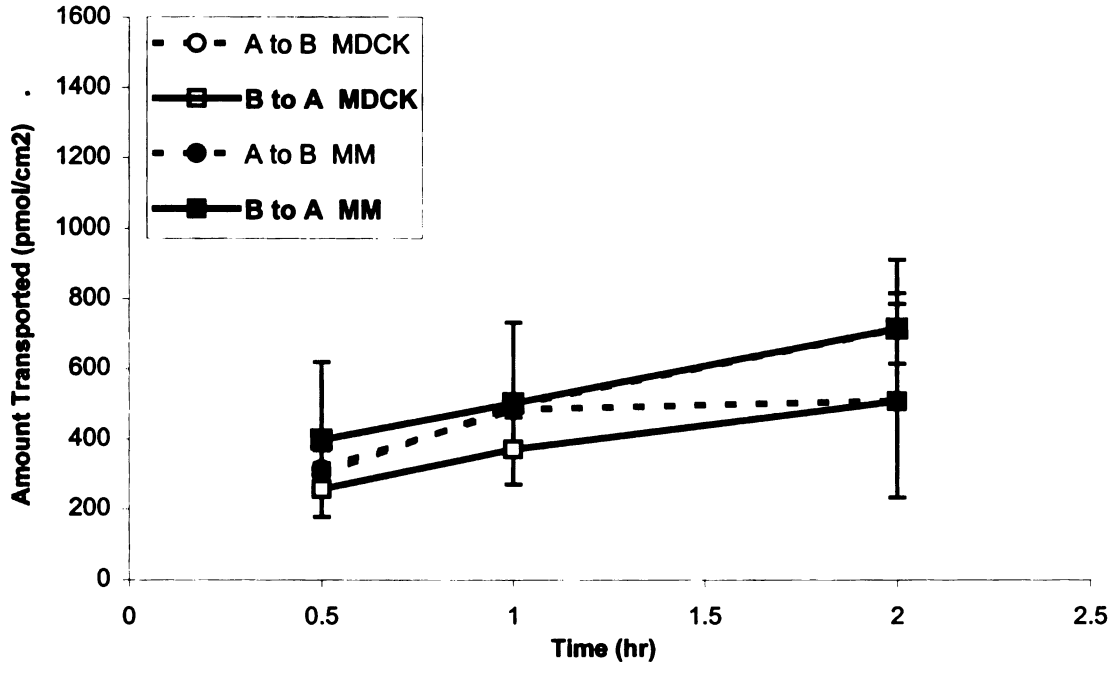

Table 3.5 Bi-directional transport of 10 μM norethindrone across *MDR1*-MDCK and MDCK cell lines.

	P_{app} x 10^{-7} cm/s (avg ± SE, n=3)		Net Efflux Ratio:
Cell Line	**B→A**	**A→B**	**(B→A/A→B)**
***MDR1*-MDCK**	43.8 ± 5.9	33.1 ± 5.2	1.3
MDCK	34.8 ± 6.8	57.3 ± 7.1	0.6

Figure 3.11 Intracellular accumulation of 10 μM norethindrone across *MDR1*-MDCK and MDCK cell lines.

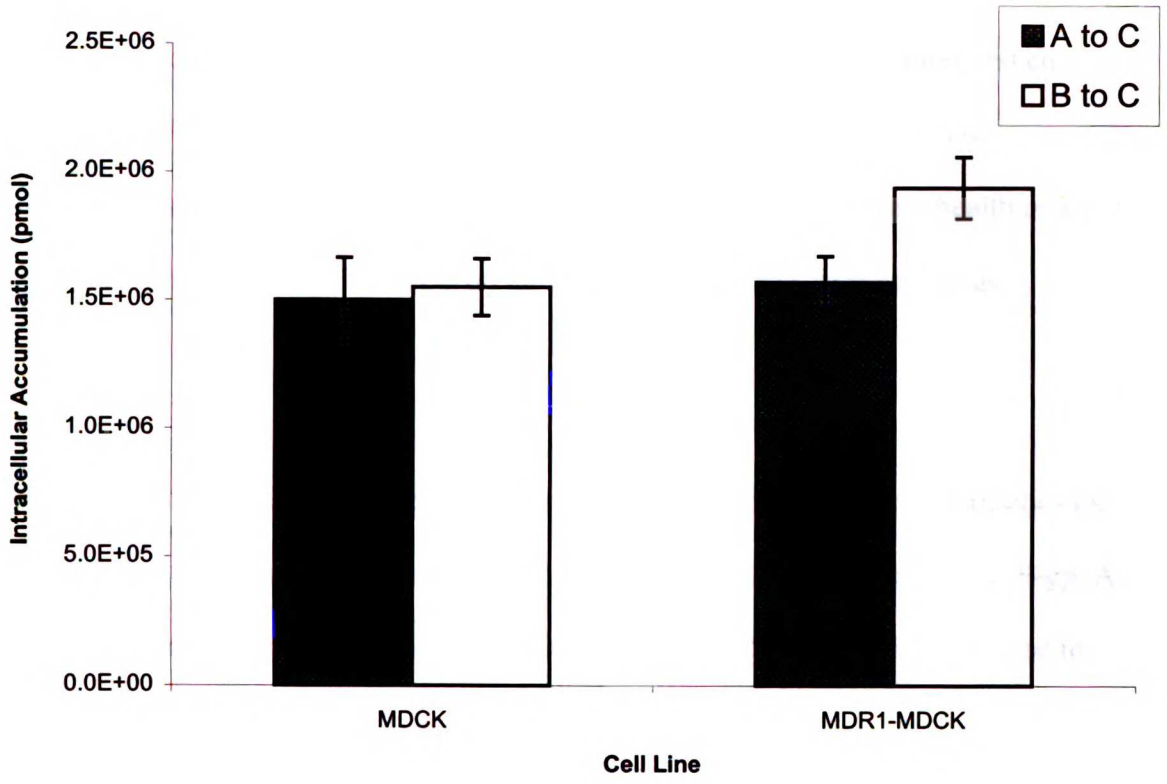

3.5 Discussion and Conclusions

Studying the integral elements that dictate the role of P-gp in major drug-eliminating organs (i.e. intestine, liver) is essential to understand better the absorption and elimination of many administered drugs and hormones prevalent in women's health. We hypothesize that steroid hormones and both their natural and synthetic metabolites can modulate the expression and function of P-gp. This in turn can affect the pharmacokinetics and bioavailability of drugs that are substrates for P-gp in women.

Upon investigation of this hormone-transporter relationship, several estrogens and their synthetic congener, ethynyl estradiol, were found to be transported by P-gp. The results of our studies have significant clinical implications in identifying potential interactions and/or complications between exogenously administered hormone therapies and co-administered P-gp substrate drugs. The discovery of P-gp induction by several endogenous estrogens has also exposed a critical need for more women's health research investigating menstrual cycle effects on the therapeutic efficacy of many drugs transported by P-gp.

A deeper exploration into the interactions between P-gp and these steroid hormones led us to question whether these steroid hormones may potentially be substrates for P-gp. A bidirectional transport system in *MDR1*-MDCK and control MDCK cells was used to measure P-gp mediated active transport of various steroid hormones. Results indicate that 20 μM β-estradiol is transported by P-gp with a net efflux ratio of 3.5 in *MDR1*-MDCK/MDCK cells. Furthermore, its synthetic derivative ethynyl estradiol (10 μM) was also discovered to be a strong P-gp substrate with a net efflux ratio (B→A/A→B) of ~11. Estrone and estriol were effluxed by P-gp substrates with ratios of ~7 and 3, respectively. The addition of the specific P-gp inhibitor, GG918, collapsed the B→A/A→B net flux ratios of these estrogens to ~1. Norethindrone was not found to be transported by P-gp. These results were confirmed by examining the impact of a P-gp inhibitor on transport. Further investigation led us to examine the accumulation of drug intracellularly following transport. Those compounds that were found to be substrates in our established *MDR1*-MDCK and MDCK transport system demonstrated a collapse of the B→A/A→B net flux

ratio in *MDR1*-MDCK cells to a ratio comparable to MDCK cells and revealed significant intracellular concentration decreases in the *MDR1*-MDCK cell line. Our studies show that estrogens, both natural and synthetic, were primarily transported by P-gp.

As progesterone is known not to be a P-gp substrate, it is important to note that the progestin synthetic derivative, norethindrone was also not transported by P-gp. Despite previous differences in the literature, β-estradiol was found to be a P-gp substrate in our studies and in the same way, its successor metabolites, which are equally important in mediating estrogenic effects, are also good substrates. Differences in chemical structure and hydrophobicity between estrogens and progestins may determine the specificity of binding, transport and antagonism of P-gp. Other possible reasons can only be attributed to the promiscuous, yet specific nature of this enigmatic transporter. This is the first report to demonstrate P-gp mediated transport of these synthetic and natural steroid hormones, many of which are known to be widely metabolized by CYP3A enzymes and eliminated thereafter (173-175), but never previously investigated as potential P-gp substrates. These natural estrogens, as well as ethynyl estradiol, can be added to the growing list of compounds that are both P-gp and CYP3A substrates, facilitating a better understanding of the elimination and overall efficacy of hormone therapies in women. Additional studies are necessary to elucidate the complex interaction between transport, induction and the effect they have on each other, not to mention their clinical relevance.

The endeavor to understand the effects of natural and synthetic steroid hormones on the expression and function of P-gp requires further *in vitro* studies investigating the regulation of P-gp at the molecular level. In humans, variations in hormone levels during the menstrual cycle have been correlated with changes in P-gp expression. Hence, the relevance of exploring hormonal effects on the pharmacokinetics of P-gp substrate drugs becomes more significant. The involvement of steroid hormones as P-gp substrates and in the modulation of P-gp expression points to an association between the effects of reproductive hormones on P-gp and potential consequential risks for drug efficacy in women. Thus, further investigations of the interactions between sex-steroids and P-gp substrate drugs are necessary to improve predictions of complications that may compromise therapeutic drug efficacy and better understand the effects of both endogenous and exogenously administered hormones on drug therapy in women.

CHAPTER IV

Ovulatory Cycle Effects on P-gp Expression and Function in HIV+/- Women

4.1 Objectives

In order to identify and address the factors that influence women's health as it relates to HIV/AIDS research, care and treatment, it is imperative to direct the focus of more research into investigating the physiologic distinctions in women. This also includes increased representation and participation of women in clinical research studies. Pharmacologic research in the last decade has revealed sex differences in both transporter and metabolizing enzyme expression, causing scientists to reassess the usual approach to prescribed medicines. To elucidate sex-specific characteristics, specifically the effects of the female reproductive system on the pharmacology of anti-HIV drugs, we implemented a longitudinal, repeated-measures analysis, clinical cohort study in women. In this study, we investigate the effect of hormone changes during the ovulatory cycle on P-gp expression and function, and its modulation of the pharmacokinetics of drugs that are substrates for P-gp. We evaluated the pharmacokinetics of the HIV protease inhibitor (PI) and P-gp substrate, nelfinavir, in both HIV-positive and negative pre-menopausal women of African-American and Caucasian descent. Changes in pharmacokinetics as it relates to menstrual cycle phase were analyzed by examining changes in the distribution of P-gp

expression in the intestinal mucosa, endometrium and lymphocytic blood cells. We hypothesize that the impact of elevated estrogen and progesterone secretion during the luteal phase of the menstrual cycle could augment P-gp expression and activity in the liver and endometrium. As nelfinavir is metabolized primarily by CYP2C19, predominantly expressed in the liver, increased biliary efflux at the canalicular surface mediated by P-gp in the liver will act to limit exposure of nelfinavir to the metabolizing enzymes (CYP2C19) and increase plasma drug levels. Conversely, reduced P-gp expression during the follicular phase (basal progestin and estrogen levels) will lessen hepatobiliary efflux and enhance exposure to metabolizing enzymes, lowering critical therapeutic plasma levels of drug. Hence, we hypothesize that P-gp (*MDR1*) expression and function varies with ovulatory phase, potentially compromising antiretroviral drug therapy in a substrate and enzyme-specific manner. We also aim to determine the effects of ethnicity based on *MDR1* SNP genotype and the presence vs. absence of HIV infection on P-gp expression, as measured by quantitative analysis of P-gp in tissue biopsies, and P-gp function, as measured in peripheral blood mononuclear cells (PBMCs) and the pharmacokinetic profile of the protease inhibitor, nelfinavir.

4.2 Background

The significance of this study lies in the role of the menstrual cycle and its hormonal effects on the efficacy of HIV protease inhibitors (PIs) and other P-gp substrate drugs as related to P-gp expression and function. This is the first study of its kind to evaluate the impact of hormones on multidrug resistance. We postulate that the impact of elevated estrogen and progestin levels may well be limiting effective intracellular concentrations

of PIs in critical HIV sanctuary sites such as the vagina-endometrium, where there is a highly exposed surface area risk for infection during sexual transmission, by upregulating P-gp expression and function. As it is known that development of HIV viral resistance to PIs could be caused by inadequate drug levels, it is very likely that many women may not be receiving adequate treatment at some point.

In the U.S., an epidemic of HIV is developing among women, particularly impacting minority populations. Among women, the Centers for Disease Control and Prevention (CDC) has estimated that African-Americans and Hispanics combined now represent the majority of AIDS cases at 76% (176). AIDS is now reportedly the third leading cause of death for women (aged 24-44) and the leading cause of death for African-American women in this same age group (176).

Treatment for HIV has developed to include a wide spectrum of combination antiretroviral therapy resulting in decreased morbidity and mortality among AIDS patients in North America and Europe (177). Among the most commonly used anti-HIV drugs, HIV protease inhibitors are known to be substrates and inhibitors of P-gp as well as several cytochrome P450 metabolizing enzymes. Other anti-retroviral drugs including non-nucleoside reverse transcriptase inhibitors (NNRTI's) appear to have little interaction with the transport and metabolism of protease inhibitors. The interaction between drug transport and metabolism works to synergistically increase or decrease the absorption and metabolism of PIs in a substrate and site-specific manner. Elucidation of the mechanisms by which sex-steroid hormones influence the activity of P-gp and

metabolizing enzymes is vital in order to further improve the pharmacology of many drugs in women.

Sex-specific effects on P-gp and CYP enzymes still remain largely undefined, but it has been suggested that such effects may contribute to interindividual variation in drug disposition, therapeutic response and drug toxicity (178). Many studies have explored the significance of sex-related differences in the pharmacokinetics and pharmacodynamics of drugs (179-181). Salphati and Benet (182) demonstrated that the basal level of hepatic P-gp expression in male rats was almost half that found in females. In human liver, expression of P-gp was found to be 2.4-fold higher in males compared to females (183). However, female subject liver samples were not identified in terms of menstrual cycle phase. The pharmacologic significance of this difference in P-gp expression may be explained by the hypothesis presented by Cummins *et al.* (181), where lower levels of hepatic P-gp expressed in women appear to elevate intracellular drug concentrations, thereby allowing for higher metabolism and clearance compared to men. However, it remains to be seen whether sex differences will become important enough to elicit adjustments in drug dosing.

It has been shown that steroids can induce P-gp and subsequently alter substrate pharmacokinetics *in vivo*. Lin *et al.* (184) investigated the inducing effect of the steroid dexamethasone on P-gp and CYP3A on the hepatic and intestinal first-pass metabolism of the HIV protease inhibitor, indinavir, in rats. Dexamethasone was able to induce both hepatic and intestinal P-gp, appearing to increase the intestinal metabolism of indinavir,

which is primarily metabolized by CYP3A. We postulate that the combined induction of both transporter (P-gp) and enzyme (CYP3A) in the intestine may have caused a synergistic decrease of indinavir absorption. In the same way, endogenously circulating estrogens and progestins may potentially alter transporter and enzyme expression in various drug-eliminating organs. Estrogen and progestin receptors are known to be expressed in both the intestine and the liver, along with androgen receptors and an abundance of heat shock proteins (90 kD, 70 kD, 27 kD) (185-189). Therefore, it is very likely that the peaks and troughs of estrogen and progestin levels during the ovulatory cycle stimulate a plethora of physiologic cascades and changes in tissue protein expression and function.

Marx *et al.* (190) discovered that progesterone enhanced the sexual transmission of SIV. Vassiliadou *et al.* (191) showed that progesterone significantly inhibited IL-2 mediated upregulation of the HIV-1 coreceptors, CCR5 and CXCR4, on activated T-cells as well as mitogen-induced HIV proliferation. These results suggest that sex-steroids may be able to inhibit HIV-1 transmission, including infection of CD4+ target cells via CXCR4/CCR5 coreceptors. Results from our investigations add a surprising twist suggesting the hypothesis that steroid hormones may in fact be inhibiting HIV by upregulating P-gp. A recent study by Lee *et al.* (108) showed that the upregulation of P-gp at the surface of CD4+ cells infected with HIV-1 demonstrated greatly decreased HIV-1 infectivity and production. An inverse relationship between P-gp and HIV was confirmed by Hulgan *et al.* (192). This reduction of viral infectivity occurred both during the fusion of viral and plasma membranes at subsequent steps in the HIV-1 life cycle.

The research that we present here in this clinical study provides information to help determine whether sex-steroids regulating P-gp can affect mechanisms underlying the sexual transmission of HIV-1.

4.3 Study Design

The study was approved by the Committee on Human Research (CHR) and the General Clinical Research Center (GCRC) at the University of California, San Francisco. It represents project IV of a larger NIH-funded study investigating HIV infection, transmission, disease progression and therapeutic intervention in women. Subjects were recruited primarily from the Women's Interagency HIV Study (WIHS) and the San Francisco Bay area. Prospective subjects were given an initial screening history and physical examination, which included blood and urine tests to verify no new developments in their overall health that could exclude them from the study. Before being accepted to participate subjects gave verbal confirmation and were tested for abstinence from alcohol and drug-abuse pre-study and during. Accepted subjects were informed of the study details, risks and benefits and gave their written informed consent.

Twenty-one HIV-positive and negative African-American and Caucasian premenopausal females were selected from a total screening popuation of 50 (Table 4.1). One individual (subject #0) withdrew from the study mid-phase due to personal inconveniences. There were four separate groups of women based on ethnicity and HIV status: 6 HIV+ African-American, 6 HIV- African-American, 5 HIV+ Caucasian and 4 HIV- Caucasian. Subjects were selected based on the following inclusion criteria: subjects were between 20-47

Table 4.1 Characteristics of premenopausal female study patients.

Patient ID #	Age	Race*	HIV status
2	44	AA	+
5	36	AA	+
7	43	AA	+
9	30	AA	+
11	51	AA	+
12	50	AA	+
4	29	AA	-
8	41	AA	-
13	34	AA	-
21	37	AA	-
17	40	AA	-
19	34	AA	-
1	39	C	+
6	38	C	+
10	49	C	+
18	32	C	+
20	41	C	+
3	23	C	-
14	35	C	-
15	26	C	-
16	32	C	-

*AA= African-American, C= Caucasian

years old; weight must be less than 30% above or below ideal body weight; subjects must be able to maintain adequate birth control during the study, independent of oral contraceptive use; subjects must be on Efavirenz. Exclusion criteria included: subjects with active medical problems; subjects who smoke tobacco; subjects who abuse drugs; subjects who are on birth control pills during study; subjects unable to follow protocol instructions or abstain from alcohol or caffeine throughout the study; subjects with clinically significant elevations in SCr, BUN or LFT's; subjects with Hct <30%; subjects who are taking any protease inhibitors, subjects who are allergic to nelfinavir, subjects on any medications that are known to induce/inhibit P-gp, MRP1, MRP2, CYP3A or CYP2C19 enzymes; subjects unable to understand the consent form.

Each qualified subject completed a total of seven procedures: one initial screening visit, two vaginal ultrasounds with endometrial biopsies, two intestinal endoscopic biopsies and two pharmacokinetic studies with nelfinavir. During the screening visit, in addition to the medical history, physical exam and blood/urine tests, a serum pregnancy test was administered to confirm non-pregnancy. All subjects were selected as "ovulatory" and then admitted to UCSF once during their follicular and once during their luteal phase. They underwent a vaginal ultrasound with an endometrial biopsy, intestinal endoscopy biopsy and a pharmacokinetic study at each phase. The ovulatory cycle for each subject was assessed by history and vaginal ultrasound to confirm that they were in the correct phase during their visit. The phases were defined based on vaginal ultrasound results as shown in Table 4.2. Accurate classification of visits as mid-follicular or mid-luteal phases of the cycle was accomplished by referring to individual subject menstrual cycle history

and scheduling visits during days 6-10 and 19-24, following the onset of menses. The criteria for inclusion in the ovulatory group also included follicular phase FSH levels of <20 mIU/mL, an increase in estradiol between the follicular and periovulatory phases and midluteal progesterone levels of > 5 ng/mL.

Table 4.2 Menstrual cycle phase as defined by vaginal ultrasound.

Phase	**Description**
Early follicular	Thin line endometrial stripe and no dominant follicle (<14mm)
Late follicular	Triple line endometrium and dominant follicle (~14 mm)
Periovulatory	Triple line endometrium and preovulatory follicle (~17 mm)
Early luteal	Isoechoic endometrium with hypoechoic corpus luteum
Late luteal	Isoechoic endometrium with hyperechoic or absent corpus luteum

Following vaginal ultrasound with endometrial biopsy, patients were transported to the UCSF endoscopy unit where an IV line was put in and the endoscopy procedure was performed by a collaborating UCSF gastroenterologist. Those patients with poor venous access had a peripherally inserted central catheter (PICC) line inserted by a radiologist. Subjects either were escorted home following the procedure or stayed overnight at the GCRC. Diet was controlled such that all patients while at the hospital maintained the same low fat diet on each study day. Breakfast, lunch and dinner were provided. Subjects

fasted for at least six hours before the endoscopy and from midnight until three hours after the morning nelfinavir dose administration on the pharmacokinetic study days. During each phase, all subjects were given one oral dose (750 mg) of nelfinavir (Viracept®) with a light snack at 0800 hours, and other necessary medications were taken at least two hours afterward. Study drug was obtained through the Department of Pharmaceutical Services, UCSF Medical Center. An indwelling peripheral venous catheter was inserted asceptically into the forearm vein and blood draw samples (8 mL) were serially collected into heparin-containing green-top tubes at the following times post-drug administration: 0, 0.5, 1, 1.5, 2, 2.5, 3, 3.5, 4, 6, 8 and 12 hours. Whole blood samples were split into two 4 mL aliquot samples, the second served as a back-up, and separated by centrifugation for plasma extraction. Plasma samples were then frozen at -80°C until LC/MS analysis. Extra blood draws were taken for DNA isolation (SNP genotyping) and peripheral blood mononuclear cell (PBMC) isolation.
Patients were allowed to go home following completion of the last 12 hour blood draw.

The risks associated with the endometrial biopsy include temporary discomfort from the biopsy, uterine spasm and bleeding, similar to menstrual cramps. The risks of venipuncture and PICC line placement include temporary discomfort, pain, bruising, swelling, infection and mental anxiety. The risks associated with taking an oral dose of nelfinavir include nausea, diarrhea, vomiting, headache, abdominal discomfort, hepatic enzyme and bilirubin elevations, rash, and taste alterations. There is also a slight theoretical chance that a single dose of a protease inhibitor may cause future viral resistance to this class of medications. The risks of the endoscopy procedure include

discomfort and possible bruising from a needle stick. Allergic reactions to sedating medications may also occur, along with respiratory depression and hypotension, albeit rare. Subjects' vital signs were monitored continuously throughout the procedure. Physical risks from the procedure are sore throat, tooth injury, injury by swallowing tube (rare) and intestinal puncture at the site of biopsy (rare). Serious potential complications (extremely rare) include hospitalization, surgery, blood transfusions, or death.

4.4 Materials and Methods

4.4.1 Materials

Ethanol, phenylmethylsulfonyl fluoride (PMSF), glycogen (Roche), Tris-HCl, EDTA, isopropyl alcohol and chloroform were purchased from Sigma chemical company (St. Louis, MO). The 18s internal standard (universal and classic), RNase-free microcentrifuge tubes (1.5, 0.5 and 0.2 mL) were purchased from Ambion, Inc (Austin, TX). *MDR1* primers were purchased from BD gentest (Woburn, MA). SuperScript OneStep RT-PCR with Platinum TAQ and DEPC-treated H_20 were purchased from the UCSF cell culture facility (CCF). Homogenizing buffer (50 mM Tris-HCl, pH 7.4, 20% glycerol, 2mM EDTA, 1mM PMSF) was pre-made and stored in -20°C. Kontes-Duall Tissue glass tissue grinders (1 mL capacity) were purchased from Fisher Scientific (Santa Clara, CA). Endoscopic biopsy forceps and endometrial biopsy catheters were purchased from the UCSF hospital. For biopsy sample preparation the following were stored in an transport ice box: ice, dry ice, ethanol, pre-labelled cryovials, tweezers, 26-gauge needles, TRIZOL (Gibco-BRL), PBS, petri-dishes, pipetman (1000, 200 and 20 mL), pipette tips and goggles.

4.4.2 Endometrial and intestinal tissue collection

The method of collection for endometrial and intestinal tissue biopsy samples was adapted from Lown *et al.* (193). Preparation for sample collection required an ethanol:dry ice bath for instantaneous freezing of homogenized samples. When endometrial biopsies were taken, the biopsy catheter with tissue sample was emptied into a petri dish and rinsed with PBS to remove excess blood and mucus. Intestinal biopsies were collected using a needle to remove the tissue sample from biopsy forceps. Tissue was then transferred in equal amounts to two chilled homogenizing tubes (one for total RNA isolation and analysis, the other for protein expression analysis) on ice. An aliquot of 800 mL of Trizol along with glycerol (final concentration 250 μg/mL) was added to the tube directed for RNA analysis, and subsequently homogenized on ice. For the tube used for protein expression analysis, 500 mL of homogenizing buffer was added and homogenized with the pestle until the mixture was completely homogeneous. Aliquots from each homogenizing tube were taken and placed into cryovials appropriately labeled with date of collection, tissue type, study ID, patient ID, HIV status, ovulatory cycle phase, and visit number. For protein analysis, aliquots were separated into 4 separate cryovials: 2 x 200 μL (Western blotting) and 2 x 50 μL (BioRad BSA protein assay). For RNA analysis, homogenate was transferred in its entirety to a 1.5 mL microcentrifuge tube for centrifugation (12,000xg for 10 minutes at 4°C) to remove extraneous insoluble material such as extracellular membranes, polysaccharides and high MW DNA. The resulting RNA-containing supernatant was then transferred to a fresh microcentrifuge tube. All samples were then frozen by dipping them into an ethanol:dry ice bath for up to 3

minutes. Tweezers were used to remove the sample, which was placed on dry ice and stored in -80°C until further analysis.

4.4.3 Semi-quantitative RT-PCR

4.4.3.1 RNA isolation

Frozen stored RNA samples were thawed to room temperature and incubated in a water bath between 20-30°C for approximately 5 minutes to allow complete dissociation of nucleoprotein complexes. Chloroform (0.2 mL/ 1mL Trizol) was added and tubes were vigorously shaken by hand for 15 seconds and incubated in the 20-30°C water bath for 2-3 minutes. Samples were then centrifuged for 13 minutes at 13,000xg at 4°C to complete phase separation. Phases consist of a lower red, phenol-chloroform phase, an interphase and a colorless upper aqueous phase. RNA remains exclusively in the aqueous phase.

To precipate RNA, the aqueous phase was transferred to a fresh 1.5 mL centrifuge tube and mixed with isopropyl alcohol (0.5 mL/ 1mL Trizol). Samples were incubated again in the 20-30°C water bath for 10 minutes and centrifuged at no more than 12,000xg for 10 minutes at 4°C. The RNA precipitate formed a gel-like pellet that was visible on the side and bottom of the tube. Supernatant was aspirated and washed with 70% ethanol diluted in DEPC-treated H_20 (1 mL 75% EtOH/ 1mL Trizol) by briefly vortexing and centrifuging at 13,000xg for 2.5 minutes at 4°C. The 75% ethanol supernatant was aspirated and the tube containing the RNA pellet placed in a negative pressure air vent to air-dry (~20-30 minutes). The RNA pellet was not dried out completely, but dried until

the pellet turned clear. To redissolve the RNA, 40-60 μL (depending on pellet size) of RNase-free water was added, incubated in a water bath at 55-60°C for 10 minutes, and mixed by passing the solution a few times through with pipette tip.

The concentration and purity of the isolated RNA sample was measured using a UV spectrophotometer and a nanodrop machine, respectively. For UV detection, samples were diluted 25 and 50-fold and subsequently read at two absorbances: 260λ and 280λ. The purity was calculated by the wavelength ratio: 260λ / 280λ, where a resulting value greater than 1.6 was considered sufficiently pure with minimal undegraded RNA product. To calculate RNA concentrations, the measured wavelength at 260 nm was multiplied by its respective fold dilution. Samples were diluted into 0.5 μg/μL aliquots and frozen to await RT-PCR analysis.

4.4.3.2 Primer design

The gene specific, intron-spanning primer sequence given in Table 4.3 was used for h*MDR1*:

Table 4.3 *MDR1* cDNA primer sequence and base location.

Primer	Sequence	Base Location
Sense	5'- TTTCATTTTGGTGCCTGGCAGC -3'	822-843
Anti-Sense	5'- AGAAGGCCAGCATAAGAT-3'	1358-1377

The expected amplified fragment size was 546 bp. The 18s internal standard (universal) expected amplified product length was 315 bp.

4.4.3.3 One-step RT-PCR

Superscript™ One-Step with Platinum® *Taq* (Gibco-BRL) was used to detect RNA by RT-PCR, in which both cDNA synthesis and PCR were performed in a single tube. Human liver total RNA obtained from Ambion, Inc. was used as a positive control. Integrity of RNA was confirmed by usage of the18S ribosomal internal standard (Ambion). The PCR reaction was performed by thawing of all components including 2x Reaction Mix (Gibco-BRL), Template RNA, *MDR1* (Sense/Anti-Sense) primers, Ambion 18s Primer:Competimer mix, and DEPC-H_20. Individual PCR reaction tubes were prepared on ice, each containing the following in the listed order:

a. 2x Reaction Mix (final concentration: 1x; 25 μL/tube)
b. DEPC-H_20 (50% v/v; 14 μL/tube)
c. 10 μM Sense and Anti-sense *MDR1* primer (0.2 μM each; 1 μL/tube)
d. 0.5 μg/μL Template RNA (2μg; 4 μL/tube)
e. 18s (3:7) 0.5 μg/μL Primer:Competimer (2 μg; 4μL/tube)
g. RT/Platinum *Taq* Mix (1μL/tube)

The final volume was attained by addition of water up to 50 μL. Samples were briefly centrifuged to make sure all components settled at bottom of the amplification tube and analyzed in the PCR Express Thermal Hybaid as depicted in Figure 4.1:

Figure 4.1 RT-PCR cycling conditions for *MDR1* cDNA amplification.

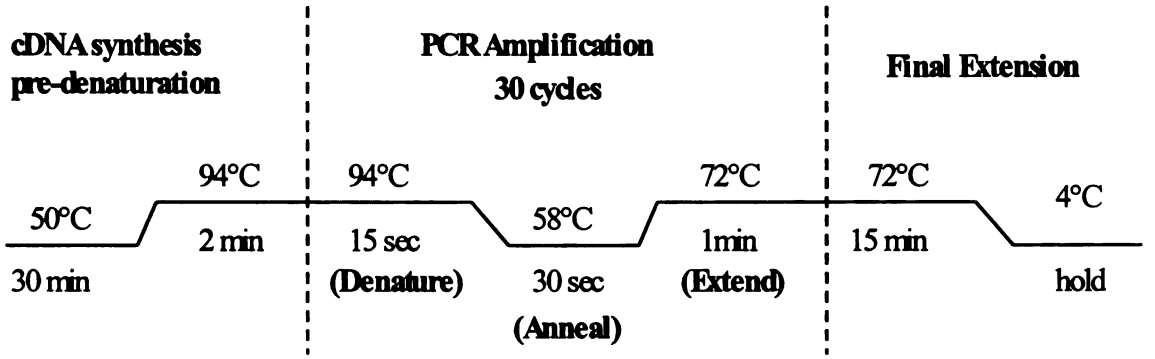

RT-PCR products were run on 2% agarose e-gels. Before loading, samples were kept on ice while e-gels were pre-run at 62 V for 2 minutes. Samples were then diluted (5 μL sample + 15 μL DEPC-H_20) and loaded onto lanes. A 100 bp DNA ladder (7 μL ladder + 13 μL DEPC-H_20) was also loaded in the first lane. Gel was run for 30 minutes at 60 V, immediately viewed under a UV transilluminator and photographed using a UV Polaroid camera.

4.4.3.4 Semi-quantitative analysis

In RT-PCR, an RNA template was copied into a complementary DNA transcript (cDNA) using a retroviral reverse transcriptase. The cDNA was then amplified exponentially using PCR. RT-PCR was utilized to quantitate transcription down to single-transcript-per-cell sensitivity. In theory, only a single copy of cDNA is necessary to be detected by PCR, but approximately one hundred copies is the practical lower limit of detection. In order to compensate for variations in RNA quality, initial quantitation errors, and random tube-to-tube variation in RT and PCR reactions, "multiplex" RT-PCR was used. This involved using a second primer set in a single PCR reaction to amplify an invariant

endogenous control (18s). The level of product from the gene of interest was normalized against the production from the 18s control. In addition, the 18s internal standard utilized competimer technology in which 18s competimers are modified at their 3' ends to block extension by DNA polymerase. By mixing 18s primers with increasing amounts of 18s competimers, the overall PCR amplification efficiency of 18s cDNA can be reduced without the primers becoming limiting and maintaining quantitative abilities.

Polaroid pictures of gels were scanned and captured electronically. Images were imported into the NIH Scion image analysis software and the image inverted for optimal quantification of band density. Pixel band density values measured were subtracted from background values and ratio values were calculated for *MDR1*/18s to normalize for inter-individual lane and technique loading variability.

4.4.4 Western blot

4.4.4.1 Materials

The P-gp antibody, C219, was obtained from Signet (Dedham, MA). The following materials were utilized for Western blotting: QiaShredder (Qiagen), BioRad gradient Tris-HCl polyacrylamide gels (4-20%), PAGE electrophoresis apparatus, PVDF membrane, nitrocellulose membrane, pre-stained broad range protein standard (BioRad), 10x Tris/Glycine/SDS running buffer (BioRad), Laemmli sample buffer, β-mercaptoethanol, microcentrifuge tubes, non-fat dry milk, Tris-HCl, Tris, glycine, NaCl, deionized H_20, Tween-20, razor, transfer cassettes, sponges, filter paper, Saran

wrap, timer, 15 mL Falcon disposable polypropylene conical tubes, ECL reagents (Amersham), Hyperfilm (Kodak) and a Kodak film developer.

4.4.4.2 Western blot method

The presence and expression level of P-gp was detected using Western blot analysis. The protein concentrations of endometrial and intestinal homogenized biopsy samples were quantified using a BioRad assay kit utilizing bovine serum albumin (BSA) as the protein standard. All samples were diluted 1:1 with Laemmli buffer (containing 5% β-mercaptoethanol) and adjusted to obtain a final loading concentration of 100 μg protein. Samples were then immediately transferred to a QiaShredder and spun for 20 seconds at 13,000xg in 4°C. This step ensured more accurate loading by precluding the sample from becoming overly viscous. Samples were then loaded unboiled onto a BioRad gradient Tris-HCl polyacrylamide gel (4-20%) electrophoresis (PAGE) in running buffer (recipe as shown in Table 2.1) at a constant 100V voltage for 90 minutes. The pre-stained SDS broad range marker was also loaded (7μL) in the first lane or last lane.

During transfer, nitrocellulose membrane was soaked briefly in methanol, then in transfer buffer (Table 2.1) for at least 15 minutes at 4°C. Sponges and filter paper were also kept soaking in transfer buffer. Gels were then blotted in transfer buffer along with nitrocellulose, sponges and filter paper overnight at 26V at 4°C. The nitrocellulose membrane was then blocked in 5% non-fat milk at room temperature for 1 hour and then washed twice for 10 minutes in TTBS (Table 2.1) before probing with the primary P-gp

antibody (C219; 1:100 in 1% non-fat milk) for another hour at room temperature. The membrane was again washed with TTBS once for 15 minutes, twice for 10 minutes and then probed with secondary goat anti-mouse horseradish peroxidase (HRP)-conjugated antibody (diluted 1:15,000 in 1% non-fat milk) for 50 minutes at room temperature. Membrane was then washed with TTBS once for 15 minutes and twice for 10 minutes, then the same set of washes repeated with TBS (Table 2.1). Membranes were then taken to the darkroom with a film developer and washed in a mixture of ECL reagents for 1 minute, blotted with Kimwipes, wrapped in plastic and exposed to film that was subsequently developed. P-gp protein was detected with the enhanced chemiluminescence system (ECL- Amersham). The resulting P-gp protein bands ran at an apparent molecular weight of ~170 kDa. Band density was scanned and quantified using the same method described above for RT-PCR.

4.4.5 Calcein-AM assay

4.4.5.1 Materials

The following reagents were used to isolate lymphocytes from normal and HIV-infected blood: Hank's Balanced Salts (HBSS) Ca^{2+}/Mg^{2+} from the UCSF cell culture facility (CCF), Histopaque-1077 from Sigma Diagnostics (St. Louis, MO), Trypan blue stain 0.4% membrane-filtered from Gibco BRL (Grand Island, NY), DMSO from Sigma-Aldrich, FBS from HyClone. The equipment used for PBMC isolation included: 50 mL polypropylene conical-bottom centrifuge tubes, internally threaded cryovials (Nunc), heparinized green-top vacutainers (Becton Dickinson), hematocytometer (Nikon, Japan), pipets (200 and 1000 μL), 5 mL polystyrene round-bottom tubes, glass serological pipets

(10 and 20 mL), Drummond pipet aid, aspirating glass pipet with bulb, goggles, face mask, surgical gown, HIV waste and a Centra-8R ultracentifugation machine (IEC, USA). The following materials were utilized for Calcein-AM uptake in the isolated lymphocytes: PBS with Ca^{2+}/Mg^{2+} from CCF, FBS from HyClone, propidium iodide, GG918, Calcein-AM from Molecular Probes (Eugene, OR), Richter's Modified Improved MEM (IMEM) with Zinc Option containing L-glutamine, L-proline at 2 mg/L, gentamicin sulfate at 50 μg/mL and without phenol red. The antibodies that were used include IgG2a-PE and UIC2-PE, which are IOTest conjugated antibodies purchased from Immunotech (Beckman Coulter). CD56+ antibodies CD56-APC and its isotype control, IgG1-APC, were purchased from BD Biosciences PharMingen. A FACSCalibur (II) flow cytometer was utilized for FACS analysis in the Laboratory for Cell Analysis (LCA) in the UCSF Cancer Research Center.

4.4.5.2 Isolation of lymphocytes

The cell preservation solution was prepared in advance, consisting of fetal bovine serum (FBS) with 10% DMSO. A ready-to-use trypan blue solution was also premade, consisting of 0.04% trypan blue diluted in HBSS. All isolations procedures using blood samples were performed at room temperature as low temperatures could result in cell clumping and poor recovery. Optimal PBMC separation from whole blood was obtained within 2-3 hours of withdrawal.

Whole blood collected in green heparin vacutainers was centrifuged at 1,500 rpm for 10 minutes at room temperature without brake. The upper plasma layer was aspirated and

the bottom layer (red blood cells) was diluted and gently mixed with HBSS (total volume of 20 mL) using serological pipets and the pipet aid. The mixture of red blood cells and HBSS was then transferred to a tube containing Histopaque (15 mL) at room temperature and carefully layered on top without mixing. As Histopaque is toxic to cells, non-mixing of Histopaque and red blood cell mixture will allow for optimal isolation. The layered tube was centrifuged at 2,000 rpm without brake for 25 minutes. The resulting top HBSS layer was aspirated and the middle buffy coat layer (at the HBSS and histopaque interphase) was collected by pipette and mixed with fresh HBSS in a separate tube for washing. The tube was centrifuged for 2,500 rpm at 4°C for 10 minutes, supernatant aspirated and washed again with HBSS by centrifugation at 4°C at 2,500 rpm for 10 minutes with brake. A small aliquot (50 μL) of the suspension mixture was taken before the final centrifugation and diluted 1:1 with trypan blue (50 μL) for staining to count lymphocytes. One to two drops were added to the hematocytometer and the number of viable lymphocytes was counted in two 4x4 chambers via microscopy. The total cell number (***Cc***) was calculated by the following equation:

$$Cc = [(\text{Count}_{mean})/(1\text{x}10^{-4})] \times 2 \times 20$$

Dead cells were subtracted from live from each chamber and averaged to determine the lymphocyte count mean. The derived ***Cc*** value was divided by the original volume of blood obtained (20 mL), giving the volume of cell preservation solution needed in which to resuspend cells in order to obtain a final concentration of twenty million cells/mL. The

cell suspension was separated into 0.2 mL (4 million cells) aliquots in 4 cryovials, slowly frozen to -80°C overnight and stored in liquid nitrogen until use.

4.4.5.3 Calcein-AM accumulation and efflux assay

The functional activity of P-gp was measured by the efflux/retention of intracellular Calcein, a P-gp substrate, from isolated lymphocytes as determined from flow cytometry. Calcein-Acetoxymethyl (Calcein-AM) (Figure 4.2) is a lipid-soluble, fluorogenic, esterase substrate that can passively cross through cellular membranes. Once inside, intracellular esterases cleave Calcein from its acetoxymethyl side group and Calcein is effluxed out in the presence of endogenous P-gp. Higher P-gp function and activity is characterized by decreased intracellular fluorescence.

Figure 4.2 Calcein-AM, a green fluorescent P-gp substrate.

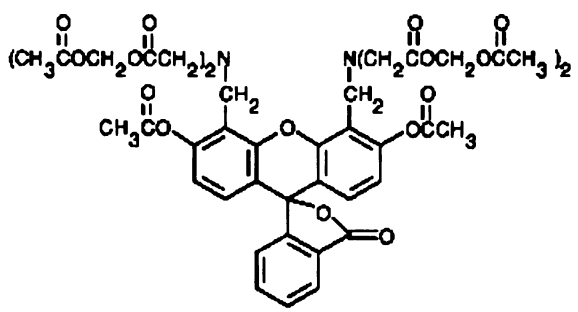

Calcein was preferentially chosen over other fluorescent substrates such as rhodamine 123 for better retention in target cells, low pH sensitivity, no stain transfer leakage among

cells and higher intesnsity of fluorescence signal. Antibodies pre-conjugated to fluorescent molecules were used (Table 4.4). To identify P-gp expressing cells, a phycoerythrin (PE) fluorescent-tagged antibody was used along with an anti-mouse IgG isotype control, also labeled with PE. CD56+ cells were identified by utilizing allophycocyanin (APC)-conjugated antibodies. To separate live cells from dead, propidium iodide (PI) was used as a viability stain, since dead cells allow uptake of PI.

Table 4.4 Pre-conjugated antibodies for P-gp expressing and CD56+ natural-killer cells.

Antibody	**Isotype Control**
UIC2-PE (P-gp)	IgG2a-PE
CD56-APC (CD56+ NK)	IgG1-APC

4.4.5.4 Flow cytometry

A FACS Calibur from the UCSF Cancer Research Center was utilized to analyze cells one at a time as they flow through two laser beams: a 488 nm argon-ion and a 635 red-diode. The method of fluorescence-activated cell sorting allows one to stain, analyze and isolate/sort cells from multiple subpopulations. The lasers analyze multiple physical characteristics of a single cell such as cell size (forward scatter, FCS), granularity (side scatter, SCC) and intensity measured by up to four fluorescent parameters (Table 4.5).

The limit of detection of rare cells is 1 x 10^4. The cells are diluted in sheath fluid before being loaded on, where the cells then pass in a single file down through several laser beams.

Table 4.5 Fluorescent parameter for measuring P-gp efflux in CD56+ and P-gp expressing lymphocytes.

Fluorescent probe	**Channel**	**Emission (nm)**
Calcein-AM	FL1	488
Phycoerythrin (PE)	FL4	525
Allophycocyanin (APC)	FL2	640
Propidium iodide (PI, viability stain)	FL3	617

Physical characteristics of the cell are measured by the scatter caused by the fluorescent light emitted from each cell. Additionally, all pre-conjugated fluorescent antibodies were carefully chosen so that they would be emitted at separate excitation wavelengths and channels to prevent inter-channel bleeding and minimize interference. The goal of our study was to measure and compare P-gp function between ovulatory cycle phase (follicular vs. luteal) through Calcein fluorescent dye extrusion.

4.4.5.5 Calcein-AM assay protocol

Frozen peripheral blood mononuclear cells (PBMCs) were rapidly thawed in a 37°C water bath until a liquid suspension was attained. Cells were washed twice in IMEM with 10% FBS by centrifugation at 1600 rpm for 5 minutes at room temperature. The cells were then resuspended in IMEM/FBS, aliquoted into separate reaction tubes, and allowed to equilibrate for 1 hour at 37°C in 5% CO_2. Those cells designated for Calcein-AM uptake (minus controls) were centrifuged at 1600 rpm for 5 minutes. IMEM/FBS supernatant was aspirated and the cells resuspended in 0.25 μM Calcein-AM with or without 250 nM GG918. Cells were incubated for 20 minutes at 37°C in 5% CO_2 (in dark, under foil). The Calcein-AM uptake reaction was terminated by placing tubes on ice and adding ice-cold IMEM/FBS. All tubes were centrifuged at 1600 rpm for 5 minutes and aspirated to prepare for addition of antibodies. Cells were then incubated and stained with appropriate antibodies and isotype controls for 40 minutes on ice in the dark. Following incubation, the addition of ice-cold PBS with 10% FBS stopped staining and cells were subsequently washed twice in PBS/FBS via centrifugation at 1600 rpm for 4 minutes at 4°C. Samples were capped, stored on ice and analyzed on a FACS Calibur instrument (Coulter). Each sample was spiked with 7.4 μM propidium iodide prior to loading to stain for and exclude dead cells from the chosen population. Data were acquired with a minimum of 3,000 events per sample and gated for CD56+ and PI-negative stained cells. The samples with the P-gp inhibitor, GG918, were normalized to the Calcein-AM only samples in order to determine a fold-difference in intracellular fluorescence caused by the inhibitor.

4.4.5.6 Data analysis

The data for Calcein-AM FACS analysis were collected as median intensity values for all samples. The intensity of Calcein fluorescence for each sample was plotted against cell counts with the following gates: (1) live only (2) live, P-gp and CD56+ expressing cells (3) live, CD56+ only cells. Of these, the gated CD56+ expressing live cells showed the most consistent results and the median Calcein-AM fluorescent values were compared between follicular vs. luteal phase samples in the presence and absence of P-gp inhibitor, GG918.

4.5 Results

4.5.1 Endometrial P-gp expression

Protein and mRNA expression of endometrial P-gp was evaluated using Western blotting and RT-PCR, respectively. *MDR1* mRNA endometrial expression for all patients are depicted in Figure 4.3 as fold induction or percent decrease during the luteal phase over follicular, normalized to the 18s internal standard. Individual study patient results are identified by patient ID number and are also grouped by ethnicity (AA= African-American; CA= Caucasian) and HIV status.

Results show that there was no pattern in induction for any particular ethnic group or based on HIV status. An average 3.2-fold induction of *MDR1* mRNA was observed during the luteal phase over the follicular in the 21 study patients. Grouped by ethnicity, African-Americans exhibited a marked 4.3-fold endometrial induction during the luteal phase over follicular. Caucasians also showed an overall induction of 1.7-fold. Amongst

Figure 4.3 Endometrial *MDR1* mRNA expression in all study patients.

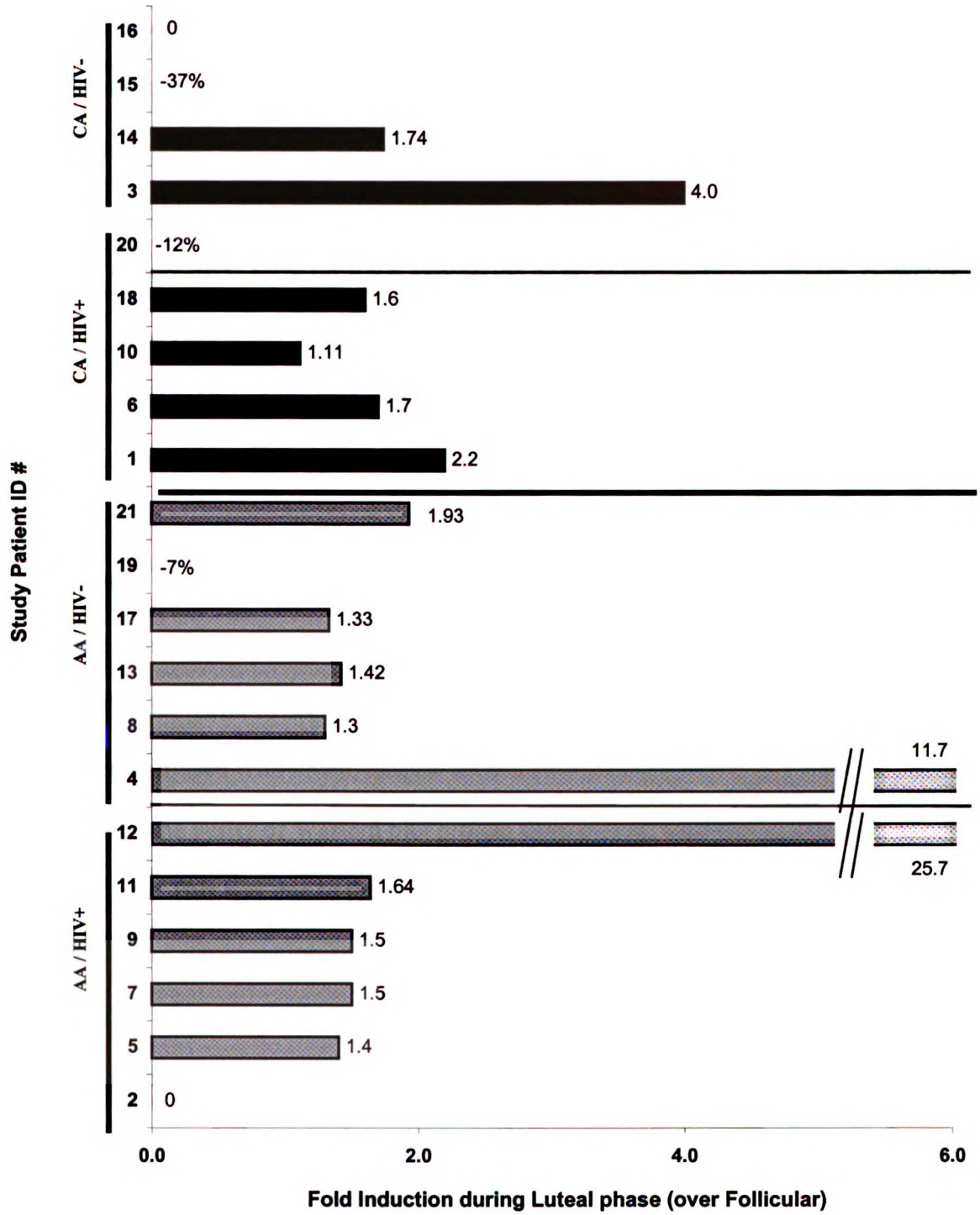

HIV-negative Caucasians, there was a 1.84-fold induction during the luteal phase (over follicular) while in HIV-positive Caucasian females, there was a similar 1.5-fold induction. HIV-negative African-American study patients exhibited a significant 3.1-fold average induction and HIV-positive females of the same ethnicity demonstrated a remarkable 5.5-fold induction during the luteal compared to follicular phase. Of the African-American study subjects, only two patients out of twelve (16.7%) showed either decreased endometrial *MDR1* mRNA expression or no change between phases. However, among the nine Caucasian subjects, 33% of study patients showed decreases with two patients showing lower decreases in endometrial *MDR1* mRNA expression and one patient with no change in expression.

Western blotting of P-gp protein using the specific C219 primary antibody demonstrated no change in expression for all subjects in the endometrium. There were a significant number of endometrial tissue samples, particularly during the follicular phase that were saturated and infused with blood, despite several PBS washes, which may have contaminated the purity of Western blot protein detection by introducing extraneous blood proteins. This was due to the very thin endometrial lining during the follicular phase following menstruation and shedding of the lining, posing a technically difficult task to obtain adequate viable tissue for this less sensitive method. In normal samples, there was no observed change between phases, using a positive control (*MDR1*-MDCK cell line) and a GAPDH internal standard with which to normalize protein expression and account for inter-lane loading technique variability.

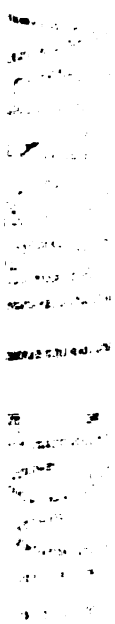

4.5.2 Intestinal P-gp expression

Changes in *MDR1* mRNA expression were investigated in intestinal biopsy tissues to determine whether induction was observed in the presence of peak β-estradiol and progesterone circulating levels during the luteal phase. Intestinal expression of *MDR1* mRNA is shown in Figure 4.4 as a percent decrease or fold induction in the luteal phase compared to the follicular phase. Expression for individual study patients is identified by ID number and grouped by ethnicity and HIV status. Electronic image analysis of pixel band density for all cDNA bands were determined and normalized to its respective 18s internal standard.

Intestinal *MDR1* mRNA expression results demonstrated an insignificant 1.11-fold overall increase during the luteal phase compared to follicular. In the nine Caucasians, we observed an average 1.33-fold induction during the luteal phase (compared to follicular), while in African-American female patients, there was a 4.8% decrease in expression. However, it was curious to note that in Caucasians, the majority of subjects (5 out of 9) demonstrated induction to some degree (up to 4.2-fold), while only 3 subjects showed a significant decrease in expression. Conversely, in African-Americans, a majority of 10 out of 12 exhibited a range from 0 to 94% decrease in intestinal *MDR1* mRNA expression during the luteal phase compared to follicular. Only 2 patients demonstrated an average 2.2-fold induction with a maximal 3.1-fold induction. We observe ethnic

Figure 4.4 Intestinal *MDR1* mRNA expression changes during the luteal compared to follicular phase in all study patients.

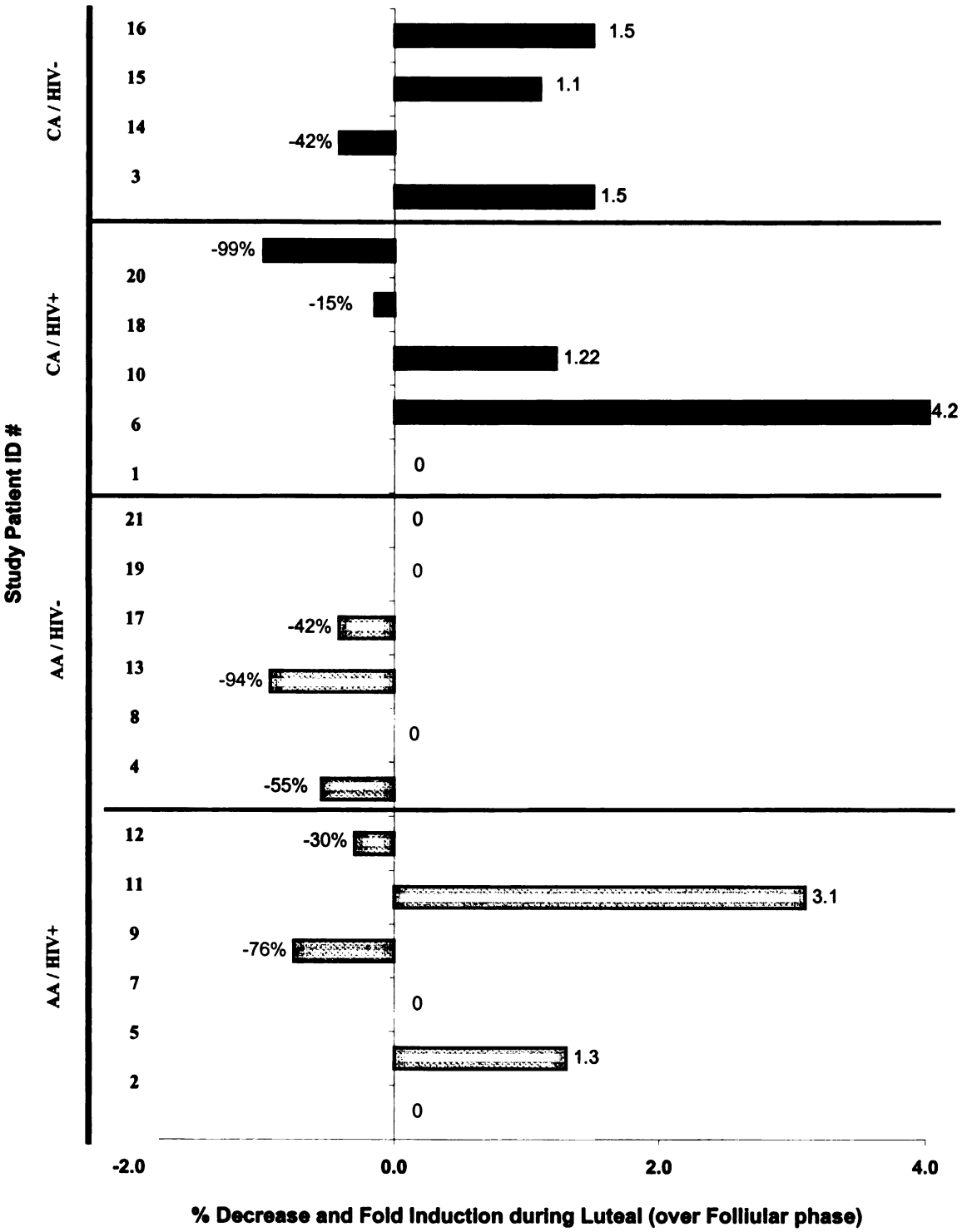

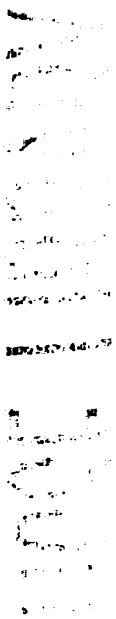

differences in *MDR1* mRNA intestinal expression between African-American and Caucasian female study patients, with African-Americans showing a general trend for lower *MDR1* mRNA intestinal expression.

Probing of P-gp protein using the C219 polyclonal antibody for intestinal expression was determined via Western blotting. Villin was utilized as an internal standard to normalize protein band densities for inter-individual variability between samples and account for variation in sample loading. We observed no change in intestinal P-gp expression between the follicular and luteal phases. We did detect a second band running at ~150 kDa below the expected P-gp protein band (170 kDa), which may be the unglycosylated form of P-gp. This was observed for both intestinal and endometrial samples. However, the two bands both did not show any inter- or intra-individual variation in density/expression.

4.5.3 P-gp function in isolated lymphocytes (Calcein-AM)

Changes in P-gp efflux function, based on menstrual cycle phase, were determined by assessing intracellular Calcein fluorescence accumulation using flow cytometry analysis. A specific inhibitor of P-gp, GG918, was used at 0.25 μM to confirm the presence and functional activity of P-gp in selected cell populations. Inhibition of P-gp in the presence of GG918 would mitigate Calcein efflux mediated by P-gp and thereby cause greater accumulation of Calcein fluorescence, resulting in a greater median fluorescence value. Tables 4.6 and 4.7 illustrate the measurements observed based on ethnicity (African-American and Caucasian, respectively) and HIV status.

Table 4.6 Comparative analysis of intracellular Calcein fluorescence accumulation between follicular and luteal phase in African-American (AA) study patients. Inhibition of P-gp was measured using GG918 (0.25 μM) to confirm transport presence and activity.

Patient ID	Ethnicity/ HIV Status	Phase	Calcein Fluorescence	+ GG918
2	AA / HIV+	1	1910.9	2308.2
		2	1526.1	2277.3
5		1	1094.1	1700.1
		2	352.3	429.4
7		1	1154.8	973.4
		2	1000	1394.9
9		1	2072.1	n/a
		2	1433	1843.4
11		1	2996.1	3337.6
		2	1910.9	2665.5
12		1	228.8	316.2
		2	248.1	347.6
4	AA / HIV-	1	562.3	n/a
		2	685.4	n/a
8		1	1684.9	n/a
		2	1433	1286.4
13		1	250.3	324.9
		2	196.3	365.2
17		1	245.8	378.6
		2	270.7	205.4
19		1	620.8	805.8
		2	865.9	1333.5
21		1	615.3	667.14
		2	395.9	1018.2

Phase 1= Follicular, Phase 2= Luteal

Table 4.7 Comparative analysis of intracellular Calcein fluorescence accumulation between follicular and luteal phase in Caucasian (C) study patients. Inhibition of P-gp was measured with GG918 to confirm transport presence and activity.

Patient ID	Ethnicity/ HIV Status	Phase	Calcein Fluorescence	+ GG918
1	C / +	1	704.1	1144.4
		2	1036.6	1240.9
6		1	1218.8	2206.7
		2	620.8	540.1
10		1	203.5	286.4
		2	152.6	289
18		1	107.5	264.2
		2	116.5	302.3
20		1	156.8	245.8
		2	140.7	245.8
3	C / -	1	609.8	938.9
		2	129.8	155.4
14		1	319.1	582.9
		2	316.2	419.8
15		1	205.4	465.6
		2	248.1	567.4
16		1	232.9	375.2
		2	179.4	399.5

Phase 1= Follicular, Phase 2= Luteal

Natural killer CD56+ lymphocytes express the highest levels of *MDR1* mRNA, followed by CD8+ (T-helper) > CD4+ (T-suppressor) = CD15+ (granulocytes) > CD19+ (B cells) > CD14+ (monocytes) (194). Samples were gated for a minimum of 3000 live, CD56+ expressing subpopulation of blood cells and measured for intracellular Calcein fluorescence. Results show a 16.8% average decrease in intracellular Calcein

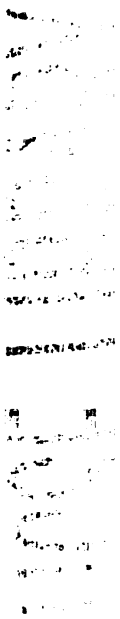

Figure 4.5 Percent change (increase or decrease) in intracellular Calcein fluorescence accumulation during the luteal phase (over follicular) in all study patients.

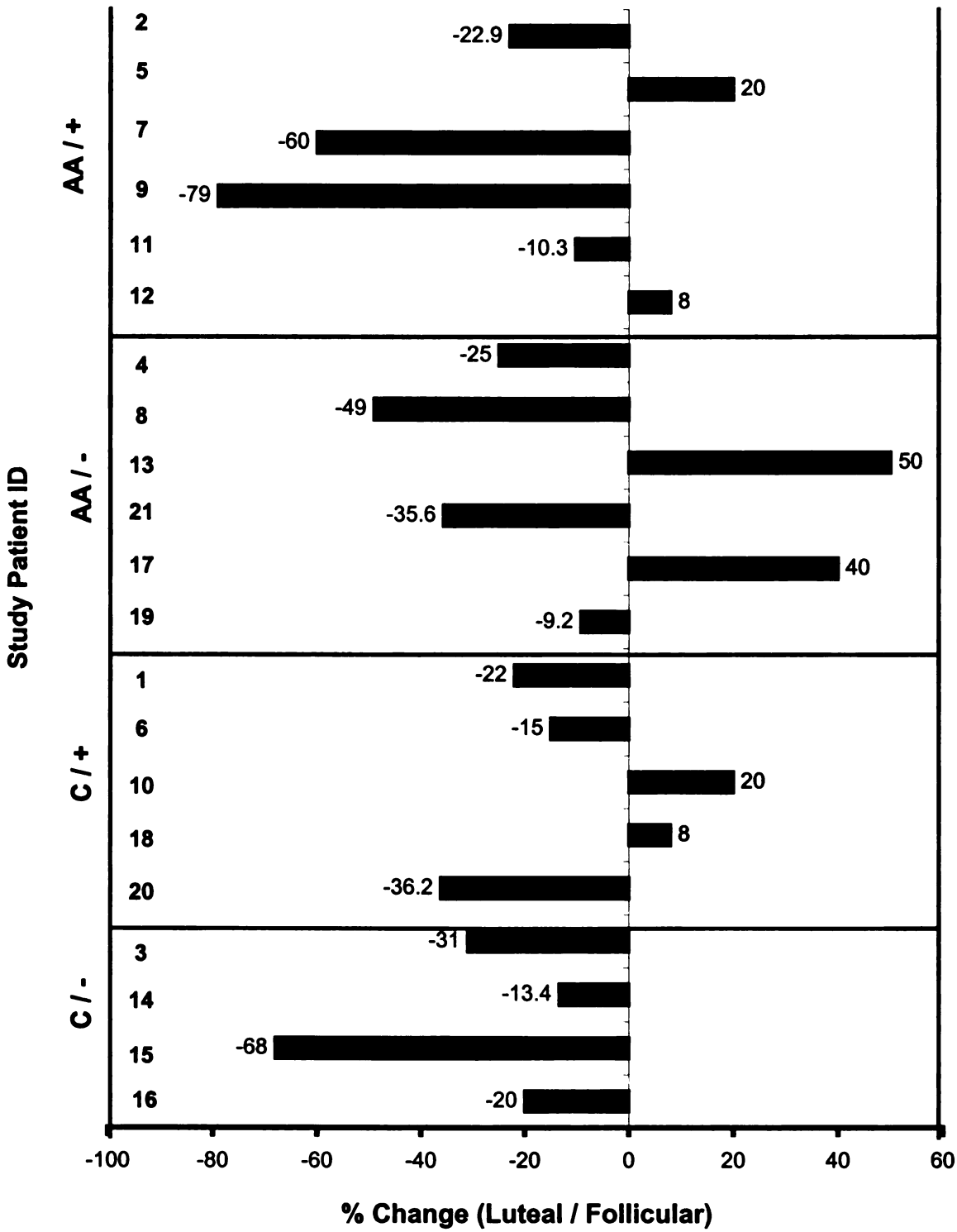

accumulation among gated CD56+ cells during the luteal phase, compared to the follicular phase in the 21 study subjects (Figure 4.5). This suggests that P-gp activity is upregulated during the luteal phase possibly due to higher endogenous circulating levels of estrogens and progestins.

4.6 Discussion and Conclusions

There are numerous studies that have shed light on the dynamic interactions between steroid hormones and multidrug resistance. It was initially demonstrated by Arceci *et al.* (86) that the expression of murine mdr1a mRNA and P-glycoprotein increased markedly in the secretory luminal and glandular epithelium of the gravid murine uterus by the combination of β-estradiol and progesterone. Data indicate that the mdr1a gene locus is hormonally responsive to estrogen and progesterone. This was further confirmed by Mallick *et al.* (77) who showed that the progesterone receptor activated mdr1b transcription indirectly at a sequence between –122 and –65. Mutations in binding sites for essential mdr transcription factors, NF-IL6 and NF-Y, found within this region reduced induction mediated by progesterone. In a more recent study, the role of estrogen receptor subtypes (ER-α and ER-β) in modulating P-gp expression and overall drug resistance was studied in cultured breast carcinoma cells by Zampieri *et al.* (118). It was shown that both ER subtypes were critical for initiating or inhibiting *MDR1* transcription via AP1 and Sp1 binding sites in the *MDR1* promoter. The importance of estrogens and progestins has been established in these *in vitro* and animal *in vivo* studies over the past 15 years. However, the clinical relevance in women's health and multidrug resistance is currently under investigation.

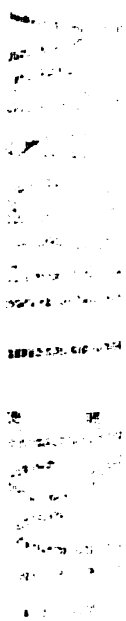

Several retrospective studies looking directly at the effect of menstrual cycle phase on P-gp expression in endometria were performed early on by Axiotis *et al.* (110, 111). The expression, distribution and intracellular localization of P-gp was investigated utilizing immunohistochemistry techniques in normal endometrial tissue (retrospectively, n=36) during the ovulatory cycle. Early follicular phase (proliferative) and menstrual endometrial showed weak or absent immunostaining for P-gp. Mid-follicular phase endometria also showed weak staining (<15%) in the glandular epithelia. However, endometria from late follicular to mid-luteal (secretory) phases exhibited strong apical paranuclear staining and spread to include luminal membraneous, sub- and supranuclear vacuolar regions (>80%) over the course of the luteal phase. Immunoreactivity was observed to diminish at the end of the luteal phase (<35%). It was suggested that P-gp expression corresponds to rising plasma and tissue levels of progesterone, which is associated with marked development in the secretory glands. P-gp expression was strongly detected in 72% of tumor samples using the same technique in endometrial adenocarcinomas (n=36) with similar apical and paranuclear type staining patterns.

In a subsequent study, Kodama *et al.* (195) also utilized immunohistochemical staining using the C219 P-gp-specific antibody to investigate retrospectively, P-gp expression changes in endometrial adenocarcinoma. Membranous and paranuclear P-gp staining was observed, with immunopositivity observed to be highest primarily during the early luteal (secretory) phase. P-gp staining was gradually increased from the late follicular phase, as observed in previous studies, peaked during the early luteal phase and gradually declined during the mid- to late luteal phase. These studies have demonstrated the ability of P-gp

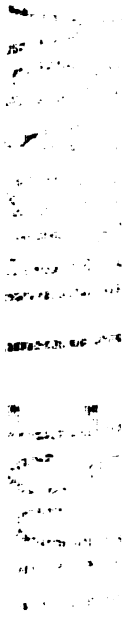

expression to vary based on ovulatory cycle phase, characterized and controlled by changes in regulated estrogen and progesterone levels.

The investigative studies that we present here are the first to examine real-time and *in vivo*, the ability of estrogens and progesterone during the ovulatory cycle to regulate P-gp expression in the intestine and endometria. The intricacies of the study extend to investigate these effects in normal and HIV+ women, as well as African-American and Caucasian women. We procured endometrial and intestinal tissue biopsy samples at both mid-follicular and mid-luteal phases from 21 study patients based on their individual cycles. In the endometria, 16 out of 21 patients (76%) exhibited induction of *MDR1* mRNA from 1.11-fold up to 25.7-fold induction during the luteal phase, compared to follicular. Only 3 out of 21 (14%) subjects showed a decrease in *MDR1* mRNA endometrial expression during the luteal phase (over follicular) and 2 (10%) demonstrated no change. A X^2-statistical analysis testing for *MDR1* mRNA upregulation during the luteal phase found the distribution to be significant with a chi-square value of 16.2 and $p \leq 0.001$. The two patients with the highest levels of induction (11.7 and 25.7-fold) were African-Americans, while the Caucasian group had the 2 patients with the largest decreases in *MDR1* mRNA expression during the luteal phase (12% and 37%). Based on ethnicity, African-Americans showed the higher average induction in *MDR1* mRNA expression during the luteal phase with a 4.3-fold average increase and Caucasians demonstrated a modest 1.7-fold increase. Interestingly, African-American HIV+ subjects revealed the greatest induction at 5.5-fold, mostly due to one patient

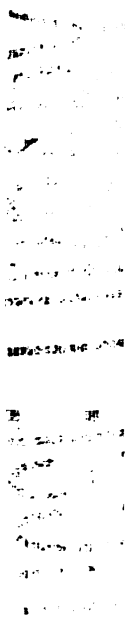

displaying a remarkable 25.7-fold increase. Overall, there was an average 3.2-fold induction observed for all 21 subjects.

Intestinal *MDR1* mRNA expression between phases proved to be more mercurial. We observed no obvious change in *MDR1* mRNA expression during the luteal phase compared to follicular with an average 1.11-fold increase. African-American subjects showed a slightly greater overall decrease in expression during the luteal phase (compared to follicular) at 4.8%. Conversely, Caucasians showed an average 1.33-fold induction, albeit insignificant. Worthy of note, the majority of Caucasians (56%) showed induction to some degree while 83% of African-Americans demonstrated 0 to 94% decrease in *MDR1* mRNA expression. It has been shown that the majority of African-Americans have a higher frequency for being homozygous wild-type (CC) for the C3435T *MDR1* SNP genotype (61%) compared to Caucasians at 26% ($p<0.0001$) (196). Further evidence of ethnic SNP genotype frequency differences between African-American and Caucasian *MDR1* have been revealed by Kim *et al.* (197) showing that 62% of European-Americans and a mere 13% of African-Americans were the homozygous variant (TT) for C3435T at exon 26 (also linked to C1236T at exon 12 and G2677T at exon 21). Although translation of allelic variation in *MDR1* into P-gp functional expression continues to be controversial, we assume that homozygous variant alleles are most likely associated with decreased P-gp expression and function. With this assumuption in mind, it is interesting to note that the majority of African-Americans exhibited decreased *MDRI* mRNA expression in the intestine, but greater overall induction in the endometrium during the luteal phase, compared to Caucasians.

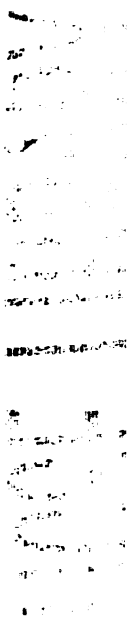

Western blotting of endometrial biopsy tissue proved to be unsuccessful, primarily due to contamination of samples with suffused blood despite washing. Additionally, there was a lack of tissue samples during the follicular phase, characterized by a thin endometrial lining, making it difficult to obtain sufficient tissue for most patients. Protein analysis of intestinal tissue was improved. However, results showed no significant change in intestinal P-gp expression between follicular and luteal phases of the menstrual cycle. This suggests that ovulatory cycle changes may not significantly affect P-gp substrate drugs that primarily undergo intestinal first-pass metabolism.

To investigate ovulatory cycle effects on P-gp function in blood cells, we utilized isolated lymphocytes from study subjects. Isolated lymphocytes were gated for CD56+ natural killer cells, which are the predominant lymphocytic subtype to express P-gp (194), and we conducted Calcein-AM assays to measure P-gp efflux activity. Intracellular accumulation of Calcein was measured and compared between phases. There was an average 16.8% average decrease in intracellular Calcein fluorescence during the luteal phase when compared to follicular for all subjects. This decrease was observed consistently throughout both ethnic and HIV status subgroups. These results suggest that P-gp activity may be enhanced during the luteal phase of the cycle in lymphocytes and may be responsible for decreased intracellular lymphocyte drug accumulation. The extent to which this correlates with P-gp genotype and phenotype relationships was subsequently examined. Statistical analyses suggest an ethnic and as well as a genotype effect on lymphocyte P-gp activity. A significant correlation was observed between African-American (AA) subjects and higher P-gp activity using baseline values

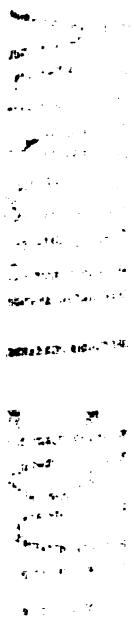

(p=0.0047). A strong correlation was also observed for African-Americans comparing control with P-gp inhibition by GG918. Increased P-gp activity in lymphocytes after subtracting background inhibition values correlated significantly (p=0.01) in the same AA subjects.

We conclude that there was no change in intestinal P-gp or *MDR1* expression. However, induction of endometrial *MDR1* mRNA during the luteal phase of the ovulatory cycle may have therapeutic implications, especially for HIV^+ patients in whom the vaginaendometrium may serve as an HIV sanctuary site. It is possible that induction of P-gp in the endometria and lymphocytes during the luteal phase may act to limit critical intracellular accumulation of anti-HIV drugs thereby jeopardizing therapeutic efficacy. Higher dosing regimens during the luteal phase may be required to maintain adequate and sufficient intracellular drug levels in critical regions subject to greater HIV infection and replication.

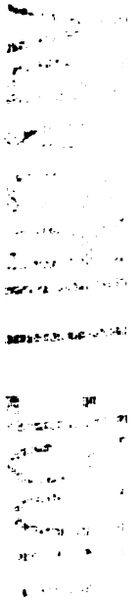

CHAPTER V

In Vivo Pharmacokinetics of Nelfinavir, Effects of HIV Status and MDR1 Polymorphisms in African-American and Caucasian Females

5.1 Objectives

In this study, we theorize that P-gp activity is upregulated in expression and activity during the luteal phase, when estrogen and progesterone levels peak. This in turn will alter the pharmacokinetics of P-gp substrate drugs such as nelfinavir, an HIV protease inhibitor. For a drug that is primarily metabolized hepatically, such as is the case for nelfinavir via CYP2C19, lower P-gp expression and activity during the follicular phase compared to luteal would mitigate hepatobiliary efflux and augment CYP2C19-mediated hepatic metabolism. The *in vivo* functional consequences would be reflected in lower plasma drug concentrations. On the other hand, increased P-gp activity during the luteal phase would restrict opportunity for hepatic metabolism and therefore lead to less hepatic metabolic clearance and higher plasma drug concentrations.

We also test whether hormonal upregulation of P-gp as it correlates to nelfinavir pharmacokinetics will be dependent upon the presence of a synonymous C3435T variant in exon 26 and respectively linked SNPs (G2677T in exon 21 and C1236T in exon 12) in the *MDR1* gene. We anticipated that the Caucasian study population would have a higher

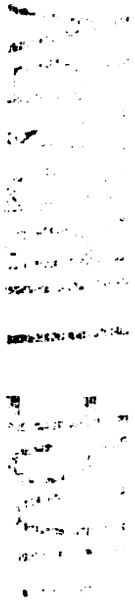

frequency of the common *MDR1*2* variant allele containing the 3 SNPs mentioned above. We also anticipated that the African-American population would have a significantly lower frequency for these variant alleles, and they would be predominantly homozygous wildtype for these 3 SNPs. We further evaluated whether a difference in nelfinavir pharmacokinetics was observed between Caucasians and African-Americans in either ovulatory phase.

5.2 Introduction

At the end of the 20th century, numerous *MDR1* single nucleotide polymorphisms (SNPs) were identified, generating conflicting and controversial predictions with regard to their role in affecting clinical outcome for P-gp substrate drugs. It was widely postulated that genetic polymorphisms in the *MDR1* gene could translate into less functional protein, thereby compromising drug disposition and response via pharmacokinetic and pharmacodynamic changes. Polymorphisms in the human *MDR1* gene are identified as random, coding or non-coding SNPs depending upon their location within the genome. Random SNPs are the most common and found in intergenic deoxyribonucleic acid regions or within introns. Coding SNPs are found in exons, which ultimately get translated, and non-coding SNPs are found within the promoter, 5' and 3' untranslated regions. Nonsynonymous coding SNPs are believed to be most significant since they represent polymorphisms that result in an amino acid change. There are approximately 30 SNPs that have been identified within the *MDR1* gene, with several groups having successfully screened the entire *MDR1* coding region (197-206).

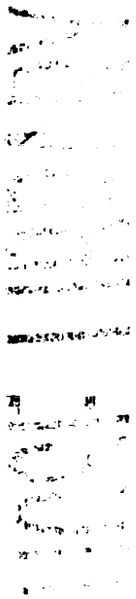

Variation in one specific allele, C3435T, located in exon 26 was found to be synonymous with no change in amino acid, but was the first SNP to be associated with altered protein expression although it did not result in an amino acid change (207). Several other laboratories have also investigated its clinical effects, resulting in contradictory data. Hoffmeyer *et al.* (207) reported lower intestinal duodenum P-gp expression in subjects with the homozygous variant 3435(T/T) allele, resulting in higher digoxin plasma concentrations at steady-state compared to subjects homozygous for the wildtype (C/C)3435 allele. In contrast, Sakaeda *et al.* (208, 209) determined that subjects possessing the homozygote wildtype allele (C/C) had the least *MDR1* mRNA expression, as determined from duodenum biopsy tissue samples, and subjects with the homozygote mutant allele (T/T) had the highest mean *MDR1* mRNA expression, with a 3-fold difference. In accordance with this data, their digoxin clinical study exhibited higher $AUC_{0\text{-}4\ hr}$ values after a single oral dose of digoxin in Japanese subjects expressing the wildtype (C/C) genotype compared to (C/T) and (T/T) subjects. Kim *et al.* (197) discovered the presence of linkage disequilibrium between SNPs in exon 26 (C3435T) and exon 21 (G2677T/A). This suggests that alterations in drug disposition due to functional differences in P-gp that were initially attributed to the C3435T allele may be the result of associated polymorphisms in exon 21. More recently, these two SNPs have also been linked to a synonymous SNP in exon 12 (C1236T) (205, 210, 211). The SNP (G2677T/A) at position 2677 in exon 21 yields two separate amino acids, Ala893Ser (G2677T) and Ala893Thr (G2677A). This particular SNP, in combination with another in exon 1 (T129C), has been associated with decreased P-gp expression in the placenta (203). *In vitro* expression of *MDR1* encoding the G2677T/A allelic variant in cells

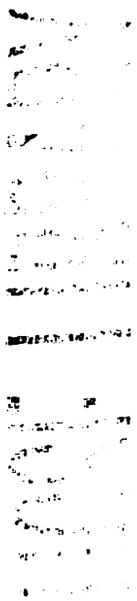

resulted in enhanced efflux of digoxin by cells. It has been suggested that the variant allele may be associated with less expression, but higher function. However, definite conclusions cannot yet be made. These results suggest that multiple genotypic combinations of *MDR1* polymorphisms, also known now as haplotypes, may work independently or synergistically to regulate P-gp expression and function.

Among lymphocyte subsets, $CD56^+$ natural killer cells have been shown to express the highest levels of P-gp at both the protein and mRNA level (194). To test whether the variant *MDR1* gene (C3435T) was related to altered P-gp function and activity in peripheral blood mononuclear cells, real-time RT-PCR was utilized to assess *MDR1* mRNA expression and flow cytometry to measure P-gp mediated rhodamine efflux among 30 healthy Caucasians (212). Subjects with the homozygous wildtype genotype (C/C) expressed the highest levels of *MDR1* mRNA and significantly lower intracellular rhodamine accumulation (indicating more P-gp efflux). *MDR1* mRNA expression was lowest in those with the variant genotype (T/T) and exhibited less rhodamine efflux. These findings were confirmed by Fellay *et al.* (213) in 59 HIV+ patients, in whom *MDR1* transcripts in PBMCs were highest among those with the wildtype (C/C) allele. This group also investigated the role of P-gp, based on C3435T allelic variations in antiretroviral treatment response, by measuring median drug concentrations of nelfinavir (P-gp substrate) and efavirenz in plasma. They identified an association between the mutant (T/T) genotype and lower plasma drug concentrations for both nelfinavir and efavirenz in 203 patients. In an effort to predict antiviral treatment response, mean CD4-cell counts were measured and determined to be higher following 6-months treatment in

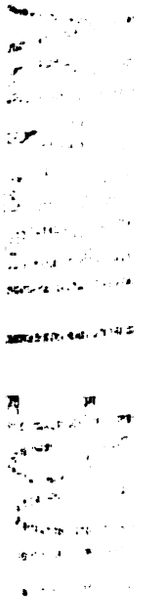

patients with the variant (T/T) genotype. This might be explained by better intracellular drug accumulation due to mutant, less functional P-gp, resulting in improved antiretroviral efficacy.

The clinical study that we present here investigates the impact of *MDR1* genotype on nelfinavir pharmacokinetics based on ethnicity (African-Americans *vs.* Caucasians) and linked *MDR1* polymorphisms, as well as HIV status. Speck *et al.* (214) demonstrated that HIV-1 protein and infectious virus production were decreased approximately 70-fold in CEM ($CD4^+$ T-cell line) cells overexpressing P-gp. HIV-infected volunteers (81% of whom were on antiretrovirals) were found to express lower levels of *MDR1* mRNA in isolated lymphocytes compared to healthy volunteers (215). Overexpression of P-gp conferred immunologic resistance by delaying and protecting against caspase-dependent apoptosis (216-221). These studies offer a piece in the puzzle to explain how the overexpression of P-gp is associated with significantly decreased HIV mRNA levels.

Other groups offer a more mechanistic approach to understanding this phenomenon. It has been suggested that HIV-1 entry into cells occurs selectively through lipid rafts, which are highly ordered sphingolipid and cholesterol rich structures in the outer leaflet of the cell membrane, of glycoplipid-enriched (GEM) domains (214, 222-224). Overexpression of P-gp and its localization to lipid rafts may disrupt critical protein-receptor interactions because of the physical size and concentration of P-gp. Furthermore, substrate binding of P-gp causes a conformational change that may interfere with CD4-gp160 binding, the formation of CD4-CXCR4 bundles or the protein-lipid ratio that may

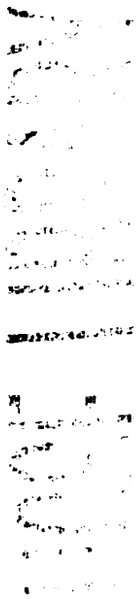

alter receptor function. Our studies will not only allow us to investigate how increased P-gp during the luteal phase of the menstrual cycle affects nelfinavir pharmacokinetics, but will also give evidence as to whether HIV has any impact on nelfinavir pharmacokinetics via P-gp, based on menstrual cycle phase. Hence, we examine the intricate interplay between reproductive hormones during the menstrual cycle, nelfinavir pharmacokinetics, HIV status and *MDR1* polymorphisms.

5.3 Materials and Methods

5.3.1 Blood collection and DNA isolation

Prior to nelfinavir dosing, a 5 mL blood sample was collected into a Vacutainer containing the anticoagulant, EDTA, and stored at 4°C before DNA analysis. A Puregene DNA Purification kit (Gentra Systems, Minneapolis, MN) was used to extract DNA from the blood and was aliquoted into concentrations of 10 ng/μL. Genotyping of *MDR1* single nucleotide polymorphisms was performed using a sequencing method. For the pharmacokinetic analysis of nelfinavir (750 mg dose), 8 mL samples of blood were collected over a period of twelve hours and placed into two separate sodium heparin vacutainers. Plasma was extracted from samples by centrifugation at -4°C for 10 min at 1300 rpm, transferred to 2 mL cryovials and stored at -80°C until analysis.

5.3.2 Sequencing analysis for *MDR1* SNP identification

The region containing the single nucleotide polymorphisms (SNPs) of interest within their respective exons was amplified by PCR. The products from the PCR assay were verified by gel electrophoresis and subsequently sequenced to genotype the selected

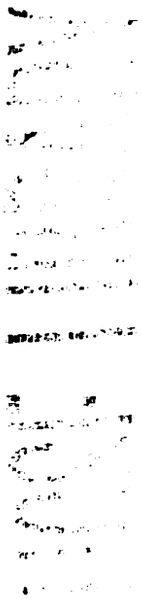

SNPs. The sequencing method utilized capillary electrophoresis and incorporation of dye-labeled dideoxyribonucleoside triphosphates (ddNTPs). The PCR conditions for the amplification of each gene are described in Figure 5.1, during which for each consecutive cycle, the annealing temperature was decreased in 0.5°C increments. For the PCR reaction, 1 μL of both forward and reverse primers (1.5 pmol/μL) for each exon (Table 5.1) were mixed with 10 ng of DNA template (1 μL of a 10 ng/μL DNA solution) and 5 μL of 2X AmpliTaq Gold Master Mix [(Applied Biosystems, Foster City, CA) containing AmpliTaq Gold DNA polymerase, GeneAmp PCR Gold Buffer, 30 mM Tris/HCl at pH 8.05, 100 mM KCl, 400 μM of each dNTP, 5 mM $MgCl_2$ and stabilizers]. DEPC-treated water (3 μL) was added, bringing the total the reaction volume to 10 μL.

Figure 5.1 PCR amplification conditions

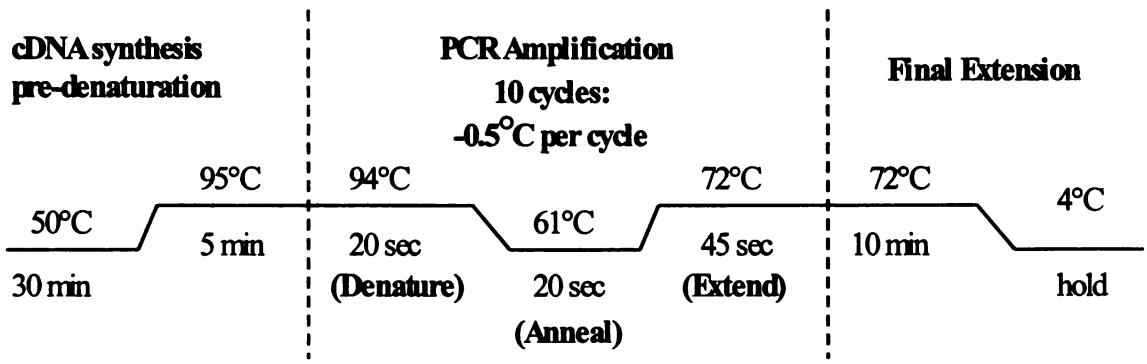

For PCR cleanup, two enzymes were utilized: shrimp alkaline phosphatase (SAP; 1μL from a 10 U/μL dilution), which acts to remove the phosphate group from any remaining dNTPs, and exonuclease I (exoI; 0.1 μL from a 1 U/μL dilution), which digests any

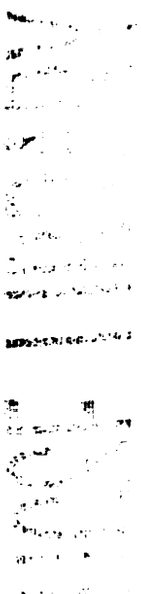

Table 5.1 PCR primers for *MDR1* exonic regions

Exon	Primer Sequence	(Sense/Anti-Sense)
2	5'- CCTCTTACTGCTCTCTGGCTTC -3'	S
	5'- TTCCATGTACCCCATTTCATAA -3'	AS
10-11	5'- ATTTATATGTTGCCTCGCCATT -3'	S
	5'- GGCAATTCACAGACACAGGATA -3'	AS
12-13	5'- CAGTTACCCATCTCGAAAAGAAGT -3'	S
	5'- TGTATCTACGACCAGTTGATACTGC -3'	AS
21	5'- CAGCATTCTGAAGTCATGGAAAT -3'	S
	5'- CCAAGAACTGGCTTTGCTACTT -3'	AS
26	5'- CTCACAGTAACTTGGCAGTTTCA -3'	S
	5'- GGTCAGGTGATCAGGTAAAGGT -3'	AS

remaining PCR primers. Distilled water (0.9 μL) was added to bring the reaction volume to 2 μL. The resulting product was then sequenced in a reaction containing polymerase (0.25 μL BigDye v3.1), 1 μL (1.5 pmol/μL) of a single sequencing primer (Table 5.2), 0.875 μL of 5x sequencing buffer, 1 μL of PCR template and a mixture of fluorescently-labeled ddNTPs and unlabeled dNTPs. Distilled water (1.875 μL) was added to bring the reaction volume to 5 μL. Sequencing conditions are delineated in Figure 5.2.

Incorporation of dNTP allows for extension of the template copy, while ddNTP incorporation results in termination of extension. Final products were run on a 3730xl

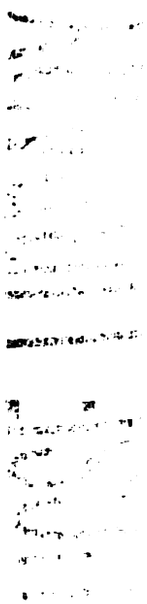

Table 5.2 Sequencing primers for *MDR1* exonic regions

Exon	Primer Sequence
2	5'- TTCCATGTACCCCATTTCATAA-3'
10-11	5'- GGCAATTCACAGACACAGGATA-3'
12-13*	5'- CAGTTACCCATCTCGAAAAGAAGT-3' 5'- TGTATCTACGACCAGTTGATACTGC -3'
21	5'- CAGCATTCTGAAGTCATGGAAAT -3'
26	5'- CTCACAGTAACTTGGCAGTTTCA -3'

*Reactions performed in both forward and reverse directions.

Figure 5.2 Sequencing conditions

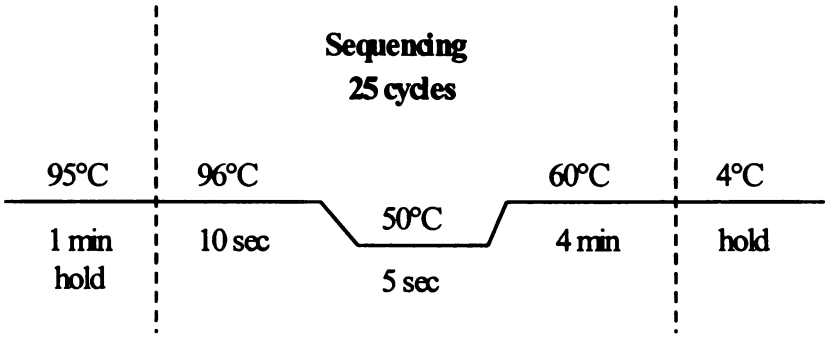

Genetic Analyzer (Applied Biosystems, Foster City, CA), where they were separated by capillary electrophoresis according to their size length. A Millipore Montage cleanup system (Millipore, Billerica, MA) was used for sequencing cleanup. Following separation, fluorescent tags attached onto the ddNTPs at the ends of the product were stimulated and excited by a laser, emitting a specific wavelength. Data was collected and

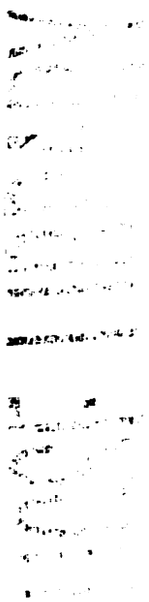

converted into an electronic format, in which each labeled ddNTP signifies a specific base (A, G, T or C) and was illustrated as a colored peak for the associated base using a Sequencer (GeneCodes, Ann Arbor, MI). The sequence of bases was then analyzed for SNPs, identified by a dissimilar base incorporated at the same particular position. Heterozygotic samples were identified as having two bases incorporated and illustrated schematically as overlapping peaks on top of each other.

5.3.3 Analytical method

For sample preparation prior to LC/MS/MS analysis, plasma samples were defrosted, vortexed for 30 seconds and aliquoted (0.1 mL) into 1.5 mL microcentrifuge tubes. Samples were spiked with the internal standard, an analogue of ritonavir kindly provided by Abbott Laboratories, A-86093 {(5*S*,8*S*,10*S*,11*S*)-9-hydroxy-2-cyclopropyl-5-(1-methylethyl)-1-[(2-1-methylethyl)-4-thiazolyl]-3,6-dioxo-8,11-bis(phenylmethyl)-2,4,7,12-tetraazatridecan-13-oic acid, 5-thiazolylmethyl ester} at 0.4 ng/μL in 85% acetonitrile, and vortexed vigorously for 30 seconds. Samples were then centrifuged at 10,000 rpm for 5 minutes and the supernatant transferred to WISP vials. Aliquots (5 μL) were injected into a Micromass Quattro LC/MS/MS and analyzed along with standard concentrations of nelfinavir (50, 100, 200, 500, 1000, 2000, 6000, 10000 ng/mL) and M8 (Figure 1.11)(25, 50, 100, 250, 500, 1000, 3000, 5000 ng/mL). Samples were injected at a flow rate of 0.8 mL/min with the following mobile phase: 60% acetonitrile, 40% H_20, 4 mM ammonium acetate and 0.15% acetic acid. Samples were initially injected into an XDB-C8 (4.6 x 12.5 mm) guard column and backflushed into an Agilent ZORBAX

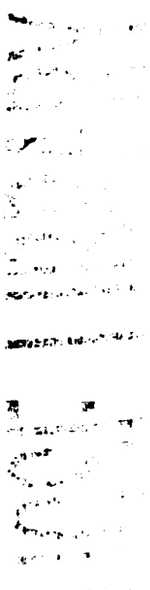

Eclipse XDB-C8 (4.6 x 2.5 μm) analytical column to achieve separation. The chromatogram for nelfinavir and M8 is profiled in Figure 5.3.

Figure 5.3 Chromatogram of nelfinavir and M8.

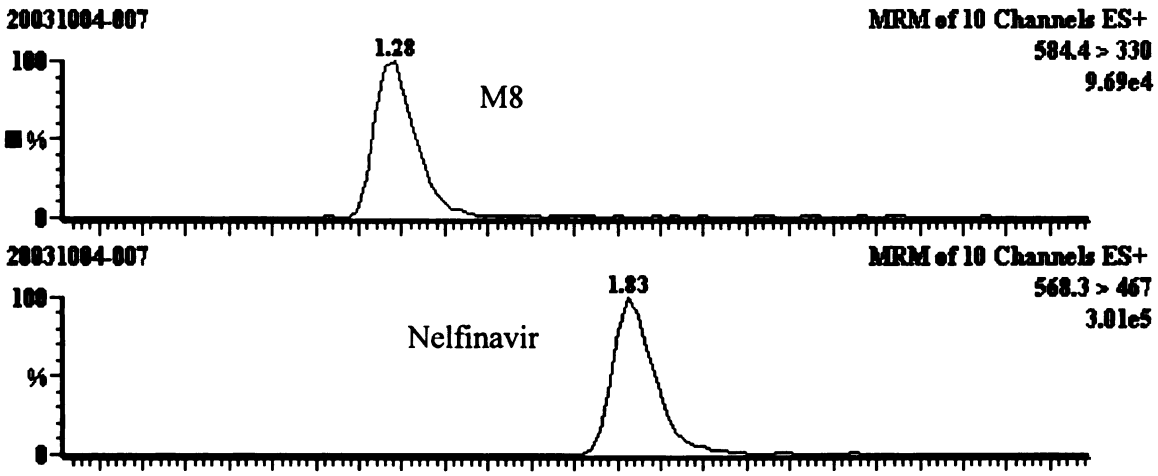

5.3.4 Pharmacokinetic analysis

Pharmacokinetic parameter values for nelfinavir were determined using WinNonlin professional edition software, version 2.1 (Pharsight Corp., Mountain View, CA). Data were analyzed using noncompartmental methods with extravascular input (model 200) to estimate area under the plasma-concentration time curve (AUC), employing the linear trapezoidal calculation method. Oral clearance (CL/F) was calculated by dividing administered oral dose (D) by $AUC_{inf.}$ The terminal half-life ($t_{1/2\lambda Z}$) was calculated as 0.693 divided by the terminal slope in a log-linear plot. Volume of distribution (V_z/F) was calculated as $V_z/F = (CL \div F) \bullet (t_{1/2\,\lambda Z} \div 0.693)$. Maximum plasma concentration (C_{max}) and the time to reach maximal plasma concentration (t_{max}) were observed from the

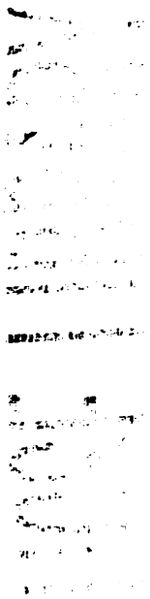

data. The mean residence time (MRT_{M8}) for nelfinavir metabolite, M8, was calculated using the following equation:

$$MRT_{M8} = \frac{AUMC_{nelfinavir}}{AUC_{nelfinavir}} - \frac{AUMC_{M8}}{AUC_{M8}}$$

5.3.5 Statistical analysis

In order to determine whether there were statistically significant changes between the follicular and luteal phases for endometrial/intestinal *MDR1* mRNA expression, for P-gp mediated-active efflux of CalceinAM and for differences in nelfinavir and M8 pharmacokinetics, all data sets analyzed by ANOVA (analysis of variance). Comprehensive univariate and multivariate (repeated measures models) analyses were performed to look at both inter-subject [ethnicity, HIV status, *MDR1* SNP genotype (C34335T, A2677T)] and intra-subject (menstrual cycle phase) factors. A univariate analysis explored each variable (i.e. pharmacokinetic parameters, endometrial *MDR1*, CalceinAM efflux) separately, examining the range, as well as the central tendency of these values. The pattern of response to the individual variables was observed. Numerous random effects models for nelfinavir and M8 pharmacokinetics were generated to see if there were any significant effects of individual pharmacokinetic parameters on HIV status, ethnicity or cycle phase. Change correlation tests were conducted between various factors to inspect whether changes in CalceinAM efflux and endometrial *MDR1* mRNA correlate with changes in pharmacokinetics. Various multivariate models were created to look at the significance of variables (i.e. CalceinAM and mRNA) as predictors of pharmacokinetics. Scatterplots were also produced to visually inspect any potential correlations between various factors. Many of the variables appeared to be skewed, so

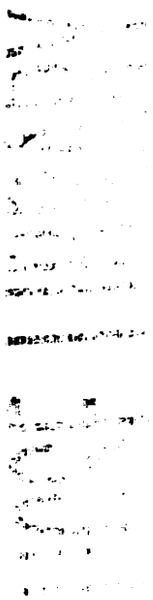

medians and nonparametric tests were utilized for the univariates, and logarithmically transformed variables were modeled for many of the multivariate models. Estimate effects (calculated as percentages for those variables that were logarithmically transformed), upper and lower confidence intervals and p-values were then determined.

A minority of the study patients had levels of the nelfinavir metabolite, M8, that were below the limit of quantification for either one or both phases of the menstrual cycle. These results could not be ignored without risking bias. Therefore, parametric methods were used for censored data to investigate changes between phases and the factors that influence them. For these women, a left-censored data value of 5 for M8 C_{max} was used. Additionally, we used 60 as a left-censored value of AUC_{last}, 90 as a left-censored value of AUC_{inf}, and 8333 as a right-censored value of CL/F. The SAS LIFEREG procedure (SAS Institute, Cary NC) was used to model these with a log-normal distribution. Coefficients for other predictors were transformed to multiplicative percentage effects by 100*(exp(coefficient)-1). P-values of ≤ 0.05 were accepted as significant.

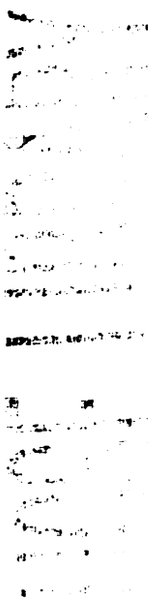

5.4 Results

5.4.1 Genotyping for *MDR1* SNPs in study patients

All study patients were genotyped for several *MDR1* variants that have been shown by previous investigators to have a potential regulatory impact on the expression and function of P-gp, consequently affecting plasma concentration drug levels of P-gp substrate drugs (197, 203, 207, 209). The frequency and distribution of the *MDR1* allelic variants were determined among the study patients and compared between those SNPs previously reported to be in linkage disequilibrium (C3435T, A61G, G2677T/A and C1236T). Our results show that indeed the allelic frequencies for these three variants are all closely linked and demonstrate ethnic differences between African-American and Caucasian patients. The allele and genotype frequencies for selected *MDR1* SNPs in all subjects are outlined in Table 5.3. The genotype frequencies are shown in Table 5.4 for the following linked SNPs: C3435T, A61G, C1236T and G2677T/A in all subjects based on ethnicity (African-American *vs.* Caucasian) and HIV status.

Results from Table 5.3 show that in all subjects, regardless of race or HIV status, the genotype and allele frequency was higher for the following variant SNPs: G44A (exon 10) and C24T (exon 13). However, the rest of the SNPs tested had higher overall frequencies for the reference wildtype. For all subjects, the A2547G (exon 21), T3322C (exon 26) and T3421A (exon 26) SNPs all exhibited 100% genotype and allele frequency for the reference nucleotide. The SNPs that showed equal distribution for the variant, heterozygote and wildtype genotype and similar frequencies between the reference

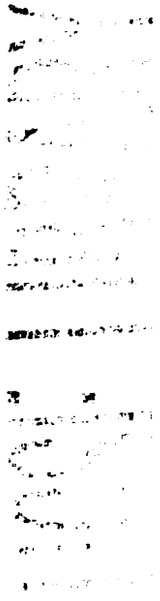

Table 5.3 Genotype and allelic frequencies for *MDR1* variants among 21 $HIV^{+/-}$ pre-menopausal women[a].

MDR1				Genotype Frequency			Allele Frequency	
Exon	**CDS Pos[b]**	**SNP**	**Amplicon Size**	**Wild-type (WT)**	**Heterozygote**	**Variant**	**Reference (WT)**	**Variant**
2	61	A to G	443	95.2	4.8	0.0	0.976	0.234
10	-44[c]	G to A	635	23.8	23.8	52.4	0.357	0.643
12	1236	C to T	816	52.4	23.8	23.8	0.643	0.357
13	24	C to T	816	23.8	38.1	38.1	0.429	0.571
21	2547	A to G	575	100.0	0.0	0.0	1.000	0.000
21	2677	G to T/A	575	66.7	4.8	28.6[(TT)d]	0.690	0.310
26	3322	T to C	500	100.0	0.0	0.0	1.000	0.000
26	3421	T to A	500	100.0	0.0	0.0	1.000	0.000
26	3435	C to T	500	47.6	23.8	28.6	0.595	0.405

[a] The reference sequence is defined by the mRNA sequence as delineated in GenBank Accession M14758 and in part by M13758.2.
[b] CDS Positions are generated from the *MDR1* cDNA GenBank Accession M13758.1.
[c] SNP located within intron, downstream of the specified exon 10.
[d] Only the (TT) homozygous variant was present among all 21 subjects.

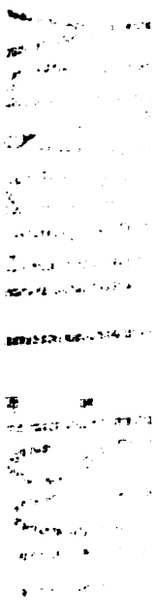

Table 5.4 Comparative genotype frequencies of *MDR1* Variants (C3435T, A61G, C1236T, G2677T/A) between African-American and Caucasian female volunteers based on HIV status.

	Caucasian (C)			African-American (AA)			
Genotype	**HIV-**	**HIV+**	**C total**	**HIV-**	**HIV+**	**AA total**	**Total**
C3435T (CC)	0/4 -	0/5 -	0/9 -	5/6 83%	5/6 83%	10/12 **83%**	10/21 48%
CT	2/4 50%	1/5 20%	3/9 33%	1/6 17%	1/6 17%	2/12 17%	5/21 24%
TT	2/4 50%	4/5 80%	6/9 **67%**	0/6 -	0/6 -	0/12 -	6/21 29%
A61G (AA)	2/4 50%	5/5 100%	7/9 **78%**	6/6 100%	6/6 100%	12/12 **100%**	19/21 90%
AG	1/4 25%	0/5 -	1/9 11%	0/6 -	0/6 -	0/12 -	1/21 5%
GG	1/4 25%	0/5 -	1/9 11%	0/6 -	0/6 -	0/12 -	1/21 5%
C1236T (CC)	1/4 25%	1/5 20%	2/9 22%	4/6 67%	5/6 83%	9/12 **75%**	11/21 52%
CT	1/4 25%	1/5 20%	2/9 22%	2/6 33%	1/6 17%	3/12 25%	5/21 24%
TT	2/4 50%	3/5 60%	5/9 **56%**	0/6 -	0/6 -	0/12 -	5/21 24%
G2677T/A (GG)	1/4 25%	1/5 20%	2/9 22%	6/6 100%	6/6 100%	12/12 **100%**	14/21 67%
GT	1/4 25%	0/5 -	1/9 11%	0/6 -	0/6 -	0/12 -	1/21 5%
TT	2/4 50%	4/5 80%	6/9 **67%**	0/6 -	0/6 -	0/12 -	6/21 29%

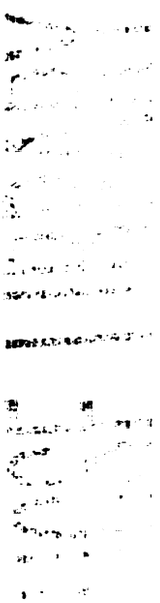

and variant allele were at the C3435T (exon 26), G2677T (exon 21), C24T (exon 13), C1236T (exon 12) and G44A (exon 10) positions. We also noted that at the G2677T/A position, there was a complete absence of the alanine (A) variant. This suggested and confirmed to us that the similarity in allele frequency between the reference and variant alleles could be further influenced by ethnic factors upon subgroup distribution analysis. Hence, based on 5 chosen SNP positions shown to be important by previous investigators, haplotype analysis was conducted.

Thus far, a total of 47 SNPs have been identified in the *MDR1* gene, along with almost 90 different *MDR1* haplotypes, which are various combinations of these known SNPs that are present simultaneously at varying degrees in all individuals. The maximum number of haplotypes that one should theoretically be able to detect is determined by the known number of SNPs and the fact that each individual has two *MDR1* alleles. Therefore, we should be able to observe $2^{47} = 1.41 \times 10^{14}$ possible *MDR1* haplotypes. However, this is not observed as some SNPs are not linked to other SNPs.

Analysis of the results as shown in Table 5.4, demonstrate that the *MDR1**1/*1 haplotype, in which the reference homozygous wildtype is closely linked between the three positions 1236CC, 2677GG and 3435CC, is predominant within the African-American subgroup compared to the *MDR1**2/*2 haplotype [homozygous variants 1236TT, 2677TT and 3435TT] prevalent among the Caucasian subgroup. In both Caucasians and African-Americans, the *MDR1**2/*26 haplotype [heterozygotes 61AA, 44GA, 1236CT, 2677GT, 3435CT] occurred at a similar, but lower frequency. Several

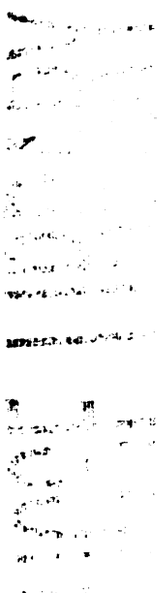

African-American subjects exhibited the *MDR1**2/*9 haplotype [61AA, 44AA, 1236CC, 2677GG, 3435CT] in which there are no variants except for the heterozygosity at the C3435T position. Some Caucasians also exhibited the *MDR1**26/*26 [all variants 44GG, 1236TT, 2677TT, 3435TT, except for 61AA], *MDR1**27/*27 [all variants 61GG, 44GG, 1236TT, 2677TT, 3435TT], and *MDR1**23/*26 haplotypes [61AA, 44GG, 1236TT, 2677GT, 3435CT], although at lower frequencies. For these analyses, ethnicity was assigned based on self-report, but *MDR1* genotyping results were consistent with prior studies of haplotypes associated with Caucasian and African-American distributions (197).

5.4.2 Nelfinavir pharmacokinetics

The mean plasma drug concentration-time profiles for nelfinavir during the follicular and luteal phases of the ovulatory cycle for the 21 study patients is illustrated in Figure 5.4. We observed that despite high interindividual variability and standard deviations, there was a significant increase in the plasma drug concentration profile during the luteal phase of the menstrual cycle. This increase was only observed after 2 hours. There appeared to be no difference in t_{max} or $t_{1/2\lambda Z}$ between the two profiles. The average pharmacokinetic parameters for nelfinavir based on cycle phase were determined as depicted in Table 5.5. Pharmacokinetic data calculations indicate that during the luteal phase, nelfinavir had a higher mean AUC (35%) and C_{max} (33%) compared to the follicular phase. We observed no apparent differences in t_{max}, $t_{1/2\lambda Z}$. or CL/F between the two phases. However, we did observe a slight decrease (21%) in V_z/F during the luteal phase, suggesting that if there was more P-gp activity due to elevated hormone levels, it would be reasonable to expect

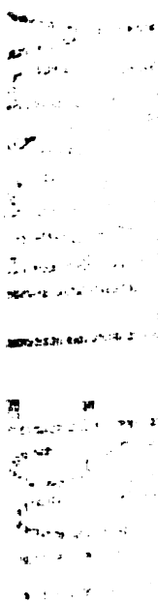

Figure 5.4 Pharmacokinetic profiles for HIV PI nelfinavir (750 mg) obtained from 21 $HIV^{+/-}$ female patients during both follicular and luteal phases of the ovulatory cycle.

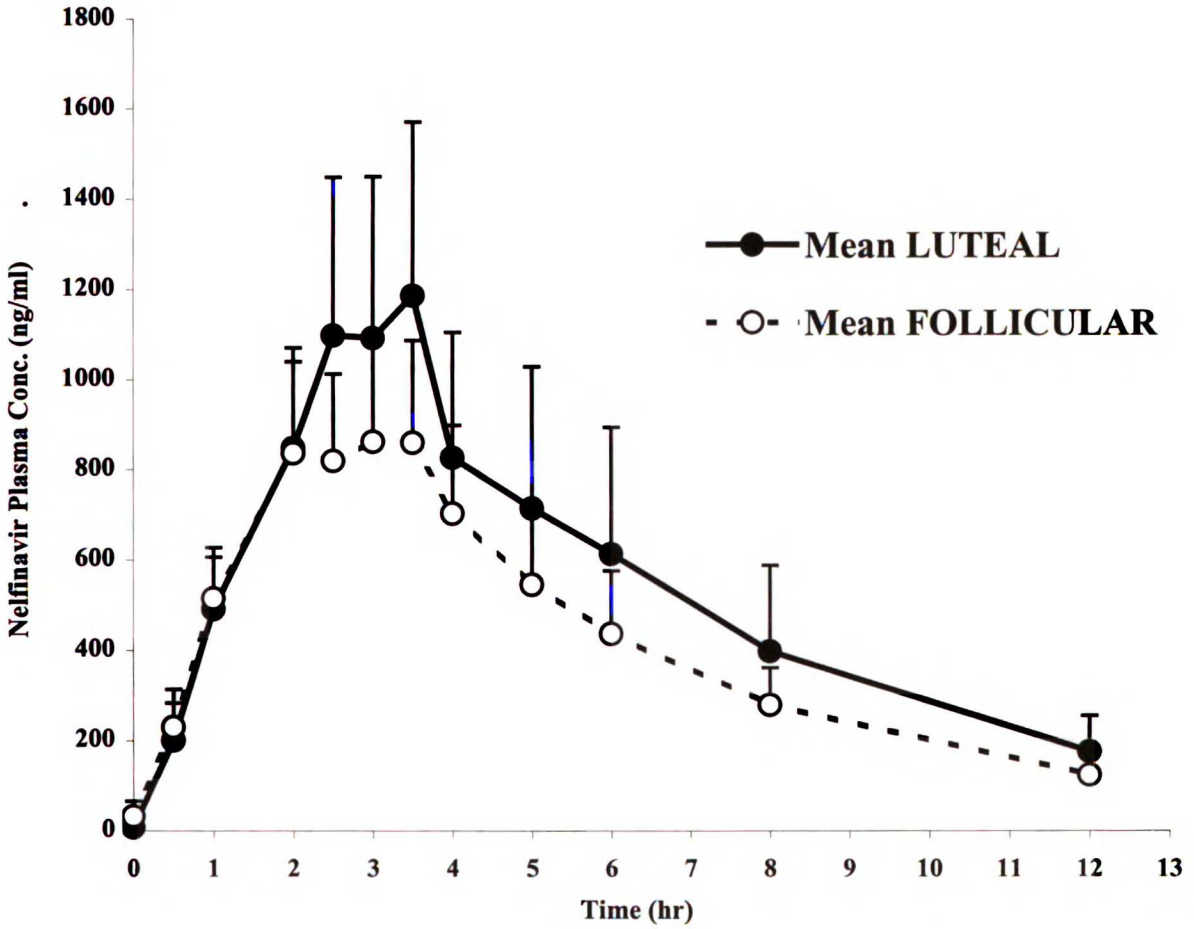

such a change. The differences seen in C_{max} and AUC_{inf} suggest that elevated estradiol (E_2) and progesterone levels during the luteal phase may be causing an increased hepatic P-gp effect, diminishing the availability of nelfinavir to undergo hepatic CYP2C19-mediated metabolism, thereby increasing drug plasma concentrations.

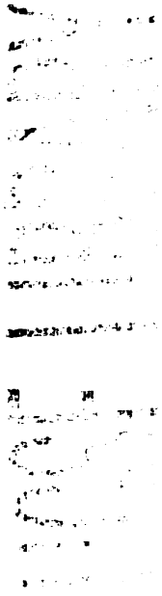

Table 5.5 Nelfinavir pharmacokinetic parameters for 21 study subjects.

PK Parameter	Mean FOLLICULAR	SD	Ratio: Luteal/Follicular
Tmax (hr)	2.6	1.1	**1.04**
Cmax (ng/mL)	987	663	**1.33**
$t_{1/2}$ (hr)	3.3	1.0	**0.94**
AUC-INF (ng*hr/mL)	5686	4186	**1.35**
Vz/F (L)	823	696	**0.79**
CL/F (L/hr)	284	118	**0.96**

PK Parameter	Mean LUTEAL	SD	P value=
Tmax (hr)	2.7	0.9	0.33
Cmax (ng/mL)	1315	1160	**0.05***
$t_{1/2}$ (hr)	3.1	1.3	0.20
AUC-INF (ng*hr/mL)	7694	7842	**0.05***
Vz/F (L)	653	467	0.08
CL/F (L/hr)	273	448	0.31

* $p \leq 0.05$, Statistically significant difference between follicular and luteal phases using paired, 2-tailed t-test.

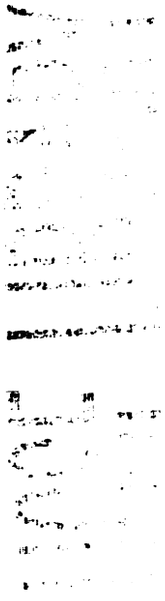

5.4.3 Pharmacokinetics of principal nelfinavir metabolite, M8

The pharmacokinetics of the active major nelfinavir metabolite, M8 was quantified by LC/MS/MS. The chromatograms characterizing the presence of nelfinavir and its major metabolite, M8, are illustrated in Figure 5.5. Several other minor metabolites, MX, M1, M10, and M11 (structures unknown) were also found to be present and are shown below. These metabolites may be products of CYP3A4, 2D6 or 2C9-mediated metabolism. The pharmacokinetic profiles for M8 during the follicular and luteal phases are depicted

Figure 5.5 Chromatogram of M8 and metabolites.

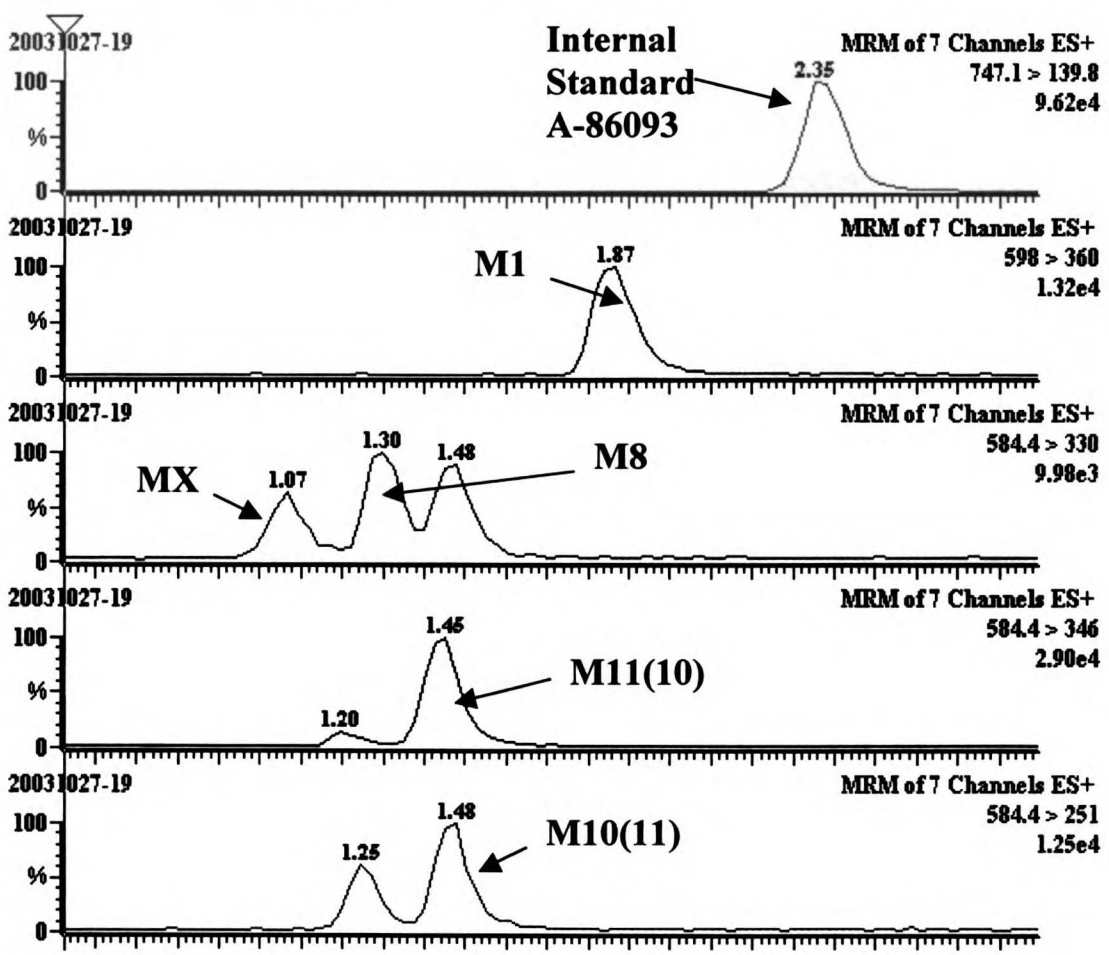

in Figure 5.6. M8 levels were undetectable in 8 patients, hence data results are shown only for the 13 remaining women (5 HIV^+ African-American, 2 HIV^- African-American, 3 HIV^+ Caucasian, 3 HIV^- Caucasian). The M8 metabolite plasma concentration-time profiles paralleled those of nelfinavir, demonstrating 1.7, 1.4 and 1.7-fold higher AUC_{last}, AUC_{inf} and significantly higher C_{max}, respectively, during the luteal compared to follicular phase (Table 5.6). The time to reach maximum drug concentration, t_{max}, of the metabolite did not change. The mean residence time (MRT) was slightly higher in the luteal phase, but not significantly, with a luteal/follicular ratio of 1.28. The metabolite/parent drug ratio (M8 AUC_{inf} / nelfinavir AUC_{inf}) during the follicular phase for the 13 subjects with detectable M8 levels was calculated to be 0.113 ± 0.075. During the luteal phase, this ratio was not found to be significantly different at 0.139 ± 0.137.

Figure 5.6 Detected pharmacokinetic profile for nelfinavir metabolite, M8, based on ovulatory cycle phase in 13 study patients.

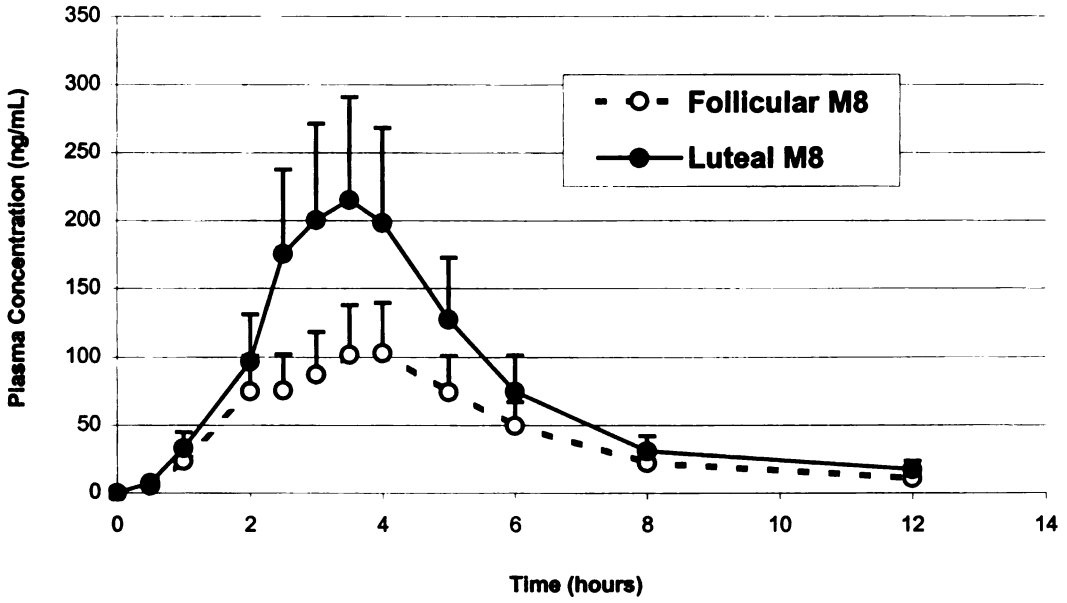

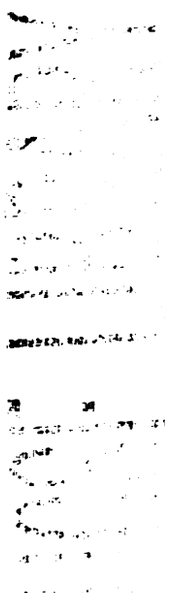

Table 5.6 Mean follicular and luteal pharmacokinetic parameters for M8.

M8	Follicular (F)	SD	Ratio: L/F
Tmax (hr)	2.9	1.2	1.05
Cmax (ng/mL)	138	112	**1.74**
AUClast (ng*hr/mL)	529	444	**1.71**
AUC-INF (ng*hr/mL)	743	511	**1.39**
MRT (hr)	3.9	2.5	1.28

M8	Luteal (L)	SD	P value=
Tmax (hr)	3.1	0.6	0.30
Cmax (ng/mL)	239	109	0.05*
AUClast (ng*hr/mL)	904	410	0.08
AUC-INF (ng*hr/mL)	1030	490	0.17
MRT (hr)	5.0	1.8	0.09

*$p \leq 0.05$, Statistically significant difference between follicular and luteal phases using paired, tailed t-test.

5.4.4 Nelfinavir pharmacokinetics based on ethnicity and HIV status

The pharmacokinetic profiles of nelfinavir were also analyzed based on the ethnicity of the women (African-American *vs.* Caucasian) and HIV status. These profiles were also investigated to determine if there were any changes in nelfinavir pharmacokinetics between the follicular and luteal phases. Results in Figure 5.7 demonstrate higher overall plasma nelfinavir levels for both African-Americans and Caucasians during the luteal phase. However, in Caucasians, the observed difference in nelfinavir plasma concentration between phases was not as large as that observed in the African-American group. We observed an average 47.9% increase in AUC_{inf} during the luteal phase, over

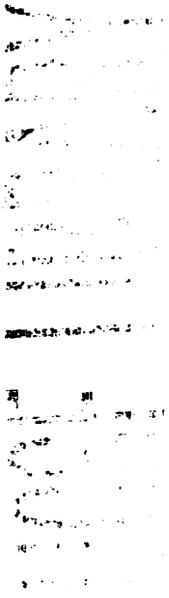

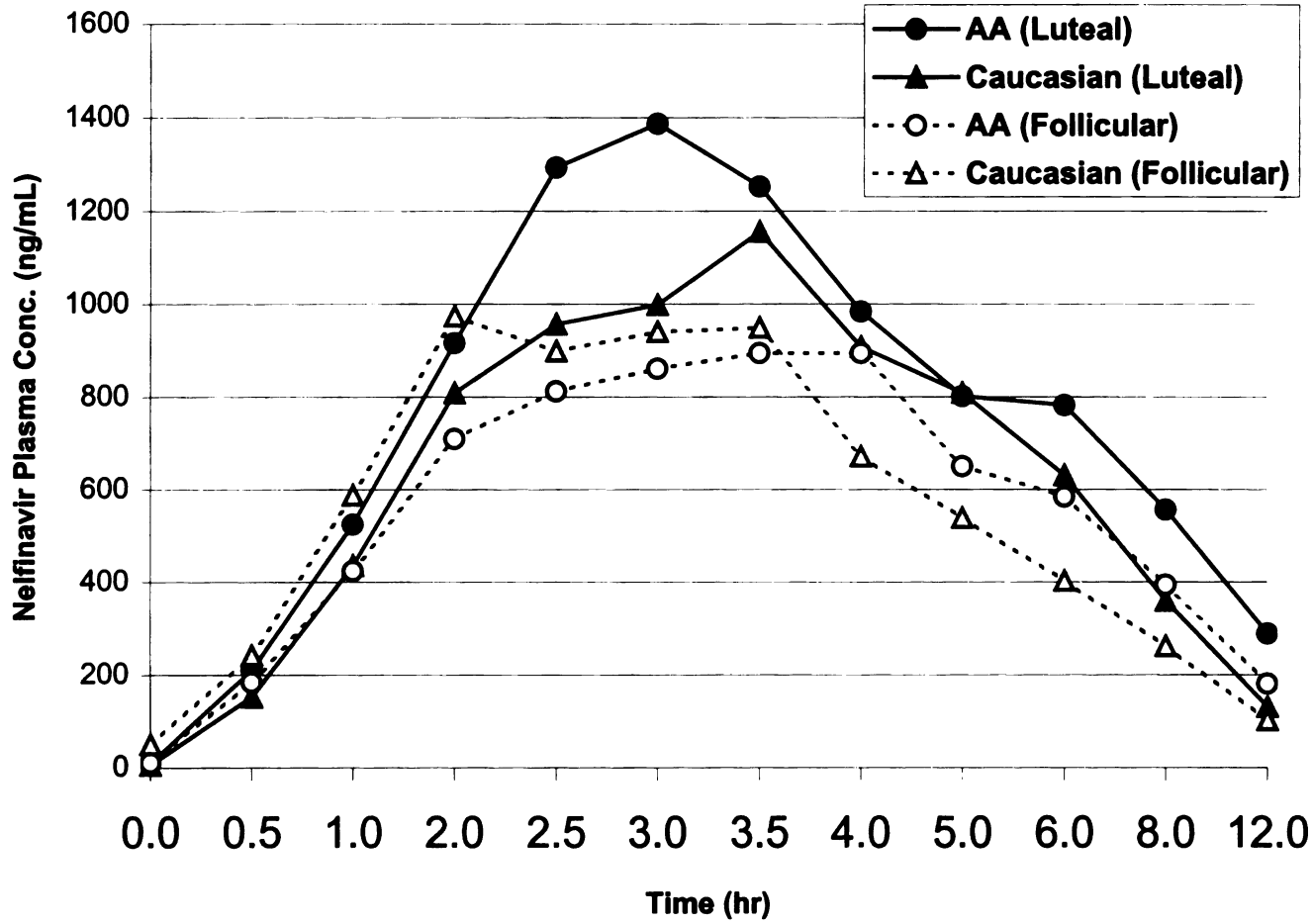

Figure 5.7 Comparison of nelfinavir pharmacokinetics based on ethnicity and ovulatory cycle phase.

follicular, among 12 African-American women and a 29.5% average increase in 9 Caucasian subjects (Figures 5.7, 5.8a and b, 5.9). Likewise, there was a 47.3% increase in C_{max} during the luteal phase (over follicular) in the African-American subgroup compared to an 18.2% increase within the Caucasian subjects. These data demonstrate that the African-American subjects had a 27.1% higher AUC_{inf} (during the luteal phase compared to follicular) and an 11.4% higher C_{max} compared to Caucasians during the luteal phase (Figures 5.8a and b, 5.10). This may be reflective of *MDR1* SNP genotyping results in which African-Americans were predominantly wildtype at various SNP positions (C3435T, C1236T, G2677T/A). We also noted that t_{max} came later at 3.5 hrs during the luteal phase compared to follicular (2.0 hrs) in Caucasians, but earlier at 3.0 hrs during the luteal phase compared to follicular (3.5 hrs) among African-Americans subjects.

Figures 5.8a and b recapitulate Figure 5.7 better to illustrate the effects of ethnicity. During the luteal phase, African-Americans had higher AUC_{inf} and C_{max} (27.1% and 11.4%, respectively) compared to Caucasians (Figures 5.8a, 5.10). However, this was not observed during the follicular phase, as there was only an 11.3% increase in AUC_{inf} and a 10.7% decrease in C_{max} in African-Americans in comparison to Caucasians (Figures 5.8b, 5.10). Although the differences observed did not meet our criteria for statistical significance due to limited sample size, the data results are in alignment with our hypothesis in that African-Americans, who were genotyped in our studies to be predominantly wild-type for the reference *MDR1**1/*1 haplotype, exhibit higher AUC and C_{max}, suggesting a more functional hepatic P-gp effect followed by less metabolism.

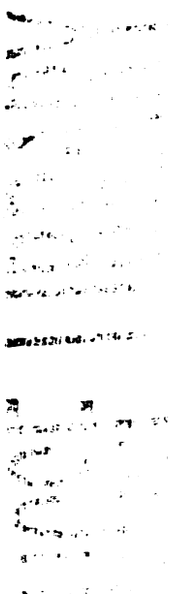

This may explain the higher AUC_{inf} and C_{max} during the luteal phase (compared to follicular) in African-Americans, compared to Caucasians.

Figure 5.8a Nelfinavir pharmacokinetics based on ethnicity, African-American (AA) *vs.* Caucasians during the luteal phase of the menstrual cycle.

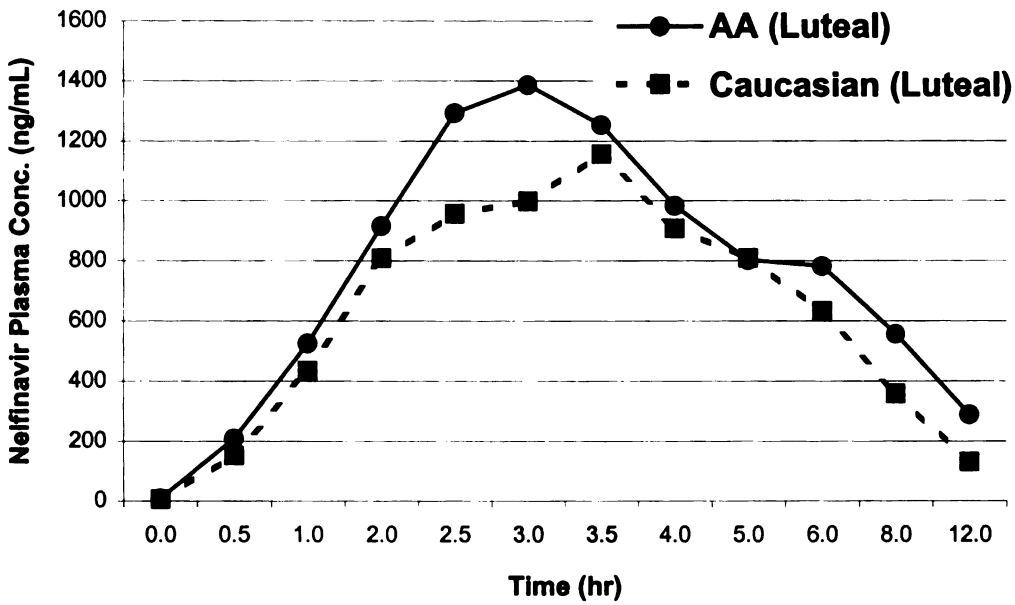

Figure 5.8b Nelfinavir pharmacokinetics during the follicular phase comparing African-American (AA) and Caucasian groups.

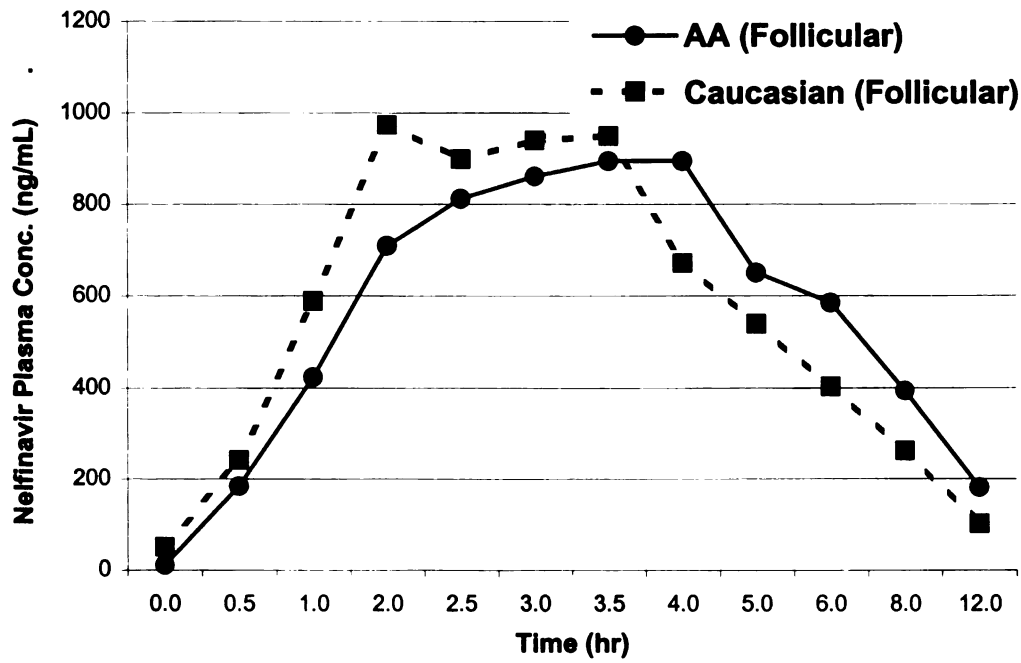

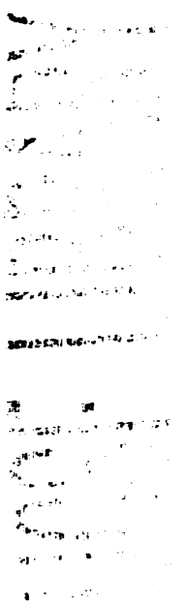

Figure 5.9 Percent increase in nelfinavir AUC_{inf} and C_{max} during the luteal phase in 12 African-American (AA) and 9 Caucasian (CA) subjects.

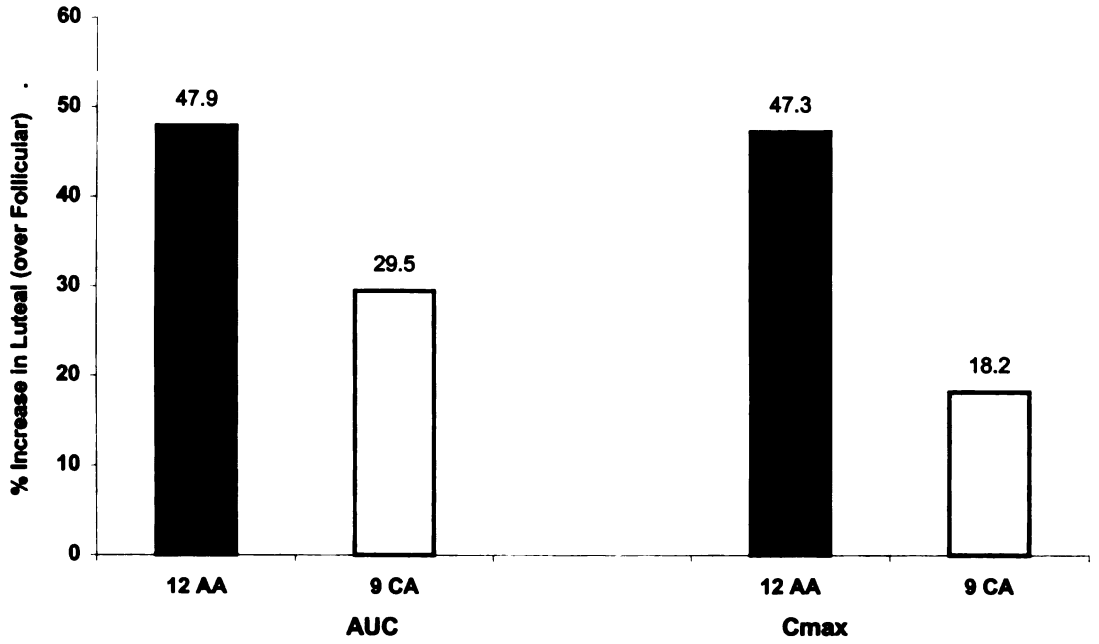

Figure 5.10 Comparison of nelfinavir AUC_{inf} and C_{max} during both phases of the menstrual cycle between African-Americans and Caucasians (CA).

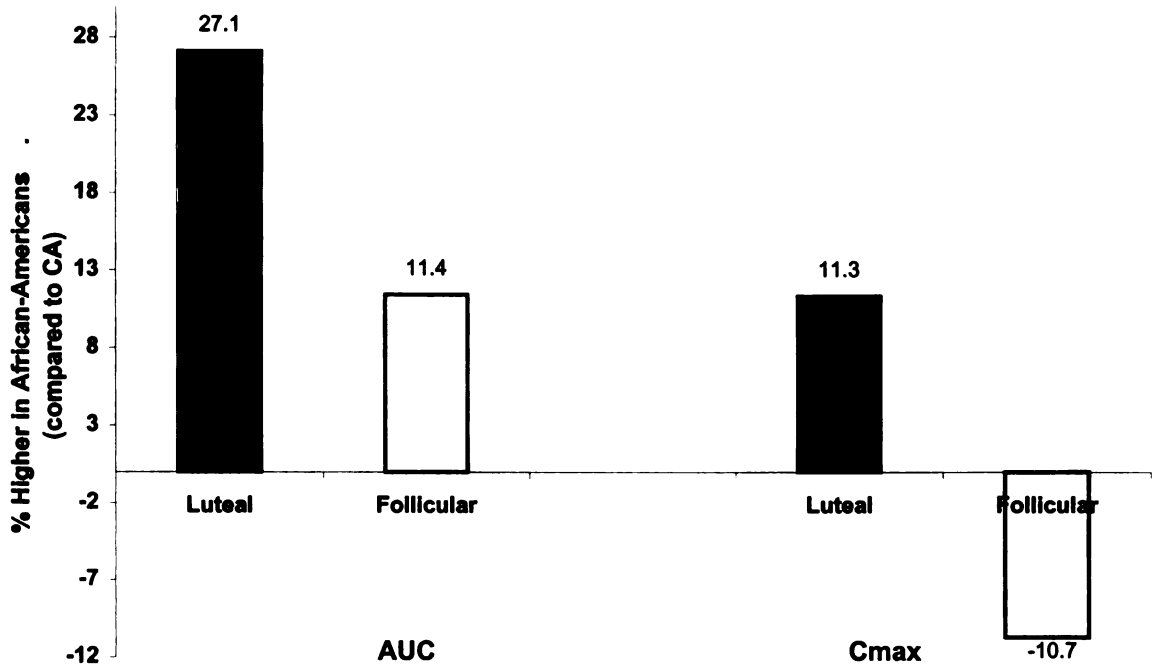

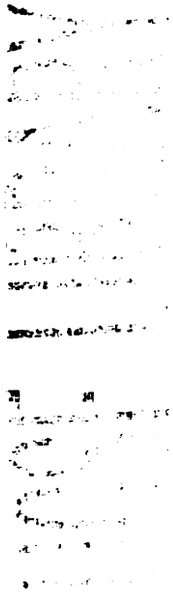

The effect of HIV on nelfinavir pharmacokinetics was investigated in all 21 subjects. Regardless of ovulatory cycle phase, there was an overall 15% increase in nelfinavir AUC_{last} in HIV^+ subjects compared to those that were HIV^-. HIV^+ subjects had a 6% increase in C_{max} compared to their HIV^- counterparts. However, HIV^+ subjects demonstrated a 35.4% higher AUC and a 25% higher C_{max} during the luteal phase. During the follicular phase, these same subjects had 7.1% and 14.5% lower AUC and C_{max}, respectively, compared to the HIV^- subjects. These differences were also observed regardless of ethnicity (Table 5.7). African-American subjects that were HIV^+ exhibited a 60.2% higher mean AUC and an 82.6% increase in mean C_{max} during the luteal phase (over follicular), while their HIV^- counterparts had a 15.5% and 15.1% higher AUC and C_{max}, respectively. HIV^+ Caucasian subjects possessed higher overall mean AUC and C_{max} values during the luteal phase, compared to their HIV^- counterparts, demonstrating a 131% higher AUC and a 69.7% higher C_{max} average values. HIV^- subjects showed an average decrease of 15.9% and 10.7% in AUC and C_{max}, respectively. However, none of these differences were statistically significant. These clinical data give some insight into the mechanistic effects of HIV on the pharmacokinetics of the P-gp substrate drug, nelfinavir. The positive correlation found between HIV-1 serum RNA levels and progesterone levels by Benki *et al.* (225) suggest that ovarian hormones may exert indirect effects on viral replication and we can speculate that it may even regulate levels of virus in the genital tract or serum though P-gp. Although the exact mechanisms are unknown, we can assert that hormonal fluctuations during the menstrual cycle affecting P-gp expression and function may act to regulate and influence drug absorption and bioavailability.

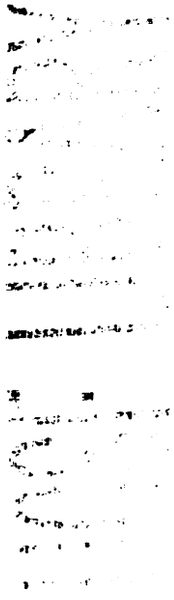

Table 5.7 Changes in nelfinavir pharmacokinetic parameters during the ovulatory cycle based on HIV and ethnicity.

	AUC		% Mean Change (±SD)	Cmax		% Mean Change (±SD)
	Follicular	**Luteal**	**[L/F]**	**Follicular**	**Luteal**	**[L/F]**
AA / HIV+	**5013** (4781)	**7829** (6741)	**60.2 (±91.1)**	**817** (751)	**1485** (1361)	**82.6 (±120)**
AA / HIV-	5915 (6629)	7056 (9707)	15.5 (±56.8)	1200 (1006)	1423 (1480)	15.1 (±45.5)
CA / HIV+	**5648** (5317)	**8754** (9915)	**131 (±171)**	**1165** (1108)	**1612** (1692)	**69.7 (±84.6)**
CA / HIV-	5356 (2581)	4748 (4248)	-15.9 (±40.3)	1052 (405)	951 (783)	-10.7 (±47.8)

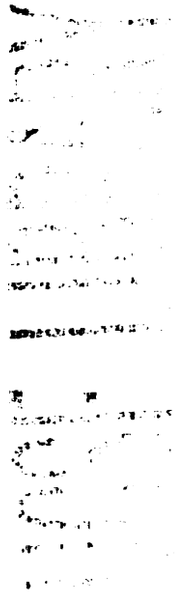

5.4.5 Effect of *MDR1* C3435T variant on nelfinavir pharmacokinetics and Calcein-AM extrusion mediated by P-gp

In support of investigating the effects of ethnicity on nelfinavir pharmacokinetics, the role of various *MDR1* SNPs was also explored to see if there were any effects on the absorption and disposition of a P-gp substrate (nelfinavir). We investigated whether nelfinavir AUC and C_{max} average values varied based on the C3435T *MDR1* SNP genotype, as previously shown by numerous investigators (Figures 5.11, 5.12).

Figure 5.11 Average nelfinavir AUC values in 21 study subjects based on *MDR1* C3435T SNP genotype.

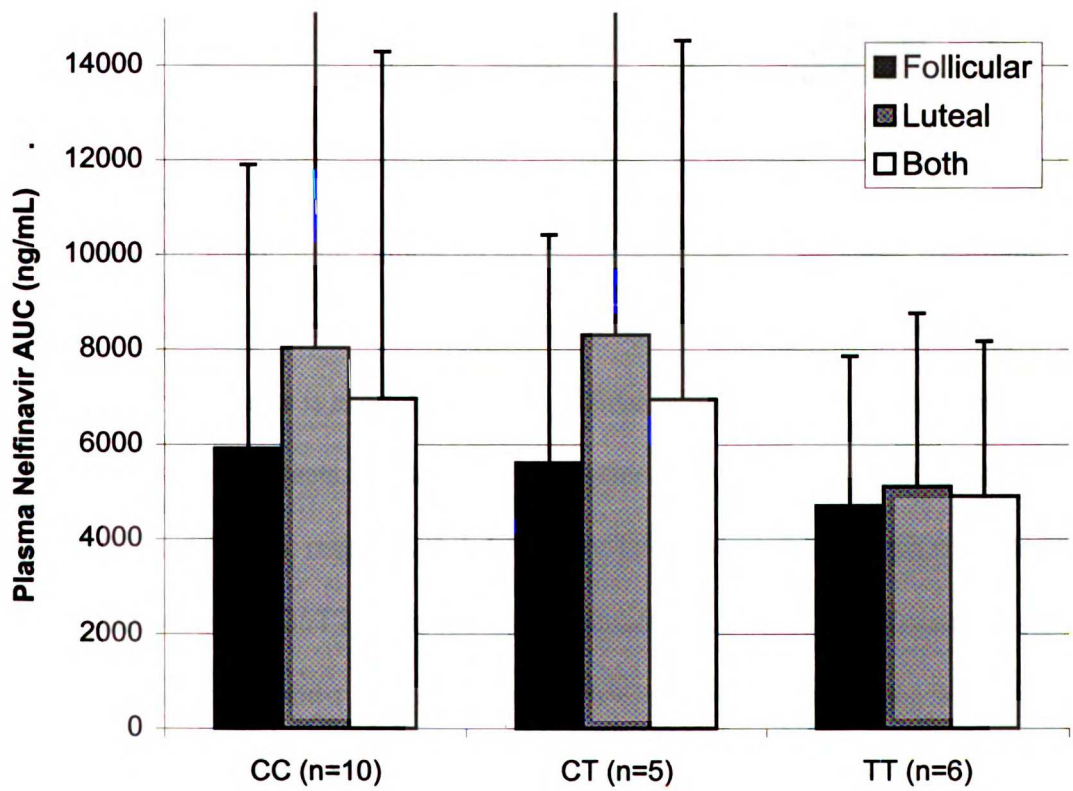

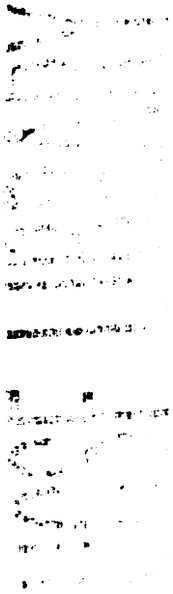

Figure 5.12 Average nelfinavir C_{max} values in 21 study patients based on *MDR1* C3435T SNP genotype.

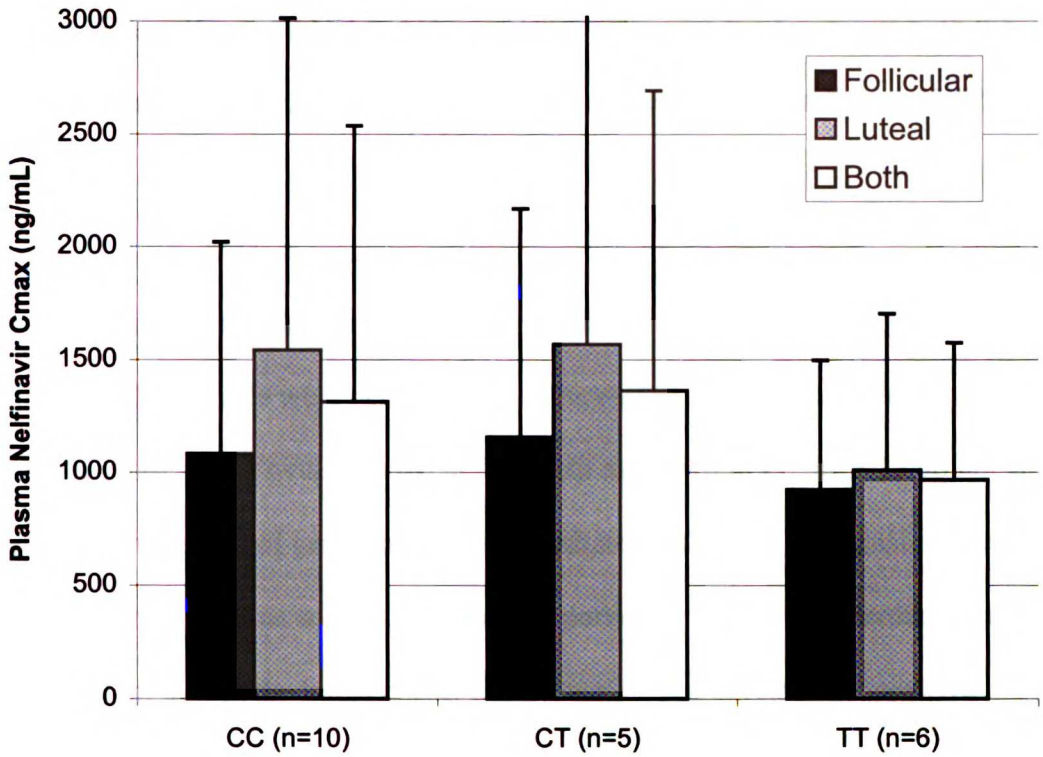

Results from our genotyping studies do not demonstrate any statistically significant changes in nelfinavir pharmacokinetics based on *MDR1* SNP genotype at the C3435T position. Although there is no statistically significant change, due to large interindividual variability between subjects, we do observe a noticeable overall decrease in AUC and C_{max} (36.0% and 34.6%, respectively) during the luteal phase for subjects with the homozygous variant 3435TT genotype (predominantly Caucasians), compared to those with the homozygous wild-type, reference 3435CC genotype (principally African-American subjects). There was also some decrease detected at 29.6% and 29.1% for AUC and C_{max}, respectively, for the combination of both follicular and luteal phases (open bars) in patients with the variant C3435T genotype, compared to wild-type subjects.

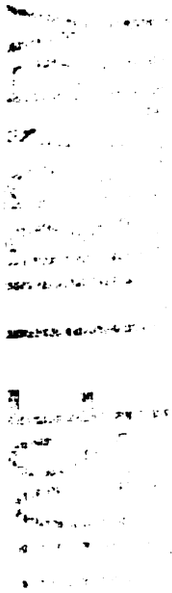

During the follicular phase, there was a 20.4% decrease in AUC and a 14.7% decrease in C_{max} for subjects exhibiting the variant (3435TT) genotype in comparison to wild-type subjects. The nelfinavir AUC and C_{max} average values for the 5 subjects with the heterozygous 3435CT genotype paralleled that of the values for reference 3435CC subjects.

We reinvestigated the Calcein-AM results to see if the *MDR1* C3435T polymorphism, ethnicity or HIV status were determinants of increased P-gp function during the luteal *vs.* follicular phase of the ovulatory cycle. The data as shown in Figure 5.13 do not suggest any significant effect of genotype on P-gp mediated Calcein-AM extrusion. Neither ethnicity nor HIV status seemed to show any particular pattern in determining increased P-gp function during the luteal phase. Hence, we did not observe any positive correlations or effects of ethnicity, *MDR1* genotype and HIV status on P-gp function in lymphocytes, nor do we expect these markers to serve as predictive tools for such.

5.5 Discussion and Conclusions

P-glycoprotein (*MDR1*) has proven to be an important factor in the disposition of many drugs. In the present study, we sought to understand the role of hormonal changes, namely estradiol (E_2) and progesterone, associated with the ovulatory cycle on P-gp expression and function, as it relates to ethnicity, *MDR1* SNP genotyping, nelfinavir pharmacokinetics and HIV status. We observed that the transporter, P-gp, was upregulated during the luteal phase in endometrial tissue. It appears that a similar change may occur in the liver increasing hepatobiliary excretion of parent drug, thereby

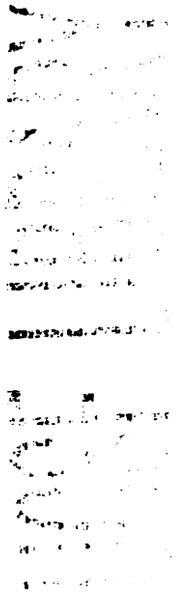

Figure 5.13 Percentage change (luteal/follicular) of Calcein fluorescence for each of the 21 subjects based on ethnicity and *MDR1* SNP genotype at the C3435T position.

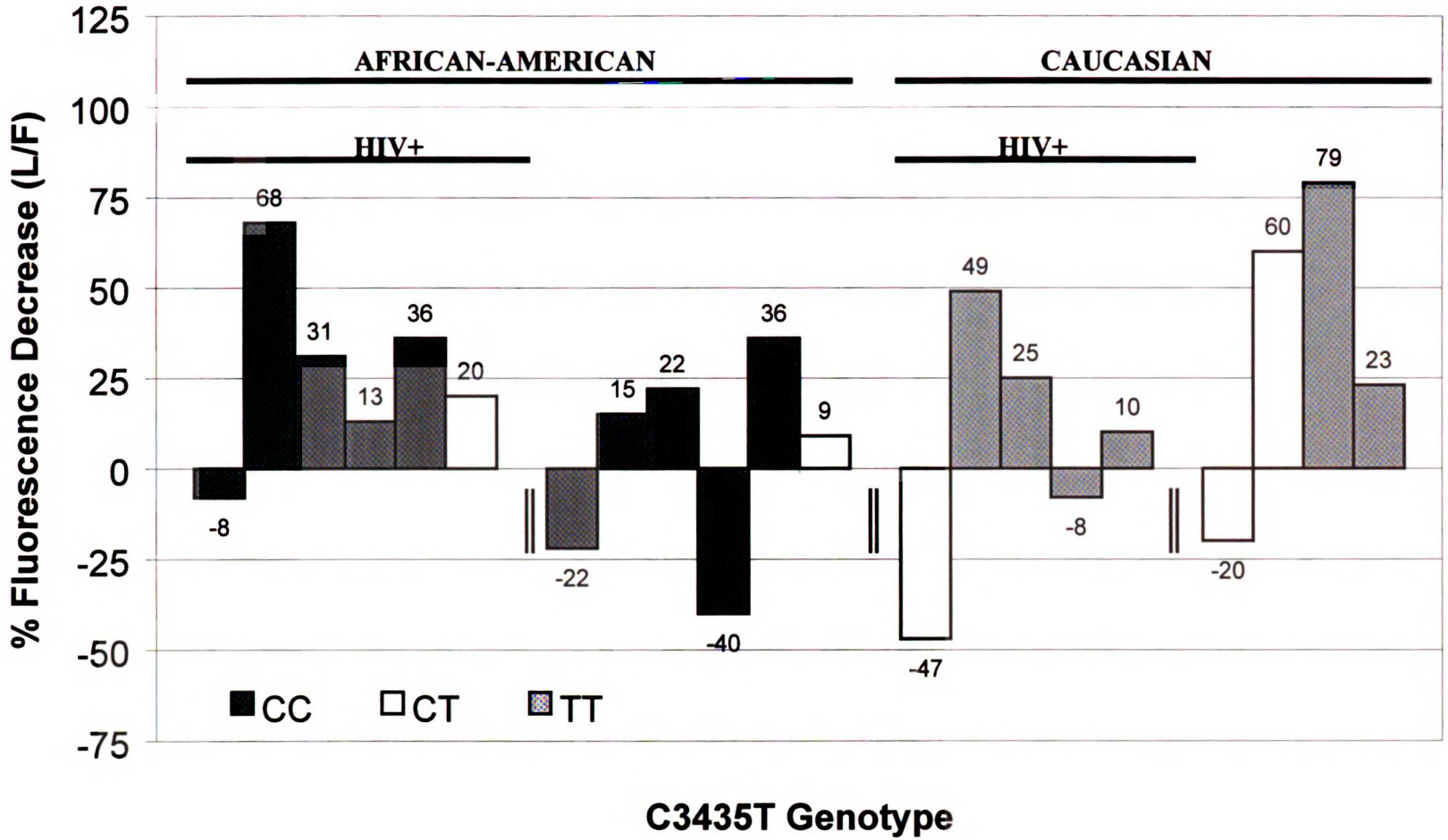

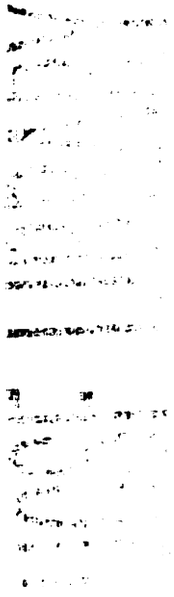

decreasing exposure to CYP2C19 and CYP3A4-mediated metabolism, the principal routes of metabolic clearance.

The upregulation of P-gp by various factors (e.g. steroid hormones, rifampin, heat-stress) may also be dependent upon the variety of haplotype polymorphisms present in transporters and metabolic enzymes. Results from our studies suggest that the wild-type *MDR1* genotype at particular sites in linkage disequilibrium (*MDR1**1/*1 haplotype) may be more susceptible to hormone-induced induction, translating into more significant clinical effects during the luteal phase of the menstrual cycle. In our studies, we examined the clinical manifestations of the C3435T *MDR1* SNP polymorphism and determined how this relates to nelfinavir pharmacokinetics.

Results from our studies have added an additional unexpected element, causing us to explore the molecular and clinical effects of HIV. Greenblatt *et al.* (226) showed that in ovulating women, the midluteal phase of the menstrual cycle, when β-estradiol and progesterone levels peak, was associated with significantly decreased HIV-1 mRNA blood levels suggesting interactions with P-gp. Data from Reichelderfer *et al.* (109), on the other hand, demonstrated that HIV-1 RNA levels measured from mucus in the genital tract varied depending on the sampling method. However, it was shown that HIV-1 RNA in endocervical canal fluid was highest during the midluteal phase and lowest during menses and the follicular phase. Additional data from their group suggested that menstrual cycle phase had no effect on HIV-1 RNA blood levels and that HIV-1 RNA levels were higher in endocervical canal fluid than in PBMCs during the luteal phase.

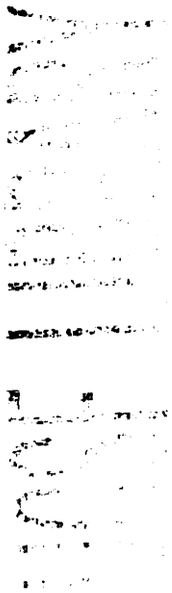

A more recent study by Benki *et al.* (225) confirmed results from both groups, demonstrating that both serum and cervical HIV-1 RNA levels varied with the menstrual cycle. A significant positive correlation between serum levels of progesterone and serum HIV-1 RNA levels was found as well as a positive correlation between cervical HIV-1 RNA and the number of days following the midcycle surge in LH (luteinizing hormone). These data contradict our hypothesis since we would expect HIV-1 RNA levels to decrease during the luteal phase due to steroid-induced P-gp expression and the inverse correlation found between HIV-1 RNA levels and P-gp expression. However, due to a dearth of research in this area, we can only speculate as to how it may actually be affecting the expression and activity of the transporter. It is possible that HIV-1 RNA may have altered mechanisms of action and interactions with P-gp within the reproductive tract itself (i.e. mucus *vs.* tissue, endometrial *vs.* vaginal) or compared to plasma due to cell-type specific differences and the presence or absence of various receptors and co-factors. We question how the disease factor plays a role in the delicate balance between P-glycoprotein, hormones and substrate-drug pharmacokinetics. Although very little is definitively known, substantial evidence continues to point to the cogent and enigmatic relationship between P-gp and HIV. We also examined whether P-gp function in blood as measured by Calcein-AM, was influenced by the *MDR1* C3435T polymorphism, HIV status or ethnicity.

By direct sequence analysis of *MDR1*, we examined the frequency and distribution of 9 previously identified *MDR1* single-nucleotide polymorphic variants. From these data, we confirmed that two synonymous SNPs (C1236T in exon 12 and C3435T in exon 26) and

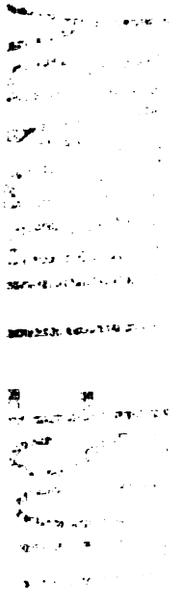

a non-synonymous SNP in exon 21 (G2677T/A) were linked. We showed that the majority (75%) of our African-American subjects (9/12) were found to exhibit the *MDR1**1/*1 haplotype, being homozygous wildtype at the linked C1236T, G2677T/A and C3435T positions (Table 5.4). The *MDR1**2/*2 haplotype was found to be largely present among the Caucasian subjects (44.4%), being homozygous variant at the same three positions. These data confirm previous results of Kim *et al.* (197), who showed that the *MDR1**2 variant occurred in 62% of 37 European-Americans and 13% of 23 African-Americans. *In vivo* functional relevance of the C3435T SNP was assessed with the HIV protease inhibitor and P-gp substrate, nelfinavir, as a probe for changes in the transporter's activity during the course of the ovulatory cycle.

Nelfinavir pharmacokinetic results show a difference in the plasma drug concentration-time profile between the follicular and luteal phases (Figure 5.4). There was a 35% increase in mean AUC_{inf} and a 33% increase in mean C_{max} during the luteal phase compared to follicular. P-values were calculated using a paired, 2-tailed t-test demonstrating marginal significance at 0.047 and 0.051 for C_{max} and AUC_{inf}, respectively. There was also a 21% non-significant decrease in volume of distribution (V_z/F), that may be explained by hormonally-induced expression and efflux activity of hepatic P-gp during the luteal phase. There were no changes in t_{max}, $t_{1/2\lambda Z}$, or CL/F between phases as shown in Table 5.5. It is possible that lower nelfinavir plasma concentrations during the follicular phase may be due to increased availability of nelfinavir to undergo hepatic CYP2C19 and CYP3A4 metabolism, as there is less P-gp to efflux nelfinavir out before it is metabolized. We conclude that the pharmacokinetic

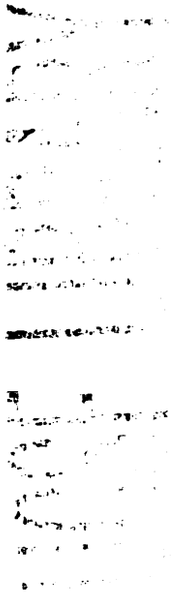

results suggest an increased clearance during the follicular phase, although decreased bioavailability cannot be ruled out.

The pharmacokinetics of the active nelfinavir metabolite, M8 were also investigated. Despite a very low limit of quantitation (LOQ), M8 levels were not detectable in 6 subjects (and not measured in 2 subjects due to lack of sample availability). In the remaining 13 subjects, the plasma-M8 AUC_{inf} and C_{max} average values between the phases, however, were slightly more pronounced, showing a non significant 1.4-fold increase ($p= 0.17$) and significant 1.7-fold ($p= 0.05$) increase, respectively, during the luteal *vs.* follicular phase (Table 5.6). There was also no observed difference in the M8/nelfinavir ratio between phases, suggesting no change in the conversion of nelfinavir to M8 in the liver or the relative contribution of M8 to the anti-viral efficacy of nelfinavir. Nelfinavir AUC_{inf} and C_{max} values in the 13 patients with detectable levels of M8 did not differ significantly from the 8 patients with undetectable M8. However, these 8 patients demonstrated greater mean nelfinavir CL/F values in both phases compared to the 13 with detectable M8. We also noted that the 8 patients with non-detectable M8 levels had a lower mean nelfinavir CL/F value during the luteal phase compared to follicular with a (L/F) ratio of 0.45.

Nelfinavir pharmacokinetics based on racial differences was also examined (Figure 5.7). In Caucasians, we did not see any difference in the pharmacokinetic profile for nelfinavir between phases. However, African-American subjects showed a higher AUC and C_{max} during the luteal *vs.* follicular phase. This may be due to the fact that African-Americans

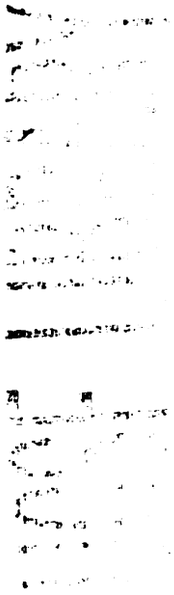

possessing the wildtype *MDR1* genotype may have more functional P-gp, less hepatic metabolism, and therefore, higher overall levels. Interestingly, when we compared nelfinavir levels between the two ethnic groups during the luteal phase, Caucasians had significantly lower AUC and C_{max} (27.1% and 11.3%, respectively). This may be due to a predominantly variant P-gp phenotype with less functional activity. The ethnic difference observed during the luteal phase was not as much as during the follicular phase (Figure 5.8b). These results are also reflected in the data illustrated in Figures 5.11 and 5.12. Despite high standard deviations (due to high interindividual variability), nelfinavir AUC and C_{max} were found to be lower during the luteal phase in subjects with the homozygous variant 3435TT genotype, compared to those in subjects with homozygous wildtype variant (3435CC). The same was seen, but to a much lesser degree, during the follicular phase. Although not statistically significant, there is still a similar, but discernable difference observed between homozygous variant and reference genotypes. These results are consistent with data of Fellay *et al.* (213) in which patients with the *MDR1* 3435TT genotype demonstrated the lowest levels of median nelfinavir concentrations compared to those with the 3435CC genotype.

We also found HIV to play a role in nelfinavir pharmacokinetics. However, ethnicity continued to play a role in the overall extent of nelfinavir plasma levels based on cycle phase. To our surprise, we found that HIV^+ subjects exhibited higher nelfinavir AUC and C_{max} compared to those of their healthy counterparts during the luteal phase (over follicular). HIV^+ subjects also had more fluctuations in drug levels during the menstrual cycle. African-American HIV^+ subjects demonstrated higher nelfinavir AUC and C_{max}

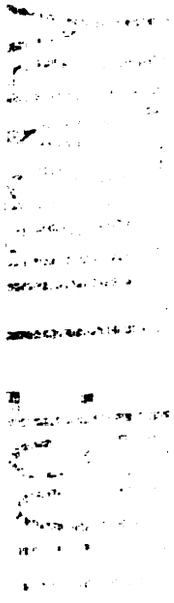

values compared to Caucasian HIV^+ subjects (luteal over follicular). It is possible that P-gp may be upregulated in HIV^+ subjects and therefore display a larger physiological P-gp effect on nelfinavir pharmacokinetics. Another explanation may be that HIV^+ subjects may have elevated steroid hormone levels in addition to immunologic factors (e.g. cytokines) that could be upregulating P-gp during the luteal phase. The direct physiological interaction between P-gp and HIV has not yet been investigated and further evidence is needed to make conclusive remarks.

P-gp function characterized by active efflux of fluorescent calcein in lymphocytes was analyzed to see if there was a correlation with ethnicity or the *MDR1* C3435T polymorphism (Figure 5.13). There was no apparent association observed with either of these factors. However, additional statistical analyses, as depicted in Figure 5.14, show that the cycle phase associated increase in lymphocytic P-gp activity as measured by Calcein-AM efflux during the luteal phase (luteal/follicular), correlates with endometrial induction of *MDR1* mRNA expression during the luteal phase, over follicular. The rank correlation between P-gp activity and endometrial *MDR1* mRNA was calculated to be 0.55 with a p-value of 0.019 [CI= 0.11 to 0.81] as depicted in Table 5.8. Our statistical results suggest an ethnic and a consequent genotype
effect on lymphocyte P-gp activity. A significant correlation was observed between African American (AA) subjects and higher P-gp activity using baseline values ($p=0.0047$) as shown in Table 5.8. Statistical significance ($p= 0.04$) was also found when looking at luteal cycle phase as a predictor for greater P-gp activity, as measured by Calcein-AM efflux. A strong correlation was seen between African-Americans and P-gp

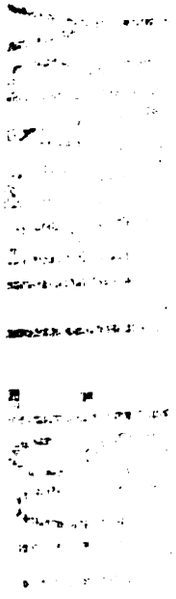

inhibition by GG918. Increased P-gp activity in lymphocytes after subtracting background inhibition values correlated significantly (p=0.01) within the AA subjects.

Table 5.8 Statistical correlation analyses between P-gp activity mediated by Calcein-AM efflux and endometrial *MDR1* mRNA expression during the luteal phase *vs.* follicular. Multivariate analysis for P-gp activity via Calcein-AM fluorescence (and GG918 inhibition) and various factors, with predictor estimates shown as percentage effects.

Variable 1 (log)	Variable 2 (log)	Rank Correlation	95% Confidence Interval lower	upper	P-value
Cal-AM efflux ratio (L/F)	**Endometrial *MDR1* mRNA ratio (L/F)**	0.548	0.109	0.808	**0.019**

Outcome	Predictor	Estimate (%)	95% Confidence Interval lower	upper	P-value
Log Cal-AM fluorescence (during luteal phase)	**HIV**	56.52	-18.29	199.8	0.17
	Ethnicity (AA)	171.6	40.96	423.5	**0.005**
	Luteal	-20.02	-34.90	-1.734	**0.035**
+ GG918	**Ethnicity (AA)**	99.97	8.59	268.3	**0.028**

Using the SAS LIFEREG statistical procedure, the changes in pharmacokinetic parameters between menstrual cycle phase, HIV status and ethnicity, were modeled with a lognormal distribution. The logarithm of the luteal phase value was modeled in terms of the logarithm of the follicular phase value, whether the follicular phase value was influenced by race and/or HIV status. The coefficient of the follicular term reflects the effect of luteal phase, with a coefficient of 1.0 indicating no systematic difference

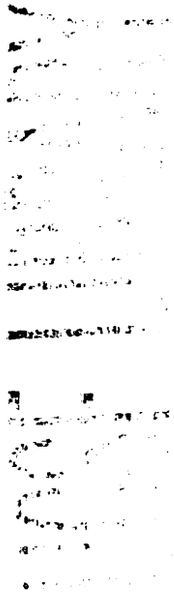

Figure 5.14 Correlation between induction of endometrial MDR1 mRNA and increased P-gp activity in lymphocytes (as measured by Calcein-AM accumulation less GG918-mediated inhibition of P-gp efflux) during the luteal phase (over follicular).

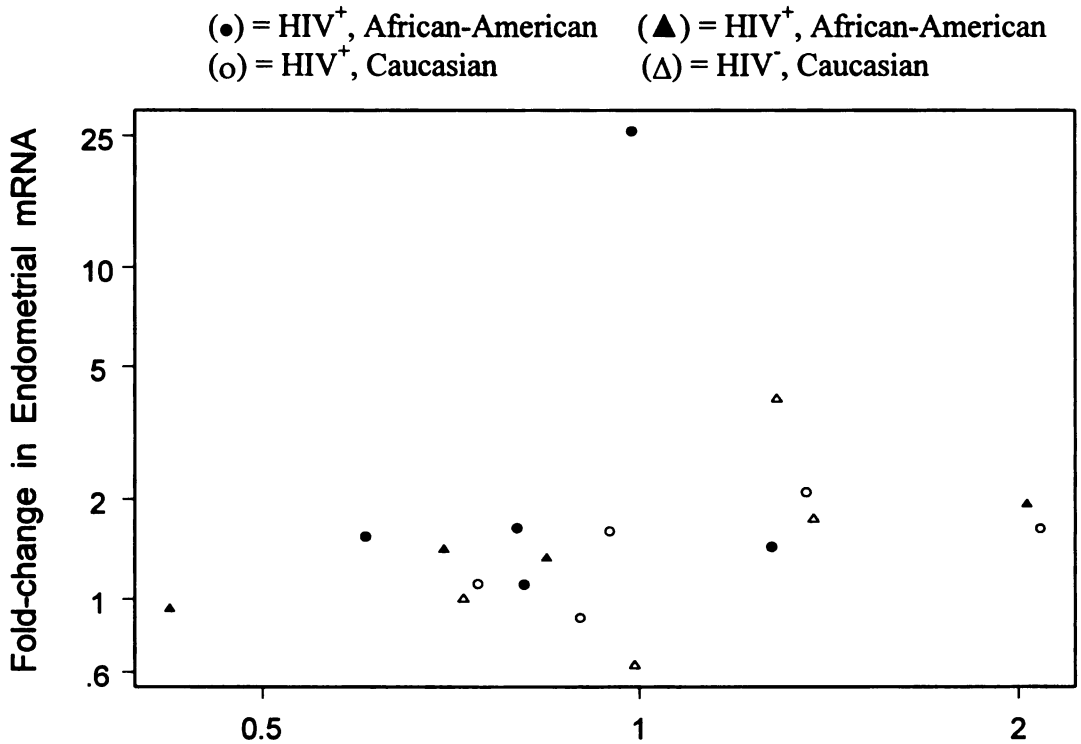

between luteal and follicular phase. We therefore show the difference from 1.0, with its confidence interval and a p-value testing for departure from 1.0.

In the multivariate analysis presented in Table 5.9, there did not appear to be an HIV effect on nelfinavir pharmacokinetics, namely C_{max} (p=0.41) and CL/F (p=0.29). As individual predictors, HIV status, ethnicity (AA) or ovulatory cycle phase (luteal) also did not show any correlations with nelfinavir AUC_{inf} (p=0.41, 0.92 and 0.60,

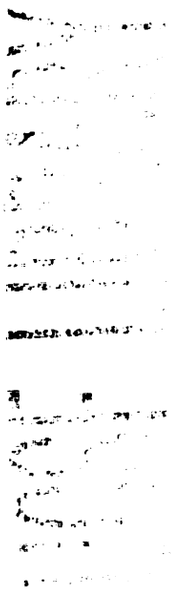

respectively). However, in HIV^+ subjects, addition of the ovulatory cycle phase variable demonstrated the combination to be a strong predictor of nelfinavir AUC_{inf} (p=0.017) (Table 5.9). The effect of cycle phase within the HIV^+ group demonstrated an estimated 90.4% increase in luteal phase nelfinavir AUC_{inf}. However, these two predictors, HIV status and luteal cycle phase, were not found to correlate significantly with the outcome of nelfinavir C_{max} (p=0.09).

Table 5.9 Multivariate statistical analyses examining the effect of HIV status, ethnicity and ovulatory cycle phase on nelfinavir pharmacokinetics. All p-values are two-tailed and significant p-values are bolded.

			95% Confidence Interval		
Outcome	**Predictor**	**Estimate (%)**	**lower**	**upper**	**P-value**
Log nelfinavir Cmax	**HIV**	-33.99	-76.41	84.72	0.41
Log nelfinavir CL/F	**HIV**	63.25	-36.27	318.2	0.29

			95% Confidence Interval		
Outcome	**Predictor**	**Estimate (%)**	**lower**	**upper**	**P-value**
Log nelfinavir AUC-inf	**HIV**	-33.99	-76.41	84.72	0.41
	Ethnicity (AA)	4.930	-61.62	186.9	0.92
	Luteal	-9.059	-37.27	31.84	0.60
	HIV-Luteal	90.40	13.97	218.1	**0.017**
Log nelfinavir Cmax	**HIV**	-42.16	-77.79	50.68	0.25
	Ethnicity (AA)	-5.264	-62.49	139.3	0.90
	Luteal	-6.16	-36.62	38.95	0.74
	HIV - Luteal	58.03	-8.12	171.8	0.09

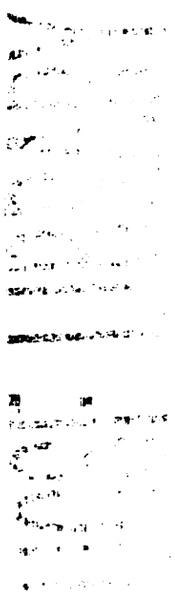

Statistical analyses depicted in Table 5.10 show that HIV^+ subjects demonstrated significant differences between the luteal *vs.* follicular phases, illustrated by larger luteal AUC and C_{max} values of M8 ($0.0064 \leq p \leq 0.025$) during the luteal phase. Hence, HIV status and cycle phase variables were mutually shown to be a strong predictor for nelfinavir metabolite, M8, pharmacokinetic parameters, such as AUC_{inf} ($p=0.006$), AUC_{last} ($p=0.007$) and C_{max} ($p=0.025$). We observed an estimated 393% significantly higher M8 C_{max} in HIV^+ subjects during the luteal phase. Additionally, we observed an estimated 375% significant increase in AUC_{inf} and a 381% increase in AUC_{last} of M8 for HIV^+ subjects during the luteal phase, versus follicular. We did not see a significant difference in M8 pharmacokinetic measurements with the ethnicity factor, as shown in Table 5.10 with our African-American (AA) subjects. These results suggest that HIV^+ subjects demonstrate a significantly larger difference in luteal versus follicular M8 pharmacokinetic measures.

From these studies, we find that increased endometrial *MDR1* mRNA expression correlated significantly with increased lymphocytic P-gp efflux activity during the luteal versus follicular phases. Ethnicity was found to play a role in predicting P-gp activity, with African-American subjects correlating strongly with higher lymphocytic P-gp activity. We also found that the luteal phase was a strong predictor of higher P-gp activity in lymphocytes. With regard to HIV status, we conclude that HIV^+ women showed significantly increased nelfinavir and M8 levels via pharmacokinetic measures during the luteal compared to the follicular phase. We observed higher overall AUC and C_{max} values

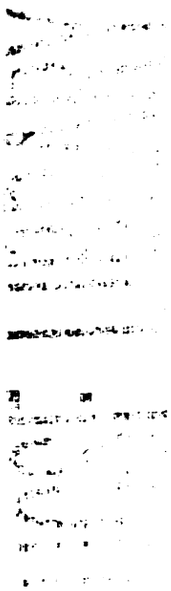

Table 5.10 Statistical significance of M8 data during the luteal phase in HIV^+ subjects. All p-values are two-tailed and significant values are bolded.

Outcome	Predictor	Estimate (%)	95% Confidence Interval		P-value
M8 Cmax	Luteal	0.043	-0.160	0.246	0.68
	Luteal	-0.057	-0.314	0.200	0.66
	AA- Luteal	+156%	-47%	+1140%	0.24
	Luteal	-0.097	-0.310	0.115	0.37
	HIV Luteal	**+393%**	+22%	+1896%	**0.025**
M8 AUC-last	Luteal	0.040	-0.095	0.175	0.56
	Luteal	-0.019	-0.198	0.161	0.84
	AA- Luteal	+95%	-51%	+682%	0.34
	Luteal	-0.072	-0.207	0.063	0.30
	HIV Luteal	**+381%**	+54%	+1402%	**0.0068**
M8 AUC-inf	Luteal	0.036	-0.094	0.167	0.59
	Luteal	-0.018	-0.194	0.158	0.84
	AA- Luteal	+87%	-53%	+644%	0.38
	Luteal	-0.073	-0.204	0.058	0.28
	HIV Luteal	**+375%**	+55%	+1354%	**0.0064**

during the luteal phase in HIV^+ subjects, regardless of ethnicity. This may be an hepatic effect since CYP2C19, the major metabolic pathway for nelfinavir, is expressed primarily in hepatocytes. In HIV^- subjects, there was no effect on nelfinavir pharmacokinetics based on hormonal phase. It is possible that HIV-1 virus and ovarian hormones may

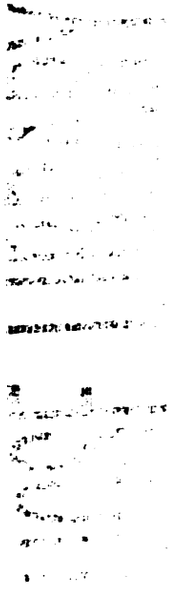

interact to regulate metabolizing enzyme or transporter function in hepatocytes. As P-gp may not be the rate-limiting step for nelfinavir metabolism, additional variables such as the presence of other transporters, hormonal effects on HIV infectivity and possible HIV effects on transporter/enzyme interplay affecting nelfinavir metabolism should also be considered.

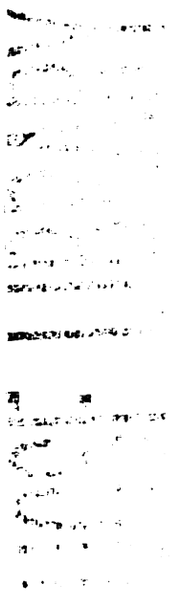

CHAPTER VI

Summary and Conclusions

6.1 Summation & Conclusions

The results summarized thoughout the course of this dissertation emphasize the significance of the impact that both endogenous and synthetically-derived sex-steroid hormones can have on the expression and activity of the multi-drug resistant transporter, P-glycoprotein. This in turn has the potential for profound pharmacokinetic consequences and, therefore, can result in therapeutic efficacy issues for those drugs that are good P-gp substrates.

We have shown through a series of *in vitro* studies, as illustrated in Chapter 2, the impact that estrogens can have on the expression of P-gp and *MDR1* in the human colon carcinoma cell line, LS180. The objective of these studies was to determine whether endogenous and synthetically-derived estrogens were capable of inducing P-gp expression and stimulating ATPase catalytic activity. For these purposes, we utilized a human colon carcinoma cell line, LS180, endogenously expressing P-gp to serve as a model for P-gp induction. Results from these studies show that the combination of 17β-estradiol and progesterone did not induce P-gp protein or *MDR1*-mRNA expression in

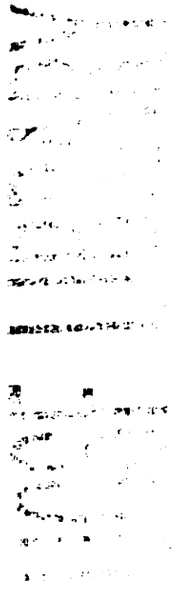

HepG2 liver cells compared to control. We also did not observe any effect with LH and FSH, 17β-estradiol alone or testosterone. These results are most likely due to the absence of estrogen or progesterone receptors and various essential co-factors.

Expression and induction of P-gp by hormones were then investigated in the LS180 cell line, which was shown by Pfrunder *et al.* (112) to express the pregnane X receptor, hPXR, an important component in the induction of *MDR1* by PXR ligands (i.e. rifampin). Our results demonstrate an induction of P-gp by estrone (3-fold), estriol (2.2-fold) and ethynyl estradiol (3.4-fold) at 50 μM. *MDR1*-mRNA expression was similarly inducible by these same steroid hormones (7.2, 6.3 and 9.0-fold, respectively), also by progesterone (3.2-fold), but insignificantly by 17β-estradiol (1.4-fold). Four steroids, ethynyl estradiol, estrone, norethindrone and norgestrel, exhibited concentration-dependent induction of *MDR1* mRNA at concentrations that were closer to physiologic conditions, ranging from 25 nM to 10 μM. However, induction at 25 nM compared to 18S control was only observed for ethynyl estradiol, estrone and norethindrone. Results from these studies allow us to conclude that there may be minimal induction of intestinal *MDR1* mRNA and P-gp by circulating 17β-estradiol and progesterone in normally cycling women *in vivo.* However, we did observe significant induction by estriol (the predominant estrogen circulating during pregnancy) and estrone (the predominant estrogen in post-menopausal women), suggesting that there may be upregulation of intestinal P-gp in women during pregnancy and possibly following menopause. Furthermore, it is very likely that daily administration of oral contraceptive drug therapy with ethynyl estradiol and norethindrone, previously only known to be metabolized by CYP3A4, may cause drug-drug interactions when co-administered with other P-gp and CYP3A4 substrate drugs.

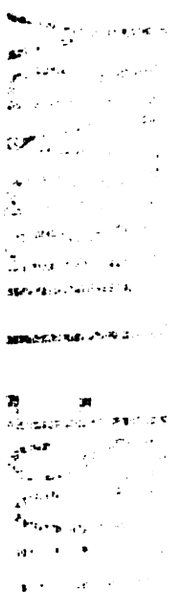

Potential dangers include toxicity and/or decreased or enhanced therapeutic efficacy of HIV medications.

Of the various estrogens tested for transcriptional activation of the *MDR1* promoter (4kb region), only ethynyl estradiol showed significant stimulation. Furthermore, ethynyl estradiol, norethindrone and norgestrel were also found to strongly induce P-gp, suggesting that oral contraceptive compounds may be metabolized significantly in the intestine due to upregulated P-gp. Utilizing the baculovirus insect cell system transfected with the human *MDR1*cDNA, we determined that progesterone and ethynyl estradiol were potent stimulators of P-gp ATPase catalytic activity, an essential component in active transport of substrates. These results suggest that a non-substrate and inhibitor such as progesterone also has the ability to bind P-gp and stimulate ATPase catalytic activity.

The specific objective of the studies detailed in Chapter 3 was to test whether sex-steroid hormones and their metabolites are specific substrates of P-gp employing an established transport cell culture system. We also confirmed in our laboratory that the HIV protease inhibitor, nelfinavir was a P-gp substrate and examined potential interactions with steroid hormone transport. The apparent permeability coefficients for the bi-directional transport of various estrogens in the presence and absence of a P-gp inhibitor, GG918, in MDCK and *MDR1*-overexpressing MDCK cells are summarized in Table 6.1. The net efflux ratios (B→A/A→B) demonstrate the extent of active efflux in the basolateral-to-apical

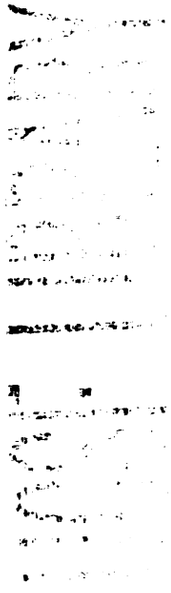

Table 6.1 Apparent permeability coefficients (P_{app}) from bi-directional transport studies for various estrogens with and without P-gp inhibitor, GG918 (1μM), across MDCK and *MDR1*-MDCK (MM) cell lines.

Cell Line	Substrate	Substrate Conc.	GG918 Inhibitor (1 μM)	P_{app} x 10^{-7} cm/s (avg ± SE), n=3		Net Efflux Ratio (B→A/ A→B)
				B→A	A→B	
MDCK	17β-Estradiol	20 μM	-	601 ± 133	589 ±123	1.0
MM			-	955 ± 778	273 ± 123	3.5
MDCK	Estrone	1 μM	-	5.90 ± 0.24	6.10 ± 0.38	0.97
			Yes	6.23 ± 1.65	6.86 ± 1.29	0.91
MM	Estrone	1 μM	-	38.7 ± 6.4	5.90 ± 1.39	6.6
			Yes	7.54 ± 3.34	6.28 ± 3.61	1.2
MDCK	Estriol	20 μM	-	112 ± 3	97.5 ± 3.9	1.1
			Yes	20.0 ± 4.4	13.2 ± 2.1	1.5
MM	Estriol	20 μM	-	147 ± 10	46.5 ± 19.4	3.2
			Yes	16.3 ± 7.2	12.3 ± 9.0	1.3
MDCK	Ethynyl-Estradiol	5 μM	-	50.1 ± 0.9	63.3 ± 1.3	0.8
			Yes	28.5 ± 6.7	27.7 ± 8.9	1.0
MM	Ethynyl-Estradiol	5 μM	-	467 ± 9	41.6 ± 2.2	11
			Yes	27.6 ± 1.4	22.6 ± 2.5	1.2
MDCK	Nor-ethindrone	10 μM	-	34.8 ± 6.8	57.3 ± 7.1	0.6
MM			-	43.8 ± 5.9	33.1 ± 5.2	1.3

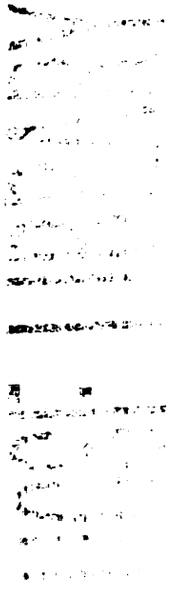

(B→A) direction compared to absorptive flux in the A→B direction for both cell lines, with or without P-gp inhibition.

We show from bi-directional transport studies that 17β-estradiol, estrone, estriol and ethynyl estradiol are all actively transported by P-gp, exhibiting net efflux ratios greater than 2.0 in *MDR1*-transfected MDCK cells. In the presence of P-gp inhibitor, GG918, these efflux ratios were reduced to approximately 1.0. These results were then corroborated with intracellular measurements in both cell monolayers, demonstrating significantly decreased accumulation in P-gp expressing cells given either a basolateral or apical dose. It was also confirmed in our laboratory that nelfinavir is a good P-gp substrate and able to competitively inhibit P-gp mediated transport of ethynyl-estradiol, estrone and estriol.

In pre-menopausal women, the cycling of the sex-steroids, estradiol and progesterone, during the course of the ovulatory cycle can also have profound physiologic effects on the activity and expression of various proteins, receptors and co-factors in a variety of tissue compartments. The effect of acute differences in steroid hormone levels between the follicular and luteal phases was studied in $HIV^{+/-}$ African-American and Caucasian women, specifically examining changes in nelfinavir pharmacokinetics as influenced by endometrial and intestinal P-gp expression and lymphocytic efflux activity. Study patients were also genotyped for specific *MDR1* polymorphisms to determine whether pharmacogenetics and ethnicity played a role in these P-gp mediated events.

Twenty-one HIV-positive and negative women of both African-American and Caucasian descent were recruited to participate in a study investigating the effect of menstrual cycle phase (follicular *vs.* luteal) on intestinal and endometrial P-gp expression. We hypothesized that induction would be observed during the luteal phase, characterized by peak estradiol and progesterone levels, compared to the follicular phase. We expected that any induction observed would be reflected in increased lymphocytic P-gp efflux activity measured using the diester fluorogenic compound, Calcein-AM, as a probe substrate.

Expression analyses of *MDR1* mRNA in intestinal tissue demonstrated no change between follicular and luteal phases, exemplified by an insignificant 1.11-fold overall increase during the luteal phase compared to follicular. We detected an ethnic difference, however, with African-Americans exhibiting lower average *MDR1* mRNA expression during the luteal phase compared to Caucasians. Endometrial *MDR1* mRNA expression showed larger differences between phases. In all subjects, an average 3.2-fold induction of *MDR1* mRNA was observed during the luteal phase compared to follicular. An ethnic difference was again observed with African-Americans characterized by an average 4.3-fold endometrial induction. In comparison, Caucasians only demonstrated an overall 1.7-fold induction during the luteal versus follicular phase. At the protein level, we failed to confirm the observations, mostly due to insufficient viable tissue during the follicular phase. These results suggest that there is hormonal induction of *MDR1* mRNA in the endometrium, but not in the intestine.

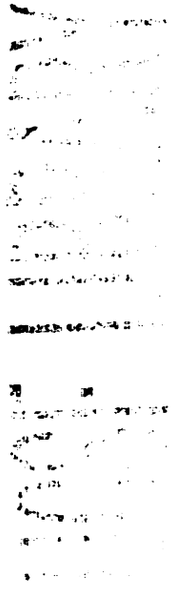

P-gp efflux activity was measured by Calcein fluorescence accumulation in isolated peripheral blood lymphocytes that were gated specifically for CD56+, P-gp expressing cells. Inhibition of P-gp efflux was mediated by use of GG918 to verify the presence of active P-gp in this cell population. Comparative analyses of intracellular Calcein fluorescence accumulation between follicular and luteal phases demonstrated a 16.8% average decrease in Calcein accumulation during the luteal phase, indicating higher P-gp activity in the luteal phase, possibly due to hormonal effects. A significant [rank] correlation was observed between endometrial induction of *MDR1* mRNA and higher P-gp activity in leukocytes during the luteal phase, strongly indicating the possibility for compromised intracellular HIV drug therapy in these tissues that may serve as sanctuary sites for HIV, as most HIV protease inhibitors are known to be excellent P-gp substrates. African-American subjects were found to have significantly higher P-gp activity during the luteal phase. This suggests that African-Americans, predominantly homozygous wildtype for the important *MDR1*2* haplotype, may have more functional P-gp due to less variant polymorphisms. This is consistent with several studies (207, 212, 213) showing that the C3435T variant was associated with lower *MDR1* expression in lymphocytes and CD56+ natural killer cells. Results from our genotyping studies for the linked *MDR1* C3435T, G3677T and C1236T polymorphisms (*MDR1*2* haplotype), confirm previous studies (196, 197) displaying the general ethnic trend for homozygous variance at these positions in Caucasians and the reference genotype in African-American subjects. Neither HIV status, ethnicity, nor genotype had an effect on the positive correlation of sex-steroid induction of endometrial *MDR1* mRNA expression and increased lymphocytic P-gp active efflux during the luteal phase.

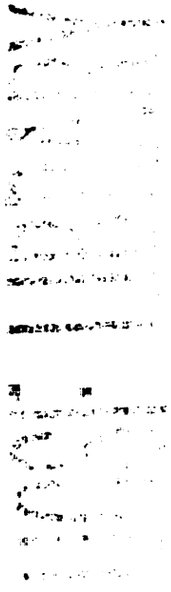

The pharmacokinetic analysis of nelfinavir between phases demonstrated a marginally significant increase in AUC (35%) and C_{max} (33%) during the luteal phase. We hypothesize that this may be due to a hepatic P-gp and CYP2C19 interaction. Increased P-gp activity and hepatobiliary efflux of nelfinavir during the luteal phase may be limiting access for nelfinavir to be metabolized by CYP2C19 or CYP3A4, thereby explaining elevated plasma levels. However, metabolite M8 pharmacokinetics exhibit the same general trend with higher plasma M8 levels during the luteal phase compared to follicular. Interestingly, the plasma M8/plasma nelfinavir (AUC_{0-12}) ratio did not change between phases for the 13 subjects with detectable M8. These findings could be explained by a possible inhibition or downregulation of CYP activity during the luteal phase, translating into no observable changes in plasma metabolite/parent drug ratios. It could also be explained by potential upregulation, during the luteal phase, of basolateral membrane hepatic efflux transporters such as MRP3 and MRP6, or downregulation of influx transporters (i.e. OATP-A), for which nelfinavir and M8 may also be substrates. Since there were no intestinal *MDR1* mRNA expression changes between phases, we also did not expect a functional effect of P-gp in the intestine. Likewise, there was no statistically significant relationship between both nelfinavir and M8 pharmacokinetics and intestinal P-gp expression. Additional studies are necessary to investigate what effects ovarian steroids may have on the expression and activity of other relevant hepatic transporters and enzymes, the affinity of nelfinavir and M8 for these transporters, or whether exogenous estrogens and progestins (e.g. in oral contraceptive pills) might affect these parameters.

We observed a non-significant *MDR1* genotype effect on the disposition of nelfinavir with higher median nelfinavir plasma levels in C3435T homozygous variant subjects. Our results are consistent with data from Fellay *et al.* (213), Kim *et al.* (197), Nakamura *et al.* (208) and Sakaeda *et al.*(209, 227), in that individuals homozygous for the *MDR1* C3435T TT variant had lower plasma nelfinavir concentrations. We also found that African-American subjects had higher nelfinavir AUC and C_{max} values during the luteal phase compared to Caucasians. It is very likely that since African-American subjects possess the wildtype *MDR1* genotype, this may be associated with greater P-gp activity during the luteal phase compared to Caucasians.

An unexpected outcome from our studies was the finding that HIV^+ subjects exhibited significantly elevated nelfinavir plasma levels during the luteal phase compared to the follicular phase. This was also seen for M8. Multivariate statistical analyses revealed that the addition of the ovulatory cycle phase variable to HIV status proved to be a strong predictor of nelfinavir AUC and M8 AUC and C_{max} in both ethnic groups. These results provide evidence to suggest the possibility that HIV^+ women may be subjected to compromised nelfinavir and M8 therapeutic efficacy during the follicular phase. Further, as HIV appears to increase the risk of anovulation (226), this phenomenon also could lead to reduced, circulating concentrations of nelfinavir. These studies strongly emphasize the importantance of investigating the myriad effects that disease states, ethnicity and menstrual cycle phase can have on drug pharmacokinetics during the course of clinical drug development.

The thesis work presented here endeavors to understand the effect that ovarian sex-steroid hormones involved in the menstrual cycle can have on P-gp substrate drug pharmacokinetics, specifically the HIV protease inhibitor, nelfinavir. Additional studies measuring intracellular HIV-1 RNA levels in lymphocytes and comparing between phases to correlate with P-gp activity would further help to understand the mechanism of interaction between HIV and transporters. Research into hormonal effects on various transporters (i.e. MDR1, MRP, OATP) and CYP enzymes in viable liver tissues (i.e. hepatocyte sandwich cultures) would also prove useful and give further evidence as to the clinical relevance of menstrual cycle phase on substrate drug pharmacokinetics. Our studies have also revealed the need to investigate the specific interactions between sex-steroid hormones and HIV, as well as HIV and P-gp. Understanding these mechanisms will provide significant insights into providing optimal care in the clinical treatment of HIV-infected women.

REFERENCES

1. S. V. Ambudkar, S. Dey, C. A. Hrycyna, M. Ramachandra, I. Pastan, and M. M. Gottesman. Biochemical, cellular, and pharmacological aspects of the multidrug transporter. *Annu Rev Pharmacol Toxicol* **39**: 361-98 (1999).

2. M. M. Gottesman, I. Pastan, and S. V. Ambudkar. P-glycoprotein and multidrug resistance. *Curr Opin Genet Dev* **6**: 610-7 (1996).

3. R. L. Juliano and V. Ling. A surface glycoprotein modulating drug permeability in Chinese hamster ovary cell mutants. *Biochim Biophys Acta* **455**: 152-62 (1976).

4. F. Thiebaut, T. Tsuruo, H. Hamada, M. M. Gottesman, I. Pastan, and M. C. Willingham. Immunohistochemical localization in normal tissues of different epitopes in the multidrug transport protein P170: evidence for localization in brain capillaries and crossreactivity of one antibody with a muscle protein. *J Histochem Cytochem* **37**: 159-64 (1989).

5. C. Cordon-Cardo, J. P. O'Brien, J. Boccia, D. Casals, J. R. Bertino, and M. R. Melamed. Expression of the multidrug resistance gene product (P-glycoprotein) in human normal and tumor tissues. *J Histochem Cytochem* **38**: 1277-87 (1990).

6. A. H. Schinkel. The physiological function of drug-transporting P-glycoproteins. *Semin Cancer Biol* **8**: 161-70 (1997).

7. P. Borst, A. H. Schinkel, J. J. Smit, E. Wagenaar, L. Van Deemter, A. J. Smith, E. W. Eijdems, F. Baas, and G. J. Zaman. Classical and novel forms of multidrug resistance and the physiological functions of P-glycoproteins in mammals. *Pharmacol Ther* **60**: 289-99 (1993).

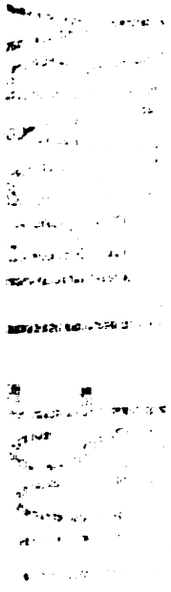

8. A. van Helvoort, A. J. Smith, H. Sprong, I. Fritzsche, A. H. Schinkel, P. Borst, and G. van Meer. MDR1 P-glycoprotein is a lipid translocase of broad specificity, while MDR3 P-glycoprotein specifically translocates phosphatidylcholine. *Cell* **87**: 507-17 (1996).

9. J. J. Smit, A. H. Schinkel, C. A. Mol, D. Majoor, W. J. Mooi, A. P. Jongsma, C. R. Lincke, and P. Borst. Tissue distribution of the human MDR3 P-glycoprotein. *Lab Invest* **71**: 638-49 (1994).

10. J. J. Smit, A. H. Schinkel, R. P. Oude Elferink, A. K. Groen, E. Wagenaar, L. van Deemter, C. A. A. M. Mol, R. Ottenhoff, N. M. van der Lugt, M. A. van Roon, M. A. van der Valk, G. J. A. Offerhaus, A. J. M. Berns, and P. Borst. Homozygous disruption of the murine mdr2 P-glycoprotein gene leads to a complete absence of phospholipid from bile and to liver disease. *Cell* **75**: 451-62 (1993).

11. A. J. Smith, J. L. Timmermans-Hereijgers, B. Roelofsen, K. W. Wirtz, W. J. van Blitterswijk, J. J. Smit, A. H. Schinkel, and P. Borst. The human MDR3 P-glycoprotein promotes translocation of phosphatidylcholine through the plasma membrane of fibroblasts from transgenic mice. *FEBS Lett* **354**: 263-6 (1994).

12. M. M. Gottesman and I. Pastan. Biochemistry of multidrug resistance mediated by the multidrug transporter. *Annu Rev Biochem* **62**: 385-427 (1993).

13. M. Azzaria, E. Schurr, and P. Gros. Discrete mutations introduced in the predicted nucleotide-binding sites of the mdr1 gene abolish its ability to confer multidrug resistance. *Mol Cell Biol* **9**: 5289-97 (1989).

14. C. Kast, V. Canfield, R. Levenson, and P. Gros. Membrane topology of P-glycoprotein as determined by epitope insertion: transmembrane organization of the N-terminal domain of mdr3. *Biochemistry* **34**: 4402-11 (1995).

15. A. R. Safa, S. Roberts, M. Agresti, and R. L. Fine. Tamoxifen aziridine, a novel affinity probe for P-glycoprotein in multidrug resistant cells. *Biochem Biophys Res Commun* **202**: 606-12 (1994).

16. A. R. Safa. Photoaffinity labeling of P-glycoprotein in multidrug-resistant cells. *Cancer Invest* **11**: 46-56 (1993).

17. S. Kajiji, J. A. Dreslin, K. Grizzuti, and P. Gros. Structurally distinct MDR modulators show specific patterns of reversal against P-glycoproteins bearing unique mutations at serine939/941. *Biochemistry* **33**: 5041-8 (1994).

18. S. V. Ambudkar, C. Kimchi-Sarfaty, Z. E. Sauna, and M. M. Gottesman. P-glycoprotein: from genomics to mechanism. *Oncogene* **22**: 7468-85 (2003).

19. E. Welker, K. Szabo, Z. Hollo, M. Muller, B. Sarkadi, and A. Varadi. Drug-stimulated ATPase activity of a deletion mutant of the human multidrug-resistance protein (MDR1). *Biochem Biophys Res Commun* **216**: 602-9 (1995).

20. I. L. Urbatsch, B. Sankaran, S. Bhagat, and A. E. Senior. Both P-glycoprotein nucleotide-binding sites are catalytically active. *J Biol Chem* **270**: 26956-61 (1995).

21. M. F. Rosenberg, R. Callaghan, R. C. Ford, and C. F. Higgins. Structure of the multidrug resistance P-glycoprotein to 2.5 nm resolution determined by electron microscopy and image analysis. *J Biol Chem* **272**: 10685-94 (1997).

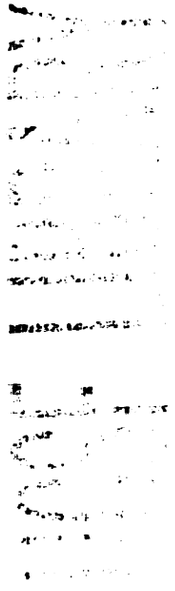

22. F. Thiebaut, T. Tsuruo, H. Hamada, M. M. Gottesman, I. Pastan, and M. C. Willingham. Cellular localization of the multidrug-resistance gene product P-glycoprotein in normal human tissues. *Proc Natl Acad Sci U S A* **84**: 7735-8 (1987).

23. A. M. Young, C. E. Allen, and K. L. Audus. Efflux transporters of the human placenta. *Adv Drug Deliv Rev* **55**: 125-32 (2003).

24. V. V. Rao, J. L. Dahlheimer, M. E. Bardgett, A. Z. Snyder, R. A. Finch, A. C. Sartorelli, and D. Piwnica-Worms. Choroid plexus epithelial expression of MDR1 P glycoprotein and multidrug resistance-associated protein contribute to the blood-cerebrospinal-fluid drug-permeability barrier. *Proc Natl Acad Sci U S A* **96**: 3900-5 (1999).

25. P. van der Valk, C. K. van Kalken, H. Ketelaars, H. J. Broxterman, G. Scheffer, C. M. Kuiper, T. Tsuruo, J. Lankelma, C. J. Meijer, H. M. Pinedo, and R. J. Scheper. Distribution of multi-drug resistance-associated P-glycoprotein in normal and neoplastic human tissues. Analysis with 3 monoclonal antibodies recognizing different epitopes of the P-glycoprotein molecule. *Ann Oncol* **1**: 56-64 (1990).

26. P. M. Chaudhary, E. B. Mechetner, and I. B. Roninson. Expression and activity of the multidrug resistance P-glycoprotein in human peripheral blood lymphocytes. *Blood* **80**: 2735-9 (1992).

27. K. Ueda, N. Okamura, M. Hirai, Y. Tanigawara, T. Saeki, N. Kioka, T. Komano, and R. Hori. Human P-glycoprotein transports cortisol, aldosterone, and dexamethasone, but not progesterone. *J Biol Chem* **267**: 24248-52 (1992).

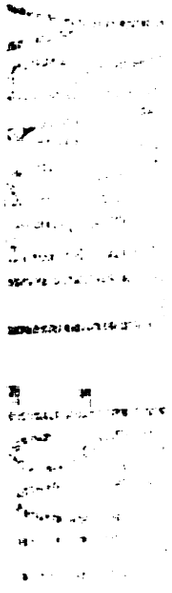

28. M. Uhr, F. Holsboer, and M. B. Muller. Penetration of endogenous steroid hormones corticosterone, cortisol, aldosterone and progesterone into the brain is enhanced in mice deficient for both mdr1a and mdr1b P-glycoproteins. *J Neuroendocrinol* **14**: 753-9 (2002).

29. A. Fojo, R. Lebo, N. Shimizu, J. E. Chin, I. B. Roninson, G. T. Merlino, M. M. Gottesman, and I. Pastan. Localization of multidrug resistance-associated DNA sequences to human chromosome 7. *Somat Cell Mol Genet* **12**: 415-20 (1986).

30. C. R. Fairchild, S. P. Ivy, C. S. Kao-Shan, J. Whang-Peng, N. Rosen, M. A. Israel, P. W. Melera, K. H. Cowan, and M. E. Goldsmith. Isolation of amplified and overexpressed DNA sequences from adriamycin-resistant human breast cancer cells. *Cancer Res* **47**: 5141-8 (1987).

31. D. F. Callen, E. Baker, R. N. Simmers, R. Seshadri, and I. B. Roninson. Localization of the human multiple drug resistance gene, MDR1, to 7q21.1. *Hum Genet* **77**: 142-4 (1987).

32. C. J. Chen, D. Clark, K. Ueda, I. Pastan, M. M. Gottesman, and I. B. Roninson. Genomic organization of the human multidrug resistance (MDR1) gene and origin of P-glycoproteins. *J Biol Chem* **265**: 506-14 (1990).

33. E. G. Schuetz and A. H. Schinkel. Drug disposition as determined by the interplay between drug-transporting and drug-metabolizing systems. *J Biochem Mol Toxicol* **13**: 219-22 (1999).

34. C. L. Cummins, W. Jacobsen, and L. Z. Benet. Unmasking the dynamic interplay between intestinal P-glycoprotein and CYP3A4. *J Pharmacol Exp Ther* **300**: 1036-45 (2002).

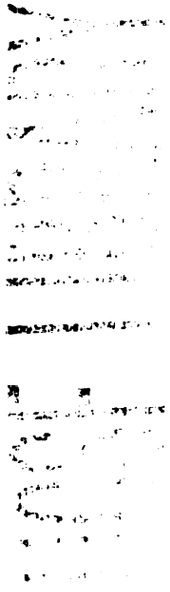

35. L. W. Hung, I. X. Wang, K. Nikaido, P. Q. Liu, G. F. Ames, and S. H. Kim. Crystal structure of the ATP-binding subunit of an ABC transporter. *Nature* **396**: 703-7 (1998).

36. M. Seigneuret and A. Garnier-Suillerot. A structural model for the open conformation of the mdr1 P-glycoprotein based on the MsbA crystal structure. *J Biol Chem* **278**: 30115-24 (2003).

37. A. B. Shapiro and V. Ling. Extraction of Hoechst 33342 from the cytoplasmic leaflet of the plasma membrane by P-glycoprotein. *Eur J Biochem* **250**: 122-9 (1997).

38. A. B. Shapiro, A. B. Corder, and V. Ling. P-glycoprotein-mediated Hoechst 33342 transport out of the lipid bilayer. *Eur J Biochem* **250**: 115-21 (1997).

39. P. D. Roepe. The role of the MDR protein in altered drug translocation across tumor cell membranes. *Biochim Biophys Acta* **1241**: 385-405 (1995).

40. C. F. Higgins and M. M. Gottesman. Is the multidrug transporter a flippase? *Trends Biochem Sci* **17**: 18-21 (1992).

41. H. Bolhuis, H. W. van Veen, D. Molenaar, B. Poolman, A. J. Driessen, and W. N. Konings. Multidrug resistance in Lactococcus lactis: evidence for ATP-dependent drug extrusion from the inner leaflet of the cytoplasmic membrane. *EMBO J* **15**: 4239-45 (1996).

42. D. F. Tang-Wai, A. Brossi, L. D. Arnold, and P. Gros. The nitrogen of the acetamido group of colchicine modulates P-glycoprotein-mediated multidrug resistance. *Biochemistry* **32**: 6470-6 (1993).

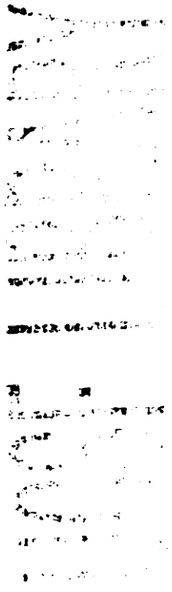

43. M. Hanna, M. Brault, T. Kwan, C. Kast, and P. Gros. Mutagenesis of transmembrane domain 11 of P-glycoprotein by alanine scanning. *Biochemistry* **35**: 3625-35 (1996).

44. S. Scala, N. Akhmed, U. S. Rao, K. Paull, L. B. Lan, B. Dickstein, J. S. Lee, G. H. Elgemeie, W. D. Stein, and S. E. Bates. P-glycoprotein substrates and antagonists cluster into two distinct groups. *Mol Pharmacol* **51**: 1024-33 (1997).

45. E. P. Bruggemann, S. J. Currier, M. M. Gottesman, and I. Pastan. Characterization of the azidopine and vinblastine binding site of P-glycoprotein. *J Biol Chem* **267**: 21020-6 (1992).

46. D. I. Morris, L. A. Speicher, A. E. Ruoho, K. D. Tew, and K. B. Seamon. Interaction of forskolin with the P-glycoprotein multidrug transporter. *Biochemistry* **30**: 8371-9 (1991).

47. A. B. Shapiro, K. Fox, P. Lam, and V. Ling. Stimulation of P-glycoprotein-mediated drug transport by prazosin and progesterone. Evidence for a third drug-binding site. *Eur J Biochem* **259**: 841-50 (1999).

48. E. E. Zheleznova, P. Markham, R. Edgar, E. Bibi, A. A. Neyfakh, and R. G. Brennan. A structure-based mechanism for drug binding by multidrug transporters. *Trends Biochem Sci* **25**: 39-43 (2000).

49. C. A. Hrycyna. Molecular genetic analysis and biochemical characterization of mammalian P-glycoproteins involved in multidrug resistance. *Semin Cell Dev Biol* **12**: 247-56 (2001).

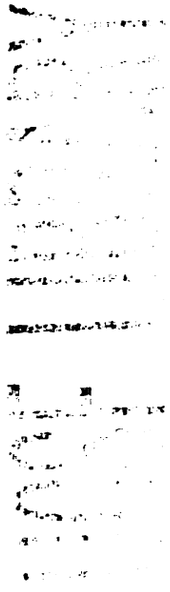

50. M. M. Gottesman, C. A. Hrycyna, P. V. Schoenlein, U. A. Germann, and I. Pastan. Genetic analysis of the multidrug transporter. *Annu Rev Genet* **29**: 607-49 (1995).

51. Q. Wu, P. Y. Bounaud, S. D. Kuduk, C. P. Yang, I. Ojima, S. B. Horwitz, and G. A. Orr. Identification of the domains of photoincorporation of the 3'- and 7-benzophenone analogues of taxol in the carboxyl-terminal half of murine mdr1b P-glycoprotein. *Biochemistry* **37**: 11272-9 (1998).

52. T. W. Loo and D. M. Clarke. Identification of residues in the drug-binding domain of human P-glycoprotein. Analysis of transmembrane segment 11 by cysteine-scanning mutagenesis and inhibition by dibromobimane. *J Biol Chem* **274**: 35388-92 (1999).

53. T. W. Loo and D. M. Clarke. Determining the structure and mechanism of the human multidrug resistance P-glycoprotein using cysteine-scanning mutagenesis and thiol-modification techniques. *Biochim Biophys Acta* **1461**: 315-25 (1999).

54. T. W. Loo and D. M. Clarke. The transmembrane domains of the human multidrug resistance P-glycoprotein are sufficient to mediate drug binding and trafficking to the cell surface. *J Biol Chem* **274**: 24759-65 (1999).

55. T. W. Loo and D. M. Clarke. The glycosylation and orientation in the membrane of the third cytoplasmic loop of human P-glycoprotein is affected by mutations and substrates. *Biochemistry* **38**: 5124-9 (1999).

56. A. Seelig. A general pattern for substrate recognition by P-glycoprotein. *Eur J Biochem* **251**: 252-61 (1998).

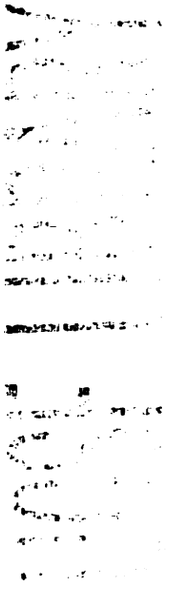

57. A. Seelig. How does P-glycoprotein recognize its substrates? *Int J Clin Pharmacol Ther* **36**: 50-4 (1998).

58. G. Ecker, M. Huber, D. Schmid, and P. Chiba. The importance of a nitrogen atom in modulators of multidrug resistance. *Mol Pharmacol* **56**: 791-6 (1999).

59. M. Demeule, A. Laplante, G. F. Murphy, R. M. Wenger, and R. Beliveau. Identification of the cyclosporin-binding site in P-glycoprotein. *Biochemistry* **37**: 18110-8 (1998).

60. E. P. Bruggemann, U. A. Germann, M. M. Gottesman, and I. Pastan. Two different regions of P-glycoprotein [corrected] are photoaffinity-labeled by azidopine. *J Biol Chem* **264**: 15483-8 (1989).

61. L. M. Greenberger. Major photoaffinity drug labeling sites for iodoaryl azidoprazosin in P-glycoprotein are within, or immediately C-terminal to, transmembrane domains 6 and 12. *J Biol Chem* **268**: 11417-25 (1993).

62. T. W. Loo and D. M. Clarke. Defining the drug-binding site in the human multidrug resistance P-glycoprotein using a methanethiosulfonate analog of verapamil, MTS-verapamil. *J Biol Chem* **276**: 14972-9 (2001).

63. T. W. Loo and D. M. Clarke. Determining the dimensions of the drug-binding domain of human P-glycoprotein using thiol cross-linking compounds as molecular rulers. *J Biol Chem* **276**: 36877-80 (2001).

64. T. W. Loo and D. M. Clarke. Identification of residues within the drug-binding domain of the human multidrug resistance P-glycoprotein by cysteine-scanning mutagenesis and reaction with dibromobimane. *J Biol Chem* **275**: 39272-8 (2000).

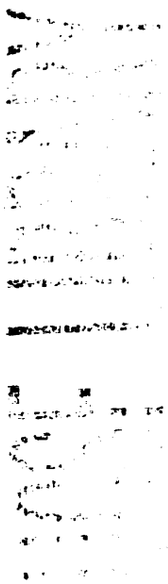

65. I. Bosch and J. Croop. P-glycoprotein multidrug resistance and cancer. *Biochim Biophys Acta* **1288**: F37-54 (1996).

66. K. Ueda, I. Pastan, and M. M. Gottesman. Isolation and sequence of the promoter region of the human multidrug-resistance (P-glycoprotein) gene. *J Biol Chem* **262**: 17432-6 (1987).

67. K. Ueda, D. P. Clark, C. J. Chen, I. B. Roninson, M. M. Gottesman, and I. Pastan. The human multidrug resistance (mdr1) gene. cDNA cloning and transcription initiation. *J Biol Chem* **262**: 505-8 (1987).

68. J. A. Silverman. Multidrug-resistance transporters. *Pharm Biotechnol* **12**: 353-86 (1999).

69. V. J. Wacher, C. Y. Wu, and L. Z. Benet. Overlapping substrate specificities and tissue distribution of cytochrome P450 3A and P-glycoprotein: implications for drug delivery and activity in cancer chemotherapy. *Mol Carcinog* **13**: 129-34 (1995).

70. C. Marzolini, E. Paus, T. Buclin, and R. B. Kim. Polymorphisms in human MDR1 (P-glycoprotein): recent advances and clinical relevance. *Clin Pharmacol Ther* **75**: 13-33 (2004).

71. M. J. Madden, C. S. Morrow, M. Nakagawa, M. E. Goldsmith, C. R. Fairchild, and K. H. Cowan. Identification of 5' and 3' sequences involved in the regulation of transcription of the human mdr1 gene in vivo. *J Biol Chem* **268**: 8290-7 (1993).

72. M. E. Goldsmith, M. J. Madden, C. S. Morrow, and K. H. Cowan. A Y-box consensus sequence is required for basal expression of the human multidrug resistance (mdr1) gene. *J Biol Chem* **268**: 5856-60 (1993).

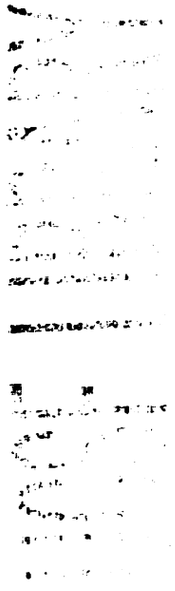

73. M. M. Cornwell and D. E. Smith. SP1 activates the MDR1 promoter through one of two distinct G-rich regions that modulate promoter activity. *J Biol Chem* **268**: 19505-11 (1993).

74. R. Sundseth, G. MacDonald, J. Ting, and A. C. King. DNA elements recognizing NF-Y and Sp1 regulate the human multidrug-resistance gene promoter. *Mol Pharmacol* **51**: 963-71 (1997).

75. T. A. Ince and K. W. Scotto. Stable transfection of the P-glycoprotein promoter reproduces the endogenous overexpression phenotype: the role of MED-1. *Cancer Res* **56**: 2021-4 (1996).

76. M. M. Cornwell. The human multidrug resistance gene: sequences upstream and downstream of the initiation site influence transcription. *Cell Growth Differ* **1**: 607-15 (1990).

77. S. Mallick and S. B. Horwitz. Transcriptional regulation of the murine multidrug resistance gene mdr1b by progesterone occurs via an indirect mechanism. *DNA Cell Biol* **16**: 807-18 (1997).

78. E. Marthinet, G. Divita, J. Bernaud, D. Rigal, and L. G. Baggetto. Modulation of the typical multidrug resistance phenotype by targeting the MED-1 region of human MDR1 promoter. *Gene Ther* **7**: 1224-33 (2000).

79. J. K. Grant and G. H. Beasthall. *Clinical Biochemistry of Steroid Hormones*, Elsevier Science Pub. Co., Inc., Amsterdam, 1993.

80. C. L. Williams and G. M. Stancel. Estrogens and progestins. Chapter 57, *Goodman & Gilman's The Pharmacological Basis of Therapeutics*, (J. G.

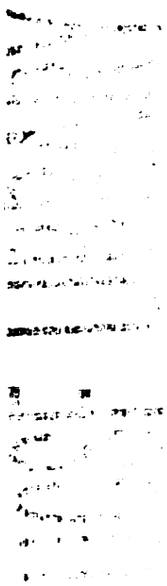

Hardman, L. E. Limbird, P. B. Molinoff, and R. W. Ruddon, eds), 9th Ed, McGraw-Hill, New York, 1996, pp. 1411-40.

81. S. P. Porterfield. *Endocrine Physiology*, Mosby Inc., St. Louis, 2001.

82. F. S. Greenspan and D. G. Gardner. *Basic and Clinical Endocrinology*, McGraw-Hill Companies, San Francisco, 2001.

83. P. F. Augustijns, T. P. Bradshaw, L. S. Gan, R. W. Hendren, and D. R. Thakker. Evidence for a polarized efflux system in CACO-2 cells capable of modulating cyclosporin A transport. *Biochem Biophys Res Commun* **197**: 360-5 (1993).

84. M. J. Tsai and B. W. O'Malley. Molecular mechanisms of action of steroid/thyroid receptor superfamily members. *Annu Rev Biochem* **63**: 451-86 (1994).

85. C. Mendelson, M. Dufau, and K. Catt. Gonadotropin binding and stimulation of cyclic adenosine 3':5'-monophosphate and testosterone production in isolated Leydig cells. *J Biol Chem* **250**: 8818-23 (1975).

86. R. J. Arceci, F. Baas, R. Raponi, S. B. Horwitz, D. Housman, and J. M. Croop. Multidrug resistance gene expression is controlled by steroid hormones in the secretory epithelium of the uterus. *Mol Reprod Dev* **25**: 101-9 (1990).

87. D. J. E. Marriott and M. McMurchie. HIV and advanced immune deficiency. *Managing HIV* **164**: 15-6 (1997).

88. F. Clavel, D. Guetard, F. Brun-Vezinet, S. Chamaret, M. A. Rey, M. O. Santos-Ferreira, A. G. Laurent, C. Dauguet, C. Katlama, C. Rouzioux, D. Klatzmann, J. L. Champalimaud, and L. Montagnier. Isolation of a new human retrovirus from West African patients with AIDS. *Science* **233**: 343-6 (1986).

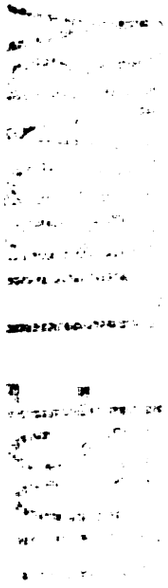

89. J. A. Levy. *HIV and the Pathogenesis of AIDS*, ASM Press, Washington, D.C., 1998.

90. J. Leis, D. Baltimore, J. M. Bishop, J. Coffin, E. Fleissner, S. P. Goff, S. Oroszlan, H. Robinson, A. M. Skalka, H. M. Temin, and V. Vogt. Standardized and simplified nomenclature for proteins common to all retroviruses. *J Virol* **62**: 1808-9 (1988).

91. T. B. Geijtenbeek, D. S. Kwon, R. Torensma, S. J. van Vliet, G. C. van Duijnhoven, J. Middel, I. L. Cornelissen, H. S. Nottet, V. N. KewalRamani, D. R. Littman, C. G. Figdor, and Y. van Kooyk. DC-SIGN, a dendritic cell-specific HIV-1-binding protein that enhances trans-infection of T cells. *Cell* **100**: 587-97 (2000).

92. A. Bukrinskaya, B. Brichacek, A. Mann, and M. Stevenson. Establishment of a functional human immunodeficiency virus type 1 (HIV-1) reverse transcription complex involves the cytoskeleton. *J Exp Med* **188**: 2113-25 (1998).

93. M. D. Miller, C. M. Farnet, and F. D. Bushman. Human immunodeficiency virus type 1 preintegration complexes: studies of organization and composition. *J Virol* **71**: 5382-90 (1997).

94. D. McDonald, M. A. Vodicka, G. Lucero, T. M. Svitkina, G. G. Borisy, M. Emerman, and T. J. Hope. Visualization of the intracellular behavior of HIV in living cells. *J Cell Biol* **159**: 441-52 (2002).

95. M. Adams, L. Sharmeen, J. Kimpton, J. M. Romeo, J. V. Garcia, B. M. Peterlin, M. Groudine, and M. Emerman. Cellular latency in human immunodeficiency

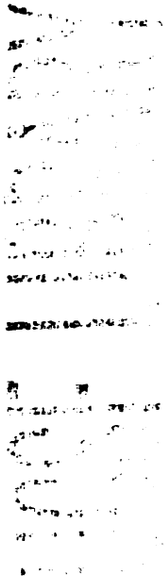

virus-infected individuals with high CD4 levels can be detected by the presence of promoter-proximal transcripts. *Proc Natl Acad Sci U S A* **91**: 3862-6 (1994).

96. O. Schwartz, V. Marechal, O. Danos, and J. M. Heard. Human immunodeficiency virus type 1 Nef increases the efficiency of reverse transcription in the infected cell. *J Virol* **69**: 4053-9 (1995).

97. M. W. Pandori, N. J. Fitch, H. M. Craig, D. D. Richman, C. A. Spina, and J. C. Guatelli. Producer-cell modification of human immunodeficiency virus type 1: Nef is a virion protein. *J Virol* **70**: 4283-90 (1996).

98. M. Sheldon, R. Ratnasabapathy, and N. Hernandez. Characterization of the inducer of short transcripts, a human immunodeficiency virus type 1 transcriptional element that activates the synthesis of short RNAs. *Mol Cell Biol* **13**: 1251-63 (1993).

99. P. A. Baede-van Dijk, P. W. Hugen, C. P. Verweij-van Wissen, P. P. Koopmans, D. M. Burger, and Y. A. Hekster. Analysis of variation in plasma concentrations of nelfinavir and its active metabolite M8 in HIV-positive patients. *AIDS* **15**: 991-8 (2001).

100. K. E. Zhang, E. Wu, A. K. Patick, B. Kerr, M. Zorbas, A. Lankford, T. Kobayashi, Y. Maeda, B. Shetty, and S. Webber. Circulating metabolites of the human immunodeficiency virus protease inhibitor nelfinavir in humans: structural identification, levels in plasma, and antiviral activities. *Antimicrob Agents Chemother* **45**: 1086-93 (2001).

101. http://www.cdc.gov/hiv/pubs/facts/youth.htm.

102. *http://www.cdc.gov/hiv/pubs/facts/women.htm*.

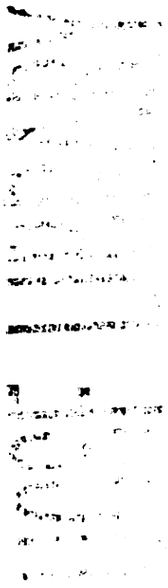

103. http://www.niaid.nih.gov/factsheets/womenhiv.htm.

104. E. F. Choo, B. Leake, C. Wandel, H. Imamura, A. J. Wood, G. R. Wilkinson, and R. B. Kim. Pharmacological inhibition of P-glycoprotein transport enhances the distribution of HIV-1 protease inhibitors into brain and testes. *Drug Metab Dispos* **28**: 655-60 (2000).

105. R. B. Kim. Drug transporters in HIV Therapy. *Top HIV Med* **11**: 136-9 (2003).

106. L. Profit, V. A. Eagling, and D. J. Back. Modulation of P-glycoprotein function in human lymphocytes and Caco-2 cell monolayers by HIV-1 protease inhibitors. *AIDS* **13**: 1623-7 (1999).

107. R. B. Kim, M. F. Fromm, C. Wandel, B. Leake, A. J. Wood, D. M. Roden, and G. R. Wilkinson. The drug transporter P-glycoprotein limits oral absorption and brain entry of HIV-1 protease inhibitors. *J Clin Invest* **101**: 289-94 (1998).

108. C. G. Lee, M. Ramachandra, K. T. Jeang, M. A. Martin, I. Pastan, and M. M. Gottesman. Effect of ABC transporters on HIV-1 infection: inhibition of virus production by the MDR1 transporter. *FASEB J* **14**: 516-22 (2000).

109. P. S. Reichelderfer, R. W. Coombs, D. J. Wright, J. Cohn, D. N. Burns, S. Cu-Uvin, P. A. Baron, M. H. Coheng, A. L. Landay, S. K. Beckner, S. R. Lewis, and A. A. Kovacs. Effect of menstrual cycle on HIV-1 levels in the peripheral blood and genital tract. WHS 001 Study Team. *AIDS* **14**: 2101-7 (2000).

110. C. A. Axiotis, C. Monteagudo, M. J. Merino, N. LaPorte, and R. D. Neumann. Immunohistochemical detection of P-glycoprotein in endometrial adenocarcinoma. *Am J Pathol* **138**: 799-806 (1991).

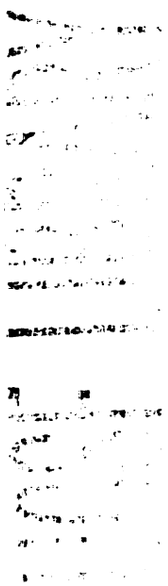

111. C. A. Axiotis, R. Guarch, M. J. Merino, N. Laporte, and R. D. Neumann. P-glycoprotein expression is increased in human secretory and gestational endometrium. *Lab Invest* **65**: 577-81 (1991).

112. A. Pfrunder, H. Gutmann, C. Beglinger, and J. Drewe. Gene expression of CYP3A4, ABC-transporters (MDR1 and MRP1-MRP5) and hPXR in three different human colon carcinoma cell lines. *J Pharm Pharmacol* **55**: 59-66 (2003).

113. S. Altuvia, W. D. Stein, S. Goldenberg, S. E. Kane, I. Pastan, and M. M. Gottesman. Targeted disruption of the mouse mdr1b gene reveals that steroid hormones enhance mdr gene expression. *J Biol Chem* **268**: 27127-32 (1993).

114. A. Nakayama, O. Eguchi, M. Hatakeyama, H. Saitoh, and M. Takada. Different absorption behaviors among steroid hormones due to possible interaction with P-glycoprotein in the rat small intestine. *Biol Pharm Bull* **22**: 535-8 (1999).

115. R. J. Arceci, J. M. Croop, S. B. Horwitz, and D. Housman. The gene encoding multidrug resistance is induced and expressed at high levels during pregnancy in the secretory epithelium of the uterus. *Proc Natl Acad Sci U S A* **85**: 4350-4 (1988).

116. C. P. Yang, S. G. DePinho, L. M. Greenberger, R. J. Arceci, and S. B. Horwitz. Progesterone interacts with P-glycoprotein in multidrug-resistant cells and in the endometrium of gravid uterus. *J Biol Chem* **264**: 782-8 (1989).

117. B. Hanstein, H. Liu, M. C. Yancisin, and M. Brown. Functional analysis of a novel estrogen receptor-beta isoform. *Mol Endocrinol* **13**: 129-37 (1999).

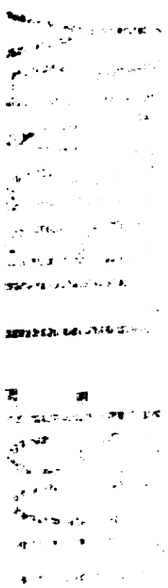

118. L. Zampieri, P. Bianchi, P. Ruff, and P. Arbuthnot. Differential modulation by estradiol of P-glycoprotein drug resistance protein expression in cultured MCF7 and T47D breast cancer cells. *Anticancer Res* **22**: 2253-9 (2002).

119. D. N. Petersen, G. T. Tkalcevic, P. H. Koza-Taylor, T. G. Turi, and T. A. Brown. Identification of estrogen receptor beta2, a functional variant of estrogen receptor beta expressed in normal rat tissues. *Endocrinology* **139**: 1082-92 (1998).

120. M. Warner, S. Nilsson, and J. A. Gustafsson. The estrogen receptor family. *Curr Opin Obstet Gynecol* **11**: 249-54 (1999).

121. K. Paech, P. Webb, G. G. Kuiper, S. Nilsson, J. Gustafsson, P. J. Kushner, and T. S. Scanlan. Differential ligand activation of estrogen receptors ERalpha and ERbeta at AP1 sites. *Science* **277**: 1508-10 (1997).

122. B. Saville, M. Wormke, F. Wang, T. Nguyen, E. Enmark, G. Kuiper, J. A. Gustafsson, and S. Safe. Ligand-, cell-, and estrogen receptor subtype (alpha/beta)-dependent activation at GC-rich (Sp1) promoter elements. *J Biol Chem* **275**: 5379-87 (2000).

123. C. Rohlff and R. I. Glazer. Regulation of multidrug resistance through the cAMP and EGF signalling pathways. *Cell Signal* **7**: 431-43 (1995).

124. C. Martin, G. Berridge, P. Mistry, C. Higgins, P. Charlton, and R. Callaghan. Drug binding sites on P-glycoprotein are altered by ATP binding prior to nucleotide hydrolysis. *Biochemistry* **39**: 11901-6 (2000).

125. C. Martin, G. Berridge, C. F. Higgins, P. Mistry, P. Charlton, and R. Callaghan. Communication between multiple drug binding sites on P-glycoprotein. *Mol Pharmacol* **58**: 624-32 (2000).

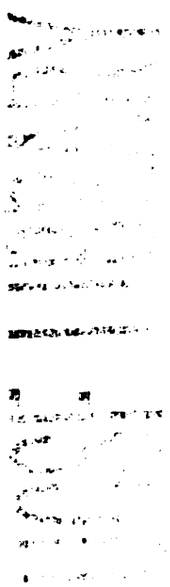

126. T. W. Loo and D. M. Clarke. Mutations to amino acids located in predicted transmembrane segment 6 (TM6) modulate the activity and substrate specificity of human P-glycoprotein. *Biochemistry* **33**: 14049-57 (1994).

127. R. Liu and F. J. Sharom. Site-directed fluorescence labeling of P-glycoprotein on cysteine residues in the nucleotide binding domains. *Biochemistry* **35**: 11865-73 (1996).

128. T. W. Loo and D. M. Clarke. Reconstitution of drug-stimulated ATPase activity following co-expression of each half of human P-glycoprotein as separate polypeptides. *J Biol Chem* **269**: 7750-5 (1994).

129. T. W. Loo and D. M. Clarke. Functional consequences of glycine mutations in the predicted cytoplasmic loops of P-glycoprotein. *J Biol Chem* **269**: 7243-8 (1994).

130. C. Martin, G. Berridge, C. F. Higgins, and R. Callaghan. The multi-drug resistance reversal agent SR33557 and modulation of vinca alkaloid binding to P-glycoprotein by an allosteric interaction. *Br J Pharmacol* **122**: 765-71 (1997).

131. C. Pascaud, M. Garrigos, and S. Orlowski. Multidrug resistance transporter P-glycoprotein has distinct but interacting binding sites for cytotoxic drugs and reversing agents. *Biochem J* **333 (Pt 2)**: 351-8 (1998).

132. M. Ichikawa-Haraguchi, T. Sumizawa, A. Yoshimura, T. Furukawa, S. Hiramoto, M. Sugita, and S. Akiyama. Progesterone and its metabolites: the potent inhibitors of the transporting activity of P-glycoprotein in the adrenal gland. *Biochim Biophys Acta* **1158**: 201-8 (1993).

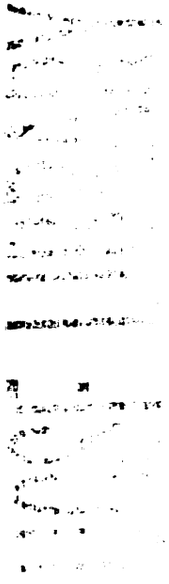

133. C. K. van Kalken, H. J. Broxterman, H. M. Pinedo, N. Feller, H. Dekker, J. Lankelma, and G. Giaccone. Cortisol is transported by the multidrug resistance gene product P-glycoprotein. *Br J Cancer* **67**: 284-9 (1993).

134. M. Naito, K. Yusa, and T. Tsuruo. Steroid hormones inhibit binding of Vinca alkaloid to multidrug resistance related P-glycoprotein. *Biochem Biophys Res Commun* **158**: 1066-71 (1989).

135. F. L. Graham and A. J. van der Eb. A new technique for the assay of infectivity of human adenovirus 5 DNA. *Virology* **52**: 456-67 (1973).

136. B. Sarkadi, E. M. Price, R. C. Boucher, U. A. Germann, and G. A. Scarborough. Expression of the human multidrug resistance cDNA in insect cells generates a high activity drug-stimulated membrane ATPase. *J Biol Chem* **267**: 4854-8 (1992).

137. A. Stavreus-Evers, P. Parini, B. Freyschuss, W. Elger, G. Reddersen, L. Sahlin, and H. Eriksson. Estrogenic influence on the regulation of hepatic estrogen receptor-alpha and serum level of angiotensinogen in female rats. *J Steroid Biochem Mol Biol* **78**: 83-8 (2001).

138. A. C. Stavreus-Evers, B. Freyschuss, and H. A. Eriksson. Hormonal regulation of the estrogen receptor in primary cultures of hepatocytes from female rats. *Steroids* **62**: 647-54 (1997).

139. B. Freyschuss, A. Stavreus-Evers, L. Sahlin, and H. Eriksson. Induction of the estrogen receptor by growth hormone and glucocorticoid substitution in primary cultures of rat hepatocytes. *Endocrinology* **133**: 1548-54 (1993).

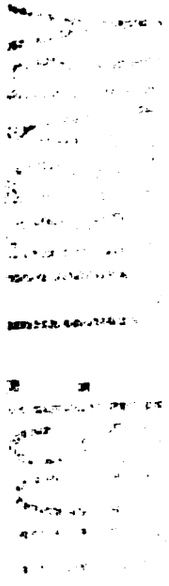

140. G. A. Kullak-Ublick and M. B. Becker. Regulation of drug and bile salt transporters in liver and intestine. *Drug Metab Rev* **35**: 305-17 (2003).

141. X. Song, M. Xie, H. Zhang, Y. Li, K. Sachdeva, and B. Yan. The pregnane X receptor binds to response elements in a genomic context-dependent manner, and PXR activator rifampicin selectively alters the binding among target genes. *Drug Metab Dispos* **32**: 35-42 (2004).

142. A. Geick, M. Eichelbaum, and O. Burk. Nuclear receptor response elements mediate induction of intestinal MDR1 by rifampin. *J Biol Chem* **276**: 14581-7 (2001).

143. B. Greiner, M. Eichelbaum, P. Fritz, H. P. Kreichgauer, O. von Richter, J. Zundler, and H. K. Kroemer. The role of intestinal P-glycoprotein in the interaction of digoxin and rifampin. *J Clin Invest* **104**: 147-53 (1999).

144. U. S. Rao and G. A. Scarborough. Direct demonstration of high affinity interactions of immunosuppressant drugs with the drug binding site of the human P-glycoprotein. *Mol Pharmacol* **45**: 773-6 (1994).

145. R. L. Piekarz, D. Cohen, and S. B. Horwitz. Progesterone regulates the murine multidrug resistance mdr1b gene. *J Biol Chem* **268**: 7613-6 (1993).

146. J. V. Wright, B. Schliesman, and L. Robinson. Comparative measurements of serum estriol, estradiol, and estrone in non-pregnant, premenopausal women; a preliminary investigation. *Altern Med Rev* **4**: 266-70 (1999).

147. R. A. Boyd, E. A. Zegarac, and M. A. Eldon. The effect of food on the bioavailability of norethindrone and ethinyl estradiol from norethindrone

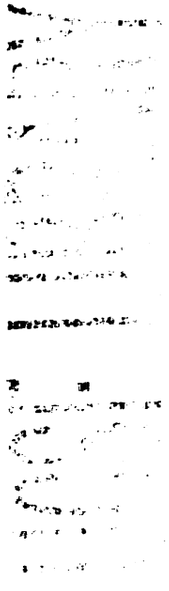

acetate/ethinyl estradiol tablets intended for continuous hormone replacement therapy. *J Clin Pharmacol* **43**: 52-8 (2003).

148. J. Endrikat, H. Blode, C. Gerlinger, P. Rosenbaum, and W. Kuhnz. A pharmacokinetic study with a low-dose oral contraceptive containing 20 microg ethinylestradiol plus 100 microg levonorgestrel. *Eur J Contracept Reprod Health Care* **7**: 79-90 (2002).

149. I. Sugawara, M. Nakahama, H. Hamada, T. Tsuruo, and S. Mori. Apparent stronger expression in the human adrenal cortex than in the human adrenal medulla of Mr 170,000-180,000 P-glycoprotein. *Cancer Res* **48**: 4611-4 (1988).

150. N. Kioka, J. Tsubota, Y. Kakehi, T. Komano, M. M. Gottesman, I. Pastan, and K. Ueda. P-glycoprotein gene (MDR1) cDNA from human adrenal: normal P-glycoprotein carries Gly185 with an altered pattern of multidrug resistance. *Biochem Biophys Res Commun* **162**: 224-31 (1989).

151. I. Sugawara. Expression and functions of P-glycoprotein (mdr1 gene product) in normal and malignant tissues. *Acta Pathol Jpn* **40**: 545-53 (1990).

152. K. M. Barnes, B. Dickstein, G. B. Cutler, Jr., T. Fojo, and S. E. Bates. Steroid treatment, accumulation, and antagonism of P-glycoprotein in multidrug-resistant cells. *Biochemistry* **35**: 4820-7 (1996).

153. K. O. Hamilton, M. A. Yazdanian, and K. L. Audus. Modulation of P-glycoprotein activity in Calu-3 cells using steroids and beta-ligands. *Int J Pharm* **228**: 171-9 (2001).

154. H. Fujise, T. Annoura, S. Sasawatari, T. Ikeda, and K. Ueda. Transepithelial transport and cellular accumulation of steroid hormones and polychlorobiphenyl

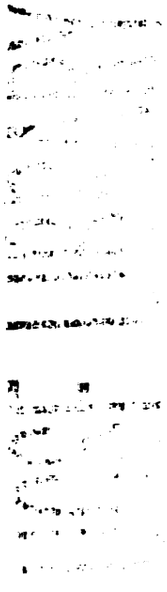

in porcine kidney cells expressed with human P-glycoprotein. *Chemosphere* **46**: 1505-11 (2002).

155. J. T. Biing, Y. F. Yang, H. S. Liu, C. T. Ye, and C. F. Chao. The induction of multidrug resistance in human cervical carcinoma cell lines by estrogenic hormones. *Proc Natl Sci Counc Repub China B* **18**: 64-70 (1994).

156. J. D. Irvine, L. Takahashi, K. Lockhart, J. Cheong, J. W. Tolan, H. E. Selick, and J. R. Grove. MDCK (Madin-Darby canine kidney) cells: A tool for membrane permeability screening. *J Pharm Sci* **88**: 28-33 (1999).

157. B. Alberts, D. Bray, J. Lewis, M. Raff, K. Roberts, and J. Watson. *Molecular Biology of the Cell*, Garland Publishing, New York, 1994.

158. P. Anderle, E. Niederer, W. Rubas, C. Hilgendorf, H. Spahn-Langguth, H. Wunderli-Allenspach, H. P. Merkle, and P. Langguth. P-Glycoprotein (P-gp) mediated efflux in Caco-2 cell monolayers: the influence of culturing conditions and drug exposure on P-gp expression levels. *J Pharm Sci* **87**: 757-62 (1998).

159. K. I. Hosoya, K. J. Kim, and V. H. L. Lee. Age-dependent expression of P-glycoprotein gp170 in Caco-2 cell monolayers. *Pharm Res* **13**: 885-90 (1996).

160. F. Tang and R. T. Borchardt. Characterization of the efflux transporter(s) responsible for restricting intestinal mucosa permeation of the coumarinic acid-based cyclic prodrug of the opioid peptide DADLE. *Pharm Res* **19**: 787-93 (2002).

161. J. A. McRoberts, M. Taub, and M. H. Saier. *Functionally Differentiated Cell Lines*, Alan R. Liss, Inc., New York, 1981.

162. J. C. Richardson, V. Scalera, and N. L. Simmons. Identification of two strains of MDCK cells which resemble separate nephron tubule segments. *Biochim Biophys Acta* **673**: 26-36 (1981).

163. A. Braun, S. Hammerle, K. Suda, B. Rothen-Rutishauser, M. Gunthert, S. D. Kramer, and H. Wunderli-Allenspach. Cell cultures as tools in biopharmacy. *Eur J Pharm Sci* **11 Suppl 2**: S51-60 (2000).

164. D. Siccardi, L. E. Kandalaft, M. Gumbleton, and C. McGuigan. Stereoselective and concentration-dependent polarized epithelial permeability of a series of phosphoramidate triester prodrugs of d4T: an in vitro study in Caco-2 and Madin-Darby canine kidney cell monolayers. *J Pharmacol Exp Ther* **307**: 1112-9 (2003).

165. C. S. Karyekar, N. D. Eddington, T. S. Garimella, P. O. Gubbins, and T. C. Dowling. Evaluation of P-glycoprotein-mediated renal drug interactions in an MDR1-MDCK model. *Pharmacotherapy* **23**: 436-42 (2003).

166. Y. Zhang and L. Z. Benet. Characterization of P-glycoprotein mediated transport of K02, a novel vinylsulfone peptidomimetic cysteine protease inhibitor, across MDR1-MDCK and Caco-2 cell monolayers. *Pharm Res* **15**: 1520-4 (1998).

167. B. F. Pan, A. Dutt, and J. A. Nelson. Enhanced transepithelial flux of cimetidine by Madin-Darby canine kidney cells overexpressing human P-glycoprotein. *J Pharmacol Exp Ther* **270**: 1-7 (1994).

168. M. Susanto and L. Z. Benet. Can the enhanced renal clearance of antibiotics in cystic fibrosis patients be explained by P-glycoprotein transport? *Pharm Res* **19**: 457-62 (2002).

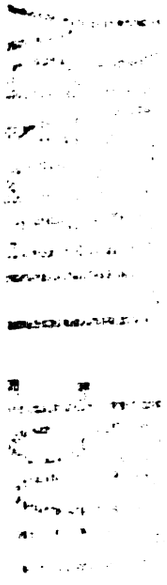

169. S. D. Flanagan, C. L. Cummins, M. Susanto, X. Liu, L. H. Takahashi, and L. Z. Benet. Comparison of furosemide and vinblastine secretion from cell lines overexpressing multidrug resistance protein (P-glycoprotein) and multidrug resistance-associated proteins (MRP1 and MRP2). *Pharmacology* **64**: 126-34 (2002).

170. S. P. Hammerle, B. Rothen-Rutishauser, S. D. Kramer, M. Gunthert, and H. Wunderli-Allenspach. P-Glycoprotein in cell cultures: a combined approach to study expression, localisation, and functionality in the confocal microscope. *Eur J Pharm Sci* **12**: 69-77 (2000).

171. F. Tang, K. Horie, and R. T. Borchardt. Are MDCK cells transfected with the human MDR1 gene a good model of the human intestinal mucosa? *Pharm Res* **19**: 765-72 (2002).

172. M. Horio, K. V. Chin, S. J. Currier, S. Goldenberg, C. Williams, I. Pastan, M. M. Gottesman, and J. Handler. Transepithelial transport of drugs by the multidrug transporter in cultured Madin-Darby canine kidney cell epithelia. *J Biol Chem* **264**: 14880-4 (1989).

173. S. Palovaara, K. T. Kivisto, P. Tapanainen, P. Manninen, P. J. Neuvonen, and K. Laine. Effect of an oral contraceptive preparation containing ethinylestradiol and gestodene on CYP3A4 activity as measured by midazolam 1'-hydroxylation. *Br J Clin Pharmacol* **50**: 333-7 (2000).

174. S. M. Tsunoda, R. Z. Harris, P. J. Mroczkowski, and L. Z. Benet. Preliminary evaluation of progestins as inducers of cytochrome P450 3A4 activity in postmenopausal women. *J Clin Pharmacol* **38**: 1137-43 (1998).

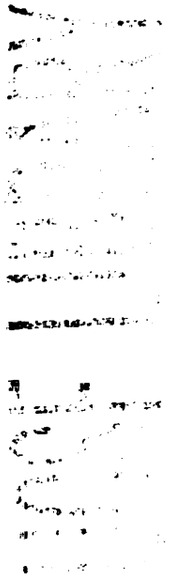

175. M. L. Orme and D. J. Back. Factors affecting the enterohepatic circulation of oral contraceptive steroids. *Am J Obstet Gynecol* **163**: 2146-52 (1990).

176. *https://statepiaps.jhsph.edu/wihs/.*

177. F. J. Palella, Jr., K. M. Delaney, A. C. Moorman, M. O. Loveless, J. Fuhrer, G. A. Satten, D. J. Aschman, and S. D. Holmberg. Declining morbidity and mortality among patients with advanced human immunodeficiency virus infection. HIV Outpatient Study Investigators. *N Engl J Med* **338**: 853-60 (1998).

178. M. E. Morris, H. J. Lee, and L. M. Predko. Gender differences in the membrane transport of endogenous and exogenous compounds. *Pharmacol Rev* **55**: 229-40 (2003).

179. R. Z. Harris, L. Z. Benet, and J. B. Schwartz. Gender effects in pharmacokinetics and pharmacodynamics. *Drugs* **50**: 222-39 (1995).

180. I. Beierle, B. Meibohm, and H. Derendorf. Gender differences in pharmacokinetics and pharmacodynamics. *Int J Clin Pharmacol Ther* **37**: 529-47 (1999).

181. C. L. Cummins, C. Y. Wu, and L. Z. Benet. Sex-related differences in the clearance of cytochrome P450 3A4 substrates may be caused by P-glycoprotein. *Clin Pharmacol Ther* **72**: 474-89 (2002).

182. L. Salphati and L. Z. Benet. Modulation of P-glycoprotein expression by cytochrome P450 3A inducers in male and female rat livers. *Biochem Pharmacol* **55**: 387-95 (1998).

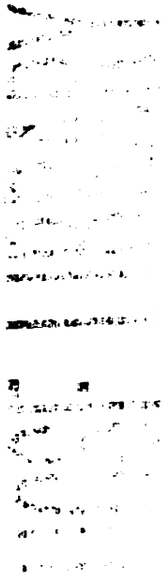

183. E. G. Schuetz, K. N. Furuya, and J. D. Schuetz. Interindividual variation in expression of P-glycoprotein in normal human liver and secondary hepatic neoplasms. *J Pharmacol Exp Ther* **275**: 1011-8 (1995).

184. J. H. Lin, M. Chiba, I. W. Chen, J. A. Nishime, F. A. deLuna, M. Yamazaki, and Y. J. Lin. Effect of dexamethasone on the intestinal first-pass metabolism of indinavir in rats: evidence of cytochrome P-450 3A [correction of P-450 A] and p-glycoprotein induction. *Drug Metab Dispos* **27**: 1187-93 (1999).

185. J. S. Macdonald, M. E. Lippman, P. V. Woolley, P. P. Petrucci, and P. S. Schein. Hepatic estrogen and progesterone receptors in an estrogen-associated hepatic neoplasm. *Cancer Chemother Pharmacol* **1**: 135-8 (1978).

186. D. R. Ciocca, A. D. Jorge, O. Jorge, C. Milutin, R. Hosokawa, M. Diaz Lestren, E. Muzzio, S. Schulkin, and R. Schirbu. Estrogen receptors, progesterone receptors and heat-shock 27-kD protein in liver biopsy specimens from patients with hepatitis B virus infection. *Hepatology* **13**: 838-44 (1991).

187. A. D. Jorge, A. O. Stati, L. V. Roig, G. Ponce, O. A. Jorge, and D. R. Ciocca. Steroid receptors and heat-shock proteins in patients with primary biliary cirrhosis. *Hepatology* **18**: 1108-14 (1993).

188. C. Cohen, D. Lawson, and P. B. DeRose. Sex and androgenic steroid receptor expression in hepatic adenomas. *Hum Pathol* **29**: 1428-32 (1998).

189. S. Singh, M. C. Sheppard, and M. J. Langman. Sex differences in the incidence of colorectal cancer: an exploration of oestrogen and progesterone receptors. *Gut* **34**: 611-5 (1993).

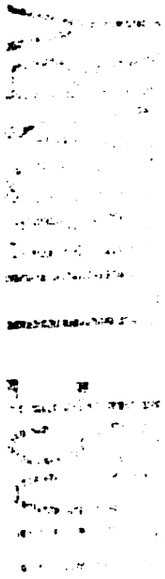

190. P. A. Marx, A. I. Spira, A. Gettie, P. J. Dailey, R. S. Veazey, A. A. Lackner, C. J. Mahoney, C. J. Miller, L. E. Claypool, D. D. Ho, and N. J. Alexander. Progesterone implants enhance SIV vaginal transmission and early virus load. *Nat Med* **2**: 1084-9 (1996).

191. N. Vassiliadou, L. Tucker, and D. J. Anderson. Progesterone-induced inhibition of chemokine receptor expression on peripheral blood mononuclear cells correlates with reduced HIV-1 infectability in vitro. *J Immunol* **162**: 7510-8 (1999).

192. T. Hulgan, J. P. Donahue, C. Hawkins, D. Unutmaz, R. T. D'Aquila, S. Raffanti, F. Nicotera, P. Rebeiro, H. Erdem, M. Rueff, and D. W. Haas. Implications of T-cell P-glycoprotein activity during HIV-1 infection and its therapy. *J Acquir Immune Defic Syndr* **34**: 119-26 (2003).

193. K. S. Lown, R. R. Mayo, A. B. Leichtman, H. L. Hsiao, D. K. Turgeon, P. Schmiedlin-Ren, M. B. Brown, W. Guo, S. J. Rossi, L. Z. Benet, and P. B. Watkins. Role of intestinal P-glycoprotein (mdr1) in interpatient variation in the oral bioavailability of cyclosporine. *Clin Pharmacol Ther* **62**: 248-60 (1997).

194. W. T. Klimecki, B. W. Futscher, T. M. Grogan, and W. S. Dalton. P-glycoprotein expression and function in circulating blood cells from normal volunteers. *Blood* **83**: 2451-8 (1994).

195. J. Kodama, H. Ryoji, H. Okuda, M. Yoshinouchi, and T. Kudo. Reverse correlation between P-glycoprotein expression and proliferative activity in endometrial adenocarcinoma. *Eur J Obstet Gynecol Reprod Biol* **59**: 45-51 (1995).

196. E. Schaeffeler, M. Eichelbaum, U. Brinkmann, A. Penger, S. Asante-Poku, U. M. Zanger, and M. Schwab. Frequency of C3435T polymorphism of MDR1 gene in African people. *Lancet* **358**: 383-4 (2001).

197. R. B. Kim, B. F. Leake, E. F. Choo, G. K. Dresser, S. V. Kubba, U. I. Schwarz, A. Taylor, H. G. Xie, J. McKinsey, S. Zhou, L. B. Lan, J. D. Schuetz, E. G. Schuetz, and G. R. Wilkinson. Identification of functionally variant MDR1 alleles among European Americans and African Americans. *Clin Pharmacol Ther* **70**: 189-99 (2001).

198. L. A. Mickley, J. S. Lee, Z. Weng, Z. Zhan, M. Alvarez, W. Wilson, S. E. Bates, and T. Fojo. Genetic polymorphism in MDR-1: a tool for examining allelic expression in normal cells, unselected and drug-selected cell lines, and human tumors. *Blood* **91**: 1749-56 (1998).

199. I. Cascorbi, T. Gerloff, A. Johne, C. Meisel, S. Hoffmeyer, M. Schwab, E. Schaeffeler, M. Eichelbaum, U. Brinkmann, and I. Roots. Frequency of single nucleotide polymorphisms in the P-glycoprotein drug transporter MDR1 gene in white subjects. *Clin Pharmacol Ther* **69**: 169-74 (2001).

200. W. Siegmund, K. Ludwig, T. Giessmann, P. Dazert, E. Schroeder, B. Sperker, R. Warzok, H. K. Kroemer, and I. Cascorbi. The effects of the human MDR1 genotype on the expression of duodenal P-glycoprotein and disposition of the probe drug talinolol. *Clin Pharmacol Ther* **72**: 572-83 (2002).

201. T. Gerloff, M. Schaefer, A. Johne, K. Oselin, C. Meisel, I. Cascorbi, and I. Roots. MDR1 genotypes do not influence the absorption of a single oral dose of 1 mg digoxin in healthy white males. *Br J Clin Pharmacol* **54**: 610-6 (2002).

202. S. Ito, I. Ieiri, M. Tanabe, A. Suzuki, S. Higuchi, and K. Otsubo. Polymorphism of the ABC transporter genes, MDR1, MRP1 and MRP2/cMOAT, in healthy Japanese subjects. *Pharmacogenetics* **11**: 175-84 (2001).

203. M. Tanabe, I. Ieiri, N. Nagata, K. Inoue, S. Ito, Y. Kanamori, M. Takahashi, Y. Kurata, J. Kigawa, S. Higuchi, N. Terakawa, and K. Otsubo. Expression of P-glycoprotein in human placenta: relation to genetic polymorphism of the multidrug resistance (MDR)-1 gene. *J Pharmacol Exp Ther* **297**: 1137-43 (2001).

204. A. Yamauchi, I. Ieiri, Y. Kataoka, M. Tanabe, T. Nishizaki, R. Oishi, S. Higuchi, K. Otsubo, and K. Sugimachi. Neurotoxicity induced by tacrolimus after liver transplantation: relation to genetic polymorphisms of the ABCB1 (MDR1) gene. *Transplantation* **74**: 571-2 (2002).

205. M. Goto, S. Masuda, H. Saito, S. Uemoto, T. Kiuchi, K. Tanaka, and K. Inui. C3435T polymorphism in the MDR1 gene affects the enterocyte expression level of CYP3A4 rather than Pgp in recipients of living-donor liver transplantation. *Pharmacogenetics* **12**: 451-7 (2002).

206. K. Tang, S. M. Ngoi, P. C. Gwee, J. M. Chua, E. J. Lee, S. S. Chong, and C. G. Lee. Distinct haplotype profiles and strong linkage disequilibrium at the MDR1 multidrug transporter gene locus in three ethnic Asian populations. *Pharmacogenetics* **12**: 437-50 (2002).

207. S. Hoffmeyer, O. Burk, O. von Richter, H. P. Arnold, J. Brockmoller, A. Johne, I. Cascorbi, T. Gerloff, I. Roots, M. Eichelbaum, and U. Brinkmann. Functional polymorphisms of the human multidrug-resistance gene: multiple sequence

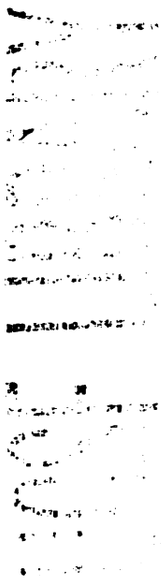

variations and correlation of one allele with P-glycoprotein expression and activity in vivo. *Proc Natl Acad Sci U S A* **97**: 3473-8 (2000).

208. T. Nakamura, T. Sakaeda, M. Horinouchi, T. Tamura, N. Aoyama, T. Shirakawa, M. Matsuo, M. Kasuga, and K. Okumura. Effect of the mutation (C3435T) at exon 26 of the MDR1 gene on expression level of MDR1 messenger ribonucleic acid in duodenal enterocytes of healthy Japanese subjects. *Clin Pharmacol Ther* **71**: 297-303 (2002).

209. T. Sakaeda, T. Nakamura, and K. Okumura. MDR1 genotype-related pharmacokinetics and pharmacodynamics. *Biol Pharm Bull* **25**: 1391-400 (2002).

210. T. Illmer, U. S. Schuler, C. Thiede, U. I. Schwarz, R. B. Kim, S. Gotthard, D. Freund, U. Schakel, G. Ehninger, and M. Schaich. MDR1 gene polymorphisms affect therapy outcome in acute myeloid leukemia patients. *Cancer Res* **62**: 4955-62 (2002).

211. A. Johne, K. Kopke, T. Gerloff, I. Mai, S. Rietbrock, C. Meisel, S. Hoffmeyer, R. Kerb, M. F. Fromm, U. Brinkmann, M. Eichelbaum, J. Brockmoller, I. Cascorbi, and I. Roots. Modulation of steady-state kinetics of digoxin by haplotypes of the P-glycoprotein MDR1 gene. *Clin Pharmacol Ther* **72**: 584-94 (2002).

212. M. Hitzl, S. Drescher, H. van der Kuip, E. Schaffeler, J. Fischer, M. Schwab, M. Eichelbaum, and M. F. Fromm. The C3435T mutation in the human MDR1 gene is associated with altered efflux of the P-glycoprotein substrate rhodamine 123 from CD56+ natural killer cells. *Pharmacogenetics* **11**: 293-8 (2001).

213. J. Fellay, C. Marzolini, E. R. Meaden, D. J. Back, T. Buclin, J. P. Chave, L. A. Decosterd, H. Furrer, M. Opravil, G. Pantaleo, D. Retelska, L. Ruiz, A. H.

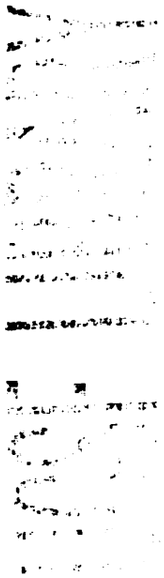

Schinkel, P. Vernazza, C. B. Eap, and A. Telenti. Response to antiretroviral treatment in HIV-1-infected individuals with allelic variants of the multidrug resistance transporter 1: a pharmacogenetics study. *Lancet* **359**: 30-6 (2002).

214. R. R. Speck, X. F. Yu, J. Hildreth, and C. Flexner. Differential effects of p-glycoprotein and multidrug resistance protein-1 on productive human immunodeficiency virus infection. *J Infect Dis* **186**: 332-40 (2002).

215. M. P. DePasquale, T. Hulgan, and L. Sutton. HIV-1 infection is associated with changes in drug transporter gene expression *in vivo*. Abstract, *10th Conference on Retroviruses and Opportunistic Infections*, Boston, MA., 2003.

216. M. Pallis and N. Russell. P-glycoprotein plays a drug-efflux-independent role in augmenting cell survival in acute myeloblastic leukemia and is associated with modulation of a sphingomyelin-ceramide apoptotic pathway. *Blood* **95**: 2897-904 (2000).

217. M. J. Smyth, E. Krasovskis, V. R. Sutton, and R. W. Johnstone. The drug efflux protein, P-glycoprotein, additionally protects drug-resistant tumor cells from multiple forms of caspase-dependent apoptosis. *Proc Natl Acad Sci U S A* **95**: 7024-9 (1998).

218. J. H. Weisburg, P. D. Roepe, S. Dzekunov, and D. A. Scheinberg. Intracellular pH and multidrug resistance regulate complement-mediated cytotoxicity of nucleated human cells. *J Biol Chem* **274**: 10877-88 (1999).

219. J. H. Weisburg, M. Curcio, P. C. Caron, G. Raghu, E. B. Mechetner, P. D. Roepe, and D. A. Scheinberg. The multidrug resistance phenotype confers immunological resistance. *J Exp Med* **183**: 2699-704 (1996).

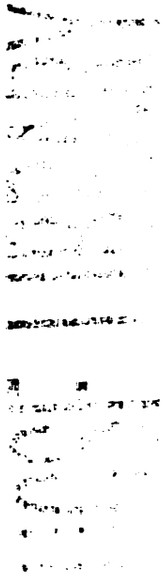

220. C. Bezombes, N. Maestre, G. Laurent, T. Levade, A. Bettaieb, and J. P. Jaffrezou. Restoration of TNF-alpha-induced ceramide generation and apoptosis in resistant human leukemia KG1a cells by the P-glycoprotein blocker PSC833. *FASEB J* **12**: 101-9 (1998).

221. L. J. Robinson, W. K. Roberts, T. T. Ling, D. Lamming, S. S. Sternberg, and P. D. Roepe. Human MDR 1 protein overexpression delays the apoptotic cascade in Chinese hamster ovary fibroblasts. *Biochemistry* **36**: 11169-78 (1997).

222. K. Simons and E. Ikonen. Functional rafts in cell membranes. *Nature* **387**: 569-72 (1997).

223. S. Manes, G. del Real, R. A. Lacalle, P. Lucas, C. Gomez-Mouton, S. Sanchez-Palomino, R. Delgado, J. Alcami, E. Mira, and A. C. Martinez. Membrane raft microdomains mediate lateral assemblies required for HIV-1 infection. *EMBO Rep* **1**: 190-6 (2000).

224. Z. Liao, L. M. Cimakasky, R. Hampton, D. H. Nguyen, and J. E. Hildreth. Lipid rafts and HIV pathogenesis: host membrane cholesterol is required for infection by HIV type 1. *AIDS Res Hum Retroviruses* **17**: 1009-19 (2001).

225. S. Benki, S. B. Mostad, B. A. Richardson, K. Mandaliya, J. K. Kreiss, and J. Overbaugh. Cyclic shedding of HIV-1 RNA in cervical secretions during the menstrual cycle. *J Infect Dis* **189**: 2192-201 (2004).

226. R. M. Greenblatt, N. Ameli, R. M. Grant, P. Bacchetti, and R. N. Taylor. Impact of the ovulatory cycle on virologic and immunologic markers in HIV-infected women. *J Infect Dis* **181**: 82-90 (2000).

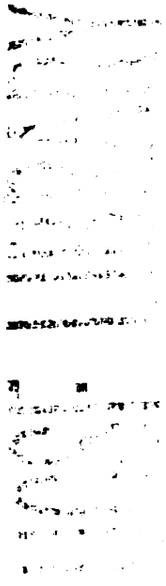

227. T. Sakaeda, T. Nakamura, M. Horinouchi, M. Kakumoto, N. Ohmoto, T. Sakai, Y. Morita, T. Tamura, N. Aoyama, M. Hirai, M. Kasuga, and K. Okumura. MDR1 genotype-related pharmacokinetics of digoxin after single oral administration in healthy Japanese subjects. *Pharm Res* **18**: 1400-4 (2001).